Volume 9
Number 3

March 4, 2009

www.cellpress.com

Cell Metabolism

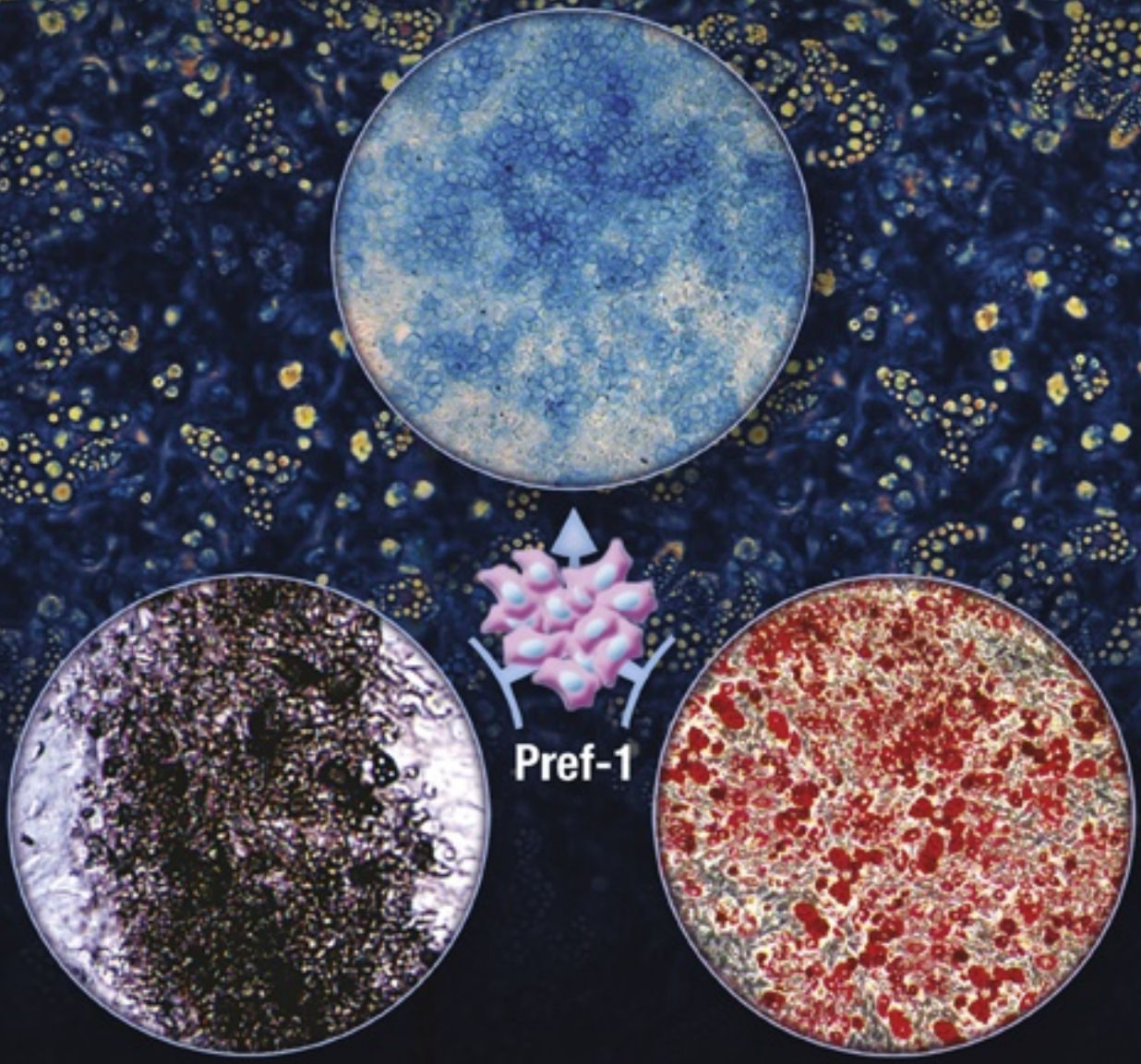

Pref-1 Controls Mesenchymal Cell Fate

Iron Sensing as a Partnership: HFE and Transferrin Receptor 2

Robert E. Fleming[1,*]
[1]Saint Louis University School of Medicine, St. Louis, MO 63104, USA
*Correspondence: flemingr@slu.edu
DOI 10.1016/j.cmet.2009.02.004

The mechanism by which HFE participates in the regulation of iron homeostasis has remained enigmatic. Gao et al. (2009) make the key discovery that the regulation of hepcidin in response to holotransferrin requires the interaction between HFE and transferrin receptor 2 (TfR2).

Among the most important breakthroughs in understanding the regulation of iron metabolism has been the discovery of the peptide hormone hepcidin (Ganz, 2008). This "master" iron regulatory hormone is the primary determinant of dietary iron absorption and body iron distribution. Hepcidin is made primarily by hepatocytes and secreted into the circulation, where it serves to downregulate iron export by certain cell populations, including splenic reticuloendothelial macrophages (the primary site of body iron turnover) and duodenal enterocytes (the primary site of body iron absorption). Hepcidin downregulates iron export by binding with and causing the internalization and degradation of the cellular iron exporter ferroportin. The consequent increase in splenic iron stores and decrease in dietary iron absorption lead to decreased circulating iron levels. Expectedly, a feedback relationship exists between body iron status and hepcidin expression; hepcidin is upregulated in response to iron loading and decreased in response to iron deficiency. Characterizing the mechanism by which iron regulates hepcidin expression has proven particularly difficult, due in no small part to the failure of cell culture systems to model the effects of iron observed in vivo. A number of the molecular participants in hepcidin regulation have been identified by the characterization of the consequences of their mutation in humans or mice. These include molecules needed for the normal upregulation of hepcidin in response to iron loading (HFE, transferrin receptor 2, hemojuvelin, SMAD4) and for downregulation in response to iron deficiency (matriptase 2) (Folgueras et al., 2008). As a result of work attempting to define in cell culture the molecular players necessary to recapitulate iron regulation observed in vivo, Gao et al. in this issue (Gao et al., 2009) made the key discovery that the regulation of hepcidin in response to holotransferrin requires the interaction between HFE and transferrin receptor 2 (TfR2).

The role of HFE in iron metabolism has been well studied, but not well understood. It is an MHC class I molecule without iron transport properties (Figure 1). As such, much of the focus of investigation has been on the interaction of HFE with other molecules with iron transport properties. Initial attention was directed toward transferrin receptor 1 (TfR1). Crystallographic studies demonstrate that the interaction between TfR1 and HFE involves the α1 and α2 domains of HFE and the transferrin-binding domain of TfR1. Experiments with mice having an engineered TfR1 mutation that interferes with HFE binding suggest that the TfR1-HFE interaction may serve to "sequester" HFE away from participation in a hepcidin upregulatory pathway (Schmidt et al., 2008). The discovery that HFE can also interact with TfR2 led to the proposal that an HFE-TfR2 complex may be involved in this hepcidin upregulation. Deletion and domain substitution studies have demonstrated that the HFE domains responsible for HFE-TfR2 interaction are entirely distinct from those involved in HFE-TfR1 interactions (Figure 1). Surprisingly, the TfR2 domain involved in this interaction appears to be likewise distinct from the homologous domain on TfR1 (and, as such, is not in competition with holotransferrin). These observations were put together to generate a model in which the interaction of holotransferrin with TfR1 frees HFE to interact with TfR2, and facilitates signal transduction to hepcidin. It had yet to be experimentally shown, however, that TfR2 is directly involved in signal transduction between holotransferrin and hepcidin. Gao et al. in this manuscript demonstrate not only that TfR2 participates in this signal transduction, but also that it requires interaction with HFE.

Several observations have supported a role for TfR2 as the hepatocellular "iron sensor" and for holotransferrin as the circulating ligand indicator of body iron status. Functional loss of TfR2 in humans, mice, and zebrafish results in abnormally low hepcidin expression and hemochromatosis. Genetic deficiencies in transferrin have likewise been shown in these same species to be associated with abnormally low hepcidin. Among the molecules known to participate in hepcidin regulation, only transferrin has been shown to directly interact with iron. While several lines of evidence lend support to these proposed roles, the effect of holotransferrin on hepcidin expression in cell culture systems has been weak or absent. These observations had led investigators to conjecture that an additional cell type is needed, or that one or more of the essential molecular players is missing. Gao et al. investigated the latter possibility and found that a hepatocellular line (WIF-B) capable of signal transduction between holotransferrin and hepcidin had substantial HFE expression, while HepG2 cells had very little. They went on to show that the regulation of hepcidin by holotransferrin requires both HFE and TfR2 in HepG2 cells and primary hepatocytes. Finally, they used a series of HFE chimeras to demonstrate that the interaction between HFE and TfR2 (but not TfR1) was

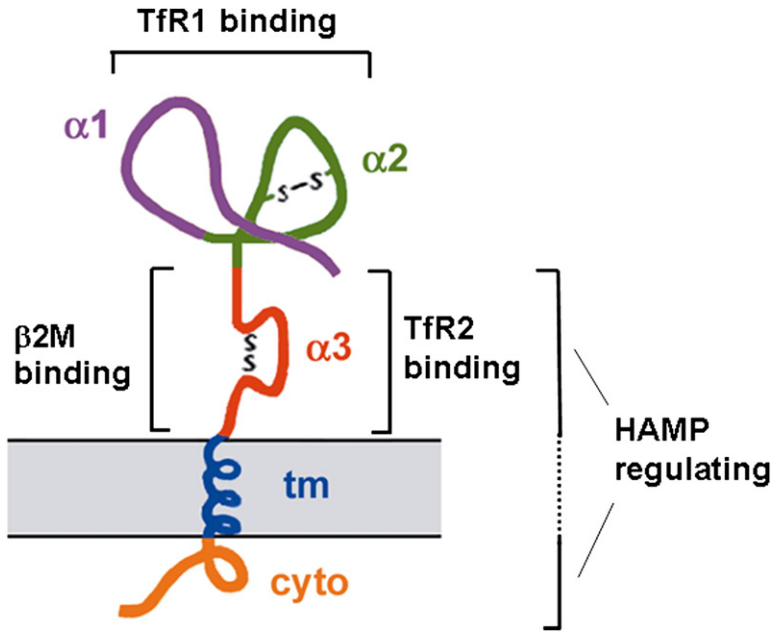

Figure 1. Schematic Representation of the HFE Protein
Colors designate HFE domains encoded by individual exons (cyto, cytoplasmic; tm, transmembrane). HFE requires interaction with β2-microglobulin (β2M) for normal cell surface localization. While transferrin receptor 1 (TfR1) interacts with the HFE α1 and α2 domains, TfR2 interacts with the HFE α3 domain. Regulation of hepcidin by holotransferrin requires HFE sequences in the α3 (and cytoplasmic) domains and interaction with transferrin receptor 2.

necessary for signal transduction. The HFE-TfR2 interaction depends upon the α3 domain of HFE, and the signal transduction depends additionally on the cytoplasmic domain of HFE (Figure 1).

These data strongly support a model in which HFE-TfR2 transduces a signal between holotransferrin and hepcidin expression. It would be informative to determine if there is a dose-response relationship between holotransferrin and hepcidin expression, as expected if this mechanism is responsible for the physiologic feedback regulation of hepcidin. It would be also be useful to know what effect overexpression of HFE had on measurements of iron status and the labile iron pool in the HepG2 cells. The overexpression of HFE has been shown to influence cellular iron status in cell lines that express neither TFR1 nor TfR2 (Carlson et al., 2004). Finally, it is not clear that the observations made in cell culture will directly translate to the situation in vivo. Some observations suggest that the absence of HFE does not completely abolish regulation of hepcidin by iron in vivo. For example, changes in dietary iron in at least certain HFE knockout mouse strains are associated with changes in hepcidin expression (Gehrke et al., 2005), albeit at an attenuated level. Also, zebrafish regulate iron metabolism by a mechanism dependent upon transferrin and on TfR2 (Fraenkel et al., 2008), yet have no identified HFE ortholog.

It is likely that hepatocellular iron sensing will found to be a group effort rather than a simple partnership. Recent studies have clearly placed hemojuvelin and matriptase 2 in a common pathway that regulates hepcidin by modulating signal transduction through bone morphogenetic proteins and SMAD4 (Silvestri et al., 2008). Several lines of evidence suggest that this pathway contributes to the regulation of hepcidin by iron (Lin et al., 2007; Yu et al., 2008). The exciting results reported here by Gao et al. provide an important step in investigating a possible relationship between HFE-TfR2 and this signal transduction pathway.

REFERENCES

Carlson, H., Zhang, A.S., Fleming, W.H., and Enns, C.A. (2004). Blood *105*, 2564–2570.

Folgueras, A.R., de Lara, F.M., Pendas, A.M., Garabaya, C., Rodriguez, F., Astudillo, A., Bernal, T., Cabanillas, R., Lopez-Otin, C., and Velasco, G. (2008). Blood *112*, 2539–2545.

Fraenkel, P.G., Gibert, Y., Holzheimer, J.L., Lattanzi, V.J., Burnett, S.F., Dooley, K.A., Wingert, R.A., and Zon, L.I. (2008). Blood. Published online December 1, 2008. 10.1182/blood-2008-06-165340.

Ganz, T. (2008). Cell Metab. *7*, 288–290.

Gao, J., Chen, J., Kramer, M., Tsukamoto, H., Zhang, A.-S., and Enns, C.A. (2009). Cell Metab. *9*, this issue, 217–227.

Gehrke, S.G., Herrmann, T., Kulaksiz, H., Merle, U., Bents, K., Kaiser, I., Riedel, H.D., and Stremmel, W. (2005). Digestion *72*, 25–32.

Lin, L., Valore, E.V., Nemeth, E., Goodnough, J.B., Gabayan, V., and Ganz, T. (2007). Blood *110*, 2182–2189.

Silvestri, L., Pagani, A., Nai, A., Dedomenico, I., Kaplan, J., and Camaschella, C. (2008). Cell Metab. *8*, 502–511.

Schmidt, P.J., Toran, P.T., Giannetti, A.M., Bjorkman, P.J., and Andrews, N.C. (2008). Cell Metab. *7*, 205–214.

Yu, P.B., Hong, C.C., Sachidanandan, C., Babitt, J.L., Deng, D.Y., Hoyng, S.A., Lin, H.Y., Bloch, K.D., and Peterson, R.T. (2008). Nat. Chem. Biol. *4*, 33–41.

Insulin Action under Arrestin

Jacqueline Stöckli[1] and David E. James[1,*]
[1]Garvan Institute of Medical Research, 384 Victoria St., Darlinghurst, NSW, Australia
*Correspondence: d.james@garvan.org.au
DOI 10.1016/j.cmet.2009.02.005

Insulin signaling is key to the etiology of metabolic syndrome. Recent work (Luan et al., 2009) uncovers a role for β-arrestin, previously known to control GPCR desensitization, in insulin signaling. In mouse models, β-arrestin-2 controls whole-body insulin action by regulating assembly of a complex containing insulin receptor, c-Src, and Akt.

Insulin resistance or impaired insulin action in muscle, fat, and liver is one of the earliest detectable defects associated with a range of metabolic diseases including type 2 diabetes (T2D). Overeating, or a lack of exercise coupled with obesity have been implicated as major factors contributing to insulin resistance. At the cellular level, a range of abnormalities (including ER stress, oxidative stress, mitochondrial defects, intracellular lipids, or inflammation) have been experimentally linked to insulin resistance. However, the molecular basis for insulin resistance remains controversial in that some studies indicate a primary role for a signaling defect at insulin receptor substrate 1 (IRS1) leading to reduced Akt activation (reviewed in Taniguchi et al., 2006), while other studies suggest otherwise (Kim et al., 1999; Hoehn et al., 2008). In a recent issue of Nature, Luan et al. (2009) now provide evidence for yet another insulin action rebel: β-arrestin-2.

β-arrestin-2 was originally identified as a mediator of β-adrenergic receptor endocytosis, leading to attenuation of β-adrenergic signaling. However, subsequent studies have revealed a broad tissue distribution and an array of interacting molecules, suggesting that β-arrestins play a general role in many signaling pathways. For example, they regulate the desensitization and downregulation of many G protein-coupled receptors (GPCRs) (DeWire et al., 2007). They also act as a scaffold for key signaling molecules including the tyrosine kinase c-Src; receptors for insulin, IGF1 and PDGF; and Ser/Thr kinases including Akt, Raf, ERK, and JNK (Hupfeld and Olefsky, 2007).

Luan et al. (2009) begin to integrate some of these disparate attributes of β-arrestin function in the context of insulin action in muscle and liver. They show that β-arrestin-2 expression in muscle and liver, but not fat, is reduced by ~50% in insulin-resistant animal models and in liver from a small cohort of T2D humans; β-arrestin-1 expression was normal. *β-arrestin-2* −/− mice were insulin resistant; results from *β-arrestin-2* haploinsufficient animals were unfortunately not described—these might have provided a direct corollary of the initial physiological data. Regardless, 2-fold overexpression of *β-arrestin-2* in mice led to increased insulin sensitivity, supporting the thesis that *β-arrestin-2* expression is correlated with insulin action.

How might β-arrestin-2 modulate insulin sensitivity? In an extensive series of experiments, Luan et al. first showed that while signaling to PI3 kinase was normal in livers from the *β-arrestin-2* −/− mice, the next step in the cascade, Akt activation, was impaired. Luan et al. showed that β-arrestin-2 acts as a scaffold for the insulin-dependent assembly of an insulin receptor/c-Src/Akt complex leading to c-Src-mediated phosphorylation of Akt at Tyr315/Tyr326. Insulin-dependent Akt tyrosine phosphorylation was defective in *β-arrestin-2* −/− mice, concomitant with reduced phosphorylation of Akt at Thr308 and Ser473, the two sites that are essential for full Akt activation. The converse was observed in *β-arrestin-2* overexpressing mice. Thus, Luan et al. suggest that, in addition to the IRS-1/PI3K pathway, a second pathway downstream of the insulin receptor is required for full Akt activation (see Figure 1B). A disruption in the formation of this complex, due to reduced *β-arrestin-2* expression, leads to impaired Akt activation followed by insulin resistance. This is potentially very exciting in view of the major role that Akt plays in numerous biological processes. However, some aspects of the study by Luan et al. seem to require clarification. The first involves the role of tyrosine phosphorylation in Akt activation and the second involves the link between β-arrestin-2 mediated Akt regulation and whole-body insulin resistance, which are discussed below.

With regard to tyrosine phosphorylation of Akt, the conventional view is that full activation of Akt in response to insulin is mediated via phosphorylation at Thr308 and Ser473 by PDK1 and PDK2 (see Figure 1A). However, several studies have shown that Akt is also phosphorylated at Tyr315, Tyr326, and Tyr474 and that this also plays a key role in kinase activation (Chen et al., 2001; Conus et al., 2002). However, in these studies, there was no evidence that Akt tyrosine phosphorylation regulated PDK-mediated phosphorylation of Akt at Thr308 and Ser473. Rather, inhibition of Akt tyrosine phosphorylation impaired Akt activity independently of PDK function via an ill-defined mechanism (Chen et al., 2001; Conus et al., 2002). In contrast to these studies, Luan et al. show that tyrosine phosphorylation of Akt at Tyr315/326 plays a major role in regulating Thr308/Ser473 phosphorylation (see Figure 1B). In *β-arrestin-2* −/− mice and under other conditions where c-Src function was inhibited, they observed almost complete inhibition of insulin-dependent phosphorylation of Akt at both Thr308 and Ser473, whereas the converse was found in *β-arrestin-2*-overexpressing animals. Thus, while the studies of Luan et al. provide a more plausible mechanism as to how Akt tyrosine phosphorylation might regulate kinase activity, the discrepancy

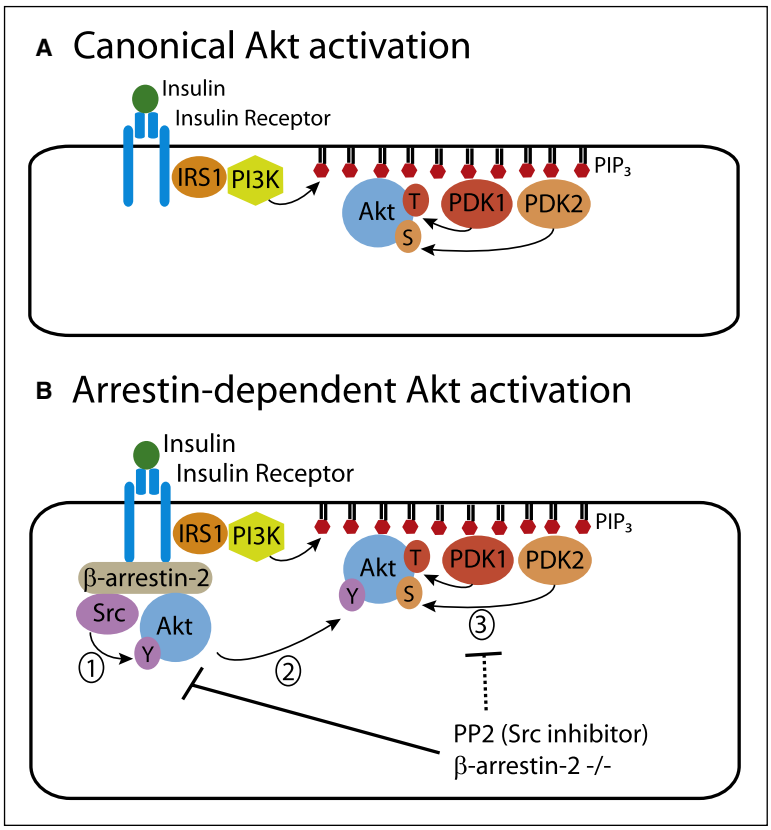

Figure 1. Models of Akt Activation

(A) The conventional model for regulation of Akt by insulin involves tyrosine phosphorylation of IRS1, which recruits PI3K to the plasma membrane, where it generates PIP_3. PIP_3 acts as a docking site for PDKs and Akt leading to the phosphorylation of Akt on Thr308 and Ser473, concomitant with its activation.

(B) Luan et al. propose a two-step model for Akt activation whereby insulin triggers the assembly of a tetrameric complex comprising insulin receptor, β-arrestin-2, c-Src, and Akt. This allows c-Src to phosphorylate Akt on Tyr315 and Tyr326 (step 1), and this step is somehow required (step 2) for phosphorylation of Akt at Thr308 and Ser473 (step 3) and its full activation. Luan et al. showed that impairment of c-Src function using PP2 or deletion of β-arrestin-2 inhibited tyrosine phosphorylation of Akt and its activation.

with previous studies needs to be resolved. These studies also need to be interpreted in light of observations that selective targeting of Akt to the plasma membrane in the absence of any stimulus that would likely activate c-Src kinase, results in robust phosphorylation of Akt at Thr308/Ser473 and kinase activity (Ng et al., 2008).

The demonstration of an insulin-regulated complex involving the insulin receptor, c-Src, Akt, and β-arrestin-2 is extremely exciting and has important implications for our understanding of insulin action. While the physiological data in animal models and the signaling data were compelling in the Luan et al. study, the linkage between these observations is still not completely clear. For example, despite having normal food intake, β-*arrestin-2* −/− mice had increased body weight on a high-fat diet while β-*arrestin-2*-overexpressing animals had reduced body weight. Assuming that these changes were accounted for by adiposity (these data were not reported), one plausible explanation is that the difference in insulin sensitivity in these animals is a simple consequence of altered body weight per se rather than a direct consequence of altered insulin signaling in muscle and liver as a function of modified β-*arrestin-2* expression. Interestingly, previous studies have shown that β-*arrestin-2* −/− mice are hypoactive (Bohn et al., 2003) with defective temperature control (Bohn et al., 1999). Both these traits likely contribute to increased body weight, particularly if they are exacerbated upon high-fat feeding. Because fat accumulation leads to insulin resistance, more work is required to justify the link between β-arrestin-2-mediated tyrosine phosphorylation of Akt and whole-body insulin action. Simultaneous analysis of insulin signaling and insulin action in isolated muscle and primary hepatocytes from wild-type and β-*arrestin-2* −/− mice would clarify matters, as well as more extensive studies of activity and thermogenesis in both chow and fat-fed animals. Despite the lack of firm evidence linking these parameters, the identification of a second insulin-regulated pathway involving Akt tyrosine phosphorylation is potentially very important, but as is often the case with challenging new ideas, more work will be required to both confirm and conquer its mechanistic architecture.

REFERENCES

Bohn, L.M., Gainetdinov, R.R., Sotnikova, T.D., Medvedev, I.O., Lefkowitz, R.J., Dykstra, L.A., and Caron, M.G. (2003). J. Neurosci. *23*, 10265–10273.

Bohn, L.M., Lefkowitz, R.J., Gainetdinov, R.R., Peppel, K., Caron, M.G., and Lin, F.T. (1999). Science *286*, 2495–2498.

Chen, R., Kim, O., Yang, J., Sato, K., Eisenmann, K.M., McCarthy, J., Chen, H., and Qiu, Y. (2001). J. Biol. Chem. *276*, 31858–31862.

Conus, N.M., Hannan, K.M., Cristiano, B.E., Hemmings, B.A., and Pearson, R.B. (2002). J. Biol. Chem. *277*, 38021–38028.

DeWire, S.M., Ahn, S., Lefkowitz, R.J., and Shenoy, S.K. (2007). Annu. Rev. Physiol. *69*, 483–510.

Hoehn, K.L., Hohnen-Behrens, C., Cederberg, A., Wu, L.E., Turner, N., Yuasa, T., Ebina, Y., and James, D.E. (2008). Cell Metab. *7*, 421–433.

Hupfeld, C.J., and Olefsky, J.M. (2007). Annu. Rev. Physiol. *69*, 561–577.

Kim, Y.B., Nikoulina, S.E., Ciaraldi, T.P., Henry, R.R., and Kahn, B.B. (1999). J. Clin. Invest. *104*, 733–741.

Luan, B., Zhao, J., Wu, H., Duan, B., Shu, G., Wang, X., Li, D., Jia, W., Kang, J., and Pei, G. (2009). Nature. Published online January 4, 2009. 10.1038/nature07617.

Ng, Y., Ramm, G., Lopez, J.A., and James, D.E. (2008). Cell Metab. *7*, 348–356.

Taniguchi, C.M., Emanuelli, B., and Kahn, C.R. (2006). Nat. Rev. Mol. Cell Biol. *7*, 85–96.

A Sweet Path to Insulin Resistance Through PGC-1β

Carlos Hernandez[1] and Jiandie D. Lin[1,*]
[1]Life Sciences Institute and Department of Cell & Developmental Biology, University of Michigan Medical Center, Ann Arbor, MI 48109, USA
*Correspondence: jdlin@umich.edu
DOI 10.1016/j.cmet.2009.02.001

Fructose is a highly lipogenic dietary nutrient that has been implicated in the pathogenesis of hyperlipidemia and insulin resistance. In this issue, Nagai et al. (2009) provide in vivo evidence that pinpoints transcriptional coactivator PGC-1β as a key factor in mediating the metabolic response to fructose intake.

The consumption of the Westernized diet is a major factor that contributes to the global epidemic of the metabolic syndrome and type 2 diabetes. Dietary intake of fructose, which is commonly derived from sweeteners based on sucrose or high-fructose corn syrup, was estimated to increase by 20%–40% over the last three decades (Havel, 2005). Numerous studies in humans and animal models have implicated fructose in the pathogenesis of insulin resistance and dyslipidemia, in particular hypertriglyceridemia (Havel, 2005; Rutledge and Adeli, 2007). Fructose is absorbed by enterocytes through GLUT5, a fructose-specific hexose transporter, and reaches the liver through the portal circulation. Compared to glucose, fructose is more potent in the stimulation of de novo hepatic lipogenesis and VLDL secretion (Hellerstein et al., 1996), which subsequently impact on systemic energy metabolism and insulin sensitivity. The exact molecular pathway that mediates the effects of fructose on hepatic lipogenesis and insulin resistance remains unclear. A new study in this issue (Nagai et al. 2009) revealed the transcriptional coactivator PPARγ coactivator-1β (PGC-1β) as a missing link between fructose intake and metabolic disorders.

The lipogenic activity of fructose is achieved through its effects on the metabolic flux as well as the induction of a genetic program that supports lipogenesis. In the liver, fructose enters the glycolytic pathway downstream of phosphofructokinase, a rate-limiting enzyme in glycolysis, and generates carbons for the synthesis of fatty acids and triglycerides. As a result, high levels of fructose intake provide an essentially unregulated source of acetyl-CoA for hepatic lipogenesis. On the other hand, fructose intake also activates the expression of lipogenic genes (Nagai et al., 2002), which involves the induction of sterol regulatory element binding proteins (SREBP), particularly SREBP1c, a major transcriptional regulator of lipogenic gene expression (Horton et al., 2002).

The PGC-1 family of transcriptional coactivators regulates glucose, lipid, and mitochondrial oxidative metabolism in response to nutritional and hormonal signals (Finck and Kelly, 2006; Lin et al., 2005a). These coactivators physically interact with selective transcription factors as well as cofactors and induce the transcription of target genes through remodeling of local chromatin structure. A case in point is PGC-1β, which coordinates hepatic lipogenesis and lipoprotein metabolism through coactivating several transcription factors, including SREBPs, the liver X receptor (LXR), and forkhead transcription factor Foxa2 (Lin et al., 2005b; Wolfrum and Stoffel, 2006). The expression of PGC-1β in the liver is induced in response to dietary saturated fats. Further, adenoviral-mediated expression of PGC-1β in the liver induces triglyceride synthesis and VLDL secretion, leading to hypertriglyceridemia in transduced rats. These effects of PGC-1β on lipid metabolism are reminiscent of the metabolic consequences of high-fructose feeding. Using an antisense oligonucleotide (ASO) strategy, Nagai et al. (2009) established an important role for PGC-1β in the pathogenesis of fructose-induced insulin resistance.

ASO treatments appear to achieve efficient knockdown of endogenous PGC-1β expression in the liver and white adipose tissue, but not in soleus and brown adipose tissue. A partial deficiency of PGC-1β in these lipogenic tissues makes it possible to assess the role of this coactivator in mediating fructose-induced lipogenesis and insulin resistance. As expected, feeding rats with a high-fructose diet leads to hypertriglyceridemia, increased epididymal fat mass, as well as significant hepatic steatosis, all of which are characteristics of enhanced lipogenesis. This dysregulation of lipid homeostasis is accompanied by insulin resistance, as evidenced by reduced whole-body glucose metabolism and elevated hepatic glucose production. PGC-1β ASO treatments result in significant improvement of metabolic profile, effectively sparing the treatment group from the deleterious effects of high-fructose feeding. Previous studies have demonstrated that PGC-1β is an important regulator of hepatic lipogenesis and VLDL secretion in response to short-term high-fat feeding (Lin et al., 2005b). While PGC-1β ASO appears to also decrease fasting plasma glucose and insulin levels in the context of high-fat feeding, it has modest effects on hepatic glucose production and whole-body glucose utilization. These findings place PGC-1β at a unique regulatory point that is apparently required for mediating the adverse metabolic effects of dietary fructose, but not dietary fats.

Parallel to the improvement of metabolic parameters, PGC-1β ASO suppresses the lipogenic response to high-fructose feeding in the liver. The induction of SREBP1a, SREBP1c, and fatty acid synthase by fructose is attenuated in rats receiving PGC-1β ASO treatments. Since LXR and SREBP1 regulate the transcription of SREBP1c itself, Nagai et al. used chromatin immunoprecipitation (chIP) to demonstrate that the occupancy of these two transcription factors on the SREBP1c promoter is reduced when PGC-1β is knocked down. It is likely that PGC-1β knockdown reduces the transcriptional activity of LXR and SREBP1, resulting in repressive chromatin

environment on the SREBP1c promoter and decreased recruitment of these factors to their respective binding sites. Additional chIP experiments using antibodies against PGC-1β and various histone marks should provide further insights into this pathway. The findings are somewhat paradoxical as PGC-1β does not appear to directly regulate the expression of SREBP1c in previous gain-of-function studies (Lin et al., 2005b). This dilemma raises the possibility that the inhibition of SREBP1 expression by PGC-1β ASO could be secondary to altered hormonal milieu, particularly insulin, which is a potent activator of SREBP1c gene expression.

It is remarkable that PGC-1β ASO drastically enhances glucose uptake by white adipose tissue when the rats were fed a fructose-rich diet. This appears to be an important contributor to the improvement in whole-body glucose utilization. Interestingly, the total levels as well as the membrane pool of GLUT4 protein are significantly elevated in the white fat following PGC-1β ASO treatments. While the exact molecular mechanisms are currently unknown, these surprising findings could potentially reveal a novel link between PGC-1β and the regulation of GLUT4 protein turnover and/or translation.

An unresolved issue is how PGC-1β interacts with dietary fructose to bring about the desirable responses. In this regard, PGC-1β knockdown apparently causes hepatic insulin resistance in the rats fed a regular chow. A plausible explanation for these findings is that PGC-1β ASO impairs mitochondrial function in the liver, in particular the expression of genes involved in fatty acid β-oxidation, and causes hepatic insulin resistance. However, similar decreases were also observed in PGC-1β ASO-treated rats fed a high-fructose diet. This discrepancy raises an intriguing possibility that PGC-1β may serve as a nodal point that modulates the interaction between dietary nutrients and the metabolic regulatory programs. The findings by Nagai et al. support the emerging role of gene/environment interaction in modulating the metabolic phenotype and disease pathogenesis. Thus, perturbations of the same regulatory motif may produce vastly different metabolic responses, depending on the specific combinations of dietary nutrients.

REFERENCES

Finck, B.N., and Kelly, D.P. (2006). J. Clin. Invest. *116*, 615–622.

Havel, P.J. (2005). Nutr. Rev. *63*, 133–157.

Hellerstein, M.K., Schwarz, J.M., and Neese, R.A. (1996). Annu. Rev. Nutr. *16*, 523–557.

Horton, J.D., Goldstein, J.L., and Brown, M.S. (2002). J. Clin. Invest. *109*, 1125–1131.

Lin, J., Handschin, C., and Spiegelman, B.M. (2005a). Cell Metab. *1*, 361–370.

Lin, J., Yang, R., Tarr, P.T., Wu, P.H., Handschin, C., Li, S., Yang, W., Pei, L., Uldry, M., Tontonoz, P., et al. (2005b). Cell *120*, 261–273.

Nagai, Y., Nishio, Y., Nakamura, T., Maegawa, H., Kikkawa, R., and Kashiwagi, A. (2002). Am. J. Physiol. Endocrinol. Metab. *282*, E1180–E1190.

Nagai, Y., Yonemitsu, S., Erion, D.M., Iwasaki, T., Stark, R., Weismann, D., Dong, J., Zhang, D., Jurczak, M.J., Löffler, M.G., et al. (2009). Cell Metab. *9*, this issue, 252–264.

Rutledge, A.C., and Adeli, K. (2007). Nutr. Rev. *65*, S13–S23.

Wolfrum, C., and Stoffel, M. (2006). Cell Metab. *3*, 99–110.

Cell Metabolism
Article

Interaction of the Hereditary Hemochromatosis Protein HFE with Transferrin Receptor 2 Is Required for Transferrin-Induced Hepcidin Expression

Junwei Gao,[1] Juxing Chen,[1] Maxwell Kramer,[1] Hidekazu Tsukamoto,[2,3] An-Sheng Zhang,[1] and Caroline A. Enns[1,*]
[1]Department of Cell and Developmental Biology, Oregon Health & Science University, Portland, OR 97239, USA
[2]Department of Pathology, Keck School of Medicine of the University of Southern California, Los Angeles, CA 90033, USA
[3]Department of Veteran Affairs, Greater Los Angeles Healthcare System, Los Angeles, CA 90073, USA
*Correspondence: ennsca@ohsu.edu
DOI 10.1016/j.cmet.2009.01.010

SUMMARY

The mechanisms that allow the body to sense iron levels in order to maintain iron homeostasis are unknown. Patients with the most common form of hereditary iron overload have mutations in the hereditary hemochromatosis protein HFE. They have lower levels of hepcidin than unaffected individuals. Hepcidin, a hepatic peptide hormone, negatively regulates iron efflux from the intestines into the blood. We report two hepatic cell lines, WIF-B cells and HepG2 cells transfected with HFE, where hepcidin expression responded to iron-loaded transferrin. The response was abolished when endogenous transferrin receptor 2 (TfR2) was suppressed or in primary hepatocytes lacking either functional TfR2 or HFE. Furthermore, transferrin-treated HepG2 cells transfected with HFE chimeras containing only the α3 and cytoplasmic domains could upregulate hepcidin expression. Since the HFE α3 domain interacts with TfR2, these results supported our finding that TfR2/HFE complex is required for transcriptional regulation of hepcidin by holo-Tf.

INTRODUCTION

Iron is essential for fundamental metabolic processes in cells and organisms. It is also toxic when in excess. Hereditary hemochromatosis (HH) is a heterogeneous group of iron overload disorders caused by mutations in a variety of proteins involved in iron homeostasis, including HFE (Feder et al., 1996), hemojuvelin (HJV) (Papanikolaou et al., 2004), hepcidin (Roetto et al., 2003), transferrin receptor 2 (TfR2) (Camaschella et al., 2000), or ferroportin (Fpn) (Montosi et al., 2001). HH manifests as increased intestinal iron absorption and liver iron overload (Vujic Spasic et al., 2008). If untreated, HH patients develop hepatic cirrhosis and hepatocellular carcinoma, cardiomyopathy and arrhythmias, diabetes, arthritis, and hypogonadotropic hypogonadism (Ajioka and Kushner, 2002; Bothwell and MacPhail, 1998).

The most common form of HH is caused by single base pair mutation in *HFE* resulting in a C260Y substitution (Feder et al., 1996). In this manuscript, we have followed the numbering system of HFE, which starts at the first amino acid after signal peptide cleavage (−22-1) (Lebron et al., 1998) and corresponds to previous numbering systems used in major histocompatibility complex class I protein (MHC1)-like molecules. *HFE* encodes an atypical MHC1. Like the MHC1 proteins, HFE is a membrane protein that consists of a signal sequence, α1–α3 domains followed by a transmembrane domain, and a short cytoplasmic domain. It also forms a heterodimeric complex with β2-microglobulin (Lebron et al., 1998). The C260Y mutation disrupts a disulfide bond in the α3 domain, leading to misfolding of HFE, lack of association with β2-microglobulin, and failure to traffic to the cell surface (Feder et al., 1997). The generation of a knockout mouse ($Hfe^{-/-}$), coupled to the finding that the C260Y substitution and the $Hfe^{-/-}$ phenotypes are similar, confirms that C260Y has a loss-of-function phenotype (Muckenthaler et al., 2004). Although the importance of HFE in iron regulation is apparent in HH patients and mouse models (Levy et al., 1999; Zhou et al., 1998), the underlying mechanism by which HFE regulates iron metabolism remains undiscovered.

Disease-causing mutations in *HFE* result in decreased hepcidin production both in HH patients and in $Hfe^{-/-}$ mice when compared to similarly iron-loaded individuals with unmutated *HFE* (Ahmad et al., 2002; Bridle et al., 2003; Muckenthaler et al., 2003; Nicolas et al., 2003). Hepcidin is a peptide hormone produced predominantly by the liver. It plays a major role in the regulation of iron homeostasis within the body by modulating iron levels through binding to and triggering the internalization and degradation of the iron exporter Fpn (Nemeth et al., 2004). Thus, hepcidin controls iron loading of Tf by negatively regulating iron efflux from enterocytes, liver macrophages, and hepatocytes into the blood.

Hepcidin production is modulated by many factors, including iron levels within the body. In response to iron loading in animal studies, hepcidin expression increases to prevent the further uptake of iron. Conversely, during iron deficiency, hepcidin expression decreases (Pigeon et al., 2001; Weinstein et al., 2002). In the liver, both hepcidin and HFE are predominantly expressed in hepatocytes (Holmstrom et al., 2003; Zhang et al., 2004). Hepatocyte-specific expression of *HFE* in $Hfe^{-/-}$ mice restores normal iron homeostasis, indicating that hepatocyte-specific expression of *HFE* is sufficient to control iron homeostasis (Vujic Spasic et al., 2008). Thus, HFE appears to function upstream of hepcidin expression to regulate iron homeostasis.

HFE has several binding partners that could participate in iron homeostasis. HFE associates with transferrin receptor 1 (TfR1) (Feder et al., 1998; Waheed et al., 1999) through its α1 and

α2 domains (Bennett et al., 2000) and with TfR2 through its α3 domain (Chen et al., 2007). The binding sites on TfR1 for HFE and iron-loaded transferrin (holo-Tf) overlap (Giannetti et al., 2003; Lebron and Bjorkman, 1999; West et al., 2001), confirming the competition between HFE and holo-Tf for binding to TfR1. More recent coimmunoprecipitation studies demonstrate that HFE also interacts with TfR2 (Chen et al., 2007; Goswami and Andrews, 2006). TfR2 is expressed predominantly in hepatocytes and is closely related to TfR1 in sequence and in its ability to bind holo-Tf but not iron-depleted Tf (apo-Tf) (Kawabata et al., 1999). Unlike TfR1, holo-Tf does not compete with HFE for binding to TfR2 (Chen et al., 2007).

Similar to *HFE*, disease-causing mutations in *TfR2* also result in decreased hepcidin levels (Wallace et al., 2007). TfR2 is hypothesized to act as a sensor for iron levels in the body because of its largely hepatocyte-specific expression and its ability to bind holo-Tf (Kawabata et al., 1999). The main limitation in determining how HFE and TfR2 regulate hepcidin expression to date has been the lack of a cell line in which the hepcidin expression is responsive to holo-Tf.

In the present study, we found that WIF-B cells, a rat hepatoma/human fibroblast hybrid, increased the expression of hepcidin in response to holo-Tf. HFE and TfR2 mRNA levels were higher in WIF-B cells compared to HepG2 cells, a human hepatoma cell line whose expression of hepcidin is not sensitive to holo-Tf. We used the HepG2/tetracycline-controlled transactivator protein (tTA) cells that express HFE under the tight control of tetracycline-inducible promoter and showed that hepcidin levels increase when cells expressing HFE are treated with holo-Tf. The involvement of HFE and TfR2 in this process was investigated using TfR2 siRNA, primary hepatocytes, and HFE chimeras. Our results show that Tf-induced hepcidin expression was dependent on the interaction of TfR2 with HFE.

RESULTS

Holo-Tf Induces Hepcidin Expression in WIF-B Cells

The positive correlation between hepcidin levels and holo-Tf in the blood leads to the hypothesis that the liver senses the level of iron in the body by sensing the amount of holo-Tf. We examined a number of hepatic cell lines for their ability to upregulate hepcidin in response to holo-Tf and found that WIF-B cells met the criterion. WIF-B cells are a rat hepatoma/human fibroblast hybrid with many functional and morphological similarities to hepatocytes (Ihrke et al., 1993). Even though they are rat/human hybrids, others have found that they express predominantly rat genes (Braiterman et al., 2008; Konieczko et al., 1998; Nies et al., 1998), and we could not detect human TfR1, TfR2, or HFE by immunoblot (M.K., unpublished data). Primers to rat hepcidin were used to determine levels of the hepcidin transcript. When treated with 25 μM holo-Tf for 24 hr, WIF-B cells expressed ~2.5-fold higher hepcidin mRNA, as determined by quantitative real-time reverse transcriptase-PCR (qRT-PCR), compared to untreated cells or cells treated with apo-Tf (Figure 1A). In contrast, HepG2 cells, a human hepatoma cell line, do not upregulate hepcidin in response to Tf (Gehrke et al., 2003). Thus WIF-B cells mimic the regulation of hepcidin levels by holo-Tf that is seen in hepatocytes in vivo.

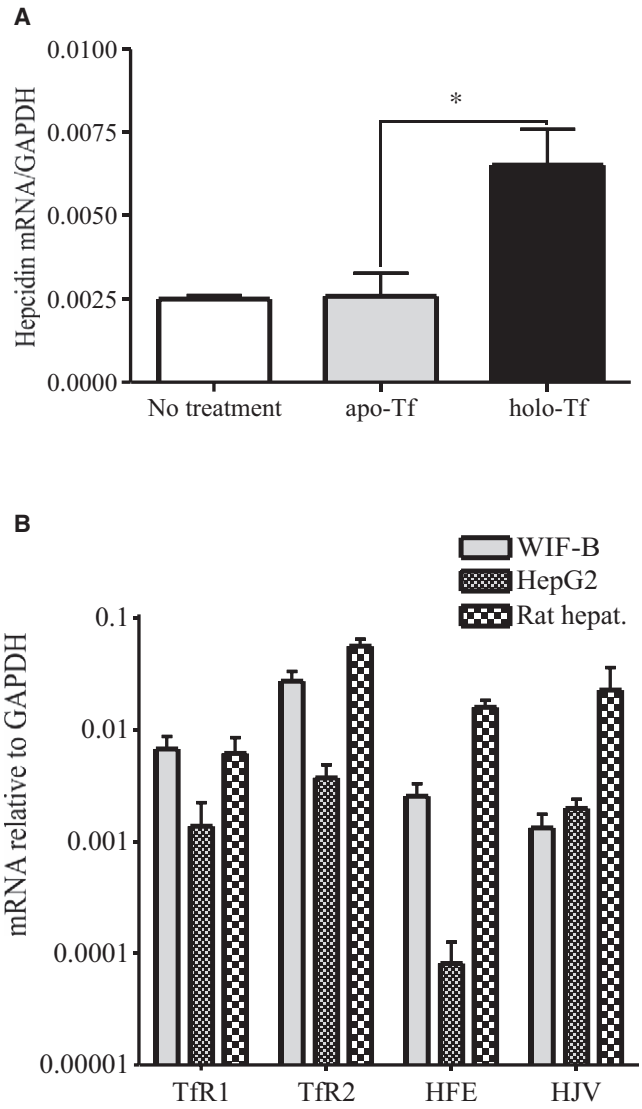

Figure 1. Hepcidin Expression in WIF-B Cells Responds to Holo-Tf

(A) Holo-Tf induces hepcidin expression in WIF-B cells. WIF-B cells were left untreated or incubated with 25 μM human apo-Tf or holo-Tf for 24 hr prior to RNA isolation. The hepcidin mRNA level was measured by qRT-PCR and normalized to GAPDH.

(B) Comparison of HFE, TfR1, TfR2, and HJV mRNA levels in WIF-B cells, HepG2 cells, and rat hepatocytes. Levels of TfR1, TfR2, HFE, and HJV mRNA, iron-related genes upstream of hepcidin, were measured by qRT-PCR. All samples were run in triplicate in three independent experiments. Data are shown as average ± SD. P values < 0.05, calculated by Student's t test, are indicated by *.

We compared the mRNA levels of the key iron-related genes in WIF-B cells, HepG2 cells, and isolated rat hepatocytes in order to determine the reason for the differences in hepcidin response to holo-Tf between the two cell lines. While the TfR1 and TfR2 levels in WIF-B cells were comparable to those of freshly isolated rat hepatocytes, HFE and HJV levels were ~6- to 10-fold less in WIF-B cells. Interestingly, the mRNA level of HFE in WIF-B cells was about 32-fold higher than in HepG2 cells. Among other genes involved in iron homeostasis in the body, TfR2 mRNA level

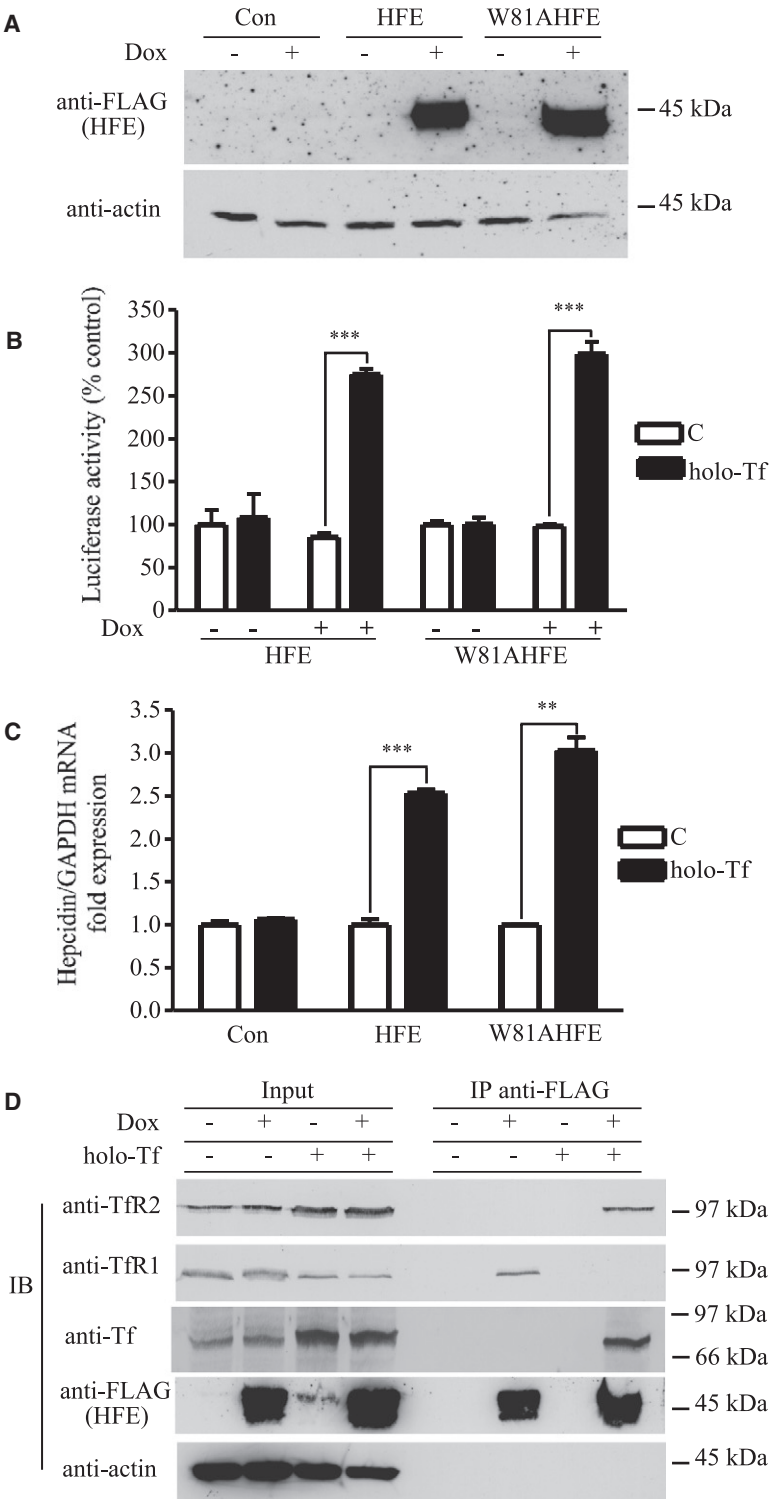

Figure 2. Tf-Induced Dissociation of HFE from TfR1 Results in the Association of HFE with TfR2 and Stimulates Hepcidin Promoter Activity

(A) Inducible expression of wild-type or W81A mutant HFE in HepG2/tTA HFE and HepG2/tTA W81AHFE cells. Lysates (25 μg) of HepG2/tTA HFE or HepG2/tTA W8AHFE cells, uninduced (−dox) or induced (+dox) to express HFE or W81AHFE, were detected with anti-FLAG antibody.

(B) HFE is required for Tf to induce hepcidin promoter activity independently of interaction with TfR1. Cells were cotransfected with pLuc-link-HAMP and pCMV-β-gal, treated without (controls, indicated by the letter C) or with holo-Tf, and analyzed as described in Experimental Procedures. Results are expressed as average ± SD of three independent experiments performed in triplicate.

(C) Hepcidin mRNA expression in HepG2/tTA (Con), HepG2/tTA HFE (HFE), and HepG2/tTA W81AHFE (W81AHFE) cells treated without (indicated by the letter C) or with holo-Tf as described in Experimental Procedures. The expression of hepcidin was measured by qRT-PCR and normalized to GAPDH. The fold of increase in hepcidin mRNA in the dox-induced group was obtained by normalization to uninduced controls. All samples were run in triplicate in three independent experiments. Data are shown as average ± SD.

(D) Tf releases HFE from TfR1 to bind to TfR2 in HepG2 cells. Cell lysates (200 μg) from HepG2/tTA HFE treated with or without 25 μM holo-Tf were immunoprecipitated with rabbit anti-FLAG antibodies, and Protein A-Sepharose 4B. Proteins were detected on immunoblots using mouse anti-TfR2, -TfR1, -FLAG, and -actin and goat anti-Tf. The input lanes correspond to one-fifth of the material used for immunoprecipitation. These results were repeated once with similar results. P values < 0.001 are indicated by *** and < 0.01 by **. P values were calculated by Student's t test.

was 8-fold higher in WIF-B than HepG2, implicating TfR2 in the response. The HJV mRNA level was comparable in the two cell lines and lower than in isolated rat hepatocytes (Figure 1B). TfR1 levels were 5-fold higher in WIF-B cells than in HepG2 cells and isolated hepatocytes, also implicating TfR1 in signaling. Since the levels of HFE mRNA were substantially lower in HepG2 cells than in WIF-B and hepatocytes, we created a cell line, HepG2/tTA HFE, which was stably transfected with HFE under the control of the tetracycline-activated promoter.

HFE Contributes to Tf-Sensitive Induction of the Hepcidin Promoter Activity Independent of TfR1

HepG2/tTA HFE cells were induced to express HFE with doxycycline (dox), a tetracycline analog, to test the possible role of HFE in the regulation of hepcidin expression (Figure 2A). To observe the effect of holo-Tf and HFE on hepcidin transcription, HepG2/tTA HFE cells were transiently transfected with a luciferase reporter vector, pLuc-link-HAMP, containing human hepcidin promoter ~2 kb in length. Hepcidin promoter activity was measured using luciferase. Holo-Tf treatment of cells had no effect on the hepcidin promoter activity in HepG2 cells as measured by luciferase in the absence of *HFE* expression (Figure 2B). The lack of response is consistent with a previous study in HepG2 cells (Gehrke et al., 2003), which we confirmed. HFE expression alone did not increase hepcidin expression (Figure 2B). However, after the induction of HFE expression with dox, holo-Tf treatment of cells increased hepcidin promoter activity by ~2.7-fold. Similar results were obtained when hepcidin mRNA levels were measured by

qRT-PCR (Figure 2C). These results indicated that the changes in mRNA levels were the result of transcriptional activation.

The finding that HepG2/tTA HFE cells increased hepcidin transcription in response to holo-Tf only in the presence of HFE made this an ideal cell line to examine the binding partners of HFE necessary for the holo-Tf-induced hepcidin response. We stably transfected HepG2/tTA cells with W81AHFE to examine the role of the TfR1/HFE complex in the regulation of hepcidin expression. W81AHFE has 5000-fold lower affinity for TfR1 (Lebron and Bjorkman, 1999) and does not detectably coimmunoprecipitate with TfR1 (Zhang et al., 2003). This mutant form of HFE does bind to TfR2 (Chen et al., 2007). Thus, if the TfR1/HFE complex was necessary for signaling to increase hepcidin levels, this cell line would not increase hepcidin mRNA in response to Tf treatment. The HepG2/tTA W81AHFE cells expressed amounts of W81AHFE comparable to cells expressing HFE (Figure 2A) and showed similarly increased hepcidin transcription (Figure 2B) and increased hepcidin mRNA levels (Figure 2C) compared to cells expressing wild-type HFE. These results suggested that the interaction between HFE and TfR1 is not required for Tf-dependent induction of hepcidin expression in HepG2 cells.

To further investigate the binding partners of HFE in the presence of holo-Tf in HepG2 cells, HFE was immunoprecipitated and blots were probed for proteins that coprecipitated with HFE. TfR1 coimmunoprecipitated with HFE in the absence of added holo-Tf, but not in the presence of high physiological levels of holo-Tf consistent with the competition between Tf and HFE for binding to TfR1 (Figure 2D). Note that these cells synthesize Tf, but not enough holo-Tf to completely abrogate the HFE/TfR1 interaction. Prolonged treatment of cells with holo-Tf increased intracellular iron loading, which decreased TfR1, presumably through the destabilization of TfR1 mRNA by the IRE/IRP pathway (reviewed in De Domenico et al., 2008). TfR2 coimmunoprecipitated with HFE in presence of high physiological levels of holo-Tf (25 μM). Holo-Tf treatment of cells resulted in increased TfR2 levels (Figure 2D), consistent with previous reports that holo-Tf stabilizes TfR2 at the protein level (Johnson and Enns, 2004; Robb and Wessling-Resnick, 2004). The lack of detectable TfR2 that coprecipitated with HFE in the absence of added holo-Tf could reflect the lower endogenous levels of TfR2 in this cell line than seen in cell lines transfected with TfR2 (Chen et al., 2007; Johnson and Enns, 2004). The coprecipitation of Tf and TfR2 with HFE in the presence of higher holo-Tf concentrations indicated the possibility that they form a signaling complex to increase hepcidin expression.

TfR2 Is Necessary for the HFE-Mediated Tf Induction of Hepcidin Expression in HepG2 Cells

We investigated the role of TfR2 in the Tf-sensitive induction of hepcidin. HepG2/tTA HFE cells were cotransfected with TfR2 siRNA to decrease TfR2 levels and with pLuc-link-HAMP to measure hepcidin promoter activity. Immunoblot analysis of TfR2 showed that TfR2 was significantly reduced after transfection of cells with TfR2 siRNA (Figure 3A). The sensitivity of hepcidin transcription to the addition of holo-Tf, as measured by the luciferase reporter activity, was abolished by TfR2 siRNA but not by control siRNA (Figure 3B). These results, along with our other results, imply that both TfR2 and HFE are necessary for Tf-induced expression of hepcidin.

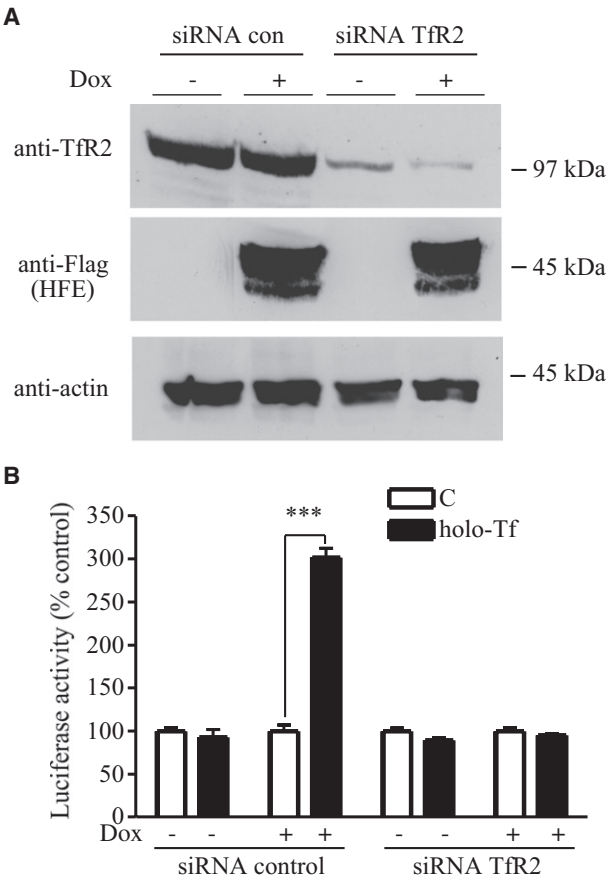

Figure 3. Knockdown of TfR2 Blocks Tf-Mediated Induction of Hepcidin Expression in HepG2/tTA HFE Cells

(A) Knockdown of endogenous TfR2 in HepG2/tTA HFE cells using specific siRNA to TfR2. Cells were transfected with control siRNA or TfR2 siRNA and cotransfected with pLuc-link-HAMP and pCMV-β-gal, as described in Experimental Procedures. To observe the efficiency of knockdown of TfR2, cell lysates (50 μg) from TfR2 siRNA- or control siRNA-transfected HepG2/tTA HFE cells were analyzed by immunoblot for TfR2, HFE, and actin expression. These results were representative of one out of three experiments. Human TfR2 siRNA significantly decreased endogenous TfR2 protein level in both HepG2/tTA control cells and HepG2/tTA HFE cells.

(B) Hepcidin promoter activity assay in HepG2/tTA HFE cells after knockdown of TfR2 and treatment without (indicated by the letter C) or with holo-Tf. Luciferase and β-galactosidase activity from cell lysates was measured as described in Experimental Procedures. Relative luciferase activity was obtained by normalization to β-galactosidase activity, and the fold increase in luciferase activity of each group was obtained by normalization to the control group without holo-Tf. Results are expressed as average ± SD of three independent experiments performed in triplicate. P values < 0.001, calculated by Student's t test, are indicated by ***.

HFE and TfR2 Are Both Necessary for the Tf-Mediated Induction of Hepcidin Expression in Mouse Primary Hepatocytes

In vitro cultures of primary hepatocytes from wild-type, *Hfe*$^{-/-}$, and *Tfr2*$^{245X/245X}$ mice were used to measure the hepcidin response of hepatocytes to holo-Tf treatment. The TfR2 (245X) mutation causes iron overload in mice, and the orthologous mutation, TfR2 (250X), causes HH in humans. *Hfe*$^{-/-}$ mice were on the 129/SvEvTac (129/S) background, and *Tfr2*$^{245X/245X}$

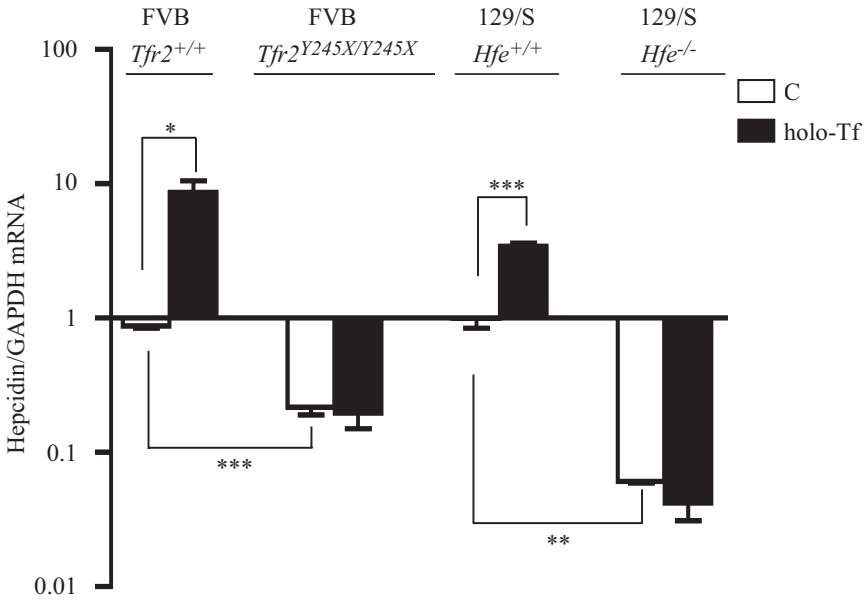

Figure 4. TfR2 and HFE Are Required for Tf-Mediated Induction of Hepcidin Expression in Mouse Primary Hepatocytes

Mouse primary hepatocytes were treated without (indicated by the letter C) or with holo-Tf, and qRT-PCR was performed on isolated RNA as described in Experimental Procedures. Average relative level of hepcidin was normalized to GAPDH. Results are expressed as average ± SD of two or four independent experiments performed in triplicate. P values < 0.05, < 0.01, and < 0.001, calculated by Student's t test, are indicated by *, **, and ***, respectively.

mice were on an FVB/NJ (FVB) background. Previous studies indicated that TfR2 (245X) binds HFE but not Tf in vitro (Chen et al., 2007; Goswami and Andrews, 2006). In the primary hepatocytes isolated from 129/S mice and FVB mice, we found that hepcidin mRNA levels increased by about 3.4- and 9.9-fold (Figure 4), respectively, in response to treatment with 25 μM holo-Tf. These differences between the ability to stimulate hepcidin expression in hepatocytes from the different strains of mice could be either strain dependent or due to the expression of the truncated TfR2. However, no significant changes of hepcidin mRNA levels were detected in the primary hepatocytes isolated from *Hfe*$^{-/-}$ or *Tfr2*$^{245X/245X}$ mice compared with their corresponding controls (Figure 4). These results strongly support the idea that both HFE and TfR2 are required for Tf-induced hepcidin expression and agree with the finding that HFE is necessary for Tf-induced hepcidin expression in HepG2 cells. Consistent with the reports that hepcidin levels are lower in *Hfe*$^{-/-}$ and in *Tfr2* mutant mice (Ahmad et al., 2002; Bridle et al., 2003; Muckenthaler et al., 2003; Nicolas et al., 2003; Wallace et al., 2007), the hepcidin mRNA levels in the isolated primary hepatocytes from *Hfe*$^{-/-}$ and *Tfr2*$^{245X/245X}$ mice were 16.5- and 4-fold lower than those in their corresponding wild-type counterparts (Figure 4). Thus, both TfR2 and HFE are necessary for the induction of hepcidin by holo-Tf.

The α3 Domain of HFE Is Insufficient for the Induction of Hepcidin Expression in HepG2 Cells in Response to Holo-Tf

To map the domains of HFE responsible for the Tf-induced upregulation of hepcidin, we took advantage of the findings that HFE binds to TfR2 through its α3 domain (Chen et al., 2007), whereas it binds to TfR1 via its α1α2 domains (Bennett et al., 2000), and that the structures of the HFE and the MHC1 molecules are similar (review in Wilson and Bjorkman, 1998). Two HFE-HLA-B7 chimeras were generated: α3(−), in which the HFE α3 domain was replaced with the HLA-B7 α3 domain, and α3(+), in which the α3 domain of HFE was substituted for the α3 domain of HLA-B7 (Figure 5A). These two constructs, along with HLA-B7, were transfected individually into HepG2/tTA cells under the control of the tetracycline-inducible system (Figure 5B). The abilities of HFE chimeras to coprecipitate TfR2 were detected by immunoblots (Figure 5C). The α3(−) chimera did not show detectable interaction with TfR2 (Figure 5C) but was able to interact with TfR1, indicating that lack of interaction with TfR2 was not due to misfolding of the chimera (Figure S1). TfR2 coprecipitated with both HFE and the chimera containing the HFE α3 domain (α3[+]) but not with the negative control HLA-B7 (Figure 5C). These results confirmed our previous observation that the α3 domain of HFE is critical for HFE binding to TfR2 (Chen et al., 2007). Surprisingly, α3(+) coprecipitated with TfR2, but it did not mediate the Tf-sensitive induction of the hepcidin promoter activity in the luciferase activity assay (Figure 5D). These results imply that α3 domain of HFE is required for binding to TfR2, but it is insufficient for regulation of hepcidin mRNA by Tf.

A Chimera Containing Both the HFE α3 Domain and Cytoplasmic Domains Is Sufficient to Mediate Tf Induction of Hepcidin Expression in HepG2 Cells

Since the chimera containing only the α3 domain of HFE was not sufficient to mediate the induction of hepcidin by Tf, we generated plasmids encoding chimeras where the domains of HFE and HLA-B7 were exchanged (Figure 6A) and stably transfected them into HepG2/tTA cell lines (Figure 6B). Only the chimeras containing both the α3 and cytoplasmic domains of HFE (α3tmcd and α3cd) were able to induce luciferase activity (Figure 6C). The α1α2 chimera interacted with TfR1, indicating that the lack of stimulation of luciferase activity is not due to misfolding of the chimera (Figure S1). Thus, the α3 and cd domains of HFE on the HLA-B7 backbone are necessary and sufficient to stimulate hepcidin transcription in response to treating cells with holo-Tf.

DISCUSSION

The liver plays a key role in the sensing of iron levels in the body and in the regulation of iron homeostasis. Hepatocytes within the liver express proteins critical to these processes, including HFE, TfR2, HJV, and Tf, as well as the peptide hormone hepcidin. Hepcidin, which negatively regulates iron efflux from cells into the blood, is controlled at the transcriptional level. Thus, when the

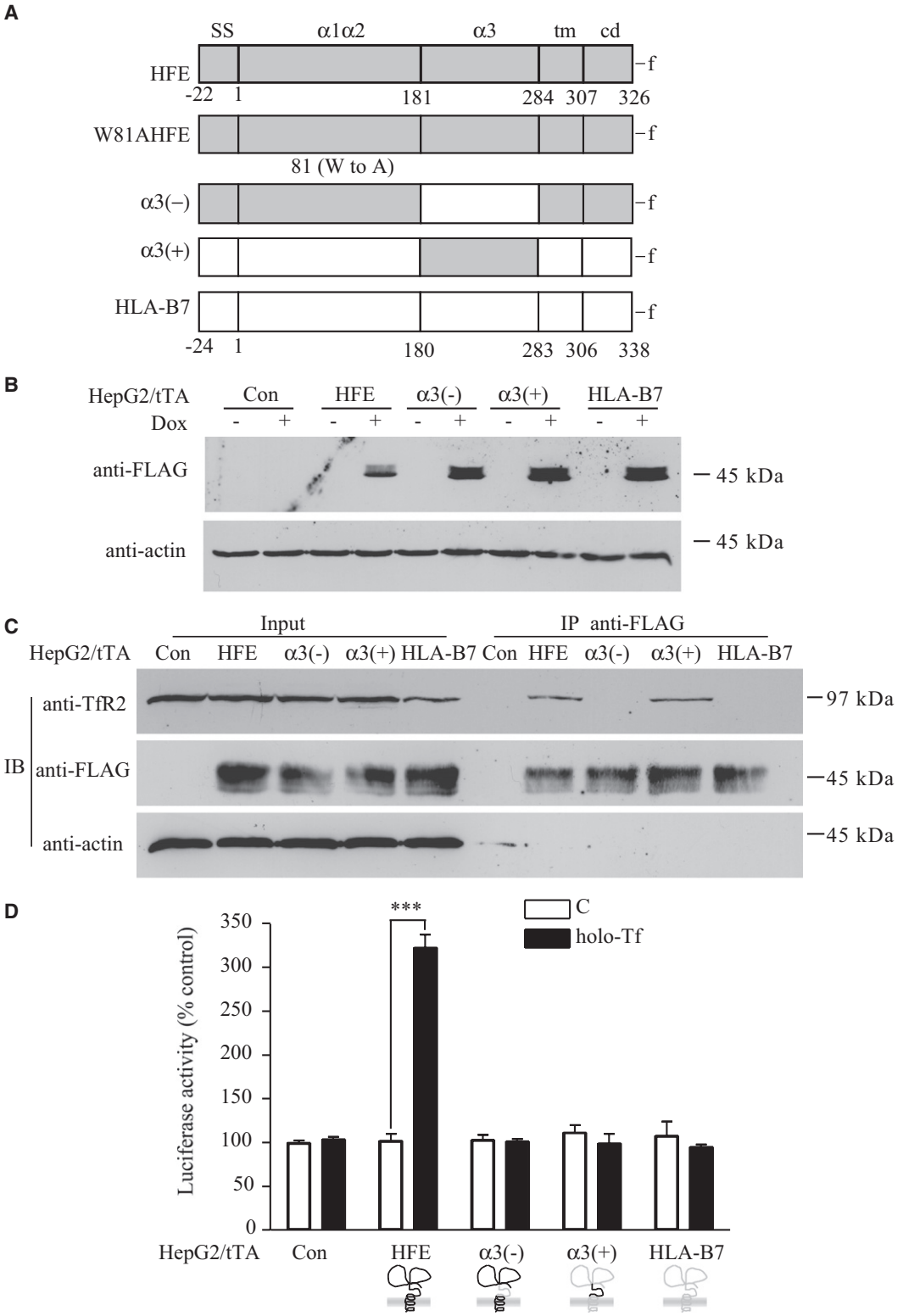

Figure 5. The α3 Domain Is Required but Insufficient for HFE-Mediated Tf Induction of Hepcidin Expression in HepG2 Cells

(A) Schematic representation of the HFE mutant and chimeras, including HFE, W81AHFE, α3(−), α3(+), and HLA-B7. HFE is shown in gray; HLA-B7 is shown in white. Numbers under diagrams for each full-length protein designate the first amino acid in the signal sequence (SS), α1α2 domain (α1α2), α3 domain (α3), transmembrane domain (tm), and cytoplasmic domain (cd). FLAG epitope tag (-f) was added to the C terminus of each protein. HFE-HLA-B7 chimeras were

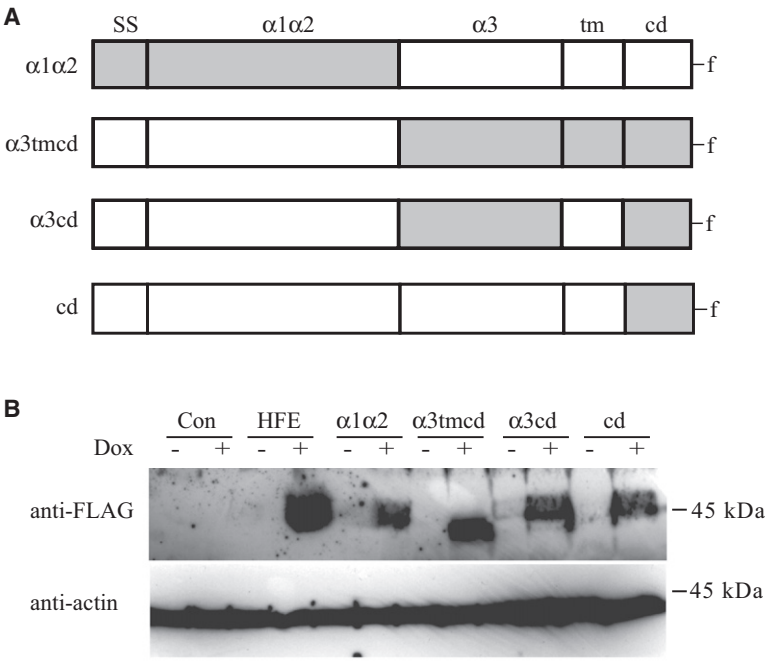

Figure 6. The α3 and Cytoplasmic Domains of HFE Mediate the Tf Induction of Hepcidin Expression in HepG2 Cells

(A) Schematic representation of the HFE chimeras, including α1α2, α3tmcd, α3cd, and cd constructs. HFE is shown in gray; HLA-B7 is shown in white. HFE chimeras were constructed by replacing the appropriate segments between the parent proteins. Individual recombinant proteins used throughout the study are referred to by the acronyms to the left of the construct cartoon.

(B) Generation of HFE-HLA-B7 chimeras. HFE chimeras, including stable cells lines HepG2/tTA α1α2, HepG2/tTA α3tmcd, HepG2/tTA α3cd, and HepG2/tTA cd, were generated as described in Experimental Procedures. Lysates (25 μg) of cells, uninduced (−dox) or induced (+dox), were used to screen the positive clones by immunoblot using anti-FLAG antibody.

(C) The α3 and cytoplasmic domains of HFE are required for HFE-mediated Tf induction of hepcidin expression in HepG2 cells. All HepG2/tTA control and HFE chimera cells were cotransfected with pLuc-link-HAMP and pCMV-β-gal, treated, and analyzed as described in Experimental Procedures. Results are expressed as average ± SD of three independent experiments performed in triplicate. P values < 0.001 are indicated by *** and < 0.01 by **. P values were calculated by Student's t test.

liver senses high iron levels, hepcidin expression increases to inhibit further iron uptake and results in iron sequestration in cells. In this study, we examined the roles of these key proteins in controlling hepcidin expression in cell lines that were engineered to mimic the increase in hepcidin in normal hepatocytes in response to treatment with a physiological concentration of holo-Tf. We found that the Tf/TfR2/HFE complex was necessary to increase hepcidin expression.

The Role of Tf in the Regulation of Hepcidin

The concentration of holo-Tf in blood has been proposed to be a regulator of hepcidin expression (Johnson and Enns, 2004; Robb and Wessling-Resnick, 2004). High holo-Tf levels correlate with increased hepcidin mRNA in the liver (Kawabata et al., 2005). The finding that hepcidin levels increase in freshly isolated mouse hepatocytes (Lin et al., 2007) in response to holo-Tf demonstrates that hepatocytes can respond directly.

Holo-Tf serves two functions in the regulation of hepcidin. First, it alters the interactions between HFE and TfR1. A recent study examined the role of TfR1 in the control of hepcidin mRNA levels by generating mice that express a mutant TfR1 that does not bind detectably to HFE (Schmidt et al., 2008). A higher level of hepcidin mRNA was detected in the TfR1 mutant mice than in the strain-matched control mice. The authors propose that increased hepcidin

constructed by replacing the appropriate segments between the parent proteins. The first coding methionine in all proteins is labeled as number 1. We refer to individual recombinant proteins used throughout the study by acronyms to the left of the construct illustration.

(B) Induction of HFE chimeras by dox. Lysates (25 μg) of HepG2/tTA HFE, HepG2/tTA α3(−), HepG2/tTA α3(+), and HepG2/tTA HLA-B7 cells, uninduced (−dox) or induced (+dox) to express wtHFE, α3(−), α3(+), or HLA-B7, were detected using mouse anti-FLAG antibody.

(C) The α3 domain of HFE is critical for interaction with TfR2 in HepG2/tTA cells. Cells lysates (200 μg) were immunoprecipitated with rabbit anti-FLAG antibody, and the blots were probed with mouse antibodies to TfR2, FLAG, and actin. The input lanes correspond to one-fifth of the material used for immunoprecipitation. These results were repeated once with similar results.

(D) The α3 domain of HFE is required but insufficient for HFE-mediated Tf induction of hepcidin expression in HepG2 cells. Cells were cotransfected with pLuc-link-HAMP and pCMV-β-gal plasmids, treated without (indicated by the letter C) or with 25 μM holo-Tf (holo-Tf), and analyzed as described in Experimental Procedures. Results are expressed as average ± SD of three independent experiments performed in triplicate. P values < 0.001, calculated by Student's t test, are indicated by ***.

mRNA results from unbound HFE or from HFE binding to another partner. They speculate that the binding partner was TfR2 based on previous evidence showing that HFE is capable of binding to TfR2 (Chen et al., 2007; Goswami and Andrews, 2006). They also suggest that the TfR2/HFE complex is responsible for hepcidin regulation, and that TfR1 sequesters HFE from binding to TfR2 under low levels of holo-Tf. In our study, we showed that disruption of the HFE/TfR1 complex alone did not regulate hepcidin expression using transfected hepatoma cell lines. Upregulation of hepcidin mRNA was achieved only in the presence of holo-Tf and TfR2. In addition, we directly demonstrated that Tf/TfR2/HFE complex is involved in the upregulation of hepcidin. Thus, the Tf/TfR2/HFE complex is critical for increased hepcidin expression. How the complex signals to accomplish this remains to be determined.

The second way that Tf can modulate the HFE/TfR2 interactions is through the downregulation of TfR1 and the upregulation of TfR2. Thus, under high-iron conditions, increased saturation of Tf with iron results in an increased amount of Tf/TfR2/HFE complex, and together with the results from mice with mutated TfR1, these findings indicate that Tf binding to TfR1 releases HFE to form a complex with Tf and TfR2. This complex is responsible for increased hepcidin expression. This model predicts that HFE is limiting for complex formation. Future experiments will focus on testing this prediction.

The Necessity of HFE in the Tf-Mediated Sensitivity of Hepcidin

The changes in hepcidin mRNA in WIF-B and HepG2/tTAHFE cells are within physiological responses. They are similar to the 3- to 4-fold increase in hepcidin levels in mice fed high-iron diets, although there is variability in response between strains (Bondi et al., 2005) and our findings in primary hepatocytes. The requirement of HFE for increased hepcidin expression in response to Tf treatment is consistent with the lack of hepcidin response in *Hfe*$^{-/-}$ mice on a high-iron diet (Ahmad et al., 2002). Our results suggest that HFE is required for the Tf-induced hepcidin expression in hepatocytes and are in keeping with the recent finding that hepatocyte-specific expression of HFE increases hepcidin levels in mice (Schmidt et al., 2008; Vujic Spasic et al., 2008). Since HFE affects other aspects of iron homeostasis independent of hepcidin (Gao et al., 2008), lack of HFE could also have other effects on iron metabolism in *Hfe*$^{-/-}$ mice.

The Role of TfR2 in the Upregulation of Hepcidin in Response to Tf

In addition to the role of HFE and Tf in the control of hepcidin mRNA, we also showed that TfR2, which binds to HFE in vitro, is required for Tf-dependent stimulation of hepcidin expression. Holo-Tf treatment of cells also increases TfR2 levels by stabilizing TfR2, thus also promoting the formation of the TfR2/HFE complex. Knockdown of TfR2 or lack of functional TfR2 results in loss of hepcidin sensitivity to Tf treatment. These results help to explain why *Tfr2*$^{-/-}$ mice have 3- to 4-fold lower basal hepcidin levels despite hepatic iron overload. They also explain the lack of hepcidin response to iron in the *Tfr2*$^{-/-}$ mice (Wallace et al., 2007) and why Tf failed to increase hepcidin expression in primary hepatocytes isolated from *Tfr2*$^{245X/245X}$ mice.

Mapping the Domains of HFE that Are Responsible for the Tf-Induced Upregulation of Hepcidin

To further investigate the involvement of TfR2/HFE complex in the Tf induction of hepcidin expression, HFE/HLA-B7 chimeras were used. Intriguingly, the HFE-HLA-B7 chimera containing only the HFE α3 domain bound to TfR2 but did not alter hepcidin expression in presence of holo-Tf. These results suggest that α3 domain of HFE is necessary but not sufficient for Tf-induced stimulation of hepcidin expression. Further domain mapping using HFE/HLA-B7 chimeras showed that both the α3 and cytoplasmic domains of HFE were required for HFE regulating hepcidin. The role of the cytoplasmic domain with respect to hepcidin regulation still remains to be clarified.

Hepcidin mRNA is transcriptionally regulated through at least three pathways. Interleukin 6 stimulates hepcidin expression through the STAT3 signaling pathway. Bone morphogenic proteins, BMPs, increase hepcidin expression through the HJV/BMP receptor/Smad 4 pathway. Tf stimulates hepcidin expression through a TfR2-/HFE-mediated pathway. The extent to which these pathways are interconnected is unknown. Mutations in HJV can cause juvenile hemochromatosis, a severe iron overload disease characterized by low hepcidin levels. Similarly, *Hjv*$^{-/-}$ mice have extremely low hepcidin levels, but the levels can be further decreased by phlebotomy (Krijt et al., 2007), implying that iron signaling can be independent of HJV, and that HJV participates in establishing a set point for BMP signaling and iron homeostasis. Whether the Tf control of hepcidin signaling is through any of these signaling pathways is still unresolved.

Taken together, our studies suggest that the Tf/TfR2/HFE complex is involved in the sensing of Tf saturation, which leads to the regulation of hepcidin expression. Based on these results, mutations in either HFE or TfR2 should result in a similar iron overload disease with respect to the regulation of hepcidin.

EXPERIMENTAL PROCEDURES

Hepcidin Promoter Construct

A fragment of the human hepcidin promoter consisting of the first 2043 nucleotides upstream of the translational start site was subcloned into the promoterless luciferase reporter vector pLuc-link as described previously (de Wet et al., 1987; Verga Falzacappa et al., 2008) and detailed in the Supplemental Data.

HFE Chimera Constructs

The plasmids containing HFE-α1α2/HLA-B7-α3 /HFE-tmcd (α3[−]), HLA-B7-α1α2/HFE-α3/HLA-B7-tm/HFE-cd (α3cd), and HLA-B7-α1α2α3tm/HFE-cd (cd) were constructed by overlapping PCR using the primers and templates listed in Table S1. The wild-type HFE, W81AHFE, HFE-α1α2/HLA-B7-α3tmcd (α1α2), HLA-B7-α1α2/HFE-α3tmcd (α3tmcd), HLA-B7-α1α2/HFE-α3/HLA-B7-tmcd (α3[+]), and wild-type HLA-B7 constructs were generated as previously described (Chen et al., 2007; Cherry et al., 2008). All constructs contain a C-terminal FLAG tag sequence for immunodetection. In all cases, the gel-purified PCR products were first inserted into the pGEM-T (Promega; Madison, WI), followed by subcloning into the pcDNA4 vector that had been modified by adding tetracycline-inducible promoter (Feng and Longmore, 2005). All of the sequences and orientations were verified.

Antibodies

Mouse anti-hTfR2 (9F8-1C11) monoclonal antibodies were described previously (Vogt et al., 2003). M2 anti-FLAG, H68.4 anti-TfR1, and anti-actin were purchased from Sigma-Aldrich (St. Louis, MO); Zymed Laboratories, Inc. (San Francisco, CA); and Sigma-Aldrich, respectively. Secondary antibodies

against rabbit and mouse IgG conjugated to horseradish peroxidase (HRP) were purchased from Chemicon (Temecula, CA).

Cell Culture and Transfection

WIF-B cells, obtained from Doctor Ann Hubbard (Johns Hopkins University), were grown in F-12 Coon's Modification with amphotericin, glutamax, penicillin/streptomycin supplemented with HAT, and 5% FCS and cultured in a humidified 7% CO_2 incubator at 37°C (Ihrke et al., 1993). Tetracycline-inducible HepG2 cells (HepG2/tTA) were obtained from Doctor Gregory D. Longmore (Washington University in St. Louis) and grown in DMEM containing 10% FBS, 2 mM L-glutamate, and 5 μg/ml blasticidin (Feng and Longmore, 2005). To generate HepG2/tTA cells stably expressing HFE chimeras, individual pcDNA4 constructs encoding the specified chimeric HFEs or HLA-B7 were introduced using Nucleofector Kit V (Amaxa Biosystems; Gaithersburg, MD). Stable cell clones were obtained under the selection with 1 mg/ml G418. Positive clones in the presence of doxycyline (dox) were screened using anti-FLAG antibody. We generated the following stable cell lines: HepG2/tTA HFE, HepG2/tTA W81AHFE, HepG2/tTA α3(−), HepG2/tTA α3(+), HepG2/tTA α1α2, HepG2/tTA α3tmcd, HepG2/tTA α3cd, HepG2/tTA cd, and HepG2/tTA HLA-B7 cells.

Isolation of Mouse Primary Hepatocyte Cells

Mouse primary hepatocytes were isolated as described in Supplemental Data.

Tf Treatment of Cells

WIF-B cells were seeded in 6-well plates and treated with 25 μM holo-Tf or apo-Tf (Athens Research and Technology; Athens, GA) for 24 hr prior to harvesting cells. HepG2/tTA cell lines were seeded in 6-well plates, and after 24 hr, the medium was replaced with FBS-free medium in the absence or presence of 25 μM human holo-Tf for 24 hr prior to harvest. To induce expression of HFE, HLA-B7, or the chimeras in HepG2/tTA cell lines, 200 ng/ml dox was added to the medium 24 hr before Tf treatment.

Immunoblot

Preparation of cell lysates is described in Supplemental Data. Immunoblot analysis was carried out using M2 anti-FLAG (1:10,000), mouse monoclonal anti-TfR2 (1:10,000, 9F8-1C11), H68.4 anti-TfR1 (1:5000), and mouse anti-actin (1:10,000) followed by anti-mouse secondary antibodies conjugated to HRP (1:10,000). Bands were detected by enhanced chemiluminescence (SuperSignal West Pico; Pierce; Rockford, IL).

Immunoprecipitation

Cell lysate (100 μg protein) was first precleared with Protein A-Sepharose 4B beads (Zymed; San Francisco, CA) for 1 hr at 4°C. The precleared lysates were rotated for 2 hr at 4°C with rabbit anti-FLAG antibody and Protein A-Sepharose 4B. Immunoprecipitated complexes were washed by centrifugation through 1% NET-Triton buffer containing 15% sucrose and eluted with 2 × Laemmli buffer (Laemmli, 1970). Immunodetection was performed as described above.

Knockdown of TfR2

Lipofectamine 2000 (Invitrogen; Carlsbad, CA) was used to cotransfect siRNA specific for human TfR2 (Dharmacon; Chicago, IL) or negative control siRNA and pLuc-link-HAMP as well as pCMV-β-gal plasmid following the manufacturer's instructions. Briefly, HepG2/tTA HFE cells in 28 cm^2 dishes were transfected with a mix of 10 μl of 20 μM TfR2 siRNA, 2 μg pLuc-link-HAMP, and 0.1 μg pCMV-β-gal plasmids using 10 μl Lipofectamine 2000 (Gao et al., 2008; Zhang et al., 2007). Control cells were incubated with the same amounts of control siRNA, pLuc-link-HAMP, and pCMV-β-gal plasmids using 10 μl Lipofectamine 2000. The concentration of siRNA (100 nM) had been optimized to maximally decrease TfR2 levels. One day after the transfection, cells were split into 12-well plates, and on the following day, cells were switched to the FBS-free medium and incubated with or without 25 μM holo-Tf for additional 24 hr prior to harvesting.

Quantitative Real-Time Reverse Transcriptase-PCR

Total RNA from HepG2 cells, WIF-B cells, rat hepatocytes, or mouse primary hepatocytes was isolated from cells using the RNeasy RNA isolation kit (QIAGEN; Valencia, CA) and treated with DNase (Roche Applied Science) to remove any contaminating genomic DNA. Rat hepatocytes (n = 3) were from normal male Wistar rats. Hepatocytes were isolated by the Cell Culture Core of the USC Research Center for Liver Diseases as previously described (Zhang et al., 2004). Oligo (dT) primers and Superscript II reverse transcriptase were used to synthesize cDNA according to manufacturer's instructions. Hepcidin, TfR1, TfR2, HFE, HJV, and GAPDH mRNA were measured using the rat or human primers listed in Table S2 and as previously described (Gao et al., 2008; Zhang et al., 2007). Results were expressed as the level relative to the corresponding GAPDH. All primers were verified for linearity of amplification.

Transient Transfections and Luciferase Assays

Control or transfected HepG2/tTA cells were seeded in 78 cm^2 dishes and cotransfected with pLuc-link-HAMP (5 μg) and pCMV-β-gal plasmids (0.25 μg) using Lipofectamine (50 μl). On the following day, the cells were split into 12 wells of a 12-well plate. They were treated with FBS-free medium ± 25 μM holo-Tf for 24 hr. Cells were lysed in NET-Triton buffer, followed by centrifugation at 16,000 *g* for 5 min at 4°C to remove cell debris. The luciferase activities of supernatants were measured and normalized to β-galactosidase activity as previously described (Kim et al., 1994; Martin et al., 1996) and normalized with the control (-Tf).

Statistical Analysis

Standard deviation (SD) and the paired and two-tailed Student's t tests were used to evaluate the statistical significance of qRT-PCR and luciferase assay data.

SUPPLEMENTAL DATA

Supplemental Data include Supplemental Experimental Procedures, two tables, and one figure and can be found online at http://www.cell.com/cellmetabolism/supplemental/S1550-4131(09)00035-7.

ACKNOWLEDGMENTS

We would like to thank Doctor Gregory D. Longmore for the gift of HepG2/tTA cells, Doctor Paul W. Howard for the pLuc-link vector, Doctor Nancy Andrews for the *Hfe*$^{-/-}$ mice, and Doctor Robert Fleming for the *Tfr2*$^{245X/245X}$ mice. We thank Doctor Maria Chloupkova for assistance in the perfusion of livers for primary hepatocyte cultures. We also thank Gary Reiness, Julia Maxson, Kristina Nicholson, and Maria Chloupkova for helpful suggestions on the manuscript. This work was supported by National Institutes of Health grant RO1-DK072166 (to C.A.E.) and Research Center for Alcoholic Liver and Pancreatic Diseases grant P50 AA011999 (to H.T.).

Received: November 8, 2008
Revised: December 29, 2008
Accepted: January 30, 2009
Published: March 3, 2009

REFERENCES

Ahmad, K.A., Ahmann, J.R., Migas, M.C., Waheed, A., Britton, R.S., Bacon, B.R., Sly, W.S., and Fleming, R.E. (2002). Decreased liver hepcidin expression in the Hfe knockout mouse. Blood Cells Mol. Dis. *29*, 361–366.

Ajioka, R.S., and Kushner, J.P. (2002). Hereditary hemochromatosis. Semin. Hematol. *39*, 235–241.

Bennett, M.J., Lebron, J.A., and Bjorkman, P.J. (2000). Crystal structure of the hereditary haemochromatosis protein HFE complexed with transferrin receptor. Nature *403*, 46–53.

Bondi, A., Valentino, P., Daraio, F., Porporato, P., Gramaglia, E., Carturan, S., Gottardi, E., Camaschella, C., and Roetto, A. (2005). Hepatic expression of hemochromatosis genes in two mouse strains after phlebotomy and iron overload. Haematologica *90*, 1161–1167.

Bothwell, T.H., and MacPhail, A.P. (1998). Hereditary hemochromatosis: etiologic, pathologic, and clinical aspects. Semin. Hematol. *35*, 55–71.

Braiterman, L.T., Heffernan, S., Nyasae, L., Johns, D., See, A.P., Yutzy, R., McNickle, A., Herman, M., Sharma, A., Naik, U.P., and Hubbard, A.L. (2008).

JAM-A is both essential and inhibitory to development of hepatic polarity in WIF-B cells. Am. J. Physiol. Gastrointest. Liver Physiol. *294*, G576–G588.

Bridle, K.R., Frazer, D.M., Wilkins, S.J., Dixon, J.L., Purdie, D.M., Crawford, D.H., Subramaniam, V.N., Powell, L.W., Anderson, G.J., and Ramm, G.A. (2003). Disrupted hepcidin regulation in HFE-associated haemochromatosis and the liver as a regulator of body iron homoeostasis. Lancet *361*, 669–673.

Camaschella, C., Roetto, A., Cali, A., De Gobbi, M., Garozzo, G., Carella, M., Majorano, N., Totaro, A., and Gasparini, P. (2000). The gene TFR2 is mutated in a new type of haemochromatosis mapping to 7q22. Nat. Genet. *25*, 14–15.

Chen, J., Chloupkova, M., Gao, J., Chapman-Arvedson, T.L., and Enns, C.A. (2007). HFE modulates transferrin receptor 2 levels in hepatoma cells via interactions that differ from transferrin receptor 1-HFE interactions. J. Biol. Chem. *282*, 36862–36870.

Cherry, J., Nieuwenhuijsen, B.W., Kaftan, E.J., Kennedy, J.D., and Chanda, P.K. (2008). A modified method for PCR-directed gene synthesis from large number of overlapping oligodeoxyribonucleotides. J. Biochem. Biophys. Methods *70*, 820–822.

De Domenico, I., McVey Ward, D., and Kaplan, J. (2008). Regulation of iron acquisition and storage: consequences for iron-linked disorders. Nat. Rev. Mol. Cell Biol. *9*, 72–81.

de Wet, J.R., Wood, K.V., DeLuca, M., Helinski, D.R., and Subramani, S. (1987). Firefly luciferase gene: structure and expression in mammalian cells. Mol. Biol. Cell *7*, 725–737.

Feder, J.N., Gnirke, A., Thomas, W., Tsuchihashi, Z., Ruddy, D.A., Basava, A., Dormishian, F., Domingo, R., Jr., Ellis, M.C., Fullan, A., et al. (1996). A novel MHC class I-like gene is mutated in patients with hereditary haemochromatosis. Nat. Genet. *13*, 399–408.

Feder, J.N., Tsuchihashi, Z., Irrinki, A., Lee, V.K., Mapa, F.A., Morikang, E., Prass, C.E., Starnes, S.M., Wolff, R.K., Parkkila, S., et al. (1997). The hemochromatosis founder mutation in HLA-H disrupts beta2-microglobulin interaction and cell surface expression. J. Biol. Chem. *272*, 14025–14028.

Feder, J.N., Penny, D.M., Irrinki, A., Lee, V.K., Lebron, J.A., Watson, N., Tsuchihashi, Z., Sigal, E., Bjorkman, P.J., and Schatzman, R.C. (1998). The hemochromatosis gene product complexes with the transferrin receptor and lowers its affinity for ligand binding. Proc. Natl. Acad. Sci. USA *95*, 1472–1477.

Feng, Y., and Longmore, G.D. (2005). The LIM protein Ajuba influences interleukin-1-induced NF-kappaB activation by affecting the assembly and activity of the protein kinase Czeta/p62/TRAF6 signaling complex. Mol. Biol. Cell *25*, 4010–4022.

Gao, J., Zhao, N., Knutson, M.D., and Enns, C.A. (2008). The hereditary hemochromatosis protein, HFE, inhibits iron uptake via down-regulation of zip14 in hepG2 cells. J. Biol. Chem. *283*, 21462–21468.

Gehrke, S.G., Kulaksiz, H., Herrmann, T., Riedel, H.D., Bents, K., Veltkamp, C., and Stremmel, W. (2003). Expression of hepcidin in hereditary hemochromatosis: evidence for a regulation in response to the serum transferrin saturation and to non-transferrin-bound iron. Blood *102*, 371–376.

Giannetti, A.M., Snow, P.M., Zak, O., and Bjorkman, P.J. (2003). Mechanism for multiple ligand recognition by the human transferrin receptor. PLoS Biol. *1*, 341–350.

Goswami, T., and Andrews, N.C. (2006). Hereditary hemochromatosis protein, HFE, interaction with transferrin receptor 2 suggests a molecular mechanism for mammalian iron sensing. J. Biol. Chem. *281*, 28494–28498.

Holmstrom, P., Dzikaite, V., Hultcrantz, R., Melefors, O., Eckes, K., Stal, P., Kinnman, N., Smedsrod, B., Gafvels, M., and Eggertsen, G. (2003). Structure and liver cell expression pattern of the HFE gene in the rat. J. Hepatol. *39*, 308–314.

Ihrke, G., Neufeld, E.B., Meads, T., Shanks, M.R., Cassio, D., Laurent, M., Schroer, T.A., Pagano, R.E., and Hubbard, A.L. (1993). WIF-B cells: an in vitro model for studies of hepatocyte polarity. J. Cell Biol. *123*, 1761–1775.

Johnson, M.B., and Enns, C.A. (2004). Diferric transferrin regulates transferrin receptor 2 protein stability. Blood *104*, 4287–4293.

Kawabata, H., Yang, R., Hirama, T., Vuong, P.T., Kawano, S., Gombart, A.F., and Koeffler, H.P. (1999). Molecular cloning of transferrin receptor 2. A new member of the transferrin receptor-like family. J. Biol. Chem. *274*, 20826–20832.

Kawabata, H., Fleming, R.E., Gui, D., Moon, S.Y., Saitoh, T., O'Kelly, J., Umehara, Y., Wano, Y., Said, J.W., and Koeffler, H.P. (2005). Expression of hepcidin is down-regulated in TfR2 mutant mice manifesting a phenotype of hereditary hemochromatosis. Blood *105*, 376–381.

Kim, D.S., Ahn, S.K., Yoon, J.H., Hong, S.H., Kim, K.E., Maurer, R.A., and Park, S.D. (1994). Involvement of a cAMP-responsive DNA element in mediating TRH responsiveness of the human thyrotropin alpha-subunit gene. Mol. Endocrinol. *8*, 528–536.

Konieczko, E.M., Ralston, A.K., Crawford, A.R., Karpen, S.J., and Crawford, J.M. (1998). Enhanced Na+-dependent bile salt uptake by WIF-B cells, a rat hepatoma hybrid cell line, following growth in the presence of a physiological bile salt. Hepatology *27*, 191–199.

Krijt, J., Niederkofler, V., Salie, R., Sefc, L., Pelichovska, T., Vokurka, M., and Necas, E. (2007). Effect of phlebotomy on hepcidin expression in hemojuvelin-mutant mice. Blood Cells Mol. Dis. *39*, 92–95.

Laemmli, U.K. (1970). Cleavage of structural proteins during the assembly of the head of bacteriophage T4. Nature *227*, 680–685.

Lebron, J.A., and Bjorkman, P.J. (1999). The transferrin receptor binding site on HFE, the class I MHC-related protein mutated in hereditary hemochromatosis. J. Mol. Biol. *289*, 1109–1118.

Lebron, J.A., Bennett, M.J., Vaughn, D.E., Chirino, A.J., Snow, P.M., Mintier, G.A., Feder, J.N., and Bjorkman, P.J. (1998). Crystal structure of the hemochromatosis protein HFE and characterization of its interaction with transferrin receptor. Cell *93*, 111–123.

Levy, J.E., Montross, L.K., Cohen, D.E., Fleming, M.D., and Andrews, N.C. (1999). The C282Y mutation causing hereditary hemochromatosis does not produce a null allele. Blood *94*, 9–11.

Lin, L., Valore, E.V., Nemeth, E., Goodnough, J.B., Gabayan, V., and Ganz, T. (2007). Iron transferrin regulates hepcidin synthesis in primary hepatocyte culture through hemojuvelin and BMP2/4. Blood *110*, 2182–2189.

Martin, C.S., Wight, P.A., Dobretsova, A., and Bronstein, I. (1996). Dual luminescence-based reporter gene assay for luciferase and beta-galactosidase. Biotechniques *21*, 520–524.

Montosi, G., Donovan, A., Totaro, A., Garuti, C., Pignatti, E., Cassanelli, S., Trenor, C.C., Gasparini, P., Andrews, N.C., and Pietrangelo, A. (2001). Autosomal-dominant hemochromatosis is associated with a mutation in the ferroportin (SLC11A3) gene. J. Clin. Invest. *108*, 619–623.

Muckenthaler, M., Roy, C.N., Custodio, A.O., Minana, B., deGraaf, J., Montross, L.K., Andrews, N.C., and Hentze, M.W. (2003). Regulatory defects in liver and intestine implicate abnormal hepcidin and Cybrd1 expression in mouse hemochromatosis. Nat. Genet. *34*, 102–107.

Muckenthaler, M.U., Rodrigues, P., Macedo, M.G., Minana, B., Brennan, K., Cardoso, E.M., Hentze, M.W., and de Sousa, M. (2004). Molecular analysis of iron overload in beta2-microglobulin-deficient mice. Blood Cells Mol. Dis. *33*, 125–131.

Nemeth, E., Tuttle, M.S., Powelson, J., Vaughn, M.B., Donovan, A., Ward, D.M., Ganz, T., and Kaplan, J. (2004). Hepcidin regulates cellular iron efflux by binding to ferroportin and inducing its internalization. Science *306*, 2090–2093.

Nicolas, G., Viatte, L., Lou, D.Q., Bennoun, M., Beaumont, C., Kahn, A., Andrews, N.C., and Vaulont, S. (2003). Constitutive hepcidin expression prevents iron overload in a mouse model of hemochromatosis. Nat. Genet. *34*, 97–101.

Nies, A.T., Cantz, T., Brom, M., Leier, I., and Keppler, D. (1998). Expression of the apical conjugate export pump, Mrp2, in the polarized hepatoma cell line, WIF-B. Hepatology *28*, 1332–1340.

Papanikolaou, G., Samuels, M.E., Ludwig, E.H., MacDonald, M.L., Franchini, P.L., Dube, M.P., Andres, L., MacFarlane, J., Sakellaropoulos, N., Politou, M., et al. (2004). Mutations in HFE2 cause iron overload in chromosome 1q-linked juvenile hemochromatosis. Nat. Genet. *36*, 77–82.

Pigeon, C., Ilyin, G., Courselaud, B., Leroyer, P., Turlin, B., Brissot, P., and Loreal, O. (2001). A new mouse liver-specific gene, encoding a protein homologous to human antimicrobial peptide hepcidin, is overexpressed during iron overload. J. Biol. Chem. *276*, 7811–7819.

Robb, A., and Wessling-Resnick, M. (2004). Regulation of transferrin receptor 2 protein levels by transferrin. Blood *104*, 4294–4299.

Roetto, A., Papanikolaou, G., Politou, M., Alberti, F., Girelli, D., Christakis, J., Loukopoulos, D., and Camaschella, C. (2003). Mutant antimicrobial peptide hepcidin is associated with severe juvenile hemochromatosis. Nat. Genet. *33*, 21–22.

Schmidt, P.J., Toran, P.T., Giannetti, A.M., Bjorkman, P.J., and Andrews, N.C. (2008). The transferrin receptor modulates Hfe-dependent regulation of hepcidin expression. Cell Metab. *7*, 205–214.

Verga Falzacappa, M.V., Casanovas, G., Hentze, M.W., and Muckenthaler, M.U. (2008). A bone morphogenetic protein (BMP)-responsive element in the hepcidin promoter controls HFE2-mediated hepatic hepcidin expression and its response to IL-6 in cultured cells. J. Mol. Med. *86*, 531–540.

Vogt, T.M., Blackwell, A.D., Giannetti, A.M., Bjorkman, P.J., and Enns, C.A. (2003). Heterotypic interactions between transferrin receptor and transferrin receptor 2. Blood *101*, 2008–2014.

Vujic Spasic, M., Kiss, J., Herrmann, T., Galy, B., Martinache, S., Stolte, J., Grone, H.J., Stremmel, W., Hentze, M.W., and Muckenthaler, M.U. (2008). Hfe acts in hepatocytes to prevent hemochromatosis. Cell Metab. *7*, 173–178.

Waheed, A., Parkkila, S., Saarnio, J., Fleming, R.E., Zhou, X.Y., Tomatsu, S., Britton, R.S., Bacon, B.R., and Sly, W.S. (1999). Association of HFE protein with transferrin receptor in crypt enterocytes of human duodenum. Proc. Natl. Acad. Sci. USA *96*, 1579–1584.

Wallace, D.F., Summerville, L., and Subramaniam, V.N. (2007). Targeted disruption of the hepatic transferrin receptor 2 gene in mice leads to iron overload. Gastroenterology *132*, 301–310.

Weinstein, D.A., Roy, C.N., Fleming, M.D., Loda, M.F., Wolfsdorf, J.I., and Andrews, N.C. (2002). Inappropriate expression of hepcidin is associated with iron refractory anemia: implications for the anemia of chronic disease. Blood *100*, 3776–3781.

West, A.P., Jr., Giannetti, A.M., Herr, A.B., Bennett, M.J., Nangiana, J.S., Pierce, J.R., Weiner, L.P., Snow, P.M., and Bjorkman, P.J. (2001). Mutational analysis of the transferrin receptor reveals overlapping HFE and transferrin binding sites. J. Mol. Biol. *313*, 385–397.

Wilson, I.A., and Bjorkman, P.J. (1998). Unusual MHC-like molecules: CD1, Fc receptor, the hemochromatosis gene product, and viral homologs. Curr. Opin. Immunol. *10*, 67–73.

Zhang, A.S., Davies, P.S., Carlson, H.L., and Enns, C.A. (2003). Mechanisms of HFE-induced regulation of iron homeostasis: Insights from the W81A HFE mutation. Proc. Natl. Acad. Sci. USA *100*, 9500–9505.

Zhang, A.S., Xiong, S., Tsukamoto, H., and Enns, C.A. (2004). Localization of iron metabolism-related mRNAs in rat liver indicate that HFE is expressed predominantly in hepatocytes. Blood *103*, 1509–1514.

Zhang, A.S., Anderson, S.A., Meyers, K.R., Hernandez, C., Eisenstein, R.S., and Enns, C.A. (2007). Evidence that inhibition of hemojuvelin shedding in response to iron is mediated through neogenin. J. Biol. Chem. *282*, 12547–12556.

Zhou, X.Y., Tomatsu, S., Fleming, R.E., Parkkila, S., Waheed, A., Jiang, J., Fei, Y., Brunt, E.M., Ruddy, D.A., Prass, C.E., et al. (1998). HFE gene knockout produces mouse model of hereditary hemochromatosis. Proc. Natl. Acad. Sci. USA *95*, 2492–2497.

Cell Metabolism
Article

Drosophila HNF4 Regulates Lipid Mobilization and β-Oxidation

Laura Palanker,[1,2] Jason M. Tennessen,[1] Geanette Lam,[1] and Carl S. Thummel[1,*]
[1]Department of Human Genetics, University of Utah School of Medicine, 15 North 2030 East Room 2100, Salt Lake City, UT 84112-5330, USA
[2]Present address: Division of Endocrinology, Metabolism, and Lipid Research, Department of Medicine, Washington University School of Medicine, Box 8127, 660 South Euclid Avenue, St. Louis, MO 63110, USA
*Correspondence: carl.thummel@genetics.utah.edu
DOI 10.1016/j.cmet.2009.01.009

SUMMARY

Drosophila **HNF4 (dHNF4) is the single ancestral ortholog of a highly conserved subfamily of nuclear receptors that includes two mammalian receptors, HNFα and HNFγ, and 269 members in *C. elegans*. We show here that *dHNF4* null mutant larvae are sensitive to starvation. Starved mutant larvae consume glycogen normally but retain lipids in their midgut and fat body and have increased levels of long-chain fatty acids, suggesting that they are unable to efficiently mobilize stored fat for energy. Microarray studies support this model, indicating reduced expression of genes that control lipid catabolism and β-oxidation. A *GAL4-dHNF4;UAS-lacZ* ligand sensor can be activated by starvation or exogenous long-chain fatty acids, suggesting that dHNF4 is responsive to dietary signals. Taken together, our results support a feed-forward model for dHNF4, in which fatty acids released from triglycerides activate the receptor, inducing enzymes that drive fatty acid oxidation for energy production.**

INTRODUCTION

Nuclear receptors are ligand-regulated transcription factors that act at the interface between chemical signaling and transcriptional control. They are defined by a conserved zinc finger DNA-binding domain (DBD) and a C-terminal ligand-binding domain (LBD) that can impart multiple functions, including hormone binding, receptor dimerization, and transactivation. Nuclear receptors are regulated by a wide range of lipophilic compounds that include dietary signals and metabolic intermediates, such as sterols, fatty acids, and bile acids. Binding of these compounds to the LBD triggers a conformational change that switches the regulatory function of the receptor, directing coordinate changes in downstream target gene expression. The resulting transcriptional programs often drive feedback or feed-forward pathways that act upon the specific class of compounds bound by the receptor (Chawla et al., 2001). Functional studies of several nuclear receptor subclasses, including ERR, LXR, and PPAR, have defined roles for these factors in regulating mitochondrial function, sterol homeostasis, and lipid metabolism—pathways that are central to human health, as manifested by the alarming rise in diabetes and obesity among human populations worldwide.

In this study, we focus on hepatocyte nuclear factor 4 (HNF4), a nuclear receptor subclass that is represented by two paralogs in mammals, HNF4α and HNF4γ. Mutations in human *HNF4α* are associated with MODY1, an autosomal dominant genetic disorder that is characterized by early onset type 2 diabetes (Yamagata et al., 1996). MODY1 patients are hyperglycemic and hypoinsulinemic, have reduced levels of circulating lipids, and display defects in the expression of genes involved in glucose and lipid metabolism (Stoffel and Duncan, 1997; Shih et al., 2000). Interestingly, similar phenotypes have been observed in *HNF4α* mutant mice. Targeted disruption of *HNF4α* leads to early embryonic lethality with defects in the expression of visceral endoderm secretory proteins that are required for maintaining gastrulation (Chen et al., 1994; Duncan et al., 1997). Tissue-specific loss of *HNF4α* in the mouse liver results in increased lipid deposits in hepatocytes, hepatomegaly, and early lethality (Hayhurst et al., 2001). Circulating cholesterol, phospholipid, and triglyceride levels are reduced in these animals, consistent with the decreased expression of hepatic genes involved in lipid metabolism and transport. An *HNF4γ* null mutant mouse strain has been reported as viable with slightly increased body weight, decreased food intake, and decreased nighttime activity, leaving it unclear what contribution this paralog might have to overall *HNF4* function (Gerdin et al., 2006).

Remarkably, the HNF4 family underwent a significant expansion during the evolution of nematodes, resulting in 269 family members in *C. elegans* (Robinson-Rechavi et al., 2005). One of these, NHR-49, has been characterized in detail (Van Gilst et al., 2005a). Like liver-specific mouse *HNF4α* mutants, *nhr-49* mutants accumulate fat and display early lethality. By examining the expression of 65 genes involved in energy metabolism, significant effects were observed in mitochondrial β-oxidation, the pathway by which fatty acids are utilized for energy production, and fatty acid desaturation, increasing the ratio of stearic acid to oleic acid in mutant worms. Overexpression of a mitochondrial acyl-CoA synthetase that is downregulated in *nhr-49* mutants was sufficient to suppress the high-fat phenotype, suggesting that this defect arises from reduced levels of β-oxidation.

Biochemical studies have provided insights into the molecular mechanisms of HNF4 function. The basal transcriptional activity of HNF4 can be enhanced by fatty acyl-CoA thioesters, suggesting that HNF4 may be modulated by a fatty acid-derived ligand (Hertz et al., 1998). Structural analysis of the HNF4α and HNF4γ LBD revealed C14–C18 long-chain fatty acids (LCFAs) almost filling a well-defined hydrophobic pocket, suggesting that they are natural ligands for the receptor (Dhe-Paganon et al., 2002; Wisely et al., 2002). These fatty acids, however, are tightly bound

and could not be dissociated from the receptor under nondenaturing conditions (Wisely et al., 2002). Mutating conserved amino acids within the LBD that disrupt fatty acid binding significantly decreases HNF4 transcriptional activity, suggesting that this interaction is essential for receptor function (Wisely et al., 2002; Aggelidou et al., 2004). Both active and inactive LBD conformations of HNF4α have bound LCFAs, implying that another mechanism is required for HNF4 transcriptional activation (Dhe-Paganon et al., 2002). Taken together, these data support a model whereby HNF4, with a tightly bound LCFA, acts as a constitutive transcriptional activator, although regulation by posttranslational modifications, cofactor interactions, or ligand exchange in vivo remains a possibility.

The presence of multiple HNF4 paralogs in mice and *C. elegans* has complicated our understanding of the physiological functions of this nuclear receptor subclass. In contrast, only a single HNF4 ortholog is encoded in the *Drosophila* genome, with 89% identity to HNF4α in its DBD and 61% identity in its LBD. Moreover, most of the basic metabolic pathways and regulatory interactions that maintain homeostasis are conserved in the fly, providing an ideal context for genetic and biological studies of HNF4 function (Baker and Thummel, 2007; Leopold and Perrimon, 2007). Here, we show that *dHNF4* null mutant larvae are sensitive to starvation. This starvation sensitivity is associated with a reduced ability to generate energy from stored lipid, as manifested by increased levels of triglycerides and LCFAs in starved animals, along with significant reduction in the transcription of genes involved in lipolysis and β-oxidation. In addition, we show that the HNF4 LBD changes its activation status during development and can be activated by starvation or exogenous LCFAs. Taken together, our data define the ancestral function of HNF4 as a key regulator of lipid mobilization and β-oxidation in response to nutrient deprivation.

RESULTS

dHNF4 Is Expressed in the Major Tissues that Control Metabolism

As a first step toward dHNF4 functional characterization, we used affinity-purified antibodies to determine its spatial pattern of expression in organs dissected from third instar larvae. dHNF4 protein is restricted to the nucleus, consistent with its role as a transcription factor (Figure 1). It is most highly expressed in four tissues: the midgut and attached gastric caeca (Figure 1A), the fat body (Figures 1B and 1C), the Malpighian tubules (Figure 1B), and the oenocytes (Figure 1D). The gastric caeca are four anterior projections off of the midgut that provide a primary site for digestive enzyme secretion and absorption of nutrients into the circulatory system. Nutrients are metabolized and stored, primarily as glycogen and triglycerides (TAG), in the fat body, the insect equivalent of the mammalian liver and white adipose tissue. Lipid mobilization is facilitated by the oenocytes, which are small clusters of cells that are embedded within the epidermis (Gutierrez et al., 2007). Waste products are transferred back into the circulatory system and absorbed by the Malpighian tubules, the principal osmoregulatory and excretory organ of the insect. Low levels of dHNF4 expression were detected in the proventriculus (Figure 1A), salivary glands (Figure 1C), epidermis (Figure 1D), brain, and ring gland (Figure S1 available online).

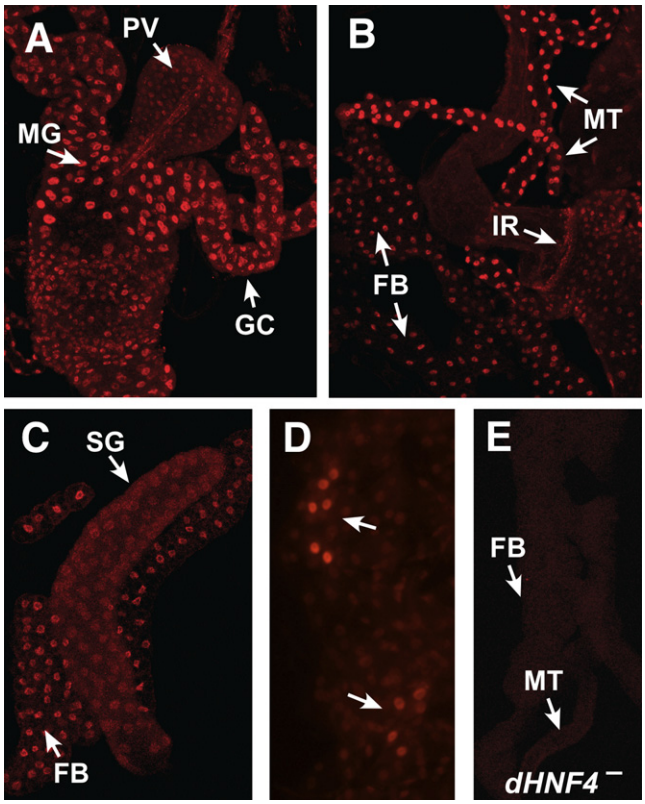

Figure 1. dHNF4 Is Expressed in Tissues that Control Metabolic Homeostasis

Affinity-purified antibodies directed against dHNF4 were used to determine its spatial pattern of expression in organs dissected from third instar larvae.

(A) dHNF4 protein is localized to the nucleus and is present at relatively high levels in the gastric caeca (GC) and anterior midgut (MG) of the digestive system, with lower levels in the proventriculus (PV).

(B and C) Relatively high levels of expression are also seen in the fat body (FB), Malpighian tubules (MT), and hindgut imaginal ring (IR), with lower levels of expression in the salivary gland (SG).

(D) dHNF4 is highly expressed in the larval oenocytes (arrows), with low-level expression in the surrounding epidermis.

(E) No expression is detectable in tissues dissected from *dHNF4* mutant tissues, indicating that the antibody is specific for dHNF4 protein.

dHNF4 was not detected in imaginal discs, although it is expressed in the ring of imaginal cells that will develop into the adult hindgut during metamorphosis (Figure 1B). dHNF4 is also not detected in the median neurosecretory cells that produce insulin-like peptides (IPCs) (Figure S1). A similar overall spatial distribution of dHNF4 expression is seen in embryos by in situ hybridization (Zhong et al., 1993), suggesting that this represents a stable pattern of expression. Northern blot analysis indicates that *dHNF4* is expressed at a constant level throughout development (Sullivan and Thummel, 2003).

dHNF4 Mutants Are Sensitive to Starvation

Imprecise excision of two *P* element insertions in *dHNF4* was used to create deletions for the locus (Figure 2A). A 8193 bp deletion of *EP2449*, designated $dHNF4^{\Delta 17}$, removes most of the *dHNF4* coding region along with three adjacent genes. Imprecise excision of *KG08976* resulted in the isolation of $dHNF4^{\Delta 33}$,

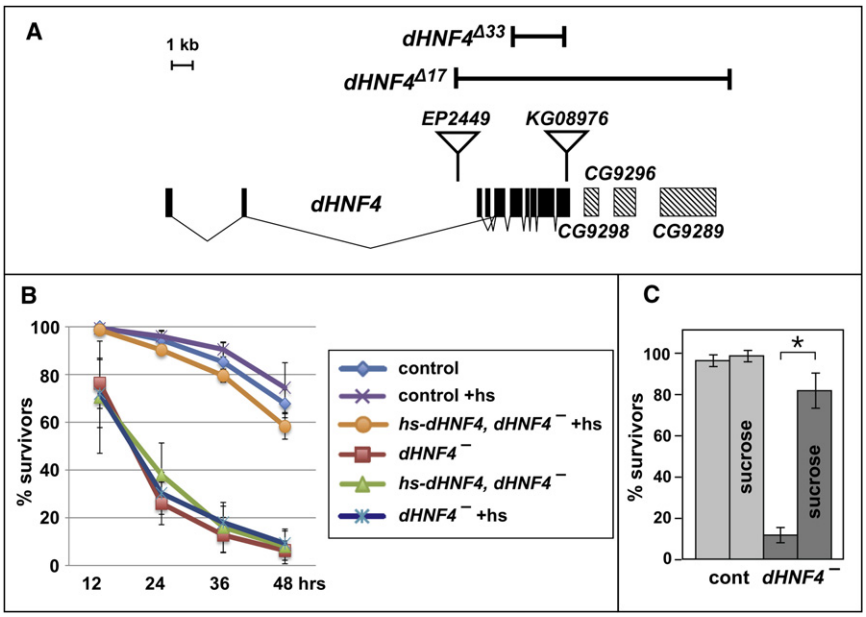

Figure 2. *dHNF4* Null Mutants Are Sensitive to Starvation

(A) A schematic representation of the *dHNF4* locus is depicted, with the gene structure shown below along with three 3′ flanking genes, *CG9298*, *CG9296*, and *CG9289*. The locations of the two *P* element insertions in *dHNF4*, *EP2449*, and *KG08976* are shown, along with the $dHNF4^{\Delta 17}$ and $dHNF4^{\Delta 33}$ deletions.

(B) A time course of the viability of starved control and *dHNF4* mutant larvae, with and without a wild-type *hs-dHNF4* transgene. Whereas most larvae that are transheterozygous for precise excisions of the *EP2449* and *KG08976 P* elements (control) can survive 2 days of starvation, most $dHNF4^{\Delta 33}/dHNF4^{\Delta 17}$ mutants ($dHNF4^{-}$) die. Heat treatment (+hs) has no effect on these animals. Heat treatment of $dHNF4^{\Delta 33}/dHNF4^{\Delta 17}$ mutants that carry a *hs-dHNF4* rescue construct (*hs-dHNF4*, $dHNF4^{-}$ +hs), however, regain their starvation resistance.

(C) Control (cont) or *dHNF4* mutant ($dHNF4^{-}$) late second instar larvae were either maintained on moist filter paper or on a 20% sucrose diet (sucrose) for 2 days at 25°C, after which the percent of surviving animals was scored and plotted. Whereas *dHNF4* mutant larvae are sensitive to starvation, they survive normally on a sucrose diet. A representative of four independent experiments is presented, with n = 10–40 animals in each experiment. Error bars are ± SE. *$p = 1.3 \times 10^{-3}$.

a 1939 bp deletion specific to *dHNF4* that removes sequences encoding most of the DBD and the entire LBD. A transheterozygous combination of these two alleles, $dHNF4^{\Delta 33}/dHNF4^{\Delta 17}$, was used for all functional studies of *dHNF4*. These mutants have no detectable dHNF4 protein, as expected for a specific *dHNF4* null allele (Figure 1E). Larvae that were transheterozygous for precise excisions of the *EP2449* and *KG08976 P* elements were used as genotypically matched controls.

dHNF4 mutants maintained under normal culture conditions progress through development until adult eclosion, when many of the animals die with their head protruding from the pupal case. The remaining *dHNF4* mutant adults die within a day of eclosion. Maintaining *dHNF4* mutants at low density under ideal culture conditions, however, results in many animals surviving this lethal period and developing into morphologically normal adults. This dependence of *dHNF4* mutant lethality on culture conditions suggests that this phenotype arises, at least in part, from metabolic defects due to the nutritional status of the animal.

As a first step toward assessing possible metabolic functions of *dHNF4*, we examined the ability of mutants to survive a period of starvation. Whereas most control larvae survive 2 days in the absence of nutrients, almost all *dHNF4* mutants succumb during this period (Figure 2B). This sensitivity can be rescued by a heat-inducible wild-type *dHNF4* transgene (*hs-dHNF4*), indicating that it is specific to *dHNF4* (Figure 2B). Significant rescue can also be achieved with expression of wild-type *dHNF4* in the midgut or fat body, but not the ring gland, oenocytes, or IPCs (Figure S2). Importantly, *dHNF4* mutants maintain the ability to survive on a sugar diet (Figure 2C). This suggests that these mutant larvae develop normally and that their basic metabolic activities (glycolysis and downstream mitochondrial energy-producing pathways) remain functional.

dHNF4 Mutants Display Defects in Lipid Metabolism

In order to identify possible causes for the starvation sensitivity of *dHNF4* mutants, glycogen and TAG levels were measured in control and *dHNF4* mutants that were either fed or starved for 1 day (Figures 3A and 3B). Levels of both metabolites did not change significantly in fed control and mutant larvae, consistent with the apparently normal developmental progression of these animals. In addition, glycogen appears to be consumed normally in *dHNF4* mutants upon starvation (Figure 3A). Starved *dHNF4* mutants, however, have significantly higher levels of TAG than do starved control larvae (Figure 3B). These observations suggest that *dHNF4* mutants are unable to properly mobilize their lipid stores upon nutrient deprivation. Starvation-induced autophagy, however, is induced normally in *dHNF4* mutant larvae (Figure S3) (Britton et al., 2002; Rusten et al., 2004).

If *dHNF4* mutants retain TAG upon starvation, then this defect should be evident by using a cellular-based assay to detect stored lipids. Accordingly, tissues were dissected from fed or starved control or *dHNF4* mutant larvae and stained with lipophilic dyes to detect neutral lipids (Figures 3C–3N). After 1 day of starvation, lipids are effectively cleared from the midgut of control animals (Figures 3C and 3E) and accumulate in the oenocytes (Figures 3G and 3I), similar to published results (Gutierrez et al., 2007). Higher levels of lipid, however, are evident in the midguts of starved *dHNF4* mutants compared to starved controls (Figures 3E and 3F). In addition, slightly elevated lipid levels are seen in the midguts and oenocytes of fed *dHNF4* mutants relative to fed controls (Figures 3C, 3D, 3G, and 3H), suggesting that metabolic dysfunction is also present in the fed state. Many small lipid droplets are evident in the fat body cells of starved control larvae relative to fed controls, consistent with the mobilization of stored lipid for energy production (Figures 3K and 3M). Moreover, fed *dHNF4* mutants have essentially normal lipid droplet morphology

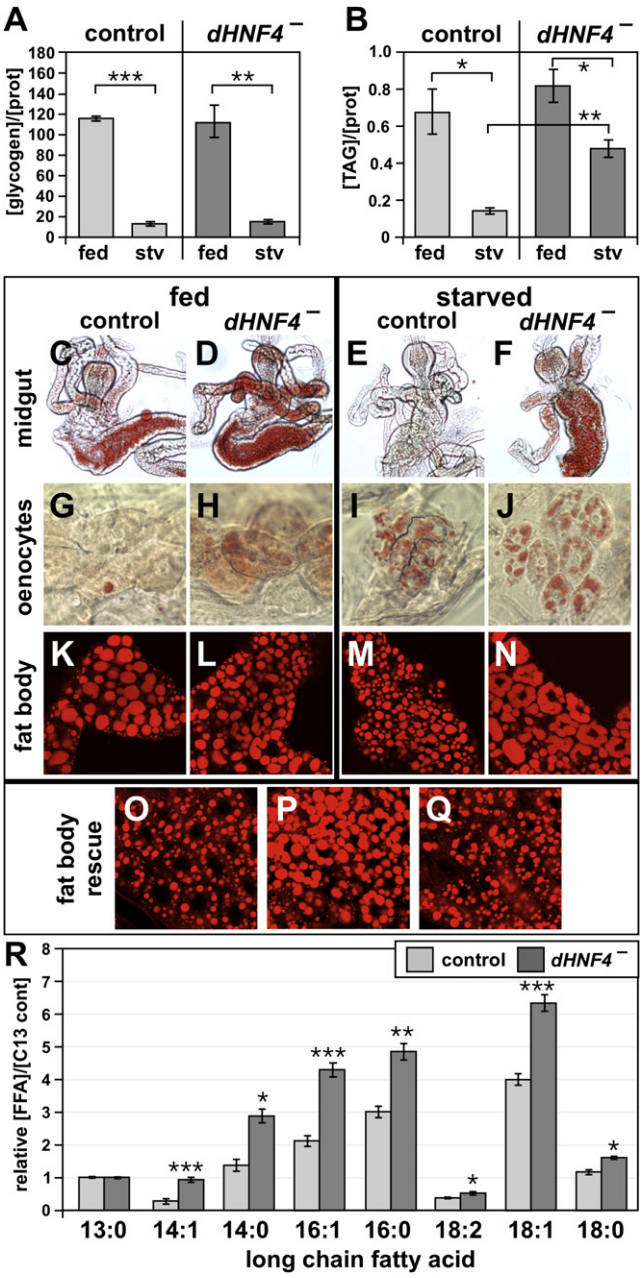

Figure 3. Starved *dHNF4* Mutants Have Excess Stored Lipid and Increased Free Fatty Acids

(A and B) Late second instar larvae that were transheterozygous for precise excisions of the *EP2449* and *KG08976 P* elements (control) or $dHNF4^{\Delta 33}$/$dHNF4^{\Delta 17}$ mutant larvae (*dHNF4*$^{-}$) were either fed or starved for 24 hr, after which homogenates were subjected to (A) glycogen or (B) TAG assays. Amounts of glycogen (in μg) and TAG (in mg) were normalized to the amount of protein (in mg), shown on the y axis. Glycogen amounts drop to similar levels in starved control and *dHNF4* mutant larvae, whereas TAG levels remain relatively high in starved *dHNF4* mutants. n = 25 animals for each sample, with each experiment using six samples. A representative of four (glycogen) or six (TAG) experiments is depicted. Error bars are ± SE. *$p < 0.01$; **$p < 1 \times 10^{-4}$; ***$p < 1 \times 10^{-8}$.

(C–J) Oil red O staining of midguts (C–F) and oenocytes (G–J) dissected from fed or 24 hr starved, control, or *dHNF4* mutant larvae. Whereas lipid levels drop significantly in the midguts of control larvae upon starvation (C and E), lipid is inefficiently depleted from the midguts of starved *dHNF4* mutants (D and F). An increase in the lipid content of oenocytes occurs normally in starved *dHNF4* mutants relative to starved controls (I and J). Fed *dHNF4* mutants, however, display a slight increase in lipids in both the midgut and oenocytes relative to fed controls (C, D, G, and H).

(K–Q) Nile Red staining of larval fat bodies. Whereas the large lipid droplets in the fat bodies of fed controls become smaller upon starvation (K and M), lipid droplets appear to aggregate in starved *dHNF4* mutant fat bodies (L and N). (O–Q) Tissue-specific rescue of lipid droplet morphology as assayed by Nile Red stains of fat bodies from starved animals. Starved *UAS-dHNF4 dHNF4*$^{-/+}$ control animals (O) display wild-type lipid droplet morphology (compare to [M]). Starved $dHNF4^{\Delta 33}$/*fb-GAL4* $dHNF4^{\Delta 17}$ mutants display lipid droplet aggregation (P), and this phenotype is largely rescued in starved *UAS-dHNF4* $dHNF4^{\Delta 33}$/*fb-GAL4* $dHNF4^{\Delta 17}$ larvae (Q).

(R) GC/MS analyses of lipid extracts reveal that *dHNF4* mutant early third instar larvae contain relatively higher levels of most free long-chain fatty acids upon starvation than control larvae. n = 20 larvae for each sample, with eight samples tested. Similar results were obtained from an independent experiment. The y axis represents the concentration of each free fatty acid (FFA) relative to a tridecanoate internal standard. Error bars represent ± SE. *$p < 1 \times 10^{-3}$; **$p < 1 \times 10^{-4}$; ***$p < 1 \times 10^{-5}$.

(Figure 3L). These droplets, however, appear to aggregate abnormally in starved mutants (Figure 3N). This observation, together with the elevated levels of lipid in the midguts of starved *dHNF4* mutants, is consistent with the retention of TAG as measured by enzymatic assay (Figure 3B).

Tissue-specific rescue was performed to further characterize the lipid metabolic defect seen in the fat body of starved *dHNF4* mutant larvae. As expected, small lipid droplets are present in the fat body of a starved control animal that carries only one mutant copy of *dHNF4* (Figure 3O), similar to that seen in wild-type animals (Figure 3M). Similarly, lipid droplet aggregation is seen in the fat body of a starved *dHNF4* mutant that carries only the fat body-specific *fb-GAL4* driver (Figure 3P). Essentially normal lipid droplet morphology, however, is recovered when wild-type *dHNF4* is expressed in the fat bodies of starved *dHNF4* mutants (Figure 3Q). This result suggests that the lipid mobilization defects seen in the fat body of starved *dHNF4* mutants are tissue autonomous.

Finally, gas chromatography and mass spectrometry (GC/MS) were used to analyze the lipid composition of fed and starved control and *dHNF4* mutant larvae. Although no significant changes were evident under fed conditions (data not shown), starved *dHNF4* mutants display reproducibly increased levels of free LCFAs compared to controls (Figure 3R). Thus, both TAG and LCFAs accumulate upon starvation in *dHNF4* mutant larvae.

Lipolysis and β-Oxidation Genes Are Downregulated in *dHNF4* Mutants

Microarray studies were performed to investigate the molecular mechanisms by which dHNF4 contributes to the starvation response. RNA extracted from fed or starved control or *dHNF4* mutant larvae was labeled and hybridized to Affymetrix *Drosophila* 2.0 microarrays. All experiments were conducted in triplicate to facilitate statistical analysis. The raw expression data files were imported into dChip (Li and Hung Wong, 2001), the background was normalized, and gene expression changes were determined by using SAM, with < 5% estimated false positives in each comparison (Tusher et al., 2001).

This study revealed that 3138 transcripts are significantly affected by starvation in wild-type larvae (≥1.5-fold), with 1809 genes upregulated and 1329 genes downregulated (Table S1). Comparison of this data set with the 2185 transcripts identified by Zinke et al. (2002) in their analysis of the 12 hr starvation response in larvae revealed that 977 (45%) transcripts are shared in common. Of these, 941 transcripts (96%) reported as either upregulated or downregulated by Zinke et al. (2002) show the same response in our study. Similarly, 145 of the 398 transcripts (36%) identified in starved adult *Drosophila* are present in our list of affected genes (Gronke et al., 2005), with 115 (79%) of these common transcripts regulated in the same manner (up or down). As expected, genes involved in gluconeogenesis and lipid mobilization, transport, and β-oxidation are upregulated in our list of starvation response genes, and genes involved in glycolysis, lipid synthesis, and mitochondrial protein biosynthesis are downregulated (Table S2).

Comparison of the transcriptional profiles in fed control and *dHNF4* mutant larvae revealed that only 85 transcripts displayed a significant change in expression level of ≥ 1.3-fold (Table S3). This number increased to 330 affected transcripts in starved *dHNF4* mutants compared to starved controls, with 45 transcripts shared in common between fed and starved conditions (Table S5). The majority of affected mRNAs are downregulated in *dHNF4* mutants, consistent with the role of HNF4 family members as transcriptional activators (Hertz et al., 1998; Van Gilst et al., 2005b).

GOstat was used to identify predicted gene functions corresponding to transcripts that are misregulated in either fed or starved *dHNF4* mutants relative to controls (Beissbarth and Speed, 2004). Interestingly, the top gene ontology categories, under both fed and starved conditions, all relate to different aspects of mitochondrial β-oxidation—the pathway by which fatty acids are converted into high-energy electron donors for energy production (Table S1). These include oxidoreductase enzymes in the β-oxidation pathway, transferases that could facilitate acyl-CoA import into mitochondria, and γ-butyrobetaine dioxygenases that synthesize the carnitine intermediate required for fatty acid import into mitochondria (Table 1 and Figure 4B). Similarly, comparison of a list of genes in *Drosophila* metabolic pathways with our *dHNF4* mutant microarray lists demonstrated major effects on β-oxidation in both fed and starved animals (Tables S4 and S6). These effects on gene expression are consistent with the results of metabolic assays described above, in that reduced flux through the β-oxidation pathway would result in an accumulation of fatty acids and TAG under starvation conditions.

Northern blot hybridizations were conducted to test the response of selected *dHNF4*-regulated genes in both fed and starved animals (Figure 4A). This study showed that *dHNF4* is significantly induced upon starvation, consistent with its role in mediating lipid mobilization, and is not detectable in the mutant, as expected. *CG5321*, *CG2107*, *fatp*, *yip2*, *CG9577*, *CG6178*, and *Acox57D-d*, many of which are predicted to act in β-oxidation (Figure 4B), are upregulated in starved controls and downregulated in both fed and starved *dHNF4* mutants (Figure 4A). Three genes were also tested that could contribute to lipid metabolism: *CG3523* (predicted to encode a fatty acid synthase), *desat1* (predicted to encode a stearoyl-CoA desaturase), and *CG11198* (predicted to encode an acetyl-CoA carboxylase). These genes are downregulated in starved control animals, and their expression is reduced in *dHNF4* mutants. Taken together, these results validate the dHNF4 targets identified by microarray and demonstrate that the receptor acts at all levels of the β-oxidation pathway.

Table 1. Top Affected Gene Functions in Fed or Starved *dHNF4* Mutants Reveal a Central Role in Fatty Acid β-Oxidation

Fed Animals		
GO Category	Number of Genes (Total)	P Value
Oxidoreductase activity	17 (541)	4.8e-07
Carnitine o-acyl transferase activity	4 (6)	2.3e-06
Mitochondrion	15 (521)	6.2e-06
Transferase activity, other than amino-acyl groups	7 (75)	1.0e-05
Acyltransferase activity	7 (75)	1.0e-05
Cytoplasmic part	22 (1537)	1.8e-05
Lipid particle	8 (129)	1.9e-05
Transferase activity, transferring acyl groups	7 (88)	1.9e-05
Fatty acid metabolic process	5 (35)	4.9e-05
Fatty acid β-oxidation	3 (5)	6.3e-05
Fatty acid oxidation	3 (6)	1.1e-04
o-Acyltransferase activity	4 (21)	1.4e-04
Starved Animals		
GO Category	Number of Genes (Total)	P Value
Oxidoreductase activity	29 (541)	3.9e-14
Fatty acid metabolic process	10 (35)	3.4e-09
Cellular lipid metabolic process	15 (113)	3.4e-09
Lipid metabolic process	15 (125)	1.1e-08
Fatty acid β-oxidation	5 (5)	4.9e-08
Monocarboxylic acid metabolic process	10 (53)	1.4e-07
Fatty acid oxidation	5 (6)	2.1e-07
Transferase activity, other than amino-acyl groups	11 (75)	2.3e-07
Acyltransferase activity	11 (75)	2.3e-07
Hydrolase activity	44 (1550)	9.5e-07
Transferase activity, transferring acyl groups	11 (88)	1.1e-06
γ-Butyrobetaine dioxygenase activity	4 (4)	1.6e-06

GOstat analysis of either the 74 genes that are downregulated in fed *dHNF4* mutants compared to fed control larvae (Table S3) or the 197 genes that are downregulated in starved *dHNF4* mutants compared to starved control larvae (Table S5). The top 12 GO categories are listed from top to bottom along with the number of affected genes in that category, the total number of genes in that category in parentheses, and the p value of the match (http://gostat.wehi.edu.au/cgi-bin/goStat.pl).

The dHNF4 LBD Can Be Activated by Starvation and Exogenous Fatty Acids

If dHNF4 plays a central role in maintaining lipid homeostasis in *Drosophila*, then it may mediate this effect by changing its

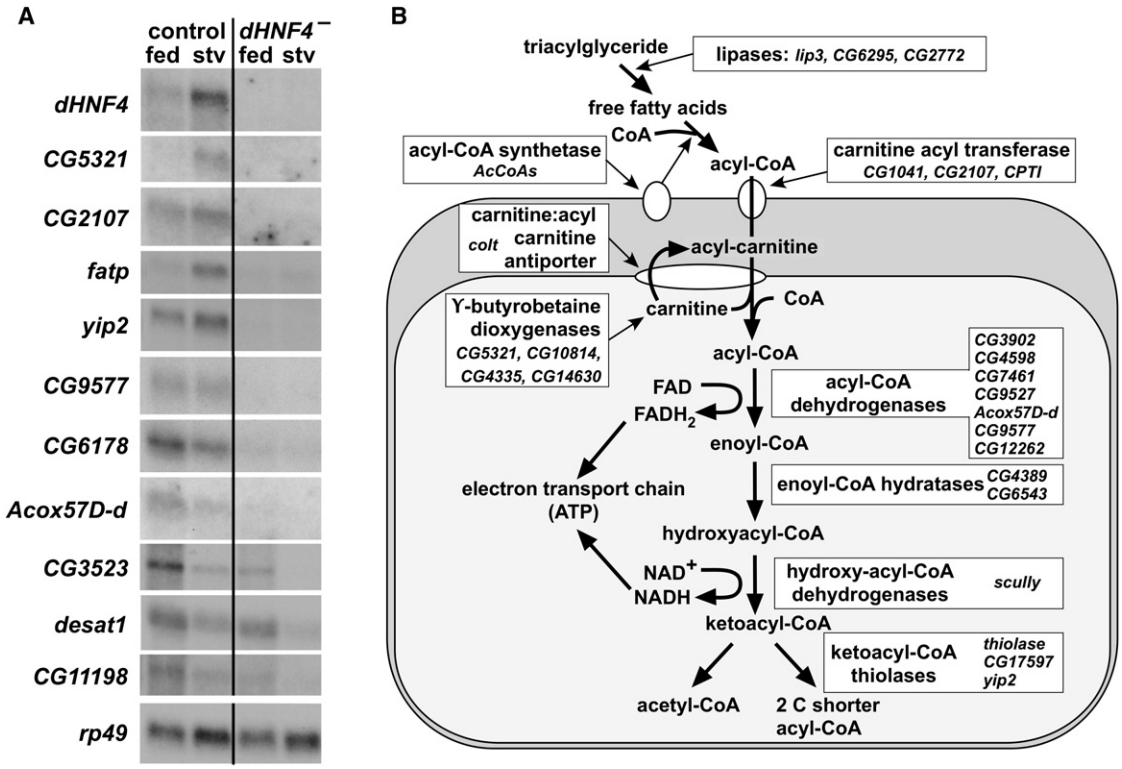

Figure 4. dHNF4 Regulates All Levels of the β-Oxidation Pathway

(A) Second instar larvae that were transheterozygous for precise excisions of the *EP2449* and *KG08976 P* elements (control) or $dHNF4^{\Delta 33}/dHNF4^{\Delta 17}$ mutants ($dHNF4^{-}$) were fed or starved for 24 hr, after which RNA was isolated and analyzed by northern blot hybridization. *dHNF4* mRNA is induced upon starvation, with no transcript seen in mutant animals. *CG5321*, *CG2107*, *fatp*, *yip2*, *CG9577*, *CG6178*, and *Acox57D-d*, which function in β-oxidation, are significantly downregulated in the *dHNF4* mutant, consistent with the microarray results. *CG3523*, which encodes a predicted fatty acid synthetase, *desat1*, which encodes a predicted stearoyl-CoA desaturase, and *CG11198*, which encodes a predicted acetyl-CoA carboxylase, are all downregulated upon starvation in both control larvae and *dHNF4* mutants, and their overall level of expression is reduced in the mutant.

(B) A schematic representation of the mitochondrial β-oxidation pathway is depicted. At the top, stored lipids in the form of triglycerides are hydrolyzed into free fatty acids by lipases. Acyl-CoA synthetases, which reside in the outer mitochondrial membrane, convert fatty acids into acyl-CoA for entry into the β-oxidation pathway. The acyl group is transported through the outer and inner mitochondrial membranes via a carnitine intermediate and then processed through four enzymatic steps, as depicted. Each cycle generates one $FADH_2$ and one NADH, which donate their high-energy electrons to the electron transport chain for ATP production. Each cycle of β-oxidation results in an acyl-CoA that is shortened by two carbons. This acyl-CoA can be processed through successive cycles to produce more $FADH_2$ and NADH. The names of genes that are downregulated in *dHNF4* mutants are listed next to their predicted enzymatic or transport functions.

transcriptional activity in response to developmental cues or dietary conditions. To test this possibility, we used the GAL4-dHNF4 ligand sensor to follow dHNF4 LBD activation during larval development, as the animal terminates feeding and growing in preparation for entry into metamorphosis. This system uses a heat-inducible transgene that encodes the yeast GAL4 DNA-binding domain fused to the dHNF4 LBD (*hsp70-GAL4-dHNF4*) in combination with a *UAS-nlacZ* reporter gene that directs the synthesis of nuclear-localized β-galactosidase. The temporal and spatial patterns of β-galactosidase expression in ligand sensor transgenic animals accurately reflect nuclear receptor LBD activation at different stages of development and in response to exogenous ligands (Palanker et al., 2006).

GAL4-dHNF4 shows low levels of LBD activation in late second instar or early third instar larvae (Figure 5A). A distinct change, however, is seen in mid-third instar larvae, with high levels of LBD activation in the fat body, at the base of the gastric caeca, and in the epidermis. Animals undergo a widespread change in physiology at this time, including downregulation of PI3K activity and initiation of autophagy, as they prepare for the cessation of feeding, the onset of wandering behavior, and metamorphosis (Britton et al., 2002; Rusten et al., 2004). Accordingly, we asked whether the dHNF4 ligand sensor could be activated by starvation, which is known to induce lipolysis and autophagy in third instar larvae (Britton et al., 2002; Rusten et al., 2004; Scott et al., 2004). Interestingly, whereas little activation is seen in early third instar larvae maintained on a regular diet or on yeast paste, high activation is seen in the fat body and epidermis of starved animals (Figures 5A and B and data not shown). Larvae fed a sugar diet, however, show no increase in activation, indicating that this response requires complete nutrient deprivation (data not shown).

Fasting normally triggers rapid breakdown of TAG into LCFAs as a first step toward β-oxidation and energy production. Given that LCFAs can bind to the HNF4 LBD and are required for its activity (Dhe-Paganon et al., 2002; Wisely et al., 2002; Aggelidou

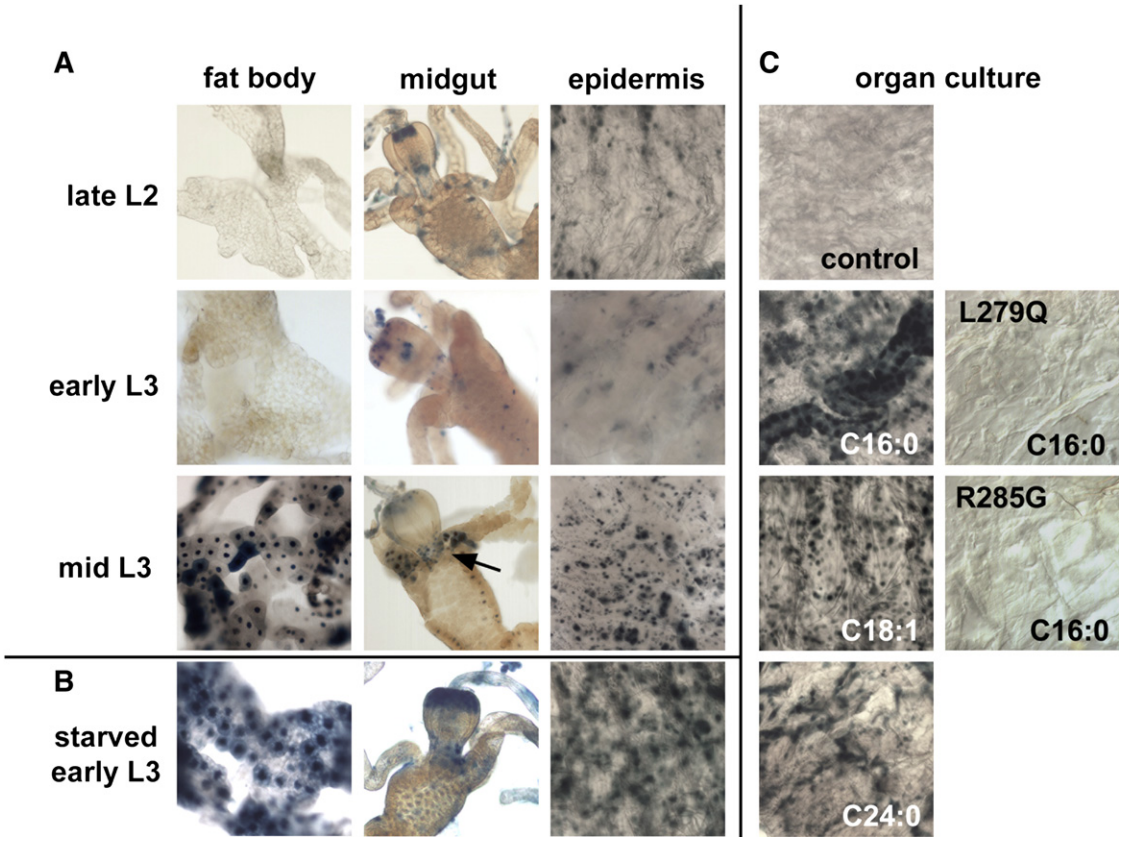

Figure 5. GAL4-dHNF4 Can Be Activated by Starvation and Exogenous Long-Chain Fatty Acids

(A) Fed larvae carrying both the *GAL4-dHNF4* and *UAS-nlacZ* transgenes were heat treated and allowed to recover for ~6 hr, and dissected organs were stained with X-gal for β-galactosidase activity. Low levels of ligand sensor activity are seen in the fat body, midgut, and epidermis of late second instar (late L2) or early third instar larvae (early L3), whereas high levels of activity are detected in mid-third instar larvae (mid L3). GAL4-dHNF4 activity in the mid-third instar midgut is restricted to the anterior region, adjacent to the proventriculus (arrow). No ligand sensor activity is detected in the oenocytes, although negative results with the ligand sensor system are difficult to interpret (Palanker et al., 2006).

(B) Late second instar *GAL4-dHNF4*; *UAS-nlacZ* larvae were fasted or fed for 3 hr, heat treated, and fasted or fed for another 3–4 hr, after which dissected organs were stained with X-gal for β-galactosidase activity. Starvation leads to strong activation of GAL4-dHNF4 in the fat body and epidermis of early third instar larvae compared to fed controls ([A], early L3).

(C) Late second instar *GAL4-dHNF4*; *UAS-nlacZ* larvae were heat treated to induce GAL4-dHNF4 expression, allowed to recover, and then bisected, inverted, and cultured overnight in either control medium or medium supplemented with fatty acids as shown. Palmitic acid (C16:0), oleic acid (C18:1), and the very long-chain fatty acid, lignoceric acid (C24:0), activate the ligand sensor in epidermis. This activation, however, is not seen in animals that express either the L279Q or R285G GAL4-dHNF4 mutant ligand sensors. Activation is also seen in the trachea, as shown in the C16:0-treated control tissue.

et al., 2004) and the dHNF4 LBD copurifies with palmitic acid (Yang et al., 2006) (H. Krause, personal communication), we wanted to test whether the dHNF4 ligand sensor could be activated by fatty acids. Consistent with this possibility, increased lipolysis driven by ectopic expression of the Brummer lipase results in increased ligand sensor activity in larval fat bodies (Figure S4) (Gronke et al., 2005). To extend this observation, we conducted organ culture studies using exogenous purified fatty acids. The addition of palmitic acid (C16:0) or oleic acid (C18:1) led to efficient GAL4-dHNF4 activation (Figure 5C). Activation was also seen upon addition of a very long-chain fatty acid, lignoceric acid (C24:0) (Figure 5C,) or an isobranched fatty acid, 14-methyl palmitic acid (Table S7). Although these compounds are not predicted to activate HNF4 based on structural studies (Dhe-Paganon et al., 2002; Wisely et al., 2002), it is possible that metabolites derived from these compounds could bind to and directly activate the dHNF4 LBD. Other LCFAs are capable of activating GAL4-dHNF4, but not cAMP, the PPAR agonist bezafibrate, vitamin D, chenodeoxycholic acid, 9-*cis* retinoic acid, cholesterol, or 20-hydroxyecdysone (Table S7). Although relatively high concentrations of fatty acids were added to the culture medium to see an effect (0.1–1 mM) it is likely that the resulting intracellular concentration is much lower.

If fatty acids activate dHNF4 through its LBD, then specific LBD mutations that disrupt fatty acid binding should reduce its transactivation function. Accordingly, transgenic lines were established that carry GAL4-dHNF4 constructs with point mutations corresponding to specific critical amino acids in the LBD conserved from *Drosophila* to mammals. One of these, R285 in dHNF4 (R226 in HNF4α), orients the fatty acid within the ligand-binding pocket via an ion pair between the carboxylic acid head group of the fatty acid and the guanidinium group of arginine (Dhe-Paganon et al., 2002). Mutation of this amino acid to glycine in HNF4α has no apparent effect on receptor

homodimerization, DNA binding, or coactivator recruitment but eliminates its transactivation function (Aggelidou et al., 2004; Iordanidou et al., 2005). The second LBD mutation tested, L279Q in dHNF4 (L220Q in HNF4α), changes a hydrophobic amino acid that is predicted to interact with the fatty acid ligand (Dhe-Paganon et al., 2002). This mutation in HNF4α also has no apparent effect on receptor homodimerization or DNA binding but eliminates the receptor transactivation function and is unresponsive to coactivators (Aggelidou et al., 2004; Iordanidou et al., 2005). Heat-induced expression of either mutated construct resulted in approximately equal levels of GAL4-dHNF4 protein in transgenic animals (Figure S5) but eliminated the activation seen in mid-third instar larvae (Figure S6) and in starved third instar larvae (Figure S7). Similarly, both mutant GAL4-dHNF4 ligand sensors show no detectable response to exogenous palmitic acid, indicating that key amino acids required for fatty acid binding are needed for GAL4-dHNF4 transcriptional activity and its responsiveness to exogenous LCFAs (Figure 5C).

DISCUSSION

The presence of multiple HNF4 family members in mice and *C. elegans* complicates our understanding of the physiological functions of this nuclear receptor subclass. Here, we characterize the single ancestral HNF4 in *Drosophila*, demonstrating its critical role in regulating the adaptive response to starvation. Our results support a feed-forward model for dHNF4 function in which fatty acids freed from triglycerides activate the receptor, inducing the expression of enzymes that drive lipid mobilization and β-oxidation for energy production.

dHNF4 Plays an Essential Role in Lipid Catabolism

Remarkably, the expression pattern of HNF4 has been conserved through evolution, from flies to mammals, with abundant dHNF4 expression in the midgut, fat body, and Malpighian tubules—tissues that are the functional equivalents of the intestine, liver, and kidney, respectively, where mammalian HNF4 is expressed (Duncan et al., 1994) (Figure 1). The only exception is a lack of dHNF4 expression in the IPCs, the functional equivalent of mammalian pancreatic β cells (Rulifson et al., 2002). dHNF4 is also expressed in the oenocytes, which have hepatocyte-like properties and contribute to lipid mobilization (Gutierrez et al., 2007). The starvation sensitivity of *dHNF4* mutants, however, cannot be rescued by expression of wild-type *dHNF4* in the oenocytes, and starvation-induced lipid accumulation occurs normally in the oenocytes of *dHNF4* mutants, leaving it unclear what role, if any, *dHNF4* plays in these cells.

Although *dHNF4* mutants can survive to adulthood under ideal culture conditions, significant defects become evident upon food deprivation, including an inability to efficiently mobilize stored lipid in the midgut and fat body, increased levels of LCFAs and TAG, and premature death. This retention of lipid is similar to the accumulation of lipids seen in the guts of *nhr-49* mutant worms and the steatosis seen in liver-specific *HNF4α* mutant mice (Hayhurst et al., 2001; Van Gilst et al., 2005a). The ability of *dHNF4* mutant larvae to survive on a sugar diet indicates that glycolysis and oxidative phosphorylation are intact in these animals. Rather, starved *dHNF4* mutant larvae appear to die from an inability to break down TAG and use the resulting free fatty acids for energy production via β-oxidation. Similar phenotypes are associated with defects in β-oxidation in mice and humans, which result in sensitivity to starvation, accumulation of lipid in the liver, and increased levels of free fatty acids (Rinaldo et al., 2002). β-oxidation takes place in the mitochondria or peroxisomes of most organisms, with very long-chain fatty acids (VLCFAs) as the substrate for the peroxisomal pathway. Although peroxisomes are present in the gut and Malpighian tubules of *Drosophila* adults (Beard and Holtzman, 1987) and VLCFAs accumulate in a VLCFA acyl-CoA synthase mutant (Min and Benzer, 1999), the existence of peroxisomes in *Drosophila* larvae remains unclear.

dHNF4 Regulates Genes that Act in Lipid β-Oxidation

Like mammalian *HNF4α*, *dHNF4* mRNA is significantly upregulated in response to starvation (Figure 4A) (Yoon et al., 2001). In addition, many genes in the β-oxidation pathway are upregulated upon starvation and display significantly reduced expression in *dHNF4* mutant larvae (Figure 4A). These include acetyl-CoA synthetase (*AcCoAs*), γ-butyrobetaine dioxygenases, and carnitine acyl transferases, the rate-limiting step in acyl import into mitochondria. In addition, genes that encode the four enzymatic steps of β-oxidation are all dependent on *dHNF4* for their proper level of expression (Figure 4). Importantly, this effect is also seen in fed *dHNF4* mutant larvae, where only 86 transcripts change ≥ 1.3-fold compared to wild-type, many of which encode components of the β-oxidation pathway (Tables S3 and S4). These include *yip2*, *Acox57D-d*, *thiolase*, *scully*, and *CPTI* (*carnitine palmitoyltransferase*) among the most highly downregulated genes in fed *dHNF4* mutants (1.8- to 4-fold as determined by dChip). Thus, *dHNF4* is required for both basal and starvation-induced β-oxidation gene transcription. Moreover, many of the genes in this pathway have at least one canonical binding site for an HNF4 homodimer within 1 kb of their predicted 5′ end, suggesting that dHNF4 directly regulates their transcription (Table S8).

The effects of dHNF4 are not, however, restricted to lipid oxidation. Three predicted lipase transcripts, *lip3*, *CG6295*, and *CG2772*, are significantly reduced in starved *dHNF4* mutants compared to starved controls (Table S5), suggesting a direct role for the receptor in the release of LCFAs from TAG. Similarly, the CGI-58 homolog encoded by *CG1882*, which activates lipolysis in mammals, is upregulated in starved *dHNF4* mutants, whereas adipokinetic hormone receptor (AKHR) is downregulated, consistent with its normal role in mobilizing stored lipids analogous to mammalian β-adrenergic signaling (Grönke et al., 2007). No effect, however, is seen on expression of *brummer*, which encodes adipose triglyceride lipase, suggesting that *dHNF4* does not have a direct impact on *brummer*-mediated lipolysis (Gronke et al., 2005). A VLCFA-CoA ligase gene (*bubblegum*) (Min and Benzer, 1999) and LCFA-CoA ligase gene (*CG6178*) (Oba et al., 2004) are also affected in starved *dHNF4* mutants. These enzymes activate free fatty acids for either catabolic or anabolic processes. We also see effects on lipid synthesis, with downregulation of a predicted fatty acid synthase (*CG3523*), a predicted acetyl-CoA carboxylase (*CG11198*), and two predicted glycerol-3-phosphate acyltransferases (GPATs) (*CG3209* and *CG17608*) in starved *dHNF4* mutants. Two predicted stearoyl-CoA desaturase genes,

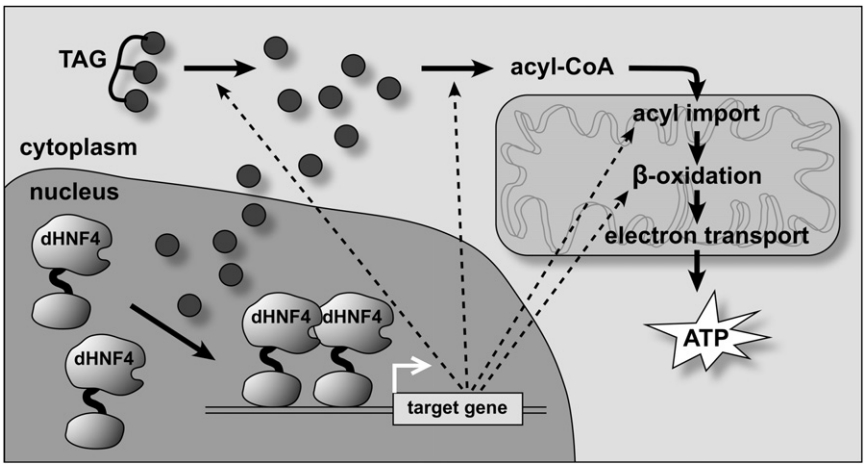

Figure 6. A Feed-Forward Model for dHNF4 in Fatty Acid β-Oxidation

In the absence of dietary nutrients, triglycerides (TAGs) are cleaved by lipases to yield long chain fatty acids (black circles). We propose that these fatty acids can directly or indirectly activate dHNF4 in the nucleus, inducing target gene transcription. The dHNF4 target genes encode lipases as well as enzymes and transporters that use fatty acids as a substrate for β-oxidation in the mitochondria, removing the activating signal for dHNF4 and maintaining energy homeostasis. See text for more details.

CG15531 and *desat1*, which catalyze the production of monounsaturated fatty acids, are also downregulated in the mutant. A similar result has been reported for NHR-49, where a stearoyl-CoA desaturase gene is a key functional target of the receptor (Van Gilst et al., 2005a). The glyoxylate pathway is also affected in *nhr-49* mutants under both fed and starved conditions (Van Gilst et al., 2005b). This pathway is analogous to mammalian ketogenesis, in which fatty acid β-oxidation products are used for energy production. Genes for the central enzymes in this pathway, malate synthase and isocitrate lyase, have not yet been identified in *D. melanogaster*. However, *CG12208*, which is predicted to contribute to glyoxylate catabolism, is downregulated in both fed and starved *dHNF4* mutants. Taken together, these effects on transcription define a central role for dHNF4 in balancing lipid anabolic and catabolic pathways in response to dietary conditions.

Although genome-wide ChIP suggests that HNF4α is a promiscuous regulator of many actively transcribed genes in pancreatic islets and hepatocytes, relatively few targets have been identified in functional studies (Odom et al., 2004). These include multiple apolipoprotein genes, NTCP, and L-FABP, indicating roles in very low-density lipoprotein secretion, high-density lipoprotein synthesis, and bile acid homeostasis (Duncan et al., 1997; Hayhurst et al., 2001). Only a few β-oxidation genes have been studied in *HNF4α* mutant mice, with contradictory results. HNF4α can bind to the promoters of liver CPT-I and MCAD (which encodes an acyl-CoA dehydrogenase), and CPT-I mRNA levels are reduced in *HNF4α* mutant livers (Carter et al., 1993; Louet et al., 2002). In contrast, other studies show that CPT-I, CPT-II, and MCAD transcripts are elevated in *HNF4α* mutant livers (Hayhurst et al., 2001; Rhee et al., 2003). Given our results, it would be interesting to resolve these contradictory observations and more broadly examine other steps in the β-oxidation pathway in *HNF4α* mutant mice.

A Feed-Forward Model for dHNF4 in Driving Fatty Acid β-Oxidation for Energy Production

Although dHNF4 is widely expressed in the larval midgut (Figure 1A), its activity appears to be spatially restricted, primarily to a band of cells at the anterior end of the midgut that lie at the base of the gastric caeca (Figure 5A, arrow) (Palanker et al., 2006). This is the primary site for nutrient absorption into the circulatory system, suggesting that dHNF4 is responsive to dietary signals (Chapman, 1998). In the fat body, the dHNF4 ligand sensor is inactive during most of larval development, when fat storage is favored over fat breakdown, but becomes activated at the end of larval growth, when lipolysis and autophagy are initiated in the fat body (Britton et al., 2002; Rusten et al., 2004) (Figure 5A). Similarly, a significant increase in GAL4-dHNF4 activation is seen in the fat body of starved larvae (Figure 5B), concurrent with the increase in fatty acid β-oxidation that is required to survive these conditions. Consistent with this model, the dHNF4 LBD can be activated by ectopic *bmm* expression or exogenous LCFAs in cultured larval organs. The most effective LCFAs, palmitic acid (C16:0) and oleic acid (C18:1), are relatively abundant in *Drosophila* larvae (Figure 3R) and are the primary constituents of triglycerides that are hydrolyzed upon starvation, making them logical signaling intermediates (Chapman, 1998). In addition, the dHNF4 LBD copurifies with palmitic acid, indicating that fatty acid binding has been conserved through evolution (Yang et al., 2006) (H. Krause, personal communication). Two different point mutations that change conserved amino acids, each of which is predicted to disrupt dHNF4 fatty acid binding, block the ability of the LBD to respond to starvation or exogenous fatty acids, suggesting that direct fatty acid binding is essential for dHNF4 transcriptional activity (Figure 5C).

Taken together, our studies support a feed-forward model in which dHNF4 functions as a sensor for free fatty acid levels in the larva, driving their catabolism through β-oxidation (Figure 6). Upon nutrient deprivation, TAG is hydrolyzed into free LCFAs. As has been shown in mammalian cells, it is likely that these cytosolic LCFAs can translocate into the nucleus, activating dHNF4 (Wolfrum et al., 2001). This, in turn, leads to the transcriptional induction of key genes involved in TAG breakdown, acyl-CoA production, acyl import into mitochondria, and β-oxidation (Figure 6). The net result of this response is consumption of the dHNF4-activating signal (LCFAs), maintaining energy homeostasis through ATP production. This feed-forward model is consistent with the phenotypes of *dHNF4* mutants, which are starvation sensitive and accumulate TAG and LCFAs.

Crystal structure studies of mammalian HNF4α have shown that the fatty acid-bound form of the LBD can assume both open and closed positions, with helix 12 either extended or held against the body of the LBD, whereas the HNF4γ LBD

appears to be locked in the open configuration (Dhe-Paganon et al., 2002; Wisely et al., 2002). Our data, however, indicate that the *Drosophila* HNF4 LBD is responsive to the nutritional status of the animal and can be activated by exogenous LCFAs. Although it is possible that fatty acids act as exchangeable ligands for dHNF4 in vivo, our model is also consistent with a role for fatty acid binding in constitutive dHNF4 transcriptional activation. *dHNF4* mRNA is significantly induced upon starvation (Figure 4A). The resultant newly synthesized protein could act as a sensor for free fatty acids, binding those molecules and thereby forming active dHNF4 transcription complexes. In contrast, dHNF4 protein that is synthesized during stages with less metabolic demand would have access to lower free fatty acid levels and thus remain less active. This model is consistent with our ligand sensor studies, in which newly synthesized GAL4-dHNF4 LBD is inactive in the presence of abundant nutrients (late L2 and early L3) (Figure 5A) and is highly active upon food deprivation (Figure 5B). Our work sets the stage for biochemical studies that address the mechanisms of dHNF4 activation in vivo and whether protein turnover, posttranslational modification, and/or differential cofactor binding modulate the activation of dHNF4 by LCFAs. It also raises the interesting possibility that vertebrate HNF4 may function as a fatty acid sensor.

dHNF4 Functions Like PPARα in Vertebrates

Our feed-forward model for dHNF4 function is reminiscent of that ascribed to a mammalian nuclear receptor, PPARα. PPARα binds LCFAs and directly regulates genes that are orthologous to dHNF4 targets, including many genes in the β-oxidation pathway (Michalik et al., 2006). PPARα mutant mice are defective in the adaptive response to starvation and display increased plasma free fatty acids and fatty liver with enlarged hepatocyte lipid droplets (Lee et al., 1995; Kersten et al., 1999; Leone et al., 1999)—phenotypes shared with *dHNF4* mutants. Van Gilst et al. (2005a) reach a similar conclusion in their characterization of *C. elegans nhr-49* mutants. There are no orthologs of the PPAR nuclear receptor subclass in lower organisms, including *Drosophila* and worms. This is in spite of the fact that PPARα functions—the ability to sense nutrient deprivation and mobilize stored forms of energy to maintain homeostasis—are essential for animal survival. Indeed, even unicellular fungi have an analogous pathway, where the Oaf1/Pip2 transcription factor heterodimer binds the fatty acid oleate and regulates peroxisomal β-oxidation (Karpichev et al., 1997; Phelps et al., 2006). We propose that the ancestral function of HNF4 has been adopted by PPARα during the course of evolution. Our studies also indicate additional functions for dHNF4 beyond lipid mobilization that provide possible directions for future research. In addition, phenotypic characterization of *dHNF4* mutants under different environmental and dietary conditions may provide new insights into dHNF4 activities and raise new implications for the regulation and function of its vertebrate counterparts.

EXPERIMENTAL PROCEDURES

Fly Stocks

Transposable *P* element insertions *EP2449* (Bloomington no. 17249) and *KG08976* (Bloomington no. 16471) were used to generate *dHNF4* mutants by imprecise excision, scoring w^- progeny for lethality in combination with *Df(2L)Te30Cb-1*. The extent of the deletion in each *dHNF4* mutant was determined by PCR and DNA sequencing. The *hs-dHNF4* transgenic line was made by PCR amplifying the *dHNF4* coding sequence (isoform A; FlyBase) using the following primers: 5′-GCGGCCGCATCGGAGAGCCACATAATGC-3′ and 5′- TCTAGAACTGCATATTGCACCGTTCG-3′. The resulting 2050 bp fragment was inserted into the *pCaSPeR-hs-act P* element vector using NotI and XbaI, and transgenic lines were established using standard methods. Flies were maintained on Standard Bloomington Stock Center medium (with malt) at 25°C, with added dry yeast, unless otherwise specified.

Metabolic Assays

For TAG assays, 25 larvae were homogenized in 100 μl PBS, 0.5% Tween 20 and immediately incubated at 70°C for 5 min. Heat-treated homogenate (20 μl) was incubated with either 20 μl PBS or Triglyceride Reagent (Sigma) for 30 min at 37°C, after which the samples were centrifuged at maximum speed for 3 min. Then, 30 μl was transferred to a 96-well plate and incubated with 100 μl of Free Glycerol Reagent (Sigma) for 5 min at 37°C. Samples were assayed using a BioTek Synergy HT microplate spectrophotometer at 540 nm. TAG amounts were determined by subtracting the amount of free glycerol in the PBS-treated sample from the total glycerol present in the sample treated with Triglyceride reagent. TAG levels were normalized to protein amounts in each homogenate using a Bradford assay (Bio-Rad), and data were analyzed using a Student's t test.

For glycogen assays, animals were prepared in an identical manner as described for the TAG assays, except that larvae were homogenized in PBS. Heat-treated homogenate was diluted 1:10 in PBS and centrifuged at maximum speed for 3 min, after which 30 μl supernatant was transferred to each of three wells of a 96-well plate. One well was treated with 100 μl PBS, the second was treated with 100 μl of glucose reagent (Sigma), and the third was treated with 100 μl of glucose reagent and 0.3 U of amyloglucosidase (Sigma). The plate was incubated at 37°C for ~30 min, after which color intensity was measured using a BioTek Synergy HT microplate reader at 540 nm. Glucose and glucose plus glycogen amounts were determined using a standard curve, and the amount of glycogen was determined by subtracting the glucose from the glucose plus glycogen. Total glycogen was normalized to protein amount as described above.

For Nile Red stains, larvae were dissected on a glass slide in 0.00002% Nile Red (Sigma), 75% glycerol and incubated for 5 min before mounting with a coverslip. Slides were imaged within 1 hr of dissection using a Leica TCS SP2 confocal microscope at 40× magnification with an excitation wavelength of 543 nm and an emission of ~626 nm. For oil red O stains, larvae were dissected and fixed for 30 min at room temperature in 4% formaldehyde in PBS. Larval organs were washed twice with PBS and twice in 100% propylene glycol, after which they were incubated with 0.5% oil red O in propylene glycol at 60°C. They were then washed twice in 85% propylene glycol and twice in PBS, both at room temperature, and mounted in 75% glycerol. Slides were imaged on a Zeiss Axioskop 2 plus microscope using a CoolSnap Pro camera and Image Pro Plus software.

Microarrays

Staged late second instar control larvae that were transheterozygous for precise excisions of the *EP2449* and *KG08976 P* elements and $dHNF4^{\Delta 33}$/$dHNF4^{\Delta 17}$ mutant larvae were either fed or starved for 24 hr. RNA was extracted from the apparently healthy animals that molted to the third instar using Trizol (GIBCO) and purified on RNAeasy columns (QIAGEN). All samples were prepared in triplicate to facilitate subsequent statistical analysis. Probe labeling, hybridization to Affymetrix GeneChip® *Drosophila* Genome 2.0 Arrays, and scanning were performed by the University of Maryland Biotechnology Institute Microarray Core Facility. Raw data were normalized using dChip (Li and Hung Wong, 2001) and analyzed using SAM 2.0 (Tusher et al., 2001), with a 5% false positive rate. Comparison between microarray data sets was performed using Microsoft Access.

Organ Culture of *GAL4-dHNF4, UAS-nlacZ* Larvae

Late second instar *hs-GAL4-dHNF4; UAS-nlacZ* larvae (Palanker et al., 2006) were heat treated at 37°C for 30 min and allowed to recover for 1–2 hr at 25°C. These animals were bisected, and the anterior half was rinsed in PBS, everted, and placed in oxygenated Grace's Insect Medium (Invitrogen) containing

0.01% NP-40. Compounds were administered at 0.1–1 mM in freshly oxygenated Grace's Medium plus 0.01% NP-40. The addition of 0.01% Nonidet P-40 to the culture medium is required to reduce the background level of GAL4-dHNF4 activation. Animals were cultured, fixed, and stained with X-gal as described (Palanker et al., 2006).

Statistical Analyses

Statistical significance was calculated using an unpaired two-tailed Student's t test with unequal variance. All quantitative data are reported as the mean ± SEM.

ACCESSION NUMBERS

The National Center for Biotechnology Information Gene Expression Omnibus accession number for the microarray data presented in this paper is GSE14531.

SUPPLEMENTAL DATA

Supplemental Data include Supplemental Experimental Procedures, eight tables, and seven figures and can be found with this article online at http://www.cell.com/cell-metabolism/supplemental/S1550-4131(09)00034-5.

ACKNOWLEDGMENTS

We thank A.-F. Ruaud and M. Sieber for helpful discussions on metabolism and associated protocols, J. Evans for help with collecting staged animals, R. Beckstead and K. Baker for help with antibody affinity purification, R. Beckstead and M. Horner for assistance with microarray analysis, A. Godinez for performing the Affymetrix microarray hybridizations and data collection, J. Cox for help with GC/MS, H. Krause for suggesting the use of NP-40 to reduce ligand sensor background activity, and lab members for critical comments on the manuscript. L.P. was supported by an NIH Predoctoral Training Grant in Genetics, T32 GM007464. This research was supported by NIH grant 1R01 DK075607.

Received: February 28, 2008
Revised: December 15, 2008
Accepted: January 28, 2009
Published: March 3, 2009

REFERENCES

Aggelidou, E., Iordanidou, P., Tsantili, P., Papadopoulos, G., and Hadzopoulou-Cladaras, M. (2004). Critical role of residues defining the ligand binding pocket in hepatocyte nuclear factor-4alpha. J. Biol. Chem. *279*, 30680–30688.

Baker, K.D., and Thummel, C.S. (2007). Diabetic larvae and obese flies—Emerging studies of metabolism in Drosophila. Cell Metab. *6*, 257–266.

Beard, M.E., and Holtzman, E. (1987). Peroxisomes in wild-type and rosy mutant Drosophila melanogaster. Proc. Natl. Acad. Sci. USA *84*, 7433–7437.

Beissbarth, T., and Speed, T.P. (2004). GOstat: Find statistically overrepresented Gene Ontologies within a group of genes. Bioinformatics *20*, 1464–1465.

Britton, J.S., Lockwood, W.K., Li, L., Cohen, S.M., and Edgar, B.A. (2002). Drosophila's insulin/PI3-kinase pathway coordinates cellular metabolism with nutritional conditions. Dev. Cell *2*, 239–249.

Carter, M.E., Gulick, T., Raisher, B.D., Caira, T., Ladias, J.A., Moore, D.D., and Kelly, D.P. (1993). Hepatocyte nuclear factor-4 activates medium chain acyl-CoA dehydrogenase gene transcription by interacting with a complex regulatory element. J. Biol. Chem. *268*, 13805–13810.

Chapman, R. (1998). The Insects: Structure and Function (Cambridge, UK: Cambridge University Press).

Chawla, A., Repa, J.J., Evans, R.M., and Mangelsdorf, D.J. (2001). Nuclear receptors and lipid physiology: Opening the X-files. Science *294*, 1866–1870.

Chen, W.S., Manova, K., Weinstein, D.C., Duncan, S.A., Plump, A.S., Prezioso, V.R., Bachvarova, R.F., and Darnell, J.E., Jr. (1994). Disruption of the HNF-4 gene, expressed in visceral endoderm, leads to cell death in embryonic ectoderm and impaired gastrulation of mouse embryos. Genes Dev. *8*, 2466–2477.

Dhe-Paganon, S., Duda, K., Iwamoto, M., Chi, Y.I., and Shoelson, S.E. (2002). Crystal structure of the HNF4 alpha ligand binding domain in complex with endogenous fatty acid ligand. J. Biol. Chem. *277*, 37973–37976.

Duncan, S.A., Manova, K., Chen, W.S., Hoodless, P., Weinstein, D.C., Bachvarova, R.F., and Darnell, J.E., Jr. (1994). Expression of transcription factor HNF-4 in the extraembryonic endoderm, gut, and nephrogenic tissue of the developing mouse embryo: HNF-4 is a marker for primary endoderm in the implanting blastocyst. Proc. Natl. Acad. Sci. USA *91*, 7598–7602.

Duncan, S.A., Nagy, A., and Chan, W. (1997). Murine gastrulation requires HNF-4 regulated gene expression in the visceral endoderm: Tetraploid rescue of Hnf-4(−/−) embryos. Development *124*, 279–287.

Gerdin, A.K., Surve, V.V., Jonsson, M., Bjursell, M., Bjorkman, M., Edenro, A., Schuelke, M., Saad, A., Bjurstrom, S., Lundgren, E.J., et al. (2006). Phenotypic screening of hepatocyte nuclear factor (HNF) 4-gamma receptor knockout mice. Biochem. Biophys. Res. Commun. *349*, 825–832.

Grönke, S., Mildner, A., Fellert, S., Tennagels, N., Petry, S., Muller, G., Jackle, H., and Kuhnlein, R.P. (2005). Brummer lipase is an evolutionary conserved fat storage regulator in Drosophila. Cell Metab. *1*, 323–330.

Grönke, S., Hirsch, J., Fellert, S., Andreou, A., Haase, T., Jäckle, H., and Kühnlein, R.P. (2007). Dual lipolytic control of body fat storage and mobilization in Drosophila. PLoS Biol. *5*, e137.

Gutierrez, E., Wiggins, D., Fielding, B., and Gould, A.P. (2007). Specialized hepatocyte-like cells regulate Drosophila lipid metabolism. Nature *445*, 275–280.

Hayhurst, G.P., Lee, Y.H., Lambert, G., Ward, J.M., and Gonzalez, F.J. (2001). Hepatocyte nuclear factor 4alpha (nuclear receptor 2A1) is essential for maintenance of hepatic gene expression and lipid homeostasis. Mol. Cell. Biol. *21*, 1393–1403.

Hertz, R., Magenheim, J., Berman, I., and Bar-Tana, J. (1998). Fatty acyl-CoA thioesters are ligands of hepatic nuclear factor-4alpha. Nature *392*, 512–516.

Iordanidou, P., Aggelidou, E., Demetriades, C., and Hadzopoulou-Cladaras, M. (2005). Distinct amino acid residues may be involved in coactivator and ligand interactions in hepatocyte nuclear factor-4alpha. J. Biol. Chem. *280*, 21810–21819.

Karpichev, I.V., Luo, Y., Marians, R.C., and Small, G.M. (1997). A complex containing two transcription factors regulates peroxisome proliferation and the coordinate induction of beta-oxidation enzymes in Saccharomyces cerevisiae. Mol. Cell. Biol. *17*, 69–80.

Kersten, S., Seydoux, J., Peters, J.M., Gonzalez, F.J., Desvergne, B., and Wahli, W. (1999). Peroxisome proliferator-activated receptor alpha mediates the adaptive response to fasting. J. Clin. Invest. *103*, 1489–1498.

Lee, S.S., Pineau, T., Drago, J., Lee, E.J., Owens, J.W., Kroetz, D.L., Fernandez-Salguero, P.M., Westphal, H., and Gonzalez, F.J. (1995). Targeted disruption of the alpha isoform of the peroxisome proliferator-activated receptor gene in mice results in abolishment of the pleiotropic effects of peroxisome proliferators. Mol. Cell. Biol. *15*, 3012–3022.

Leone, T.C., Weinheimer, C.J., and Kelly, D.P. (1999). A critical role for the peroxisome proliferator-activated receptor alpha (PPARalpha) in the cellular fasting response: the PPARalpha-null mouse as a model of fatty acid oxidation disorders. Proc. Natl. Acad. Sci. USA *96*, 7473–7478.

Leopold, P., and Perrimon, N. (2007). Drosophila and the genetics of the internal milieu. Nature *450*, 186–188.

Li, C., and Hung Wong, W. (2001). Model-based analysis of oligonucleotide arrays: Model validation, design issues and standard error application. Genome Biol. *2*, RESEARCH0032.

Louet, J.F., Hayhurst, G., Gonzalez, F.J., Girard, J., and Decaux, J.F. (2002). The coactivator PGC-1 is involved in the regulation of the liver carnitine palmitoyltransferase I gene expression by cAMP in combination with HNF4 alpha and cAMP-response element-binding protein (CREB). J. Biol. Chem. *277*, 37991–38000.

Michalik, L., Auwerx, J., Berger, J.P., Chatterjee, V.K., Glass, C.K., Gonzalez, F.J., Grimaldi, P.A., Kadowaki, T., Lazar, M.A., O'Rahilly, S., et al. (2006).

International Union of Pharmacology. LXI. Peroxisome proliferator-activated receptors. Pharmacol. Rev. *58*, 726–741.

Min, K.T., and Benzer, S. (1999). Preventing neurodegeneration in the Drosophila mutant bubblegum. Science *284*, 1985–1988.

Oba, Y., Ojika, M., and Inouye, S. (2004). Characterization of CG6178 gene product with high sequence similarity to firefly luciferase in Drosophila melanogaster. Gene *329*, 137–145.

Odom, D.T., Zizlsperger, N., Gordon, D.B., Bell, G.W., Rinaldi, N.J., Murray, H.L., Volkert, T.L., Schreiber, J., Rolfe, P.A., Gifford, D.K., et al. (2004). Control of pancreas and liver gene expression by HNF transcription factors. Science *303*, 1378–1381.

Palanker, L., Necakov, A.S., Sampson, H.M., Ni, R., Hu, C., Thummel, C.S., and Krause, H.M. (2006). Dynamic regulation of Drosophila nuclear receptor activity in vivo. Development *133*, 3549–3562.

Phelps, C., Gburcik, V., Suslova, E., Dudek, P., Forafonov, F., Bot, N., MacLean, M., Fagan, R.J., and Picard, D. (2006). Fungi and animals may share a common ancestor to nuclear receptors. Proc. Natl. Acad. Sci. USA *103*, 7077–7081.

Rhee, J., Inoue, Y., Yoon, J.C., Puigserver, P., Fan, M., Gonzalez, F.J., and Spiegelman, B.M. (2003). Regulation of hepatic fasting response by PPARgamma coactivator-1alpha (PGC-1): Requirement for hepatocyte nuclear factor 4alpha in gluconeogenesis. Proc. Natl. Acad. Sci. USA *100*, 4012–4017.

Rinaldo, P., Matern, D., and Bennett, M.J. (2002). Fatty acid oxidation disorders. Annu. Rev. Physiol. *64*, 477–502.

Robinson-Rechavi, M., Maina, C.V., Gissendanner, C.R., Laudet, V., and Sluder, A. (2005). Explosive lineage-specific expansion of the orphan nuclear receptor HNF4 in nematodes. J. Mol. Evol. *60*, 577–586.

Rulifson, E.J., Kim, S.K., and Nusse, R. (2002). Ablation of insulin-producing neurons in flies: Growth and diabetic phenotypes. Science *296*, 1118–1120.

Rusten, T.E., Lindmo, K., Juhász, G., Sass, M., Seglen, P.O., Brech, A., and Stenmark, H. (2004). Programmed autophagy in the Drosophila fat body is induced by ecdysone through regulation of the PI3K pathway. Dev. Cell *7*, 179–192.

Scott, R.C., Schuldiner, O., and Neufeld, T.P. (2004). Role and regulation of starvation-induced autophagy in the Drosophila fat body. Dev. Cell *7*, 167–178.

Shih, D.Q., Dansky, H.M., Fleisher, M., Assmann, G., Fajans, S.S., and Stoffel, M. (2000). Genotype/phenotype relationships in HNF-4alpha/MODY1: Haploinsufficiency is associated with reduced apolipoprotein (AII), apolipoprotein (CIII), lipoprotein(a), and triglyceride levels. Diabetes *49*, 832–837.

Stoffel, M., and Duncan, S.A. (1997). The maturity-onset diabetes of the young (MODY1) transcription factor HNF4alpha regulates expression of genes required for glucose transport and metabolism. Proc. Natl. Acad. Sci. USA *94*, 13209–13214.

Sullivan, A.A., and Thummel, C.S. (2003). Temporal profiles of nuclear receptor gene expression reveal coordinate transcriptional responses during Drosophila development. Mol. Endocrinol. *17*, 2125–2137.

Tusher, V.G., Tibshirani, R., and Chu, G. (2001). Significance analysis of microarrays applied to the ionizing radiation response. Proc. Natl. Acad. Sci. USA *98*, 5116–5121.

Van Gilst, M.R., Hadjivassiliou, H., Jolly, A., and Yamamoto, K.R. (2005a). Nuclear hormone receptor NHR-49 controls fat consumption and fatty acid composition in C. elegans. PLoS Biol. *3*, e53.

Van Gilst, M.R., Hadjivassiliou, H., and Yamamoto, K.R. (2005b). A Caenorhabditis elegans nutrient response system partially dependent on nuclear receptor NHR-49. Proc. Natl. Acad. Sci. USA *102*, 13496–13501.

Wisely, G.B., Miller, A.B., Davis, R.G., Thornquest, A.D., Jr., Johnson, R., Spitzer, T., Sefler, A., Shearer, B., Moore, J.T., Miller, A.B., et al. (2002). Hepatocyte nuclear factor 4 is a transcription factor that constitutively binds fatty acids. Structure *10*, 1225–1234.

Wolfrum, C., Borrmann, C.M., Borchers, T., and Spener, F. (2001). Fatty acids and hypolipidemic drugs regulate peroxisome proliferator-activated receptors alpha - and gamma-mediated gene expression via liver fatty acid binding protein: A signaling path to the nucleus. Proc. Natl. Acad. Sci. USA *98*, 2323–2328.

Yamagata, K., Furuta, H., Oda, N., Kaisaki, P.J., Menzel, S., Cox, N.J., Fajans, S.S., Signorini, S., Stoffel, M., and Bell, G.I. (1996). Mutations in the hepatocyte nuclear factor-4alpha gene in maturity-onset diabetes of the young (MODY1). Nature *384*, 458–460.

Yang, P., Sampson, H.M., and Krause, H.M. (2006). A modified tandem affinity purification strategy identifies cofactors of the Drosophila nuclear receptor dHNF4. Proteomics *6*, 927–935.

Yoon, J.C., Puigserver, P., Chen, G., Donovan, J., Wu, Z., Rhee, J., Adelmant, G., Stafford, J., Kahn, C.R., Granner, D.K., et al. (2001). Control of hepatic gluconeogenesis through the transcriptional coactivator PGC-1. Nature *413*, 131–138.

Zhong, W., Sladek, F.M., and Darnell, J.E., Jr. (1993). The expression pattern of a Drosophila homolog to the mouse transcription factor HNF-4 suggests a determinative role in gut formation. EMBO J. *12*, 537–544.

Zinke, I., Schutz, C.S., Katzenberger, J.D., Bauer, M., and Pankratz, M.J. (2002). Nutrient control of gene expression in Drosophila: Microarray analysis of starvation and sugar-dependent response. EMBO J. *21*, 6162–6173.

Cell Metabolism
Article

TORC2 Regulates Hepatic Insulin Signaling via a Mammalian Phosphatidic Acid Phosphatase, LIPIN1

Dongryeol Ryu,[1,6] Kyoung-Jin Oh,[1,6] Hee-Yeon Jo,[1] Susan Hedrick,[2] Yo-Na Kim,[3] Yu-Jin Hwang,[3] Tae-Sik Park,[3] Joong-Soo Han,[5] Cheol Soo Choi,[3,4] Marc Montminy,[2] and Seung-Hoi Koo[1,*]
[1]Department of Molecular Cell Biology, Sungkyunkwan University School of Medicine, 300 Chunchun-dong, Jangan-gu, Suwon, Gyeonggi-do 440-746, Korea
[2]Peptide Biology Laboratories, Salk Institute for Biological Studies, La Jolla, CA 92037, USA
[3]Lee Gil Ya Cancer and Diabetes Institute
[4]Division of Endocrinology
Gil Medical Center, Gachon University of Medicine and Science, Incheon 405-760, Korea
[5]Institute of Biomedical Science and Department of Biochemistry and Molecular Biology, College of Medicine, Hanyang University, Seoul 133-791, Korea
[6]These authors contributed equally to this work
*Correspondence: shkoo@med.skku.ac.kr
DOI 10.1016/j.cmet.2009.01.007

SUMMARY

TORC2 is a major transcriptional coactivator for hepatic glucose production. Insulin impedes gluconeogenesis by inhibiting TORC2 via SIK2-dependent phosphorylation at Ser171. Interruption of this process greatly perturbs hepatic glucose metabolism, thus promoting hyperglycemia in rodents. Here, we show that hyperactivation of TORC2 would exacerbate insulin resistance by enhancing expression of LIPIN1, a mammalian phosphatidic acid phosphatase for diacylglycerol (DAG) synthesis. Diet-induced or genetic obesity increases *LIPIN1* expression in mouse liver, and TORC2 is responsible for its transcriptional activation. While overexpression of LIPIN1 disturbs hepatic insulin signaling, knockdown of LIPIN1 ameliorates hyperglycemia and insulin resistance by reducing DAG and PKCε activity in *db/db* mice. Finally, TORC2-mediated insulin resistance is partially rescued by concomitant knockdown of LIPIN1, confirming the critical role of LIPIN1 in the perturbation of hepatic insulin signaling. These data propose that dysregulation of TORC2 would further exaggerate insulin resistance and promote type 2 diabetes in a LIPIN1-dependent manner.

INTRODUCTION

Insulin resistance is a major predicament for the development of type 2 diabetes. Increased infusion of free fatty acids into the peripheral tissues due to the atherogenic diets or obesity directs to the accumulation of intracellular free fatty acids, which then leads to the generation of various second messengers for signaling cascades, including diacylglycerol (DAG), a major activator for protein kinase C (PKC) families (Savage et al., 2007). Among family members, PKCε is known to be involved in reducing insulin receptor (IR) kinase activity, thus inhibiting insulin-mediated signaling cascades in liver (Samuel et al., 2004, 2007).

Previously identified as a gene product that is responsible for the pathophysiology of *fld* mice, which show occurrence of neonatal fatty liver that is accompanied by hypertriglyceridemia and lipodystrophy phenotypes, LIPIN1 is later shown to be involved in various pathways in lipid metabolism in diverse cell types such as liver, adipose tissues, muscle, and neuronal cells (Finck et al., 2006; Peterfy et al., 2001, 2005; Phan et al., 2004; Phan and Reue, 2005; Reue and Zhang, 2008; Verheijen et al., 2003). Depletion of *LIPIN1* gene in preadipocytes delays the fat cell differentiation, and *fld* mice that lack expression of functional LIPIN1 display lipodystrophy-associated insulin resistance, perhaps due to the lack of adipokine generation, showing the importance of adipose-specific LIPIN1 function in lipid homeostasis and systemic insulin signaling. On the other hand, muscle-specific *LIPIN1* transgenic mice show insulin resistance and obesity phenotypes, suggesting the presence of differential functions of LIPIN1 in different cell types. The role of LIPIN1 in liver is somewhat more complicated. LIPIN1 appears to function as a coactivator for PPARα/PGC-1α to transcriptionally regulate fatty acid oxidation gene expression. At the same time, two recent reports suggest contradicting results regarding functions of LIPIN1 in the regulation of triglyceride synthesis and VLDL secretion, depending on the systems utilized (Chen et al., 2008; Khalil, 2009). The presence of other isoforms, LIPIN2 and LIPIN3, makes it hard to determine the sole contribution of LIPIN1 in hepatic lipid metabolism (Reue and Dwyer, 2008). Surprisingly, LIPIN1 is later identified as a cytosolic phosphatidic acid phosphatase (PAP) that would generate DAG in response to increase in intracellular free fatty acid levels (Carman and Han, 2006; Donkor et al., 2007; Han et al., 2006, 2007; Reue and Zhang, 2008). The PAP function of LIPIN1 could potentially link this protein with free fatty acid-induced perturbation of insulin signaling that is observed in muscle-specific *LIPIN1* transgenic mice (Phan and Reue, 2005).

TORC2 is a major transcriptional coregulator for hepatic glucose output in response to fasting in mammals (Koo et al., 2005). While fasting triggers a rapid dephosphorylation and nuclear entry of TORC2 to promote hepatic gluconeogenesis,

feeding induces insulin signaling cascades that would enhance the activity of inhibitory serine/threonine kinase SIK2 to reverse the process by phosphorylating Ser171 residue of TORC2, resulting in the retention of this factor in the cytoplasm in association with 14-3-3 proteins (Dentin et al., 2007; Screaton et al., 2004). During insulin-resistant conditions, however, TORC2 remains in the nucleus and is actively involved in coactivating CREB-target gluconeogenic gene expression, in part due to the inactivation of AKT-mediated SIK2, which results in hyperglycemia that would further exacerbate the insulin-resistant phenotype and ultimately bring about the type 2 diabetes.

Here, we report that TORC2 transcriptionally activates *LIPIN1* expression during fasting and insulin-resistant conditions in mouse liver. Overexpression of LIPIN1 in primary hepatocytes indeed increases DAG production and results in inactivation of AKT due to the activation of PKCε. Furthermore, adenovirus-mediated knockdown of hepatic LIPIN1 in diabetic *db/db* mice greatly alleviates hyperglycemia as well as hepatic insulin resistance. These data support that TORC2-mediated induction of *LIPIN1* expression during insulin resistance would greatly contribute to the further exacerbation of hyperglycemia and the progression of type 2 diabetes.

RESULTS

S171A TORC2 Promotes Hepatic Insulin Resistance

As reported previously, Ser171 residue of TORC2 is targeted by AMPK and AMPK-related kinases, including SIK kinases, and is critical for determining its cellular localization (Koo et al., 2005; Shaw et al., 2005). Mutation of this residue into alanine results in constant nuclear localization of TORC2, which leads to the unregulated activation of TORC2/CREB target genes. Indeed, mice injected with adenovirus for Ser171 to alanine mutant TORC2 (S171A TORC2) show higher blood glucose levels as well as increased expression of gluconeogenic genes (Figures 1A and 1C) relative to mice with GFP control adenovirus injection. Unexpectedly, S171A TORC2 mice show impaired glucose tolerance compared with GFP mice (Figure 1B). We would speculate this is due to either the increased gluconeogenic/decreased glycolytic gene expression or the increased TORC2 target gene expression in S171A mouse that would potentially perturb insulin signaling in this setting.

LIPIN1 Is a Transcriptional Target of TORC2 in Liver

To gain a further insight into the nature of this phenomenon, we performed microarray analysis using RNAs from mouse liver infected with either TORC2 RNAi adenovirus or US control RNAi adenovirus. As shown previously, several TORC2/CREB target genes in the gluconeogenesis are downregulated by TORC2 knockdown in microarray analysis (Table 1) and are confirmed by quantitative PCR (Q-PCR) (Figure 1E). Knockdown of TORC2 does not promote changes in expression of several glycolytic enzyme genes. Surprisingly, we noticed a change in gene expression levels of *LIPIN1*, a member of mammalian PAP families, by TORC2 knockdown. Fasting and either diet-induced or genetic insulin resistance in mouse enhance hepatic *LIPIN1* expression (Figures 2A, 2B, and S1–S4), while SIK expression greatly inhibits it (Figures S5–S7), showing similar regulatory patterns with gluconeogenic *PEPCK* gene in these settings. Indeed, we were able to confirm the increased expression of *LIPIN1*, but not of *LIPIN2* or *3*, by S171A TORC2 infection in mouse liver or in primary hepatocytes (Figures 1C, 1D, and 2C). Furthermore, expression of *LIPIN1* is increased by TORC2 and inhibited by CREB inhibitor ACREB in primary hepatocytes, further confirming that TORC2/CREB might regulate *LIPIN1* expression in liver (data not shown). To verify whether TORC2/CREB would regulate *LIPIN1* expression at the transcriptional level, we obtained *LIPIN1* promoter from mouse genomic DNA and performed transient transfection assays in HepG2 cells. We chose to utilize sequences upstream of exon 1b as a hepatic promoter for *LIPIN1*, since exon 1b appears to be selectively expressed over exon 1a in hepatocytes. Moreover, hepatic *LIPIN1* transcript with exon 1b is regulated by fasting or insulin–resistance mouse models, as shown by RT-PCR analysis using differential exon-specific primers (Figure S8). Interestingly, *LIPIN1* promoter is upregulated by TORC2 cotransfection in the presence of PKA, and TORC2-/cAMP-responsive region is localized −85 to +56 from the putative transcriptional start site (Figures 2D and 2E). TORC2 occupies promoter regions of several CREB target genes, such as *PEPCK* or *G6Pase*, and the occupancy of TORC2 on the *LIPIN1* promoter is also confirmed by chromatin immunoprecipitation assay in mouse primary hepatocytes, further confirming that TORC2 regulates *LIPIN1* expression at the transcriptional level in vivo (Figure 2F).

LIPIN1 Expression Increases DAG Production and Inhibits Insulin Signaling in Primary Hepatocytes

Increased production of DAG is linked to obesity-related insulin resistance in peripheral tissues (Samuel et al., 2004, 2007; Savage et al., 2007). Since LIPIN1 was previously reported as a mammalian cytosolic PAP in other cell types, we wanted to verify whether this protein functions similarly in liver. Adenovirus-mediated overexpression of wild-type (WT) LIPIN1 or LIPIN2 induces DAG production in response to palmitate treatment, while LIPIN1 with mutations in previously defined phosphatase active sites does not promote such events in primary hepatocytes (Figures 3A and S9). In accordance with increased DAG production by WT LIPIN1, Ser729 phosphorylation of PKCε, a major noncanonical PKC isoform in liver, is much more pronounced with WT LIPIN1-infected cells compared with cells infected with GFP or PAP mutant LIPIN1 in response to phosphatidic acid (PA) treatments, a direct substrate for LIPIN1 (Figure 3C). In addition, Ser473 phosphorylation of AKT is accordingly more dramatically reduced in WT LIPIN1 infected cells with treatment of PA (over 34-fold in WT LIPIN1 versus less than 10-fold in PAP mutant LIPIN1) (Figures 3B and 3C), suggesting that increased expression of LIPIN1 in the abundance of its substrates could promote insulin resistance in liver. To test whether the disturbance of insulin signaling may affect gluconeogenic gene expression, we infected primary hepatocytes with GFP control, WT LIPIN1, or PAP mutant LIPIN1 adenoviruses in the absence or in the presence of PA/insulin. Expression of either WT or PAP mutant LIPIN1 does not promote significant changes in *PGC-1α* or *PEPCK* mRNA levels in the absence or in the presence of PA without insulin treatment (Figure 3D). As expected, short-term treatment of insulin (4 hr) dramatically reduces mRNA levels of both genes. Indeed, PA treatment slightly blocks insulin-mediated inhibition of *PEPCK* gene

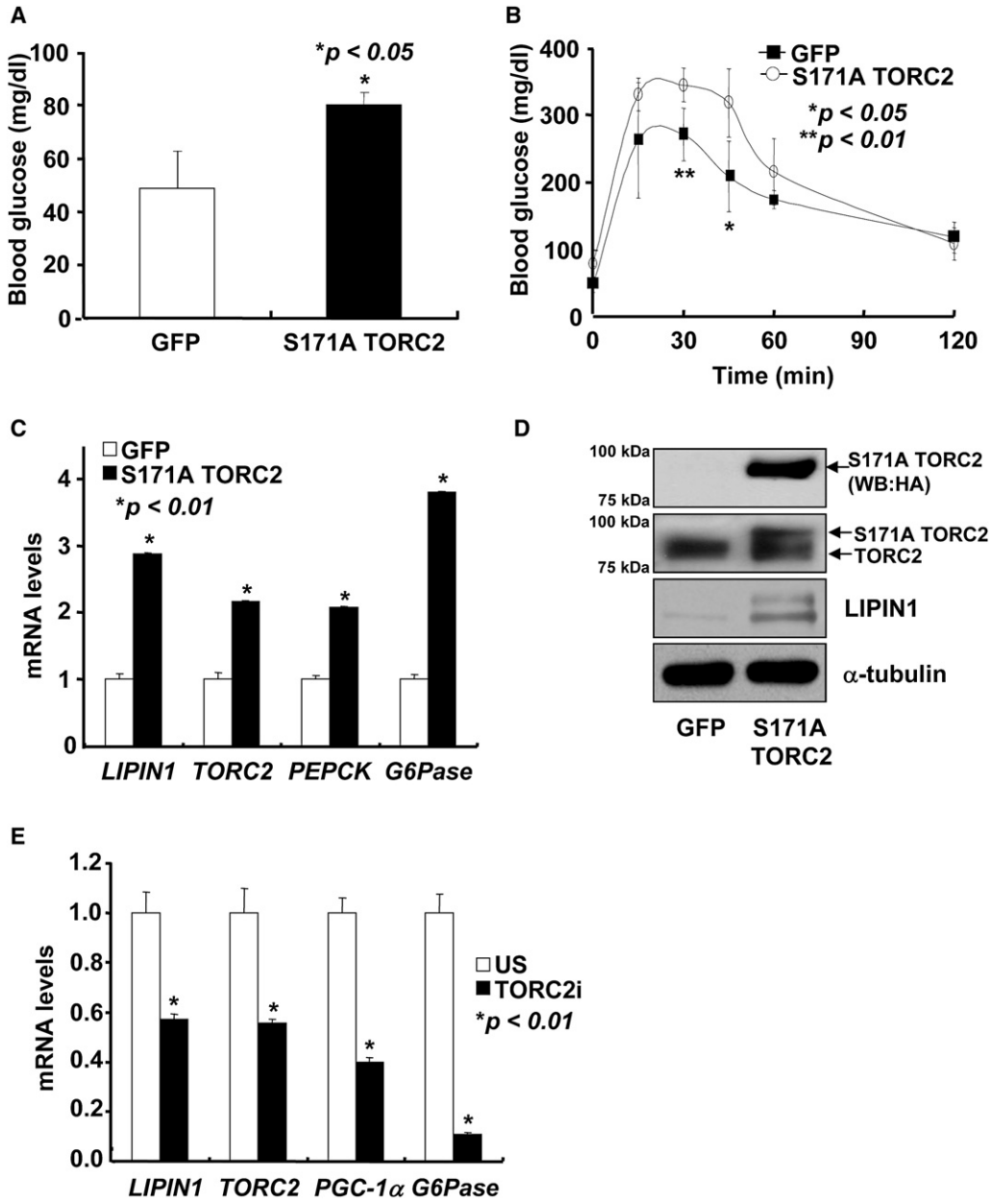

Figure 1. TORC2 Promotes Elevations in Blood Glucose Levels and Glucose Intolerance

(A) Sixteen hour fasting glucose levels in mice expressing Ad-GFP or Ad-S171A TORC2 (*p < 0.05; n = 3).

(B) Glucose tolerance test (GTT) of Ad-GFP and Ad-S171A TORC2 mice (*p < 0.05; **p < 0.01; n = 3).

(C) Effects of Ad-S171A TORC2 infection on *LIPIN1* gene expression; Q-PCR analysis of hepatic *LIPIN1*, *TORC2*, *PEPCK*, and *G6Pase* expression using hepatic RNAs from Ad-GFP or Ad-S171A TORC2-injected mice (*p < 0.01; n = 3).

(D) Western blot analysis of hepatic TORC2 and LIPIN1 levels in mice infected with Ad-GFP or Ad-S171A TORC2 virus. HA-TORC2 levels are shown on the top panel.

(E) Effects of TORC2 knockdown on *LIPIN1* gene expression; Q-PCR analysis of hepatic *LIPIN1*, *TORC2*, *PEPCK*, and *G6Pase* expression using hepatic RNAs from Ad-US control RNAi adenovirus or Ad-TORC2 RNAi virus-injected mice (*p < 0.01; n = 3). Data in (A)–(C) and (E) represent mean ± SD.

expression; the effect of PA is significantly augmented by overexpression of WT but not PAP mutant LIPIN1. These data suggest that LIPIN1 may not directly regulate gluconeogenic expression at the transcriptional level, but block insulin-dependent regulation of these genes by disturbing hepatic insulin signaling via its DAG-producing activity.

Knockdown of Hepatic LIPIN1 Improves Diabetic Conditions in *db/db* Mice

To verify the functional significance of LIPIN1 in the insulin resistance in vivo, we prepared adenovirus for *LIPIN1* shRNA and injected it into the *db/db* diabetic mice, widely utilized rodent models displaying peripheral insulin resistance. Interestingly,

Table 1. Results of cDNA Microarray Data

	Gene symbol	Fold induction
shTORC2/US	*LIPIN1**	0.733
	LIPIN2	1.018
	LIPIN3	1.131
	*G6pase**	0.478
	*PGC-1α**	0.809
	PC	0.803
	FBP1	0.702
	GCK	1.023
	PFK1	0.871
	ADOLB	1.192
	PFKFB2	0.923

G6pase, glucose-6-phosphatase; *PGC-1α*, peroxisome proliferator-activated receptor gamma coactivator 1 α; *PC*, pyruvate carboxylase; *FBP1*, Fructose-1,6-bisphosphatase 1;. *GCK*, glucokinase; *PFK1*, liver-type phosphofructokinase; *ALDOB*, aldolase B; *PFKFB2*, 6-phosphofructo-2-kinase/fructose-2,6-bisphosphatase 2. n = 3, C57BL/6, liver.
*Confirmed by Q-PCR (Figure 1E).

LIPIN1 expression is highly induced in livers of diabetic mice, as shown in Figure 2B and in the previous report (Finck et al., 2006). Knockdown of hepatic LIPIN1 is verified by Q-PCR as well as western blot analysis (Figures 4C, 4D, and 5A). Surprisingly, LIPIN1 knockdown greatly lowers blood glucose level that is associated with reduction in key gluconeogenic gene expression (Figures 4A, 5A, and S10). Moreover, intraperitoneal glucose tolerance test (GTT) reveals the improvement in glucose intolerance of *db/db* mice with LIPIN1 knockdown compared with mice with control viruses, suggesting a notion of increased hepatic insulin sensitivity with reduced hepatic LIPIN1 expression (Figure 4B). Indeed, tyrosine phosphorylation of IR, as well as serine phosphorylation of AKT, FOXO1, and GSK3β, is greatly increased by LIPIN1 knockdown both in basal and insulin-induced conditions (Figures 4C, 4D, and S11). While there are no changes in plasma TAG and NEFA levels (Figure S12), hepatic DAG and TAG levels are greatly reduced with Ad-LIPIN1 RNAi infection (Figure 5B). Moreover, phosphorylation level of PKCε is also significantly diminished (Figures 4C and 4D), further corroborating the notion that hepatic LIPIN1 knockdown improves insulin sensitivity in insulin-resistant conditions. To further evaluate the functional consequences of LIPIN1 deficiency in insulin and glucose metabolism in vivo, we performed the 140 min hyperinsulinemic-euglycemic clamp studies in conscious *db/db* mice. Basal hepatic glucose production of LIPIN1 knockdown mice tends to be lower than that of control mice ($p = 0.09$) (Figure 5C). During the clamp periods, plasma insulin was infused at a constant rate (30 pmol/kg/min) to raise plasma insulin within a physiological range, and plasma glucose was clamped at about 6.7 mM. Indeed, knockdown of LIPIN1 increases hepatic insulin sensitivity, as reflected by ~70% higher suppression of endogenous glucose production from LIPIN1-deficient mice compared to control groups (Figure 5C). However, there are no significant differences in whole-body glucose uptake, glycolysis, and glycogen synthesis between the two groups (Figure 5E). Consistent with no changes in peripheral insulin sensitivity other than that of liver, muscle glucose uptake does not show differences between the two groups of mice (Figure 5D).

LIPIN1 Knockdown Prevents S171A TORC2-Induced Insulin Resistance

Finally, we wanted to confirm whether S171A TORC2-induced glucose intolerance in mice is due to the increased expression of *LIPIN1*. Thus, Ad-LIPIN1 RNAi virus was coinjected with Ad-S171A TORC2 virus in normal mice and compared with Ad-GFP + Ad-US groups and Ad-S171A TORC2 + Ad-US groups. Ad-GFP + Ad-LIPIN1 RNAi group is not included, since we did not observe changes in blood glucose or glucose tolerance with LIPIN1 knockdown only in WT mice (data not shown). Indeed, the elevation of both 4 hr fasting and regular-feeding blood glucose levels caused by S171A TORC2 expression alone is resolved by the additional infection of LIPIN1 RNAi adenovirus (Figures 6A and 6B). Consistent with the role of LIPIN1 in the disturbance of insulin-mediated regulation of gluconeogenic gene expression, LIPIN1 RNAi-mediated reduction of *PEPCK*, *G6Pase*, or *PGC-1α* mRNA levels is much more pronounced in feeding conditions than in 4 hr fasting conditions (Figure 6E). Improved insulin sensitivity is also indicated by enhanced glucose clearance in GTT assay with S171A TORC2 + LIPIN1 RNAi groups over S171A TORC2 + US mice (Figure 6C). Moreover, reduction in serine phosphorylation of AKT or FOXO1 and induction of serine phosphorylation of PKCε in S171A TORC2 mice are restored to control levels by additional LIPIN1 knockdown both in basal state and insulin-injected conditions, showing that S171A TORC2-mediated insulin resistance is indeed partially rescued by LIPIN1 deficiency (Figures 6D and S13). The insulin levels tend to be lower with S171A TORC2 + LIPIN1 RNAi groups over S171A TORC2 + US mice under both 4 hr fasting and feeding conditions, reflecting the normalized glycemia in this setting (Figure S14).

DISCUSSION

TORC2 has been shown to be a major regulator for hepatic glucose production by directing transcriptional activation of gluconeogenic genes (Koo et al., 2005). In our study, we would now suggest another role for this coactivator as an instigator of the hepatic insulin resistance by activating LIPIN1. Hepatic expression of LIPIN1, a member of mammalian Mg^{2+}-dependent PAPs, is transcriptionally controlled by TORC2 in a CREB-dependent manner. Hepatic *LIPIN1* expression is higher in mouse models with diet-induced or genetic obesity and insulin resistance, conditions previously associated with constitutive activation of TORC2 due to the impaired insulin actions (Dentin et al., 2007; Screaton et al., 2004). We found that high-level expression of LIPIN1 increases intracellular DAG levels and perturbs insulin signaling in part via a PKCε-mediated pathway. We showed that reducing LIPIN1 expression in liver indeed improves hepatic insulin sensitivity and normalizes hyperglycemia by reducing hepatic DAG levels and PKCε activity in diabetic *db/db* mice. Furthermore, constitutively active TORC2-mediated hepatic insulin resistance is partially blunted by concomitant knockdown of LIPIN1, suggesting that TORC2-dependent expression of LIPIN1 could indeed be responsible for this phenomenon (see Figure 6F for a model).

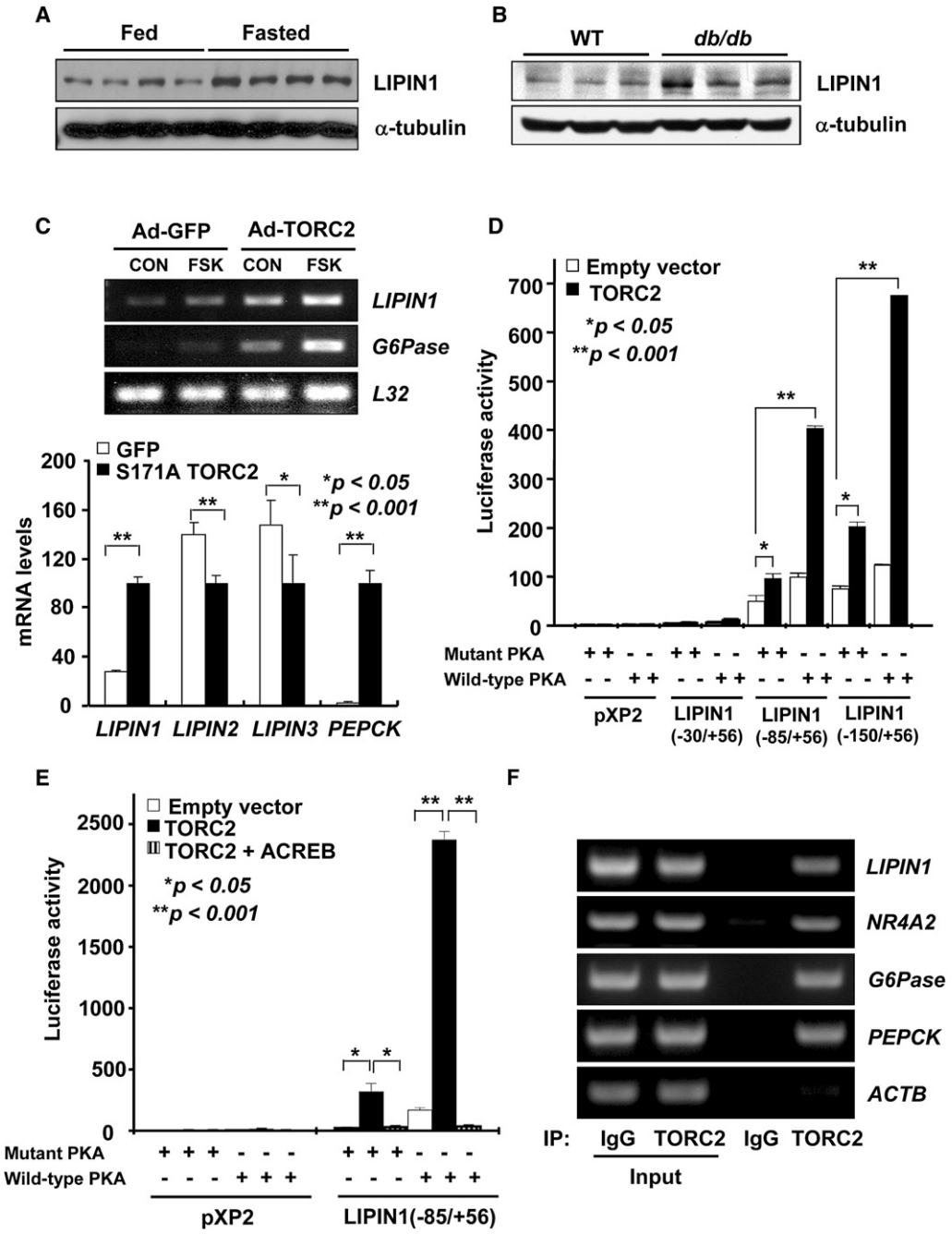

Figure 2. TORC2 Activates Transcription of Hepatic *LIPIN1*

(A) Western blot assay showing hepatic LIPIN1 expression in mice under fed or fasted conditions.

(B) Western blot assay showing hepatic LIPIN1 expression in WT or *db/db* mice.

(C) RT-PCR analysis showing effect of TORC2 pathway on mRNA levels of *LIPIN1* and *G6Pase* (top) or *LIPIN* family members and *PEPCK* (bottom) in rat primary hepatocytes. Cells were infected with adenoviruses for GFP, TORC2, or S171A TORC2 for 48 hr and then exposed to forskolin or DMSO for 2 hr (*$p < 0.05$; **$p < 0.001$; n = 3).

(D) Transient assays of HepG2 cells transfected with LIPIN1 luciferase constructs (*$p < 0.05$; **$p < 0.001$; n = 3).

(E) Transient assays of HepG2 cells transfected with LIPIN1 luciferase construct showing effects of expression vector for CREB dominant-negative polypeptide (ACREB) on *LIPIN1* transcription (*$p < 0.05$; **$p < 0.001$; n = 3).

(F) Chromatin immunoprecipitation showing the occupancy of TORC2 on *LIPIN1* and gluconeogenic promoters in mouse primary hepatocytes. Data in (C)–(E) represent mean ± SD.

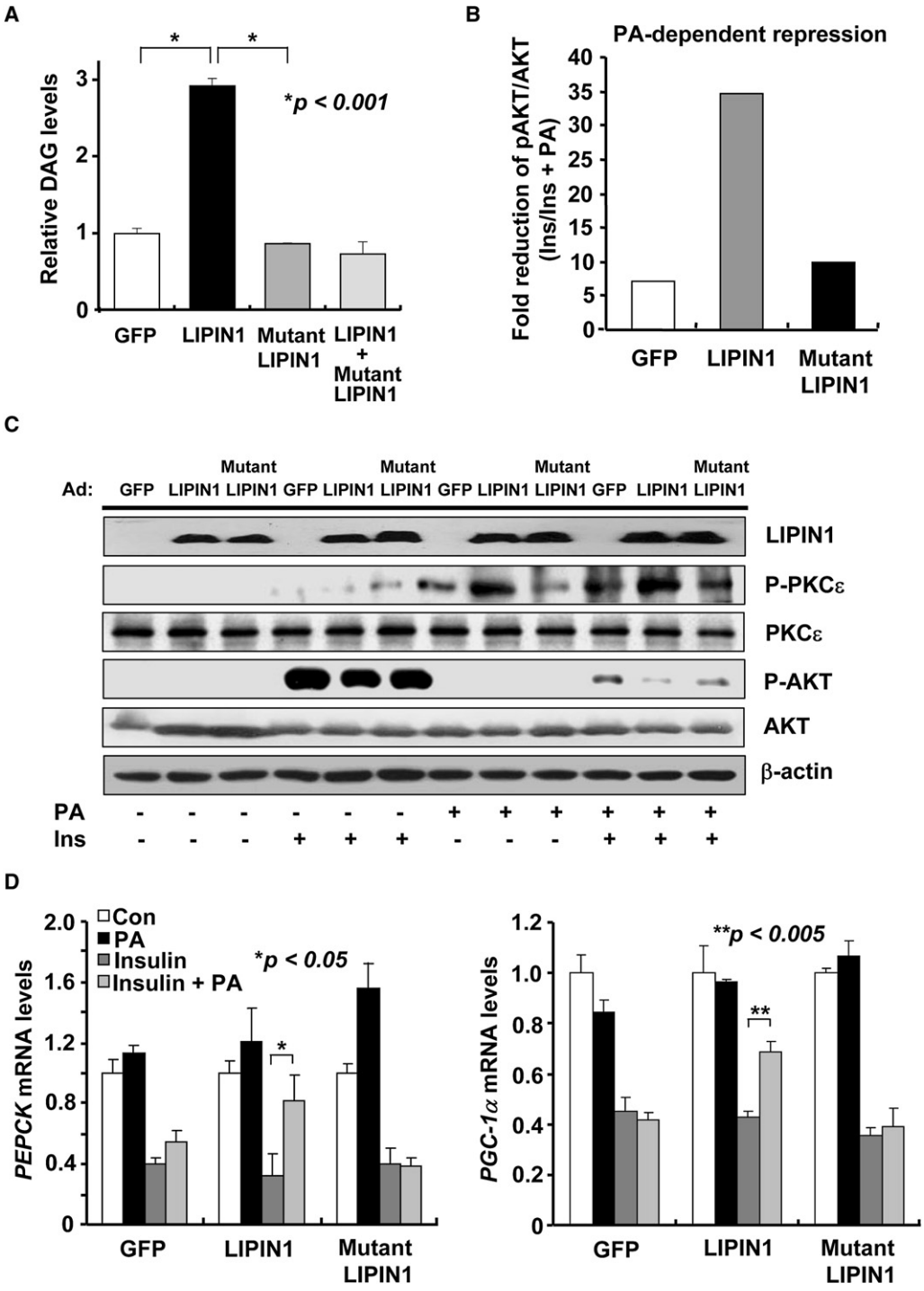

Figure 3. LIPIN1-Mediated DAG Production Is Linked to Hepatic Insulin Resistance

(A) Representative thin-layer chromatography analysis of formation of DAG in mouse primary hepatocytes infected with Ad-GFP, Ad-WT LIPIN1, or mutant Ad-LIPIN1 (D712E, D714E) (*$p < 0.001$; n = 3).

(B) Quantitation showing relative effects of PA on insulin-dependent AKT phosphorylation from cells infected with Ad-GFP, Ad-LIPIN1, or mutant Ad-LIPIN1 as in (C). The intensities of the bands were quantified by ImageJ (version 1.36×, NIH).

(C) Western blot analysis showing effects of Ad-GFP, Ad-LIPIN1, or mutant Ad-LIPIN1 on phospho-serine and total levels of AKT and PKCε. Mouse primary hepatocytes were infected with Ad-GFP, Ad-LIPIN1, or mutant Ad-LIPIN1 and then exposed to PA (50 μM) for 2 hr prior to 10 min stimulation of 100 nM insulin.

(D) Q-PCR analysis showing effect of LIPIN1 on mRNA levels of *PEPCK* (left) and *PGC-1α* (right). Cells were infected with adenoviruses for GFP, LIPIN1, or mutant LIPIN1 for 48 hr and then cultured in the absence or in the presence of 100 μM PA (2 hr) and/or 100 nM insulin (4 hr) (*$p < 0.05$; **$p < 0.005$; n = 3). Data in (A) and (D) represent mean ± SD.

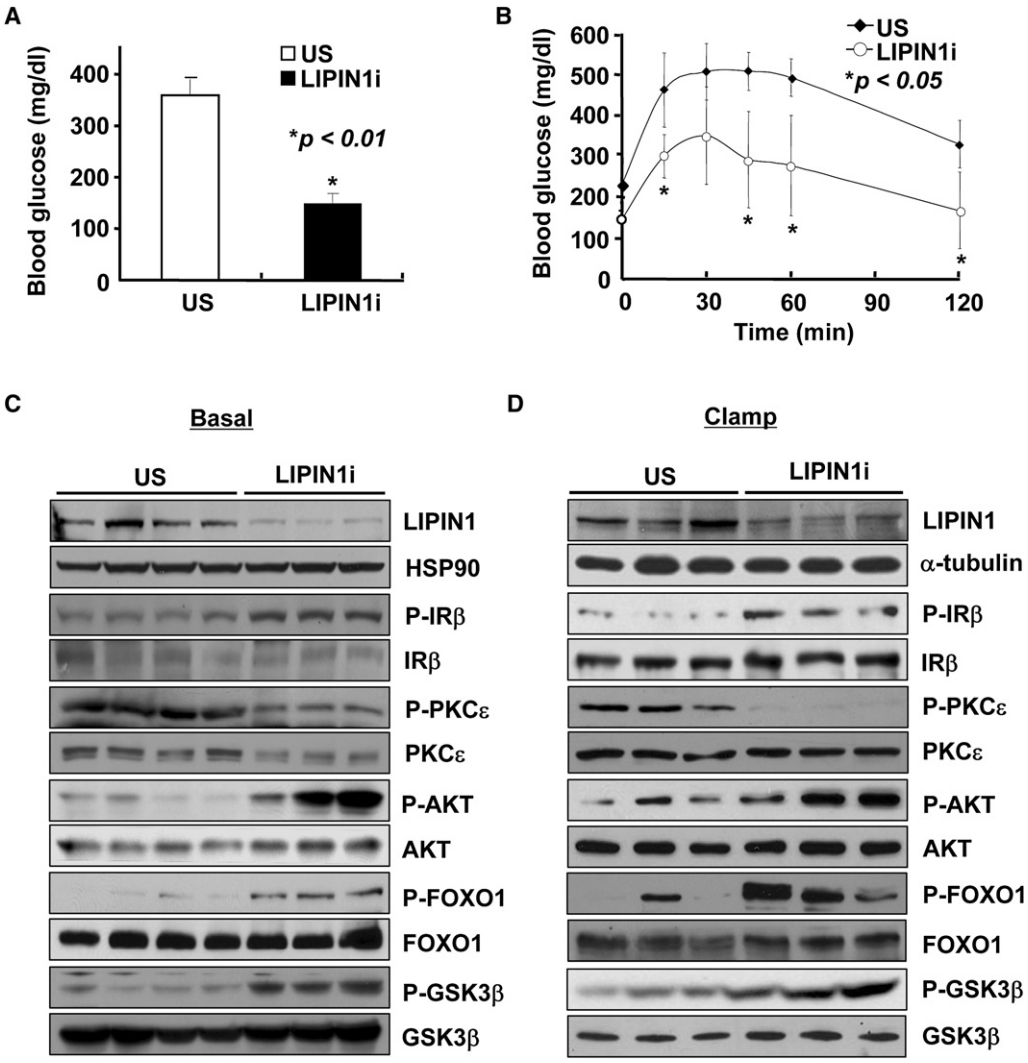

Figure 4. Knockdown of LIPIN1 Improves Hepatic Glucose Tolerance and Insulin Signaling in *db/db* Mice

(A and B) Four hour fasting glucose levels (*p < 0.01) (A) and GTT (*p < 0.05) (B) from *db/db* mice injected with either Ad-US (n = 4) or Ad-LIPIN1 RNAi (n = 3).

(C) Western blot analysis of total and phosphorylated forms of IR, PKCε, AKT, FOXO1, and GSK3β using extracts from 4 hr fasted mouse liver infected with either Ad-US or Ad-LIPIN1 RNAi virus.

(D) Western blot analysis of total and phosphorylated forms of IR, PKCε, AKT, FOXO1, and GSK3β using liver extracts generated from adenovirus-infected mice after clamp studies. (A) and (B) represent mean ± SD.

In a study conducted by Finck et al., LIPIN1 seems to also function as a coactivator for PPARα and PGC-1α to promote fatty acid beta oxidation in livers of WT C57BL/6 mice (Finck et al., 2006). In our study, we were unable to observe the reduction in expression of genes involved in the beta oxidation, such as *ACOX* or *CPT-Iα*, by LIPIN1 knockdown in *db/db* mouse liver (Figures S15 and S17). Interestingly, *PPARα* mRNA levels are significantly higher with LIPIN1 knockdown, perhaps compensating for the reduced expression of hepatic LIPIN1 in insulin-resistant condition that we tested in this study. Moreover, genes involved in the lipogenesis, such as *L-PK*, *FAS*, or *SCD-1*, were reciprocally decreased (Figure S16), suggesting that an equilibrium between fatty acid oxidation and fatty acid synthesis could be achieved even in the absence of LIPIN1. Alternatively, the presence of other LIPIN families in liver would partially compensate for the loss of LIPIN1 (Donkor et al., 2007; Reue and Zhang, 2008), although there are no significant changes in either *LIPIN2* or *LIPIN3* mRNA levels by LIPIN1 knockdown (Figures S16 and S18). The relative importance between coactivator function and PAP activity of LIPIN1 in normal or disease conditions would be an interesting subject for future studies.

While this work was under review, two reports came out regarding the role of LIPIN1 in triglyceride formation and VLDL secretion in liver. In a study conducted in cultured hepatocytes, LIPIN1 overexpression leads to increased triglyceride synthesis and secretion, whereas siRNA-mediated knockdown of LIPIN1 selectively decreased VLDL assembly and secretion among lipoproteins measured (Khalil et al., 2009). On the other hand, adenovirus-mediated overexpression of LIPIN1 in cultured *fld* mouse hepatocytes or in liver of UCP-DTA mouse, a brown-fat-deficient

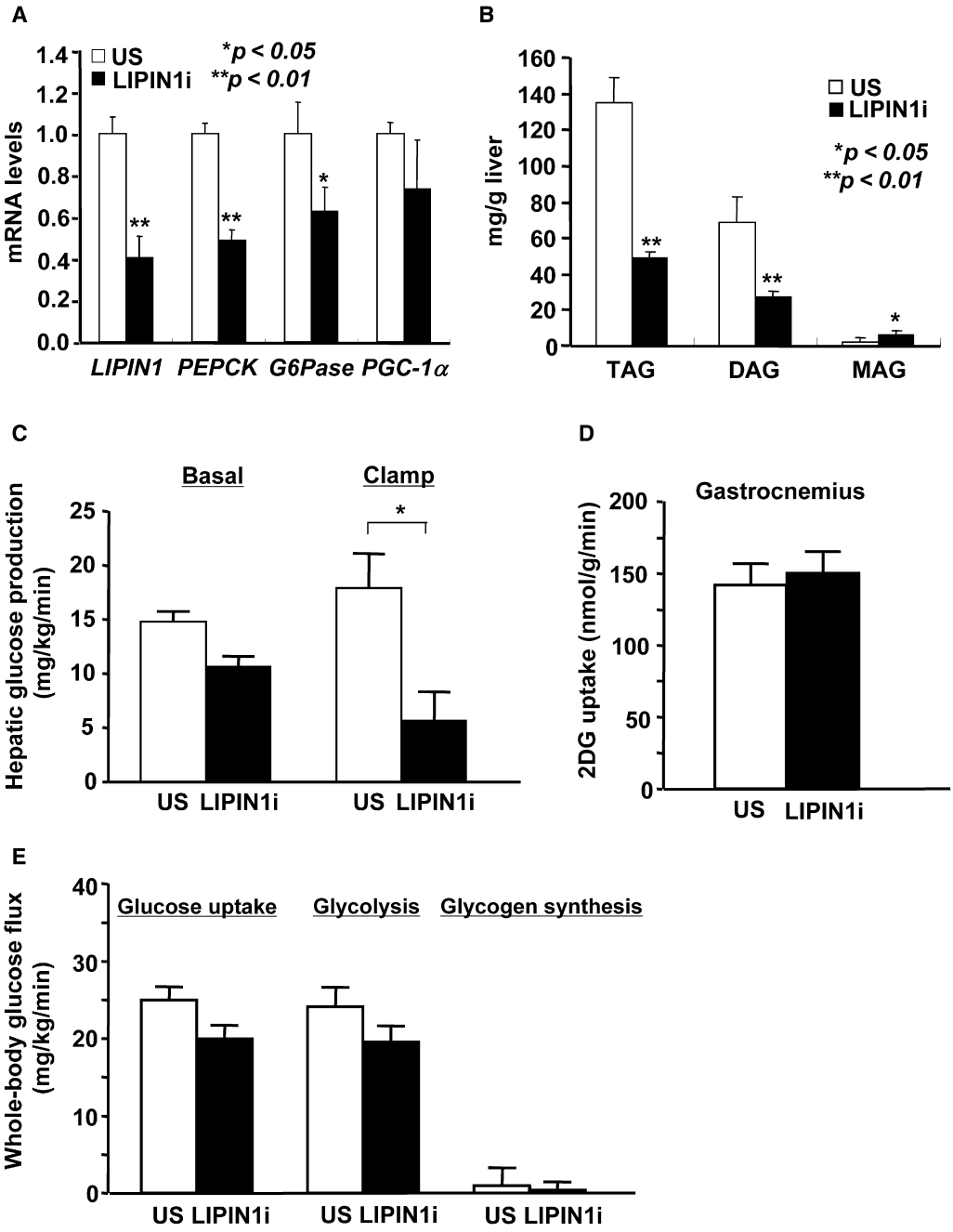

Figure 5. Knockdown of LIPIN1 Improves Hepatic Insulin Sensitivity in *db/db* Mice

(A) Q-PCR analysis showing effect of Ad-US or Ad-LIPIN1 RNAi infection on hepatic expression of gluconeogenic genes in *db/db* mice fasted for 4 hr. (*$p < 0.05$; **$p < 0.01$; $n = 3$).

(B) Tri-, di-, and mono-acylglycerols in liver of Ad-US- and Ad-LIPIN1 RNAi-injected *db/db* mice (*$p < 0.05$; **$p < 0.001$; $n = 3$).

(C–E) Peripheral and hepatic insulin sensitivity was assessed by means of hyperinsulinemic-euglycemic clamps. Shown are hepatic glucose production (C), skeletal muscle (gastrocnemius) glucose uptake (D), whole-body glucose uptake (E), and glycolysis and glycogen synthesis (*$p < 0.05$, $n = 5$). (A)–(E) represent mean ± SD.

FVB mouse model that displays hyperinsulinemia (~7500 pg/ml), significantly decreased total TAG secretion, including VLDL, showing a result somewhat inconsistent from the aforementioned study (Chen et al., 2008). To resolve differences in the proposed functions of hepatic LIPIN1, generation of liver-specific transgenic or knockout mice would be desirable to avoid secondary effects from LIPIN1 overexpression/knockout on other tissues, such as adipose tissue. These mouse models would also be useful to study the longer-term effects of hepatic LIPIN1 expression on lipid metabolism or insulin signaling in liver.

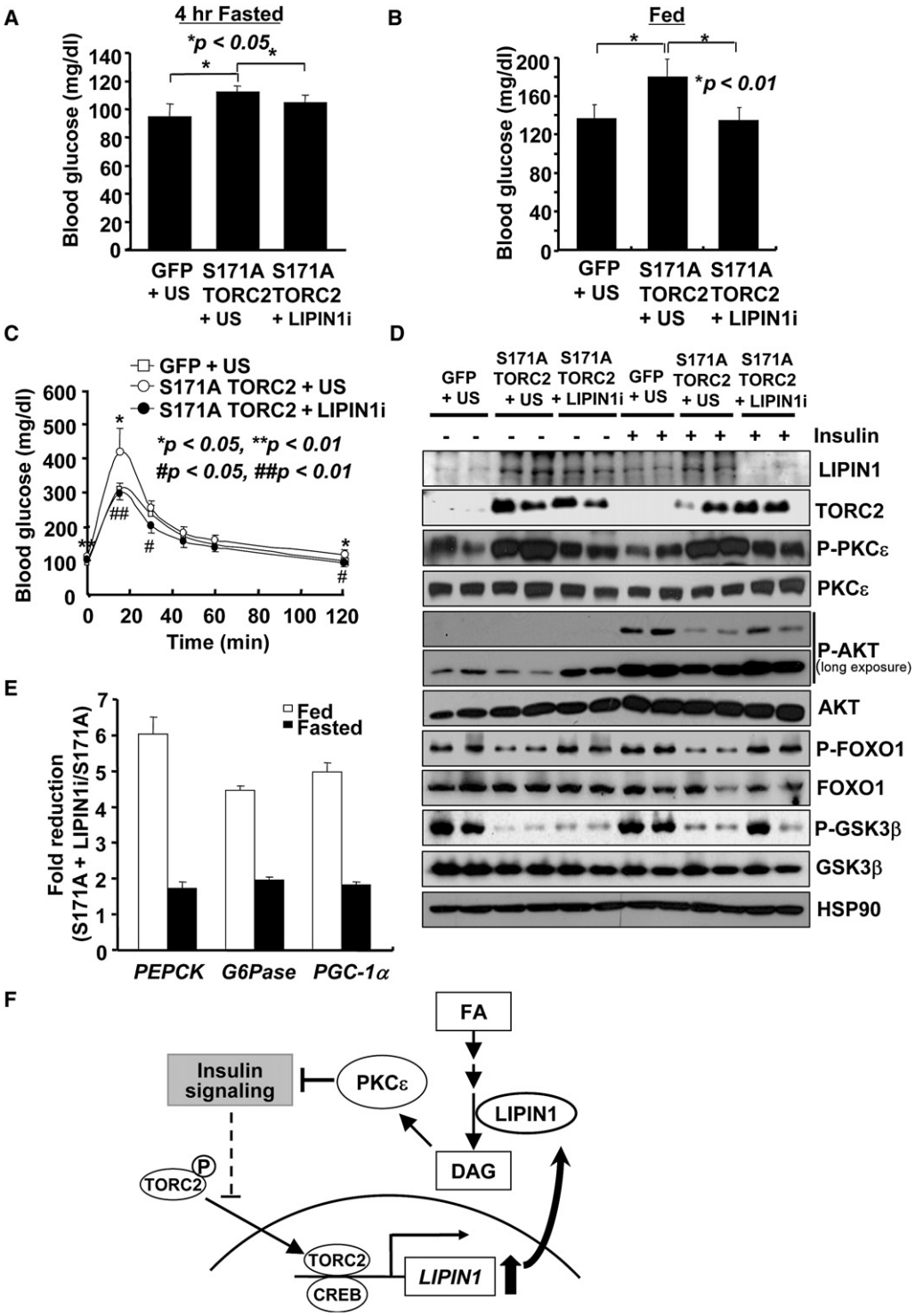

Figure 6. LIPIN1 Knockdown Improves TORC2-Induced Hepatic Glucose Intolerance in Mice

(A–B) Four hour fasting plasma glucose levels (A) and ad libitum feeding plasma glucose levels (B) of WT C57BL/6 mice infected with Ad-GFP + Ad-US (n = 5), Ad-S171A TORC2 + Ad-US (n = 4), or Ad-S171A TORC2 + Ad-LIPIN1i (n = 4) (*$p < 0.05$ for 4 hr fasting glucose and *$p < 0.01$ for ad libitum feeding glucose).

(C) GTT using mice as in (A). Statistically significant differences between GFP + US and S171A TORC2 + US (*$p < 0.05$; **$p < 0.01$) or S171A TORC2 + US and S171A TORC2 + LIPIN1i ($^{\#}p < 0.05$; $^{\#\#}p < 0.01$) were shown.

(D) Western blot analysis showing combined effects of Ad-S171A TORC2 and Ad-LIPIN1 RNAi on insulin singling pathway.

(E) Q-PCR analysis showing combined effects of Ad-S171A TORC2 and Ad-LIPIN1 RNAi on expression of gluconeogenic genes during 4 hr fasting or ad libitum feeding conditions (n = 3).

(F) A proposed model of TORC2 and LIPIN1-mediated hepatic insulin resistance. Data in (A)–(C) and (E) represent mean ± SD.

Increased accumulation of free fatty acids in peripheral tissues has long been regarded as a major predicament for the progression of insulin resistance (Chibalin et al., 2008; Holland et al., 2007; Holland and Summers, 2008; Kraegen and Cooney, 2008; Savage et al., 2007). Various metabolic intermediates, including ceramide, DAG, or their metabolites, were proposed to be major signaling molecules for activating serine/threonine kinases such as JNK, noncanonical PKC, S6K, or mTOR to target IR or IR substrates to hamper insulin signaling in the cell (Jaeschke and Davis, 2007; Nguyen et al., 2005; Samuel et al., 2004, 2007; Um et al., 2004, 2006). A recent review from Shulman's group revealed the importance of DAG as a signaling molecule to activate PKCθ in muscle or PKCε in liver to target either IR substrates or IR, respectively (Savage et al., 2007). However, results from other studies implied that increase in hepatic DAG alone may not be a direct indication for insulin resistance in liver, suggesting that the involvement of other related mechanisms, including inflammation, is further required (Choi et al., 2007b; Minehira et al., 2008; Monetti et al., 2007). In our study, decreased expression of LIPIN1 reduces cellular DAG levels that are concomitant with decreased phosphorylation of PKCε and enhanced tyrosine phosphorylation of IR in previously established insulin-resistant setting, at least supporting the hypothesis that relieving the higher hepatic DAG levels might be beneficial to improve insulin signaling and deter the progression of type 2 diabetes. Further study will be necessary to discern the relative contribution of various signaling cascades that would promote insulin-resistant phenotypes in mammals.

EXPERIMENTAL PROCEDURES

Plasmids and Recombinant Adenoviruses

LIPIN1 promoter sequences were PCR-amplified from mouse genomic DNA and inserted into the pXP2-luc vector. To generate LIPIN1 and LIPIN2 expression vectors, the coding sequences of mouse *LIPIN1* and *LIPIN2* were PCR-amplified from mouse hepatic cDNA and subcloned into pcDNA3-FLAG vector. LIPIN1 mutant (D712E, D714E) was generated using site-directed mutagenesis (Finck et al., 2006). Adenoviruses expressing GFP only, nonspecific RNAi control (US), LIPIN1, LIPIN1 RNAi, and PKCε were generated as described previously (Koo et al., 2005).

Animal Experiments

Seven-week-old male C57BL/6 or *db/db* mice were purchased from Charles River Laboratories. Recombinant adenovirus (0.5×10^9 pfu) was delivered by tail-vein injection to mice. To measure fasting blood glucose levels, animals were fasted for 16 hr or 4 hr with free access to water. For GTT, mice were fasted for 16 hr and then injected intraperitoneally with 1 g/kg (for *db/db* mice) or 2 g/kg (for C57BL/6 mice) body weight of glucose (Koo et al., 2004). Blood glucose was measured from tail-vein blood collected at the designated times.

All procedures were approved by the Sungkyunkwan University School of Medicine Institutional Animal Care and Use Committee (IACUC).

Quantitative PCR

Total RNA from either primary hepatocytes or liver tissue was extracted using RNeasy Mini Kit (QIAGEN). cDNAs generated by Superscript II enzyme (Invitrogen) were analyzed by Q-PCR using a SYBR Green PCR Kit and TP800 Thermal Cycler Dice Real Time System (TAKARA). All data were normalized to ribosomal *L32* expression.

Western Blot Analyses

Western blot analyses on 50–150 g of whole-cell extracts were performed as described (Koo et al., 2004). LIPIN1 antibody was from Novus. Antisera against IRS1, IRS2, AKT, phospho-Ser473 AKT, GSK3β, phospho-Ser9 GSK3β, FOXO1, phospho-Ser256 FOXO1, IRβ, phospho-Tyr1162/1163 IRβ, and phospho-Tyrosine were purchased from Cell Signaling. Antibodies against total PKCε and phospho-Ser729 PKCε were obtained from Upstate and Santa Cruz, respectively. Antibodies against HSP90 (Santa Cruz) and α-tubulin (Sigma) were used to assess equal loading.

Culture of Primary Hepatocytes

Primary hepatocytes were prepared from 200–300 g Sprague-Dawley rats or 8- to 10-week-old C57BL/6 mice by collagenase perfusion method as described previously (Koo et al., 2005). Cells were plated with medium 199 supplemented by 10% FBS, 10 units/ml penicillin, 10 μg/ml streptomycin, and 10 nM dexamethasone. After attachment, cells were infected with various adenoviruses, indicated in figure legends, for 16 hr. Subsequently, cells were maintained in the same media without FBS overnight and treated with 100 nM dexamethasone and 10 μM forskolin for 2 hr with or without 100 nM insulin for 16 hr.

Transfection Assays

Human hepatoma HepG2 cells were maintained with Ham's F12 medium supplemented with 10% FBS, 10 units/ml penicillin, and 10 μg/ml streptomycin. Each transfection was performed with 300 ng of luciferase construct, 50 ng of β-galactosidase plasmid, and 2.5–100 ng of expression vector for TORC2, PKA, or mutant PKA using Fugene 6 reagent, according to manufacturer's instruction.

Chromatin Immunoprecipitation Assays

Nuclear isolation, cross-linking, and chromatin immunoprecipitation assays on primary mouse hepatocyte samples were performed as described previously (Jaeschke and Davis, 2007). Precipitated DNA fragments were analyzed by PCR using primers against relevant mouse promoters.

Thin-Layer Chromatographic Analyses

Lipids from rat primary hepatocytes, which were labeled with 1 μCi/ml of [^{3}H]palmitic acid (Moravek Biochemicals, Inc.) in the serum-free medium for 18 hr, were extracted using the Bligh and Dyer method (Bligh and Dyer, 1959). DAG was separated from other phospholipids by thin-layer chromatography using a solvent system of toluene/ether/ethanol/concentrated NH_4OH (50/30/20/0.2, v/v). DAG bands corresponding to 1,2-diacyl glycerol (Avanti Polar Lipids) were identified with primulin, scraped, and counted using a scintillation counter.

Measurement of Metabolites

Blood glucose for basal conditions and during GTT was monitored from tail-vein blood using an automatic glucose monitor (OneTouch; LifeScan, Inc.). Blood triglycerides and NEFA were measured by colorimetric assay kits (Wako). Insulin was measured by Mouse Insulin ELISA Kit (U-Type; Shibayagi Corp.). Total liver lipids were extracted with chloroform-methanol (2:1, v/v) mixture according to Folch method (Folch et al., 1957). The extracts were dissolved in chloroform, and the solutions were loaded on Sep-Pak NH_2 columns (Sep-Pak Vac 6cc [500 mg] NH_2 cartridge; Waters Corp.). The fractions were separated into triacylglyceride, diacylglyceride, and monoacylglyceride (Giacometti et al., 2002; Kaluzny et al., 1985). The contents were analyzed with lipid standard (1787-1AMP, Lipid Standard, Mono-, Di-, & Triglyceride Mix; Supelco) on HPLC-ELSD system (Evaporative Light Scattering Detector [ELSD] ZAM 3000; Schambeck SFD GmbH) as described (Bravi et al., 2006).

Hyperinsulinemic-Euglycemic Clamp Study

Seven days prior to the hyperinsulinemic-euglycemic clamp studies, indwelling catheters were placed into the right internal jugular vein extending to the right atrium. After an overnight fast, [3-^{3}H]glucose (HPLC purified; PerkinElmer) was infused at a rate of 0.05 μCi/min for 2 hr to assess the basal glucose turnover. Following the basal period, hyperinsulinemic-euglycemic clamp was conducted for 140 min with a primed/continuous infusion of human insulin (210 pmol/kg prime, 30 pmol/kg/min infusion) (Novo Nordisk; Denmark). Blood samples (10 μl) were collected at 10–20 min intervals, plasma glucose was immediately analyzed during the clamps by a glucose oxidase method (GM9 Analyzer; Analox Instruments; London), and 20% dextrose

was infused at variable rates to maintain plasma glucose at basal concentrations (~6.7 mM). To estimate insulin-stimulated whole-body glucose fluxes, [3-^{3}H]glucose was infused at a rate of 0.1 μCi/min throughout the clamps, and 2-deoxy-D-[1-^{14}C]glucose (2-[^{14}C]DG; PerkinElmer) was injected as a bolus at the 85th minute of the clamp to estimate the rate of insulin-stimulated tissue glucose uptake, as previously described (Choi et al., 2007a). Blood samples (10 μl) for the measurement of plasma ^{3}H and ^{14}C activities were taken at the end of the basal period and during the last 45 min of the clamp.

Glucose Flux Calculation

For the determination of plasma [^{3}H]glucose, plasma was deproteinized with $ZnSO_4$ and $Ba(OH)_2$, dried to remove $[^3H]_2O$, resuspended in water, and counted in scintillation fluid (Ultima Gold; PerkinElmer) on a PerkinElmer scintillation counter. Rates of basal and insulin-stimulated whole-body glucose turnover were determined as the ratio of the [3-^{3}H]glucose infusion rate (disintegrations per minute [dpm]) to the specific activity of plasma glucose (dpm/mg) at the end of the basal period and during the final 30 min of the clamp experiment, respectively. Hepatic glucose production was determined by subtracting the glucose infusion rate from the total glucose appearance rate.

The plasma concentration of $[^3H]_2O$ was determined by the difference between ^{3}H counts without and with drying. Whole-body glycolysis was calculated from the rate of increase in plasma $[^3H]_2O$ concentration divided by the specific activity of plasma [^{3}H]glucose, as previously described (Youn and Buchanan, 1993). Whole-body glycogen synthesis was estimated by subtracting whole-body glycolysis from whole-body glucose uptake, assuming that glycolysis and glycogen synthesis account for the majority of insulin-stimulated glucose uptake (Rossetti and Giaccari, 1990).

Statistical Analyses

Results are shown as mean ± SD. The comparison of different groups was carried out using two-tailed unpaired Student's t test, and differences at or under to $p < 0.05$ were considered statistically significant and reported as in legends.

SUPPLEMENTAL DATA

Supplemental Data include 18 figures and can be found online at http://www.cell.com/cellmetabolism/supplemental/S1550-4131(09)00008-4.

ACKNOWLEDGMENTS

We would like to thank Sun Myung Park and Bo-Kyoung Kim for the technical assistance. This work was supported by a Research Program for New Drug Target Discovery (M10648000089-08N4800-08910) grant; a Korea Science and Engineering Foundation (KOSEF) grant (R01-2008-000-11935-0); a Korea Research Foundation (KRF) grant (2006-E00037) by the Ministry of Education, Science, and Technology; and a grant from the Marine Biotechnology Program funded by the Ministry of Land, Transport, and Maritime Affairs, Republic of Korea.

Received: July 5, 2008
Revised: November 13, 2008
Accepted: January 14, 2009
Published: March 3, 2009

REFERENCES

Bligh, E.G., and Dyer, W.J. (1959). A rapid method of total lipid extraction and purification. Can. J. Biochem. Physiol. *37*, 911–917.

Bravi, E., Perretti, G., and Montanari, L. (2006). Fatty acids by high-performance liquid chromatography and evaporative light-scattering detector. J. Chromatogr. A. *1134*, 210–214.

Carman, G.M., and Han, G.S. (2006). Roles of phosphatidate phosphatase enzymes in lipid metabolism. Trends Biochem. Sci. *31*, 694–699.

Chen, Z., Gropler, M.C., Norris, J., Lawrence, J.C., Jr., Harris, T.E., and Finck, B.N. (2008). Alterations in hepatic metabolism in fld mice reveal a role for lipin 1 in regulating VLDL-triacylglyceride secretion. Arterioscler. Thromb. Vasc. Biol. *28*, 1738–1744.

Chibalin, A.V., Leng, Y., Vieira, E., Krook, A., Bjornholm, M., Long, Y.C., Kotova, O., Zhong, Z., Sakane, F., Steiler, T., et al. (2008). Downregulation of diacylglycerol kinase delta contributes to hyperglycemia-induced insulin resistance. Cell *132*, 375–386.

Choi, C.S., Savage, D.B., Abu-Elheiga, L., Liu, Z.X., Kim, S., Kulkarni, A., Distefano, A., Hwang, Y.J., Reznick, R.M., Codella, R., et al. (2007a). Continuous fat oxidation in acetyl-CoA carboxylase 2 knockout mice increases total energy expenditure, reduces fat mass, and improves insulin sensitivity. Proc. Natl. Acad. Sci. USA *104*, 16480–16485.

Choi, C.S., Savage, D.B., Kulkarni, A., Yu, X.X., Liu, Z.X., Morino, K., Kim, S., Distefano, A., Samuel, V.T., Neschen, S., et al. (2007b). Suppression of diacylglycerol acyltransferase-2 (DGAT2), but not DGAT1, with antisense oligonucleotides reverses diet-induced hepatic steatosis and insulin resistance. J. Biol. Chem. *282*, 22678–22688.

Dentin, R., Liu, Y., Koo, S.H., Hedrick, S., Vargas, T., Heredia, J., Yates, J., 3rd, and Montminy, M. (2007). Insulin modulates gluconeogenesis by inhibition of the coactivator TORC2. Nature *449*, 366–369.

Donkor, J., Sariahmetoglu, M., Dewald, J., Brindley, D.N., and Reue, K. (2007). Three mammalian lipins act as phosphatidate phosphatases with distinct tissue expression patterns. J. Biol. Chem. *282*, 3450–3457.

Finck, B.N., Gropler, M.C., Chen, Z., Leone, T.C., Croce, M.A., Harris, T.E., Lawrence, J.C., Jr., and Kelly, D.P. (2006). Lipin 1 is an inducible amplifier of the hepatic PGC-1alpha/PPARalpha regulatory pathway. Cell Metab. *4*, 199–210.

Folch, J., Lees, M., and Sloane Stanley, G.H. (1957). A simple method for the isolation and purification of total lipides from animal tissues. J. Biol. Chem. *226*, 497–509.

Giacometti, J., Milosevic, A., and Milin, C. (2002). Gas chromatographic determination of fatty acids contained in different lipid classes after their separation by solid-phase extraction. J. Chromatogr. A. *976*, 47–54.

Han, G.S., Wu, W.I., and Carman, G.M. (2006). The Saccharomyces cerevisiae Lipin homolog is a Mg2+-dependent phosphatidate phosphatase enzyme. J. Biol. Chem. *281*, 9210–9218.

Han, G.S., Siniossoglou, S., and Carman, G.M. (2007). The cellular functions of the yeast lipin homolog PAH1p are dependent on its phosphatidate phosphatase activity. J. Biol. Chem. *282*, 37026–37035.

Holland, W.L., and Summers, S.A. (2008). Sphingolipids, insulin resistance, and metabolic disease: new insights from in vivo manipulation of sphingolipid metabolism. Endocr. Rev. *29*, 381–402.

Holland, W.L., Knotts, T.A., Chavez, J.A., Wang, L.P., Hoehn, K.L., and Summers, S.A. (2007). Lipid mediators of insulin resistance. Nutr. Rev. *65*, S39–S46.

Jaeschke, A., and Davis, R.J. (2007). Metabolic stress signaling mediated by mixed-lineage kinases. Mol. Cell *27*, 498–508.

Kaluzny, M.A., Duncan, L.A., Merritt, M.V., and Epps, D.E. (1985). Rapid separation of lipid classes in high yield and purity using bonded phase columns. J. Lipid Res. *26*, 135–140.

Khalil, M.B., Sundaram, M., Zhang, H.Y., Links, P.H., Raven, J.F., Manmontri, B., Sariahmetoglu, M., Tran, K., Reue, K., Brindley, D.N., and Yao, Z. (2009). The level and compartmentalization of phosphatidate phosphatase-1 (lipin-1) control the assembly and secretion of hepatic VLDL. J. Lipid Res. *50*, 47–58.

Koo, S.H., Satoh, H., Herzig, S., Lee, C.H., Hedrick, S., Kulkarni, R., Evans, R.M., Olefsky, J., and Montminy, M. (2004). PGC-1 promotes insulin resistance in liver through PPAR-alpha-dependent induction of TRB-3. Nat. Med. *10*, 530–534.

Koo, S.H., Flechner, L., Qi, L., Zhang, X., Screaton, R.A., Jeffries, S., Hedrick, S., Xu, W., Boussouar, F., Brindle, P., et al. (2005). The CREB coactivator TORC2 is a key regulator of fasting glucose metabolism. Nature *437*, 1109–1111.

Kraegen, E.W., and Cooney, G.J. (2008). Free fatty acids and skeletal muscle insulin resistance. Curr. Opin. Lipidol. *19*, 235–241.

Minehira, K., Young, S.G., Villanueva, C.J., Yetukuri, L., Oresic, M., Hellerstein, M.K., Farese, R.V., Jr., Horton, J.D., Preitner, F., Thorens, B., and Tappy, L. (2008). Blocking VLDL secretion causes hepatic steatosis but does not affect peripheral lipid stores or insulin sensitivity in mice. J. Lipid Res. *49*, 2038–2044.

Monetti, M., Levin, M.C., Watt, M.J., Sajan, M.P., Marmor, S., Hubbard, B.K., Stevens, R.D., Bain, J.R., Newgard, C.B., Farese, R.V., Sr., et al. (2007). Dissociation of hepatic steatosis and insulin resistance in mice overexpressing DGAT in the liver. Cell Metab. *6*, 69–78.

Nguyen, M.T., Satoh, H., Favelyukis, S., Babendure, J.L., Imamura, T., Sbodio, J.I., Zalevsky, J., Dahiyat, B.I., Chi, N.W., and Olefsky, J.M. (2005). JNK and tumor necrosis factor-alpha mediate free fatty acid-induced insulin resistance in 3T3-L1 adipocytes. J. Biol. Chem. *280*, 35361–35371.

Peterfy, M., Phan, J., Xu, P., and Reue, K. (2001). Lipodystrophy in the fld mouse results from mutation of a new gene encoding a nuclear protein, lipin. Nat. Genet. *27*, 121–124.

Peterfy, M., Phan, J., and Reue, K. (2005). Alternatively spliced lipin isoforms exhibit distinct expression pattern, subcellular localization, and role in adipogenesis. J. Biol. Chem. *280*, 32883–32889.

Phan, J., and Reue, K. (2005). Lipin, a lipodystrophy and obesity gene. Cell Metab. *1*, 73–83.

Phan, J., Peterfy, M., and Reue, K. (2004). Lipin expression preceding peroxisome proliferator-activated receptor-gamma is critical for adipogenesis in vivo and in vitro. J. Biol. Chem. *279*, 29558–29564.

Reue, K., and Dwyer, J.R. (2008). Lipin proteins and metabolic homeostasis. J. Lipid Res., in press. Published online October 21, 2008. 10.1194/jlr.R800052-JLR200.

Reue, K., and Zhang, P. (2008). The lipin protein family: dual roles in lipid biosynthesis and gene expression. FEBS Lett. *582*, 90–96.

Rossetti, L., and Giaccari, A. (1990). Relative contribution of glycogen synthesis and glycolysis to insulin-mediated glucose uptake. A dose-response euglycemic clamp study in normal and diabetic rats. J. Clin. Invest. *85*, 1785–1792.

Samuel, V.T., Liu, Z.X., Qu, X., Elder, B.D., Bilz, S., Befroy, D., Romanelli, A.J., and Shulman, G.I. (2004). Mechanism of hepatic insulin resistance in nonalcoholic fatty liver disease. J. Biol. Chem. *279*, 32345–32353.

Samuel, V.T., Liu, Z.X., Wang, A., Beddow, S.A., Geisler, J.G., Kahn, M., Zhang, X.M., Monia, B.P., Bhanot, S., and Shulman, G.I. (2007). Inhibition of protein kinase Cepsilon prevents hepatic insulin resistance in nonalcoholic fatty liver disease. J. Clin. Invest. *117*, 739–745.

Savage, D.B., Petersen, K.F., and Shulman, G.I. (2007). Disordered lipid metabolism and the pathogenesis of insulin resistance. Physiol. Rev. *87*, 507–520.

Screaton, R.A., Conkright, M.D., Katoh, Y., Best, J.L., Canettieri, G., Jeffries, S., Guzman, E., Niessen, S., Yates, J.R., 3rd, Takemori, H., et al. (2004). The CREB coactivator TORC2 functions as a calcium- and cAMP-sensitive coincidence detector. Cell *119*, 61–74.

Shaw, R.J., Lamia, K.A., Vasquez, D., Koo, S.H., Bardeesy, N., Depinho, R.A., Montminy, M., and Cantley, L.C. (2005). The kinase LKB1 mediates glucose homeostasis in liver and therapeutic effects of metformin. Science *310*, 1642–1646.

Um, S.H., Frigerio, F., Watanabe, M., Picard, F., Joaquin, M., Sticker, M., Fumagalli, S., Allegrini, P.R., Kozma, S.C., Auwerx, J., and Thomas, G. (2004). Absence of S6K1 protects against age- and diet-induced obesity while enhancing insulin sensitivity. Nature *431*, 200–205.

Um, S.H., D'Alessio, D., and Thomas, G. (2006). Nutrient overload, insulin resistance, and ribosomal protein S6 kinase 1, S6K1. Cell Metab. *3*, 393–402.

Verheijen, M.H., Chrast, R., Burrola, P., and Lemke, G. (2003). Local regulation of fat metabolism in peripheral nerves. Genes Dev. *17*, 2450–2464.

Youn, J.H., and Buchanan, T.A. (1993). Fasting does not impair insulin-stimulated glucose uptake but alters intracellular glucose metabolism in conscious rats. Diabetes *42*, 757–763.

Cell Metabolism
Article

The Role of Peroxisome Proliferator-Activated Receptor γ Coactivator-1 β in the Pathogenesis of Fructose-Induced Insulin Resistance

Yoshio Nagai,[1,4] Shin Yonemitsu,[1,4] Derek M. Erion,[1,2,4] Takanori Iwasaki,[1] Romana Stark,[1] Dirk Weismann,[1] Jianying Dong,[1] Dongyan Zhang,[1,4] Michael J. Jurczak,[1,4] Michael G. Löffler,[1] James Cresswell,[1] Xing Xian Yu,[5] Susan F. Murray,[5] Sanjay Bhanot,[5] Brett P. Monia,[5] Jonathan S. Bogan,[1,3] Varman Samuel,[1] and Gerald I. Shulman[1,2,4,*]
[1]Department of Internal Medicine
[2]Department of Cellular & Molecular Physiology
[3]Department of Cell Biology
[4]Howard Hughes Medical Institute
Yale University School of Medicine, New Haven, CT 06536-8012, USA
[5]ISIS Pharmaceuticals, Carlsbad, CA 92008, USA
*Correspondence: gerald.shulman@yale.edu
DOI 10.1016/j.cmet.2009.01.011

SUMMARY

Peroxisome proliferator-activated receptor γ coactivator-1 β (PGC-1β) is known to be a transcriptional coactivator for SREBP-1, the master regulator of hepatic lipogenesis. Here, we evaluated the role of PGC-1β in the pathogenesis of fructose-induced insulin resistance by using an antisense oligonucleotide (ASO) to knockdown PGC-1β in liver and adipose tissue. PGC-1β ASO improved the metabolic phenotype induced by fructose feeding by reducing expression of SREBP-1 and downstream lipogenic genes in liver. PGC-1β ASO also reversed hepatic insulin resistance induced by fructose in both basal and insulin-stimulated states. Furthermore, PGC-1β ASO increased insulin-stimulated whole-body glucose disposal due to a threefold increase in glucose uptake in white adipose tissue. These data support an important role for PGC-1β in the pathogenesis of fructose-induced insulin resistance and suggest that PGC-1β inhibition may be a therapeutic target for treatment of NAFLD, hypertriglyceridemia, and insulin resistance associated with increased de novo lipogenesis.

INTRODUCTION

Insulin resistance is a common feature of the metabolic syndrome and type 2 diabetes mellitus (T2DM). Both have reached epidemic proportions worldwide (Zimmet et al., 2001) with the global adoption of the westernized diet along with increased consumption of fructose, stemming from the wide and increasing use of high-fructose corn syrup sweeteners (Elliott et al., 2002; Basciano et al., 2005). It is well established that fructose is more lipogenic than glucose, and high-fructose diets have been linked to hypertriglyceridemia, nonalcoholic fatty liver disease (NAFLD), and insulin resistance (Daly et al., 1997; Sleder et al., 1980; Havel, 2005; Petersen et al., 2007). Despite a clear relationship between fructose and increased hepatic lipogenesis, the mechanisms responsible for this association remain poorly defined.

Hepatic lipogenesis is regulated by the action of sterol regulatory element-binding protein (SREBP) transcription factors, especially SREBP-1c, the principal inducer of hepatic lipogenic gene expression (Shimano et al., 1997). Dietary fructose, per se, activates lipogenesis partly through inducing expression of SREBP-1 (Nagai et al., 2002). Among strains of inbred mice, a genetic polymorphism within the SREBP-1c promoter region underlies a differential sensitivity to fructose-induced lipid synthesis, further suggesting that this transcription factor mediates the lipogenic effects of fructose (Nagata et al., 2004). Although there is evidence linking induction of SREBP-1c to fructose-induced lipogenesis in vivo, the mechanism responsible for fructose-induced alterations in SREBP-1c transcription remains unknown.

Recent studies implicate the peroxisome proliferator-activated receptor gamma (PPARγ) coactivator-1 (PGC-1) family in regulating liver glucose and lipid metabolism. Though initially described as a coactivator of PPARγ (Lin et al., 2002), PGC-1 is now recognized to coactivate multiple other transcription factors. Through these interactions, they can coordinate both hepatic glucose and lipid metabolism, the former via forkhead transcription factor-1 (FOXO1) (Puigserver et al., 2003); hepatocyte nuclear factor 4 alpha (HNF4α) (Rhee et al., 2003) and myocyte enhancer factor-2 (MEF-2) (Michael et al., 2001), the latter via peroxisome proliferator-activated receptor α (PPARα) (Vega et al., 2000); liver X receptor (LXR) (Lin et al., 2005); and SREBP (Lin et al., 2005). PGC-1β, but not PGC-1α, activates the expression of genes involved in lipogenesis and triglyceride secretion via direct coactivation of SREBPs (Lin et al., 2005). Thus, PGC-1β, a regulator of both carbohydrate and lipid metabolism, is poised to play a pivotal role in fructose-induced lipogenesis.

We hypothesized that PGC-1β mediates fructose-induced lipogenesis via upregulation of SREBP-1c, and knockdown of PGC-1β would prevent this from occurring. To test this hypothesis, we knocked down the expression of PGC-1β using

antisense oligonucleotides (ASOs) in chronically (4 weeks) fructose-fed rats. ASOs are ideal for these studies, as they can target both liver and adipose tissues in adult animals. Our studies reveal an important role for PGC-1β in the pathogenesis of fructose-induced insulin resistance and suggest that PGC-1β inhibition may be a therapeutic target for treatment of NAFLD, hypertriglyceridemia, and insulin resistance.

RESULTS

PGC-1β ASO Decreases PGC-1β Expression in Rat Livers and White Adipose Tissue

Rats were divided into two diet groups and two ASO treatment groups. They received either a regular chow diet, which provided 60% calories from carbohydrates, predominantly in the form of starch, or a high-fructose diet that provided 66.8% calories from fructose. Within each diet group, rats were treated with either control ASO or PGC-1β ASO at 25 mg/kg body weight twice weekly for 4 weeks. Caloric intake and weight gain were similar in all treated groups. Compared to control ASO, PGC-1β ASO treatment reduced PGC-1β mRNA expression by approximately 75% in the liver (Figure 1A) and 70% in the white adipose tissue (WAT) (Figure 1B). The reduction in mRNA with PGC-1β ASO translated into a similar reduction in PGC-1β protein (Figures 1C and 1D). In contrast, PGC-1β ASO did not significantly reduce expression of PGC-1β in either brown adipose tissue (BAT) or skeletal muscle (Figures 1E and 1F). Finally, rats remained free of hepatotoxicity, as reflected by the absence of alanine amino transaminase elevation in all four groups (Table 1).

PGC-1β ASO Improves Metabolic Parameters Induced by High-Fructose Feeding

To evaluate the effect of knocking down PGC-1β on whole-body physiology, we performed detailed metabolic characterization, including measures of morphology and serum chemistry as well as glucose and lipid kinetics. As shown in Table 1, epididymal fat mass and plasma concentrations of glucose, triglyceride, fatty acids, insulin, and leptin were significantly higher in the high-fructose-fed rats. Knockdown of PGC-1β protected rats from all these fructose-induced changes. Compared with the rats fed high-fructose diet, the plasma glucose and insulin levels were significantly lower in PGC-1β ASO-treated rats, 12% and 37%, respectively. The plasma triglyceride and leptin levels and epididymal fat mass were also significantly lower: 40%, 50%, and 13%, respectively. On the other hand, plasma concentrations of total cholesterol, HDL cholesterol, and β-hydroxybutyrate were significantly higher in PGC-1β ASO-treated rats: 58%, 63%, and 11%, respectively. Finally, there were no differences in plasma concentrations of glucagon, adiponectin, or retinol-binding protein 4 (RBP4).

The changes in plasma triglyceride and cholesterol concentrations seen with PGC-1β ASO treatment prompted further analysis of their respective pathways. Using primary hepatocytes, we quantified the impact of PGC-1β inhibition on lipid and sterol synthesis in vitro. Specifically, the synthesis was assessed by measuring the incorporation of [^{14}C]acetic acid into fatty acid and cholesterol. PGC-1β ASO inhibited the synthesis of fatty acids (Figure 2A) but not of cholesterol (Figure 2B). The decreased lipid synthesis in vitro was reflected in vivo, where PGC-1β ASO prevented the accumulation of liver triglyceride observed with high-fructose feeding (Figure 2C).

PGC-1β ASO Reduces Lipogenic Gene Expression

Gene expression was profiled by RT-qPCR to determine what genes were affected by PGC-1β ASO in fructose-fed rats. Under fasting condition, SREBP-1c and -1a mRNA levels were similar among the four groups (Figures 3A and 3B). Though with refeeding, SREBP-1c expression increased in all groups, and SREBP-1a expression increased in high-fructose-fed groups; there were marked differences in the degree of induction. SREBP-1c and -1a expression increased 5 times and 1.5 times, respectively, with feeding. This exaggerated induction of SREBP-1c by fructose was attenuated 40% with PGC-1β ASO treatment (Figure 3A). The changes in SREBP-1a/-1c expression were confirmed by quantifying SREBP-1 protein with western blot analysis (Figure 3C). The decreased induction of SREBP-1 with PGC-1β ASO was reflected in decreased activation of fatty acid synthase (FAS) gene by fructose (Figure 3D).

It has been reported that rat SREBP-1c promoter contains binding sites for SREBP (Cagen et al., 2005) and LXR (Dif et al., 2006), which are both coactivated by PGC-1β (Lin et al., 2005). We next examined whether the binding of SREBP-1 or LXR to the SREBP-1c promoter was affected by PGC-1β ASO treatment. Formaldehyde treatment of fresh liver samples was used to cross link the transcription factors with the chromosomal DNA. Chromatin immunoprecipitation (ChIP) assays were performed using anti-SREBP-1 (H-160) or anti-LXRα/β (S-20) antibodies to immunoprecipitate fragments of DNA where there was interaction. Figure 3E shows the amplification by PCR (33 cycles) of a specific portion of the proximal promoter of the SREBP-1c gene. We quantified the PCR products using real-time PCR and confirmed that the amplification of the negative control using normal rabbit IgG was less than 0.05% of that of the input sample (data not shown). Moreover, we also confirmed that there was no difference in LXR mRNA and protein expression among all four groups (Table S1 and data not shown). When rats were refed with a high-fructose diet, there was a marked increase in the association of both SREBP-1 and LXRα/β with the SREBP-1c promoter. PGC-1β ASO decreased both bindings. These data were consistent with SREBP-1c mRNA (Figure 3A) and protein (Figure 3C) expressions. Thus, the ability of fructose to activate a program of lipogenesis via SREBP-1 was inhibited by PGC-1β ASO.

While PGC-1β ASO decreased liver and plasma triglyceride concentrations in fructose-fed rats, plasma cholesterol concentrations were increased in both diet groups (Table 1). We also measured the expression of key genes that regulate cholesterol metabolism. Neither high-fructose feeding nor PGC-1β ASO treatment increased expression of SREBP-2 or downstream targets such as HMG-CoA reductase (HMGCoAR) and LDL-receptor (Table S1). LXRα, a nuclear receptor that balances cholesterol and bile metabolism (Kalaany et al., 2005), is also coactivated by PGC-1α/-1β (Lin et al., 2005). Although LXRα expression was unchanged by either diet or ASO treatment (Table S1), target gene cholesterol-7α-hydroxylase (CYP7A1) protein expression was significantly decreased in all PGC-1β ASO-treated groups independent of diet (Figure 3F). CYP7A1

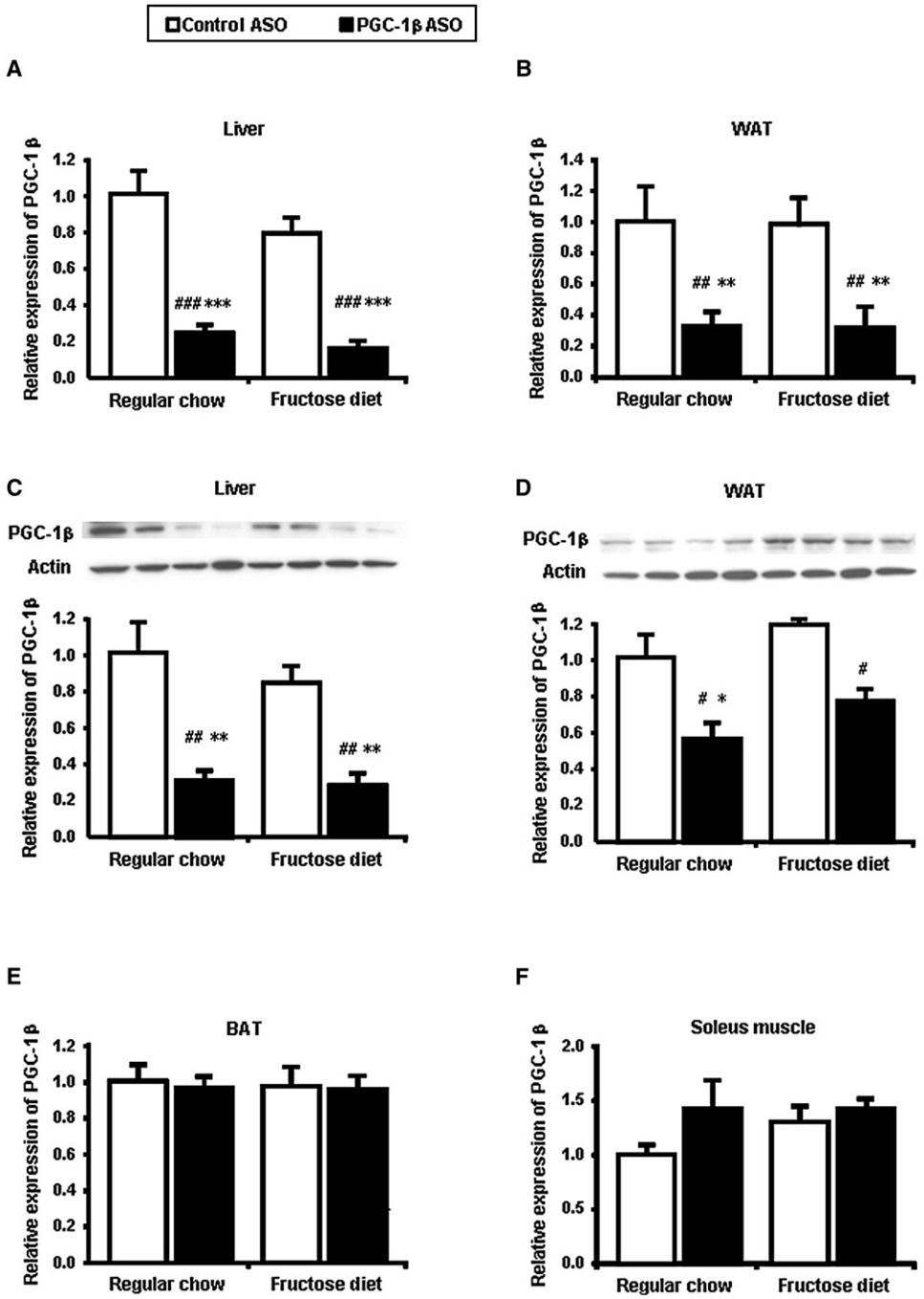

Figure 1. PGC-1β ASO Treatment Is Effective and Well Tolerated

(A–F) The amount of PGC-1β mRNA was determined by quantitative RT-qPCR after 4 weeks of feeding with fructose and treatment with a control ASO and an ASO against PGC-1β (PGC-1β ASO) in liver (A), epididymal WAT (B), BAT (E), and soleus muscle (F). PGC-1β protein levels are shown in liver (C) and WAT (D). Two separate samples are shown for each group fraction. Data are means ± SEM. Data are expressed as relative to expression in regular chow-fed control ASO-treated rats (n = 7–9 rats per treatment group). $^{\#}p < 0.05$, $^{\#\#}p < 0.01$, $^{\#\#\#}p < 0.001$ versus regular chow-fed control ASO-treated rats; $^{*}p < 0.05$, $^{**}p < 0.01$, $^{***}p < 0.001$ versus high-fructose-fed control ASO-treated rats.

converts cholesterol into 7α-hydroxycholesterol and is responsible for the rate-limiting step in the classical bile acid synthesis pathway. Thus, CYP7A1 mediates clearance of cholesterol from the circulation, and it is possible that the decrease in CYP7A1 protein expression is responsible for the observed increased concentrations of cholesterol in the PGC-1β ASO-treated rats. Some other target genes of LXR (SR-B1, ABCG8) had decreased transcription by PGC-1β ASO treatment (Table S1); however, there was no difference in protein expression (data not shown).

Table 1. Physiologic and Plasma Parameters in Control and PGC-1β ASO-Treated Rats

	Regular chow		Fructose diet	
	Control ASO	PGC-1β ASO	Control ASO	PGC-1β ASO
Physiologic parameters				
Body weight (g)	356 ± 6	344 ± 7	363 ± 5	343 ± 6
Epididymal fat mass (g)	3.82 ± 0.21	4.57 ± 0.36[d]	6.16 ± 0.40[c]	5.33 ± 0.18[a]
Plasma metabolites				
Glucose (mg/dl)	117.5 ± 1.8	112.9 ± 1.7[f]	129.2 ± 2.6[c]	113.3 ± 1.6[f]
Triglyceride (mg/dl)	49.2 ± 4.1	52.4 ± 5.6[e]	92.0 ± 10.4[c]	55.2 ± 3.9[e]
Total cholesterol (mg/dl)	64.1 ± 4.1	88.1 ± 5.8[b,d]	68.9 ± 3.1	108.7 ± 5.4[c,f]
HDL cholesterol (mg/dl)	23.1 ± 0.9	32.1 ± 1.4[b,d]	25.3 ± 0.9	41.3 ± 2.3[c,f]
Nonesterified fatty acid (meq/l)	1.04 ± 0.06	1.22 ± 0.10	1.50 ± 0.12[b]	1.39 ± 0.10
β-hydroxybutyrate (mmol/l)	0.84 ± 0.05	1.18 ± 0.07[a]	1.11 ± 0.08	1.23 ± 0.08[b]
ALT (units/l)	47.1 ± 5.2	55.8 ± 6.0	38.9 ± 3.8	43.8 ± 3.4
Plasma hormones and adipocytokines				
Insulin (mU/l)	10.4 ± 1.1	8.0 ± 1.4[f]	19.8 ± 2.1[c]	12.5 ± 1.0[e]
Glucagon (pg/ml)	46.9 ± 8.8	51.9 ± 5.4	40.5 ± 5.0	54.6 ± 5.4
Adiponectin (mg/ml)	2.82 ± 0.07	3.11 ± 0.13	3.15 ± 0.04	2.78 ± 0.11
Leptin (ng/ml)	1.02 ± 0.19	0.74 ± 0.15	1.82 ± 0.28	0.91 ± 0.12[d]
RBP4 (μg/ml)	43.5 ± 4.33	35.1 ± 3.92	45.7 ± 2.99	53.2 ± 4.24

Data are means ± SEM; n = ~25 rats in each group.
[a]$p < 0.05$, [b]$p < 0.01$, and [c]$p < 0.001$ versus regular chow-fed control ASO-treated rats.
[d]$p < 0.05$, [e]$p < 0.01$, and [f]$p < 0.001$ versus high-fructose-fed control ASO-treated rats.

PGC-1β ASO Protects High-Fructose-Fed but Not Regular Chow-Fed Rats from Hepatic Insulin Resistance

PGC-1β ASO lowered fasting plasma glucose and insulin concentrations in high-fructose-fed rats, suggesting improved insulin sensitivity. We performed hyperinsulinemic-euglycemic clamps in order to further understand the mechanisms of improved insulin sensitivity. The basal rate of hepatic glucose production (HGP) was significantly increased in high-fructose-fed rats compared with regular chow-fed rats (Figure 4A). In fructose-fed rats, PGC-1β ASO treatment decreased HGP along with plasma glucose and insulin concentrations.

Under hyperinsulinemic-euglycemic conditions, plasma insulin concentrations were raised to ~80 mU/l while plasma glucose levels were maintained at approximately 5.5 mM in all groups with a variable infusion of glucose (data not shown). Under these conditions, HGP was significantly higher in high-fructose-fed rats (Figure 4B). PGC-1β ASO treatment improved the ability of insulin to suppress HGP in high-fructose-fed rats (Figure 4B).

We measured hepatic diacylglycerol (DAG), which has previously been associated with insulin resistance (Samuel et al., 2004). In the basal state, DAG concentration was markedly increased in high-fructose-fed rats (Figure 4C). PGC-1β ASO treatment decreased DAG concentrations 60% (Figure 4C). In the past, we have shown that DAG accumulation leads to PKCε activation (Samuel et al., 2007). The decreased DAG concentrations seen with PGC-1β ASO were associated with decreased PKCε membrane to cytosol ratio (Figure 4E) and increased hepatic Akt activity (Figure 4G).

In contrast with fructose feeding, HGP was paradoxically higher in the regular chow-fed PGC-1β ASO-treated rats (Figure 4B). Hepatic DAG concentration was significantly increased, ~2-fold, in regular chow-fed PGC-1β ASO-treated rats after insulin stimulation (Figure 4D). PKCε membrane to cytosol ratio was increased over six times in regular chow-fed PGC-1β ASO-treated rats after insulin stimulation (Figure 4F).

The unexpected hepatic insulin resistance seen in the regular chow groups is consistent with previous studies in mice lacking exons 3–4 of the PGC-1β gene (PGC-1β$^{E3,4-/E3,4-}$ mice) (Vianna et al., 2006). In these mice, defects in mitochondrial oxidative capacity were implicated in the development of insulin resistance. PGC-1β has been reported to coactivate both PPARα (Lin et al., 2003), which plays a key role in control of fatty acid oxidation, and nuclear respiratory factor (NRF)-1 (Wu et al., 1999), which regulates proteins required for mitochondrial function (Scarpulla, 2002). PGC-1β ASO significantly decreased PPARα mRNA expression and its target genes LCAD, MCAD, and CPT1a in both regular chow-fed and high-fructose-fed rats by ~30% (Figures 5A and 5B). NRF-1 mRNA expression was significantly decreased by 40% (Figure 5C). Consistent with this reduction, mitochondrial copy numbers were also significantly reduced by 30% in PGC-1β ASO-treated groups (Figure 5D). Additionally, PGC-1β ASO decreased expressions of ATPase synthase subunit 6 (ATP6), a mitochondrial encoded gene, and cytochrome C, a nuclear encoded mitochondrial gene (Figure 5E).

In order to determine whether PGC-1β ASO has any effect on other diet-induced insulin resistance models, we tested PGC-1β ASO on rats fed a high-fat diet. Though both fasting plasma glucose and insulin concentrations were significantly decreased in PGC-1β ASO-treated high-fat-fed rats (Figures S1A and S1B), there was no difference in HGP both under basal and insulin-stimulated conditions (Figure S1C). In addition, the degree of induction of SREBP-1c with refeeding was less than that observed compared to high-fructose-fed rats. PGC-1β ASO did not decrease SREBP-1c mRNA expression (Figure S1E).

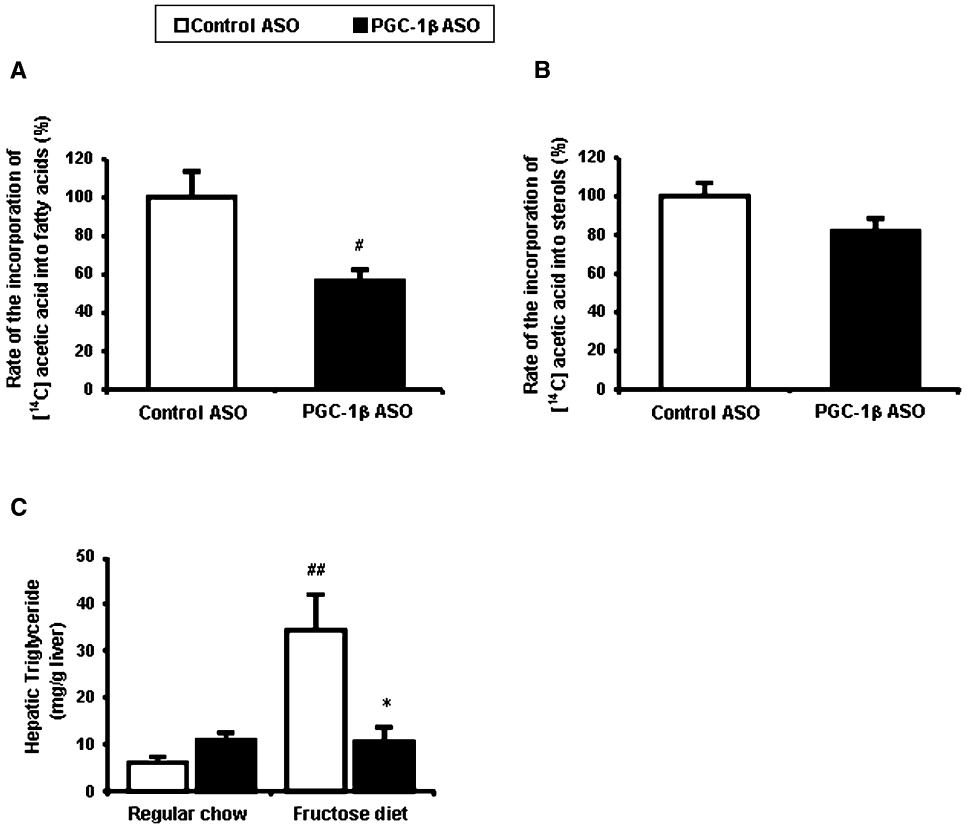

Figure 2. PGC-1β ASO Treatment Reduces Fatty Acid Synthesis In Vitro and Triacylglycerol Content In Vivo

(A and B) Synthesis of fatty acids (A) and sterols (B) in rat hepatocytes. $^{\#}p < 0.05$ versus control ASO.

(C) Hepatic triglyceride content. Data are means ± SEM (n = 11–14 rats per treatment group). $^{\#}p < 0.01$ versus regular chow-fed control ASO-treated rats; $^{*}p < 0.05$ versus high-fructose-fed control ASO-treated rats.

The unchanged expression of SREBP-1c was reflected by unchanged DAG accumulation in liver (Figure S1E).

PGC-1β ASO Treatment Improves Adipose Insulin Action in High-Fructose-Fed Rats

Insulin-stimulated whole-body glucose disposal was decreased by ~50% in the high-fructose-fed rats compared to the regular chow-fed rats (Figure 6A). PGC-1β ASO rescued the fructose-induced insulin resistance, as shown by the 90% increase in insulin-stimulated whole-body glucose uptake.

In order to determine the organs' response to the increased insulin-stimulated glucose uptake seen in high-fructose-fed PGC-1β ASO-treated rats, we assessed [^{14}C]2-deoxyglucose uptake in muscle and adipose tissue. There was no significant increase in either muscle or BAT [^{14}C]2-deoxyglucose uptake (Figures 6B and 6C). However, in high-fructose-fed PGC-1β ASO-treated rats, glucose uptake in the epididymal WAT was increased nearly 4-fold compared with that in the other three groups (Figure 6D). The augmented adipose insulin sensitivity is corroborated by a decreased plasma fatty acid concentration during the hyperinsulinemic-euglycemic clamps (data not shown). To further explore the mechanism for the increased WAT glucose uptake, we first examined the gene expression of PPARγ and its target genes in epididymal WAT. Surprisingly, the expression of PPARγ was decreased by 50%, and adipocyte protein 2 (aP2), adiponectin, and acyl-CoA synthetases (ACS) were decreased in PGC-1β ASO-treated groups (Table S2). PGC-1β also induces mRNA expression of GLUT4 in cultures of primary rat skeletal muscle cells (Mortensen et al., 2006). In the present study, GLUT4 mRNA in WAT was decreased by 50% in PGC-1β ASO-treated groups (Table S2). In contrast, the protein expression in both total tissue lysate and plasma membrane was increased ~2-fold in only PGC-1β ASO-treated high-fructose-fed rats (Figures 6E and 6F), consistent with the result of 2-deoxyglucose uptake in WAT. There were no differences in the expression of other glucose transporters (GLUT1 and GLUT5 [known as a fructose transporter]) (data not shown).

The discordance between GLUT4 mRNA and protein could possibly be explained by increased expression of associated proteins that regulate GLUT4 trafficking and stability. However, we were unable to detect any changes in the expression of these proteins that accounted for the increased WAT GLUT4 protein content in the PGC-1β ASO-treated rats (Table S2). Furthermore, one report suggests that GLUT4 can be degraded by calpain-2 (Otani et al., 2004). But calpain-1/-2 activity was similar across all groups (data not shown).

Interestingly, this amelioration of diet-induced insulin resistance by PGC-1β ASO was not seen in high-fat-fed rats (Figure 6A). Consistent with this result, GLUT4 protein expression in WAT was not increased in high-fat-fed rats (Figure S1F).

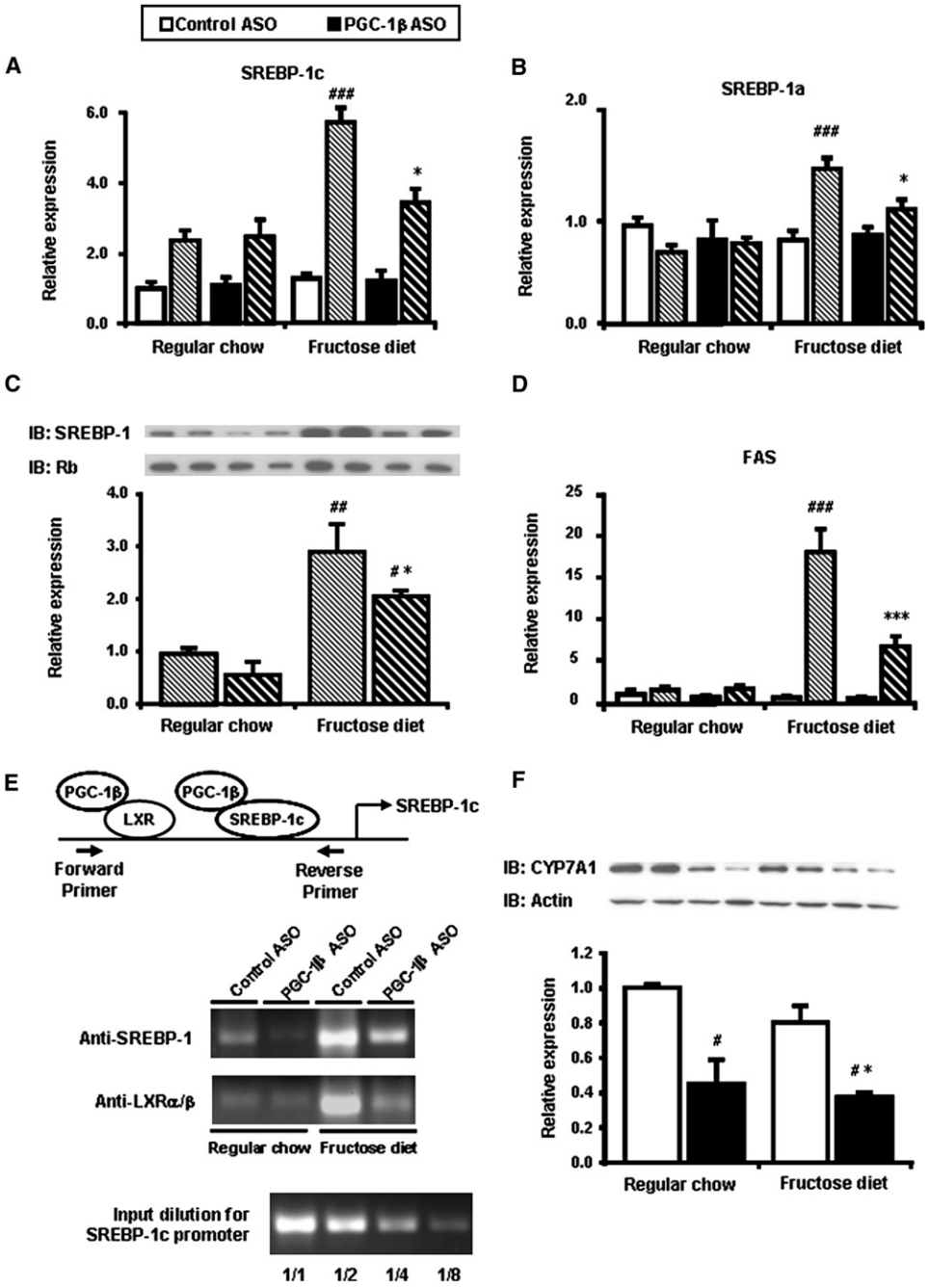

Figure 3. PGC-1β ASO Treatment Reduces Expression of Lipogenic Genes in Liver

(A and B) Total mRNA was isolated from fasted and fed liver and quantified using primers for SREBP-1c (A) and -1a (B).

(C) Representative immunoblots of liver homogenates from liver in fed state. Two separate samples are shown for each group.

(D) Total mRNA was isolated from fasted and fed liver and quantified using primers for key enzymes in FAS.

(E) ChIP assay of SREBP-1c gene promoter. After cross linking chromatin DNA to the interacting proteins, specific immunoprecipitation with anti-SREBP-1 or anti-LXRα/β antibodies was performed as described in Experimental Procedures. PCR products of the SREBP-1c promoter were analyzed after PCR amplification (33 cycles). The lower part of the figure shows verification of the quantitative aspect of the PCR amplification using serial dilutions of the input.

(F) Liver gene expression of CYP7A1. Data are means ± SEM (n = 7–9 rats per treatment group). Solid bars represent fasted values, and striped bars represent fed values. $^{\#}p < 0.05$, $^{\#\#}p < 0.01$, $^{\#\#\#}p < 0.001$ versus regular chow-fed control ASO-treated rats; $^{*}p < 0.05$, $^{**}p < 0.01$, $^{***}p < 0.001$ versus high-fructose-fed control ASO-treated rats.

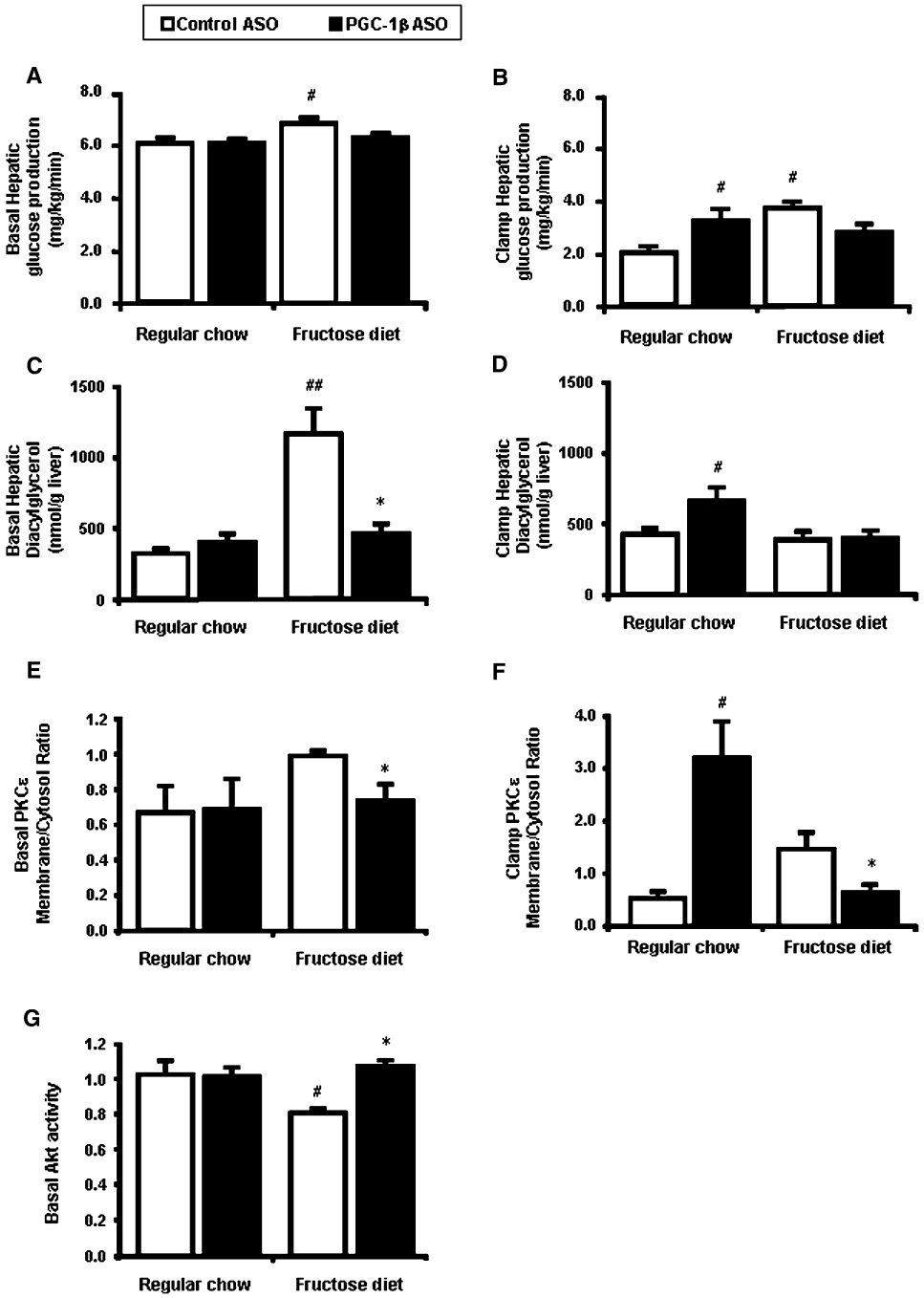

Figure 4. PGC-1β ASO Treatment Protects against Fructose-Induced Hepatic Insulin Resistance but Induces Hepatic Insulin Resistance in Regular Chow-Fed Rats

(A and B) Rate of basal (A) and clamp (B) endogenous glucose production.

(C and D) Hepatic total DAG obtained from basal (C) and clamp (D) liver.

(E and F) Representative western blots showing basal (E) and clamp (F) membrane to cytosol fractions ratio for PKCε. The relative densities of the bands in the membrane fraction were compared with the cytosol fraction to derive a quantifiable measure of activation.

(G) Basal Akt activity in liver. Data are means ± SEM (n = 6–20 rats per treatment group) $^{\#}p < 0.05$ versus regular chow-fed control ASO-treated rats; $^{*}p < 0.05$ versus high-fructose-fed control ASO-treated rats.

DISCUSSION

It is becoming increasingly clear that PGC-1β plays an important role as a regulator of both carbohydrate and lipid metabolism. In the present study, we evaluated the metabolic effects of PGC-1β knockdown in rats with fructose-induced insulin resistance. Here we show that hepatic de novo lipogenesis and hepatic triglyceride synthesis induced by fructose are both decreased by

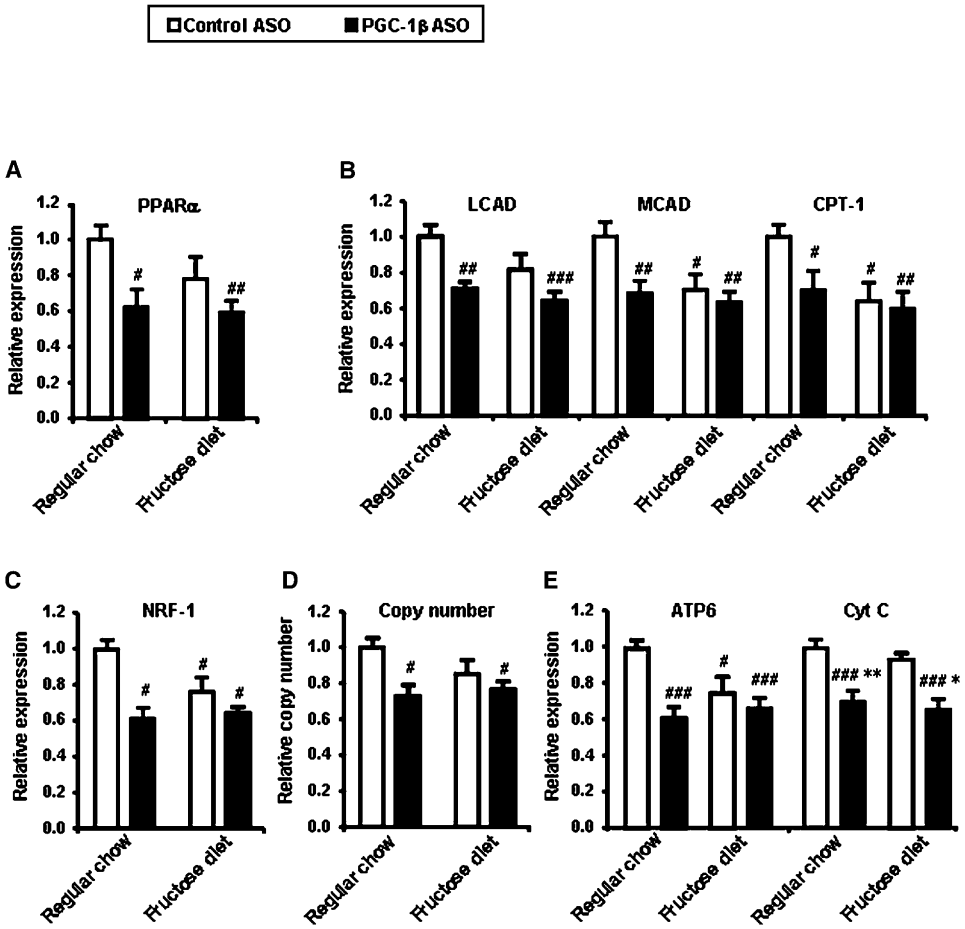

Figure 5. PGC-1β ASO Treatment Reduces Genes Involved with Mitochondrial Fatty Acid Oxidation, Biogenesis, and Function

(A and B) Liver gene expression of PPARα (A) and target enzymes in fatty acid oxidation (B).

(C–E) Liver gene expression of NRF-1 (C) and target enzymes in mitochondrial oxidative phosphorylation (E). mtDNA copy number is determined by real-time qPCR using primers for mitochondrial encoded gene (ATP6) and nuclear encoded gene (β-actin) (D). mtDNA copy number is calculated as the ratio of ATP6 to β-actin. Data are means ± SEM (n = 6–8 rats per treatment group). $^{\#}p < 0.05$, $^{\#\#}p < 0.01$, $^{\#\#\#}p < 0.001$ versus regular chow-fed control ASO-treated rats; $^{*}p < 0.05$, $^{**}p < 0.01$ versus high-fructose-fed control ASO-treated rats.

PGC-1β ASO treatment. Furthermore, we show that knockdown of PGC-1β prevents fructose-induced hypertriglyceridemia and hepatic and peripheral insulin resistance.

PGC-1β has been reported to coactivate its partners through augmentation of their transcriptional activity (Lin et al., 2005). Though initially described to pair with PPARγ, the number of partners for PGC-1 transcription factors is rapidly growing. One of its partners is SREBP-1c. The transcriptional control of this key regulator of lipogenesis is complex. It has been reported that rat and human SREBP-1c promoter contains binding sites for both SREBP itself (Cagen et al., 2005) and LXR (Dif et al., 2006), which are both regulated by PGC-1β (Lin et al., 2005).

The ChIP assay data showed a marked increase in the association of both SREBP-1 and LXRα/β with the SREBP-1c promoter on a high-fructose diet. The bindings were both decreased by PGC-1β ASO treatment. Undoubtedly, the binding of SREBP-1 to SREBP-1c promoter might be reflected with the amount of SREBP-1 total protein, but the binding of LXR to SREBP-1c promoter was also decreased by PGC-1β ASO treatment. LXR protein was unchanged between all groups, implying that the decreased binding to the SREBP-1c promoter was due to the decreased coactivation with PGC-1β. Thus, these data suggest that PGC-1β ASO treatment reduces SREBP-1c expression by decreased coactivation of LXR and SREBP.

Consistent with the reduction of SREBP-1 expression, FAS, a target lipogenic gene of SREBP-1, was downregulated in high-fructose-fed PGC-1β ASO-treated rats. This likely accounted for the observed decrease in hepatic de novo lipogenesis and hepatic triglyceride content and reductions in hypertriglyceridemia in the high-fructose-fed PGC-1β ASO-treated rats. Supporting these observations, we found that in vitro hepatic triglyceride synthesis was significantly inhibited in primary rat hepatocytes by PGC-1β ASO treatment.

Knockdown of PGC-1β in liver protected rats from fructose-induced hepatic insulin resistance. This protection from fructose-induced hepatic insulin resistance could mostly be attributed to reduction in hepatic lipogenesis resulting in reduced hepatic DAG content and decreased PKCε activation. These data were also reflected in Akt activity.

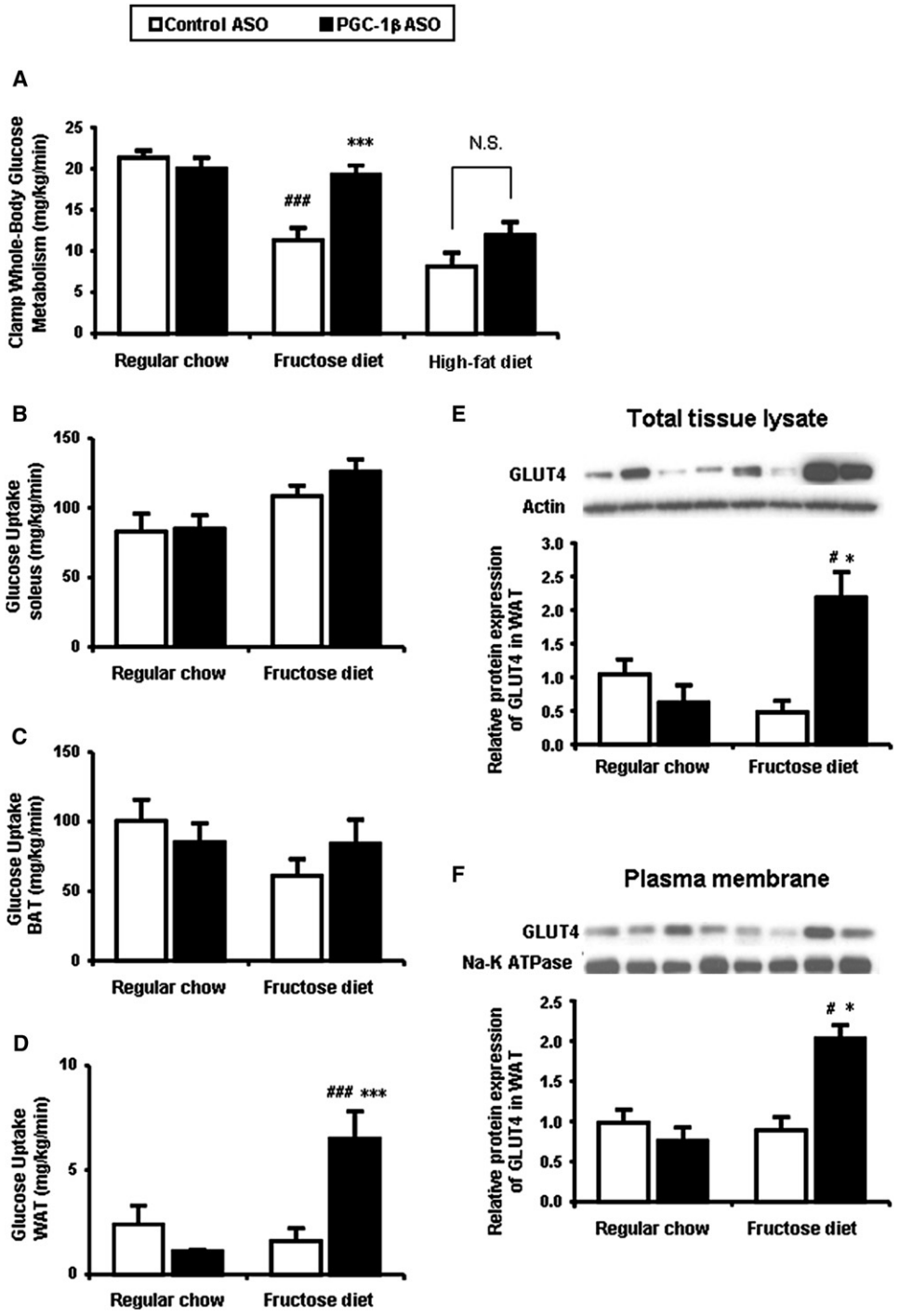

Figure 6. PGC-1β ASO Treatment Improves Peripheral Insulin Sensitivity Due to an Increase in White Adipose Tissue Glucose Uptake in High-Fructose-Fed Rats

(A) Rate of insulin-stimulated whole-body glucose uptake.

(B) Soleus [^{14}C]2-deoxyglucose (2DG) uptake.

(C) BAT 2DG uptake.

(D) Epididymal WAT 2DG uptake.

(E and F) Western blotting of extract from total tissue (E) and plasma membrane fraction (F) using the GLUT4-specific mouse monoclonal antibody (1F8). Two separate samples are shown for each group fraction. Data are means ± SEM (n = 6–20 rats per treatment group). $^{\#}p < 0.001$ versus regular chow-fed control ASO-treated rats; $^{*}p < 0.05$, $^{***}p < 0.001$ versus high-fructose-fed control ASO-treated rats.

In marked contrast to these findings, the effects of PGC-1β ASO on the liver differed in the regular chow- and high-fructose-fed rats. In regular chow-fed rats, PGC-1β ASO induced slight but significant reductions in insulin suppression of HGP. These reductions in insulin responsiveness could be attributed to decreased mitochondrial fatty acid oxidation resulting in increased DAG content and to increased PKCε activation resulting in decreased insulin signaling (Samuel et al., 2007). PGC-1s have been reported to coactivate both PPARα and NRF-1. PPARα plays a key role in the transcriptional control of genes encoding mitochondrial fatty acid oxidation enzymes such as LCAD and MCAD. NRFs regulate expression of mitochondrial transcription factor A (Tfam), a nuclear-encoded transcription factor essential for replication, maintenance, and transcription of mitochondrial DNA. NRFs also control the expression of nuclear genes encoding respiratory chain subunits and other proteins required for mitochondrial function (Scarpulla, 2002). PGC-1β ASO decreased expression of genes encoding fatty acid oxidation and oxidative phosphorylation as well as mitochondrial copy number, suggesting that PGC-1β is required in liver for normal expression of genes encoding fatty acid oxidation and oxidative phosphorylation. These results are consistent with previous studies in PGC-1β$^{E3,4-/E3,4-}$ mice (Vianna et al., 2006) and LCAD knockout mice, which both develop hepatic steatosis and hepatic insulin resistance due to decreased hepatic fat oxidation, resulting in increased hepatic DAG content and increased PKCε activation (Zhang et al., 2007).

PGC-1β ASO also prevented fructose-induced insulin resistance in peripheral tissue. This preservation of insulin responsiveness could be attributed largely to a 3-fold increase in insulin-stimulated WAT glucose uptake. Since the PGC family members are known coactivators of PPARs, we examined the expression of PPARγ and its target genes. The expression of PPARγ itself, as well as of key target genes, was reduced with PGC-1β ASO treatment and could not explain the observed improvements in insulin action.

We next investigated GLUT4 expression and found that the GLUT4 protein expression in WAT was increased more than 4-fold in the high-fructose-fed PGC-1β ASO-treated rats. This was compatible with our findings in the glucose uptake, although the mRNA expression of GLUT4 was surprisingly decreased by PGC-1β ASO treatment. A similar dissociation between GLUT4 protein and mRNA expression has been reported by Otani et al. (Otani et al., 2004). We believe this result may reflect enhanced stability of GLUT4 protein, leading to its accumulation. However, in the present study, we did not find any explanations in the gene expression of GLUT4 trafficking proteins. Further studies are required to explain why the increases of 2-deoxyglucose uptake and GLUT4 protein expression were seen in only high-fructose-fed PGC-1β ASO-treated rats.

We tested PGC-1β ASO on rats fed a high-fat diet to understand if the protection from diet-induced insulin resistance was specific for high-fructose diet. PGC-1β ASO failed to ameliorate both hepatic and peripheral insulin resistance in high-fat-fed rats. The degree of SREBP-1 induction with high-fat diet was less than that with high-fructose diet, and PGC-1β ASO did not affect the SREBP-1 mRNA expression on high-fat diet. Consequently, the unaffected lipogenesis resulted in similar hepatic lipid content between control ASO and PGC-1β ASO groups. These findings raise the possibility that fructose can directly induce the transcriptional activity of SREBP-1 via PGC-1β.

Interestingly, we also found that PGC-1β ASO treatment increased plasma cholesterol concentrations. We did not observe any increases in the expression of SREBP-2, a key transcriptional regulator of cholesterol biosynthesis, or in the SREBP-2 responsive genes HMGCoAR or LDL-R following PGC-1β ASO treatment. These data suggest that cholesterol biosynthesis in liver and LDL uptake from plasma by liver were unlikely to be responsible for the observed increases in plasma cholesterol in the PGC-1β ASO-treated groups. Consistent with these observations, we found that reduction in PGC-1β expression in primary rat hepatocytes had no effect on the incorporation rate of [^{14}C]acetic acid into sterol. We next investigated the effects of PGC-1β knockdown on the expression of LXRα and its target genes. LXRα has been shown to be an important regulator of cholesterol (Kalaany et al., 2005) and is coactivated by PGC-1s (Lin et al., 2005). Although we found that LXRα expression was not different in the four groups, hepatic CYP7A1 expression was decreased in both PGC-1β ASO-treated groups. Since CYP7A1 is responsible for the rate-controlling step in the bile acid synthesis pathway, it is likely that this reduction in CYP7A1 may explain the increased plasma cholesterol concentrations in the PGC-1β ASO-treated rats.

In conclusion, these data support an important role for PGC-1β in the pathogenesis of fructose-induced hypertriglyceridemia and insulin resistance. Furthermore, given recent studies suggesting an important role for increased hepatic de novo lipogenesis in the pathogenesis of hypertriglyceridemia and NAFLD associated with the metabolic syndrome (Petersen et al., 2007), these data suggest that PGC-1β inhibition may be a therapeutic target for treatment of this condition.

EXPERIMENTAL PROCEDURES

Animals

All rats were maintained in accordance with the Institutional Animal Care and Use Committee of Yale University School of Medicine. Healthy male Sprague-Dawley rats weighing ~200 g were obtained from Charles River Laboratories and acclimated for 1 week after arrival before initiation of the experiment. Rats received water ad libitum and were maintained on a 12:12 hr light/dark cycle (lights on at 6:00 a.m.). They received regular rodent chow (60% carbohydrate, 10% fat, 30% protein calories), a high-fructose diet (66.8% carbohydrate, 13% fat, 20.2% protein calories, TD.89247) (Harlan Teklad; Madison, WI), or a high-fat diet (24.0% carbohydrate, 54.8% fat, 21.2% protein calories, TD.93075) (Harlan Teklad; Madison, WI) three times per week at a weight of 225 g per week for 4 weeks. Intraperitoneal (i.p.) ASO therapy was initiated 3 days after commencing the high-fructose diet. All ASOs (control and PGC-1β) were prepared in normal saline, and the solutions were sterilized through a 0.2 μm filter. Rats were dosed with ASO solutions twice per week via i.p. injection at a dose of 50 mg/kg per week for 4 weeks. During the treatment period, body weight was measured weekly. After 14–20 days of ASO treatment, rats underwent the placement of jugular venous and carotid artery catheters. They recovered their presurgical weights by 5–7 days after the operation.

Selection of Rat PGC-1β ASOs

To identify rat PGC-1β ASO inhibitors, rapid throughput screens were performed in vitro as described previously (Qu et al., 1999). In brief, 80 ASOs were designed to the rat PGC-1β mRNA sequences, and initial screens identified several potent and specific ASOs, all of which targeted a binding site within the coding region of the PGC-1β mRNAs. After extensive dose-response characterization, the most potent ASO from the screen was chosen: ISIS-384891, with the following sequence: 5-CTGGAAGTCCTGGGAGACAC-3.

The control ASO, ISIS-141923, has the following sequence: 5-CCTTCCCTGAA GGTTCCTCC-3, and does not have perfect complementarity to any known gene in public databases.

Hyperinsulinemic-Euglycemic Clamp Studies

After 4 weeks of the assigned diet, rats were fasted overnight. The following morning, the clamp study began with a prime (1 mg/kg for 8 min) of [6,6-^{2}H]glucose followed by a continuous infusion at a rate of 0.1 mg/kg per minute for 2 hr to assess the basal glucose turnover. After the basal period, the hyperinsulinemic-euglycemic clamping was conducted for 140 min with a primed/continuous infusion of human insulin (400 mU/kg prime for 5 min, 4 mU/kg/min infusion) (Novo Nordisk) and a variable infusion of 20% dextrose to maintain euglycemia (approximately 100 mg/dl). The 20% glucose was enriched with [6,6-^{2}H]glucose to approximately 2.5% to match the enrichment in the plasma achieved after the basal period. A 30 μCi bolus of 2-deoxy-d-[1-^{14}C]glucose (PerkinElmer) was injected 120 min into the clamp to estimate the rate of insulin-stimulated tissue glucose uptake. At the end of the clamp, rats were anesthetized with pentobarbital sodium injection (150 mg/kg), and all tissues were taken within 4 min, frozen immediately with the use of liquid N_2-cooled aluminum tongs, and stored at −80°C for subsequent analysis.

Biochemical Analysis and Calculations

Plasma glucose was analyzed during the clamping with the use of 10 μl plasma by a glucose oxidase method on a Beckman Glucose Analyzer II (Beckman Coulter). Plasma insulin and adiponectin were measured by RIA using kits from Linco. Plasma leptin was measured using the LINCOplex Assay system (Linco). Plasma RBP4 was measured using EIA Kit from ALPCO.

Plasma fatty acid concentrations were determined using an acyl-CoA oxidase-based colorimetric kit (Wako). To determine the enrichment of [6,6-^{2}H]glucose in plasma, samples were deproteinized with five volumes of 100% methanol, dried, and derivatized with 1:1 acetic anhydride/pyridine to produce the pentacetate derivative of glucose. The atom percentage enrichment of glucoseM + 2 was then measured by gas chromatographic/mass spectrometric analysis using a Hewlett-Packard 5890 Gas Chromatograph interfaced to a Hewlett-Packard 5971A Mass Selective Detector operating in the electron ionization mode (Hundal et al., 2002). GlucoseM + 2 enrichment was determined from the m/z ratio 202:200. Rates of basal and insulin-stimulated whole-body glucose turnover were determined as the ratio of the rate of [6,6-^{2}H]glucose infusion (mg/kg per min) to the atom percentage excess glucoseM + 2 (%) in the plasma. This rate was corrected by subtraction of the rate of [6,6-^{2}H]glucose infusion. HGP was determined by subtraction of the glucose infusion rate from the rate of total glucose appearance. For the determination of muscle and WAT [^{14}C]2-deoxyglucose-6-phosphate content, tissue samples were homogenized, and the supernatants were subjected to an ion-exchange column to separate [^{14}C]2-deoxyglucose-6-phosphate from 2-deoxyglucose as previously described (Youn and Buchanan, 1993).

Tissue Lipid Measurement

The DAG extraction and analysis were performed as previously described (Yu et al., 2002). After purification, DAG fractions were dissolved in methanol/H_2O (1:1, vol/vol) and subjected to liquid chromatography-tandem mass spectrometry (LC/MS/MS) analysis. A Turbo Ion Spray source was interfaced with an API 3000 Tandem Mass Spectrometer (Applied Biosystems) in conjunction with two PerkinElmer Series 200 Micro Pumps and a PerkinElmer Series 200 Autosampler. Total DAG content is expressed as the sum of individual species. Tissue triglyceride was extracted by the method of Bligh and Dyer (Bligh and Dyer, 1959) and measured with the use of a DCL Triglyceride Reagent (Diagnostic Chemicals Ltd.).

Total RNA Preparation and RT-qPCR Analysis

Total RNA was extracted from liver samples using the RNeasy Kit (QIAGEN). RNA was reverse-transcribed into cDNA with the use of M-MuLV Reverse Transcriptase (New England Biolabs). The abundance of transcripts was assessed by real-time PCR on an Applied Biosystems 7500 Real-Time PCR System (Applied Biosystems) with a SYBR Green detection system. For each run, samples were run in duplicate for both the gene of interest and actin. The expression data for each gene of interest and actin were normalized for the efficiency of amplification, as determined by a standard curve included on each run (Pfaffl, 2001).

mtDNA Content

Total DNA was isolated from 20 mg of each basal liver using a QIAamp DNA Micro Kit (QIAGEN). Fifty nanograms of total DNA was used as a template in 20 μl PCR reaction using an Applied Biosystems 7500 Real-Time PCR System with a SYBR Green detection system against ATP6 (mitochondrial encoded gene) and β-actin (nuclear encoded gene). mtDNA copy number was presented as a ratio of ATP6 to β-actin as previously described (Bhat and Epelboym, 2004).

Determination of Fatty Acid and Sterol Synthesis in Transfected Rat Hepatocytes In Vitro

Primary rat hepatocytes were isolated as previously described and plated onto collagen-coated 25 cm^2 flasks for 60 mm plates for the synthesis measurement. Hepatocytes were treated with ASO (150 nM) and Lipofectin (Invitrogen) mixture for 4 hr in serum-free Williams' Media E (Invitrogen). ASO and Lipofectin were mixed in a ratio of 3 μg of Lipofectin for every 1 ml of 100 nM ASO concentration. After 4 hr, ASO reaction mixture was replaced with normal maintenance media (Williams' Media E with 10% FBS and 10 nM insulin). The cells were incubated under normal conditions for 20–24 hr, and then fatty acid and sterol synthesis (incorporation of [^{14}C]acetic acid into fatty acid and sterol) were measured as described previously (Yu et al., 2005).

Western Blotting

For SREBP-1 quantification, nuclear protein was extracted using NE-PER Nuclear and Cytoplasmic Extraction Reagents (Pierce). The protein extracts were resolved by SDS-PAGE using 4%–12% gradient gel (Invitrogen) and electroblotted onto PVDF membrane (DuPont) with the use of a wet transfer cell (Bio-Rad). The membrane was then blocked for 2 hr at room temperature in PBS-Tween (10 mmol/l NaH_2PO_4, 80 mmol/l Na_2HPO_4, 0.145 mol/l NaCl, and 0.1% Tween-20, pH 7.4) containing 5% (weight/vol) nonfat powder dried milk, washed twice, and incubated overnight with rabbit anti-peptide antibody against SREBP-1 (H-160; Santa Cruz Biotechnology, Inc.) diluted 1:100 in rinsing solution. After further washings, membranes were incubated with HRP-conjugated IgG fraction of goat anti-rabbit IgG (Bio-Rad), diluted 1:5,000 in PBS-Tween, for 2 hr. These blots were stripped and reblotted with rabbit anti-retinoblastoma-associated protein (Rb) IgG to normalize for variations in protein loading. Blots were scanned and analyzed with ImageJ (NIH).

A separate group of rats was used to assess the impact of hepatic DAG accumulation and PKCε quantification. These rats were treated exactly as described above and underwent 20 min of hyperinsulinemic-euglycemic clamping after a basal infusion. Tissues were harvested in situ immediately at the end of the clamping. For PKCε quantification, plasma membrane and cytosol protein were extracted using ProteoExtract Native Membrane Protein Extraction Kit (Calbiochem). Western blotting was performed as described above. Twenty micrograms of homogenized samples were blotted on PVDF membranes. The membrane was incubated overnight with rabbit anti-peptide antibody against PKCε (1:1000; Santa Cruz Biotechnology, Inc.). These blots were stripped and reblotted with plasma membrane marker, mouse sodium potassium ATPase IgG (abcam), and rabbit anti-actin IgG to normalize for variations in protein loading. The polyclonal PGC-1β antibodies were a kind gift provided by Doctor B. Spiegelman, Harvard Medical School, and purchased from Novus.

Chromatin Immunoprecipitation Assay

ChIP assays were performed according to the procedure described previously (Gosmain et al., 2005; Deng et al., 2007) with minor modifications using ChampionChIP One-Day Kit (SABiosciences). Fresh liver samples (300 mg) were minced and treated for 15 min with 10 ml formaldehyde (1% final concentration in DMEM) at room temperature. Cross linking was stopped by the addition of glycine to a final concentration of 125 mM. Chromatin extracts were prepared from tissue homogenates and further fragmented by sonication. The sonicated chromatin was first precleared for 1 hr with protein G agarose/salmon sperm DNA beads (Millipore). After centrifugation, supernatants were incubated overnight at 4°C with 4 μg of an anti-SREBP-1 antibody (H-160; Santa-Cruz Biotechnology), 4 μg of anti-LXRα/β antibody (S-20; Santa-Cruz

Biotechnology), or normal-rabbit IgG. The immunoprecipitated DNA/protein complex was bound to protein A-Sepharose beads during 1 hr at 4°C and washed in low-salt buffer, high-salt buffer, LiCl buffer, and Tris-EDTA buffer. Proteins were eliminated using Proteinase K for 30 min at 45°C. The DNA was purified and used as a template for PCR. The sets of PCR primers used for the analysis of the rat SREBP-1c proximal promoter were 5-TGGTTGCCTGTGCGGCAG-3 (SREBP-1c-Pro-S) and 5-TCAGGCCCCGC CAGGCTTTAA-3 (SREBP-1c-Pro-AS). Real-time PCR analyses were performed using 7500 Real-Time PCR System (Applied Biosystems). The PCR amplification products were analyzed on ethidium bromide-stained 2% agarose gels.

Akt Activity

Liver Akt activity was measured using a commercially available kit (Assay Designs).

Calpain Activity

Calpain activity in WAT was determined using a commercially available kit (Calbiochem).

Statistics

Values are expressed as mean ± SEM. The significance of the differences in mean values among different treatment groups was evaluated by two-tailed Student's t tests or one-way ANOVA followed by post hoc analysis using the Tukey's Honestly Significant Differences (HSD) test. P values less than 0.05 were considered significant.

SUPPLEMENTAL DATA

Supplemental Data include two tables and one figure and can be found online at http://www.cell.com/cellmetabolism/supplemental/S1550-4131(09)00036-9.

ACKNOWLEDGMENTS

We thank Aida Grossmann, Yanna Kosover, Todd May, Mario Kahn, Rebecca Pongratz, Gary Cline, Takeshi Yoshizaki, and Katsutaro Morino for excellent technical assistance. This work was supported by grants from the United States Public Health Service (R01 DK-40936 and P30 DK-45735 to G.I.S., K23 RR-17404 to V.S., R01 DK-075772 to J.S.B.) and a Distinguished Clinical Scientist Award from the American Diabetes Association. G.I.S. is an investigator of the Howard Hughes Medical Institute. V.S. also receives support from the Veterans Administration Medical Center, West Haven, CT. J.S.B. also receives support from the W.M. Keck Foundation.

Received: July 29, 2008
Revised: December 12, 2008
Accepted: January 29, 2009
Published: March 3, 2009

REFERENCES

Basciano, H., Federico, L., and Adeli, K. (2005). Fructose, insulin resistance, and metabolic dyslipidemia. Nutr. Metab. (Lond) *2*, 5.

Bhat, H.K., and Epelboym, I. (2004). Quantitative analysis of total mitochondrial DNA: competitive polymerase chain reaction versus real-time polymerase chain reaction. J. Biochem. Mol. Toxicol. *18*, 180–186.

Bligh, E.G., and Dyer, W.J. (1959). A rapid method of total lipid extraction and purification. Can. J. Biochem. Physiol. *37*, 911–917.

Cagen, L.M., Deng, X., Wilcox, H.G., Park, E.A., Raghow, R., and Elam, M.B. (2005). Insulin activates the rat sterol-regulatory-element-binding protein 1c (SREBP-1c) promoter through the combinatorial actions of SREBP, LXR, Sp-1 and NF-Y cis-acting elements. Biochem. J. *385*, 207–216.

Daly, M.E., Vale, C., Walker, M., Alberti, K.G., and Mathers, J.C. (1997). Dietary carbohydrates and insulin sensitivity: a review of the evidence and clinical implications. Am. J. Clin. Nutr. *66*, 1072–1085.

Deng, X., Yellaturu, C., Cagen, L., Wilcox, H.G., Park, E.A., Raghow, R., and Elam, M.B. (2007). Expression of the rat sterol regulatory element-binding protein-1c gene in response to insulin is mediated by increased transactivating capacity of specificity protein 1 (Sp1). J. Biol. Chem. *282*, 17517–17529.

Dif, N., Euthine, V., Gonnet, E., Laville, M., Vidal, H., and Lefai, E. (2006). Insulin activates human sterol-regulatory-element-binding protein-1c (SREBP-1c) promoter through SRE motifs. Biochem. J. *400*, 179–188.

Elliott, S.S., Keim, N.L., Stern, J.S., Teff, K., and Havel, P.J. (2002). Fructose, weight gain, and the insulin resistance syndrome. Am. J. Clin. Nutr. *76*, 911–922.

Gosmain, Y., Dif, N., Berbe, V., Loizon, E., Rieusset, J., Vidal, H., and Lefai, E. (2005). Regulation of SREBP-1 expression and transcriptional action on HKII and FAS genes during fasting and refeeding in rat tissues. J. Lipid Res. *46*, 697–705.

Havel, P.J. (2005). Dietary fructose: implications for dysregulation of energy homeostasis and lipid/carbohydrate metabolism. Nutr. Rev. *63*, 133–157.

Hundal, R.S., Petersen, K.F., Mayerson, A.B., Randhawa, P.S., Inzucchi, S., Shoelson, S.E., and Shulman, G.I. (2002). Mechanism by which high-dose aspirin improves glucose metabolism in type 2 diabetes. J. Clin. Invest. *109*, 1321–1326.

Kalaany, N.Y., Gauthier, K.C., Zavacki, A.M., Mammen, P.P., Kitazume, T., Peterson, J.A., Horton, J.D., Garry, D.J., Bianco, A.C., and Mangelsdorf, D.J. (2005). LXRs regulate the balance between fat storage and oxidation. Cell Metab. *1*, 231–244.

Lin, J., Puigserver, P., Donovan, J., Tarr, P., and Spiegelman, B.M. (2002). Peroxisome proliferator-activated receptor gamma coactivator 1beta (PGC-1beta), a novel PGC-1-related transcription coactivator associated with host cell factor. J. Biol. Chem. *277*, 1645–1648.

Lin, J., Tarr, P.T., Yang, R., Rhee, J., Puigserver, P., Newgard, C.B., and Spiegelman, B.M. (2003). PGC-1beta in the regulation of hepatic glucose and energy metabolism. J. Biol. Chem. *278*, 30843–30848.

Lin, J., Yang, R., Tarr, P.T., Wu, P.H., Handschin, C., Li, S., Yang, W., Pei, L., Uldry, M., Tontonoz, P., et al. (2005). Hyperlipidemic effects of dietary saturated fats mediated through PGC-1beta coactivation of SREBP. Cell *120*, 261–273.

Michael, L.F., Wu, Z., Cheatham, R.B., Puigserver, P., Adelmant, G., Lehman, J.J., Kelly, D.P., and Spiegelman, B.M. (2001). Restoration of insulin-sensitive glucose transporter (GLUT4) gene expression in muscle cells by the transcriptional coactivator PGC-1. Proc. Natl. Acad. Sci. USA *98*, 3820–3825.

Mortensen, O.H., Frandsen, L., Schjerling, P., Nishimura, E., and Grunnet, N. (2006). PGC-1alpha and PGC-1beta have both similar and distinct effects on myofiber switching toward an oxidative phenotype. Am. J. Physiol. Endocrinol. Metab. *291*, E807–E816.

Nagai, Y., Nishio, Y., Nakamura, T., Maegawa, H., Kikkawa, R., and Kashiwagi, A. (2002). Amelioration of high fructose-induced metabolic derangements by activation of PPARalpha. Am. J. Physiol. Endocrinol. Metab. *282*, E1180–E1190.

Nagata, R., Nishio, Y., Sekine, O., Nagai, Y., Maeno, Y., Ugi, S., Maegawa, H., and Kashiwagi, A. (2004). Single nucleotide polymorphism (−468 Gly to A) at the promoter region of SREBP-1c associates with genetic defect of fructose-induced hepatic lipogenesis. J. Biol. Chem. *279*, 29031–29042.

Otani, K., Han, D.H., Ford, E.L., Garcia-Roves, P.M., Ye, H., Horikawa, Y., Bell, G.I., Holloszy, J.O., and Polonsky, K.S. (2004). Calpain system regulates muscle mass and glucose transporter GLUT4 turnover. J. Biol. Chem. *279*, 20915–20920.

Petersen, K.F., Dufour, S., Savage, D.B., Bilz, S., Solomon, G., Yonemitsu, S., Cline, G.W., Befroy, D., Zemany, L., Kahn, B.B., et al. (2007). The role of skeletal muscle insulin resistance in the pathogenesis of the metabolic syndrome. Proc. Natl. Acad. Sci. USA *104*, 12587–12594.

Pfaffl, M.W. (2001). A new mathematical model for relative quantification in real-time RT-PCR. Nucleic Acids Res. *29*, e45.

Puigserver, P., Rhee, J., Donovan, J., Walkey, C.J., Yoon, J.C., Oriente, F., Kitamura, Y., Altomonte, J., Dong, H., Accili, D., et al. (2003). Insulin-regulated hepatic gluconeogenesis through FOXO1-PGC-1alpha interaction. Nature *423*, 550–555.

Qu, X., Seale, J.P., and Donnelly, R. (1999). Tissue and isoform-selective activation of protein kinase C in insulin-resistant obese Zucker rats—effects of feeding. J. Endocrinol. *162*, 207–214.

Rhee, J., Inoue, Y., Yoon, J.C., Puigserver, P., Fan, M., Gonzalez, F.J., and Spiegelman, B.M. (2003). Regulation of hepatic fasting response by PPARgamma coactivator-1alpha (PGC-1): requirement for hepatocyte nuclear factor 4alpha in gluconeogenesis. Proc. Natl. Acad. Sci. USA *100*, 4012–4017.

Samuel, V.T., Liu, Z.X., Qu, X., Elder, B.D., Bilz, S., Befroy, D., Romanelli, A.J., and Shulman, G.I. (2004). Mechanism of hepatic insulin resistance in nonalcoholic fatty liver disease. J. Biol. Chem. *279*, 32345–32353.

Samuel, V.T., Liu, Z.X., Wang, A., Beddow, S.A., Geisler, J.G., Kahn, M., Zhang, X.M., Monia, B.P., Bhanot, S., and Shulman, G.I. (2007). Inhibition of protein kinase Cepsilon prevents hepatic insulin resistance in nonalcoholic fatty liver disease. J. Clin. Invest. *117*, 739–745.

Scarpulla, R.C. (2002). Nuclear activators and coactivators in mammalian mitochondrial biogenesis. Biochim. Biophys. Acta *1576*, 1–14.

Shimano, H., Horton, J.D., Shimomura, I., Hammer, R.E., Brown, M.S., and Goldstein, J.L. (1997). Isoform 1c of sterol regulatory element binding protein is less active than isoform 1a in livers of transgenic mice and in cultured cells. J. Clin. Invest. *99*, 846–854.

Sleder, J., Chen, Y.D., Cully, M.D., and Reaven, G.M. (1980). Hyperinsulinemia in fructose-induced hypertriglyceridemia in the rat. Metabolism *29*, 303–305.

Vega, R.B., Huss, J.M., and Kelly, D.P. (2000). The coactivator PGC-1 cooperates with peroxisome proliferator-activated receptor alpha in transcriptional control of nuclear genes encoding mitochondrial fatty acid oxidation enzymes. Mol. Cell. Biol. *20*, 1868–1876.

Vianna, C.R., Huntgeburth, M., Coppari, R., Choi, C.S., Lin, J., Krauss, S., Barbatelli, G., Tzameli, I., Kim, Y.B., Cinti, S., et al. (2006). Hypomorphic mutation of PGC-1beta causes mitochondrial dysfunction and liver insulin resistance. Cell Metab. *4*, 453–464.

Wu, Z., Puigserver, P., Andersson, U., Zhang, C., Adelmant, G., Mootha, V., Troy, A., Cinti, S., Lowell, B., Scarpulla, R.C., et al. (1999). Mechanisms controlling mitochondrial biogenesis and respiration through the thermogenic coactivator PGC-1. Cell *98*, 115–124.

Youn, J.H., and Buchanan, T.A. (1993). Fasting does not impair insulin-stimulated glucose uptake but alters intracellular glucose metabolism in conscious rats. Diabetes *42*, 757–763.

Yu, C., Chen, Y., Cline, G.W., Zhang, D., Zong, H., Wang, Y., Bergeron, R., Kim, J.K., Cushman, S.W., Cooney, G.J., et al. (2002). Mechanism by which fatty acids inhibit insulin activation of insulin receptor substrate-1 (IRS-1)-associated phosphatidylinositol 3-kinase activity in muscle. J. Biol. Chem. *277*, 50230–50236.

Yu, X.X., Murray, S.F., Pandey, S.K., Booten, S.L., Bao, D., Song, X.Z., Kelly, S., Chen, S., McKay, R., Monia, B.P., et al. (2005). Antisense oligonucleotide reduction of DGAT2 expression improves hepatic steatosis and hyperlipidemia in obese mice. Hepatology *42*, 362–371.

Zhang, D., Liu, Z.X., Choi, C.S., Tian, L., Kibbey, R., Dong, J., Cline, G.W., Wood, P.A., and Shulman, G.I. (2007). Mitochondrial dysfunction due to long-chain Acyl-CoA dehydrogenase deficiency causes hepatic steatosis and hepatic insulin resistance. Proc. Natl. Acad. Sci. USA *104*, 17075–17080.

Zimmet, P., Alberti, K.G., and Shaw, J. (2001). Global and societal implications of the diabetes epidemic. Nature *414*, 782–787.

Cell Metabolism
Article

Cyclic AMP Produced inside Mitochondria Regulates Oxidative Phosphorylation

Rebeca Acin-Perez,[1] Eric Salazar,[2] Margarita Kamenetsky,[3] Jochen Buck,[3] Lonny R. Levin,[3] and Giovanni Manfredi[1,*]
[1]Department of Neurology and Neuroscience
[2]Tri-Institutional MD/PhD Program
[3]Department of Pharmacology
Weill Medical College of Cornell University, New York, NY 10065, USA
*Correspondence: gim2004@med.cornell.edu
DOI 10.1016/j.cmet.2009.01.012

SUMMARY

Mitochondria constantly respond to changes in substrate availability and energy utilization to maintain cellular ATP supplies, and at the same time control reactive oxygen radical (ROS) production. Reversible phosphorylation of mitochondrial proteins has been proposed to play a fundamental role in metabolic homeostasis, but very little is known about the signaling pathways involved. We show here that protein kinase A (PKA) regulates ATP production by phosphorylation of mitochondrial proteins, including subunits of cytochrome c oxidase. The cyclic AMP (cAMP), which activates mitochondrial PKA, does not originate from cytoplasmic sources but is generated within mitochondria by the carbon dioxide/bicarbonate-regulated soluble adenylyl cyclase (sAC) in response to metabolically generated carbon dioxide. We demonstrate for the first time the existence of a CO_2-HCO_3^--sAC-cAMP-PKA (mito-sAC) signaling cascade wholly contained within mitochondria, which serves as a metabolic sensor modulating ATP generation and ROS production in response to nutrient availability.

INTRODUCTION

The Krebs Cycle (TCA cycle) produces the electron donors, which drive mitochondrial production of ATP via oxidative phosphorylation (OXPHOS). OXPHOS is subject to complex regulation, including short-term modulations essential for responding to transient changes in nutritional availability, environmental conditions, and energy requirements. If the reducing equivalents generated by the TCA cycle are not efficiently utilized by the OXPHOS machinery, reactive oxygen species (ROS) production may increase, and oxidative damage may ensue. It has been proposed that dynamic protein phosphorylation plays a major role in these rapid modulations (Hopper et al., 2006).

Evidence has emerged suggesting that cyclic AMP (cAMP)-mediated phosphorylation of mitochondrial enzymes plays a role in OXPHOS regulation. Consistent with this hypothesis, both protein kinase A (PKA) (reviewed in Pagliarini and Dixon, 2006; Thomson, 2002) and A kinase-anchoring proteins (AKAPs) have been identified in mammalian mitochondria (Feliciello et al., 2005; Lewitt et al., 2001). In particular, PKA in the mitochondrial matrix has been demonstrated by several independent groups using biochemical, pharmacological, and immunological methods, including immunoelectron microscopy (Livigni et al., 2006; Prabu et al., 2006; Ryu et al., 2005; Schwoch et al., 1990). However, if PKA plays a role in phosphorylating mitochondrial proteins, it remains unclear how the cAMP that activates PKA is modulated. Specifically, cAMP does not diffuse far from its source (Bornfeldt, 2006; Zaccolo and Pozzan, 2002), and as we show here, it does not enter mitochondria. Papa et al. postulated that a source of this second messenger might reside inside mitochondria (Papa et al., 1999), but an intramitochondrial adenylyl cyclase had not been demonstrated so far.

In mammalian cells, cAMP can be produced by a family of plasma membrane-bound forms of adenylyl cyclase (tmAC), or by a "soluble" adenylyl cyclase (sAC) (Buck et al., 1999). We previously showed that sAC resides at multiple subcellular organelles, including mitochondria (Zippin et al., 2003). Unlike tmACs, sAC is insensitive to heterotrimeric G protein regulation or forskolin; instead, it is stimulated by bicarbonate (Chen et al., 2000) and sensitive to ATP (Litvin et al., 2003) and calcium levels (Jaiswal and Conti, 2003; Litvin et al., 2003). Bicarbonate stimulates sAC activity by facilitating active site closure, while calcium promotes activity by increasing the affinity for ATP (Litvin et al., 2003; Steegborn et al., 2005). In physiological systems, including mitochondria (Dodgson et al., 1980), carbonic anhydrases (CA) convert CO_2 into bicarbonate. While generating electron donors for OXPHOS, the TCA cycle generates CO_2 and therefore bicarbonate. Thus, sAC represents an excellent candidate OXPHOS regulator, which ensures that respiration can keep pace with changes in nutritional availability and prevent ROS accumulation.

Here we show that PKA modulation of OXPHOS activity is regulated by cAMP generated inside mitochondria by sAC in response to metabolically generated CO_2. This study provides a functional understanding of the modulation of OXPHOS in direct response to nutrient metabolism by the mito-sAC signaling pathway.

RESULTS

cAMP-PKA Regulation of OXPHOS

To test whether mitochondrial OXPHOS can be modulated by PKA, we stimulated HeLa cells with membrane-permeant

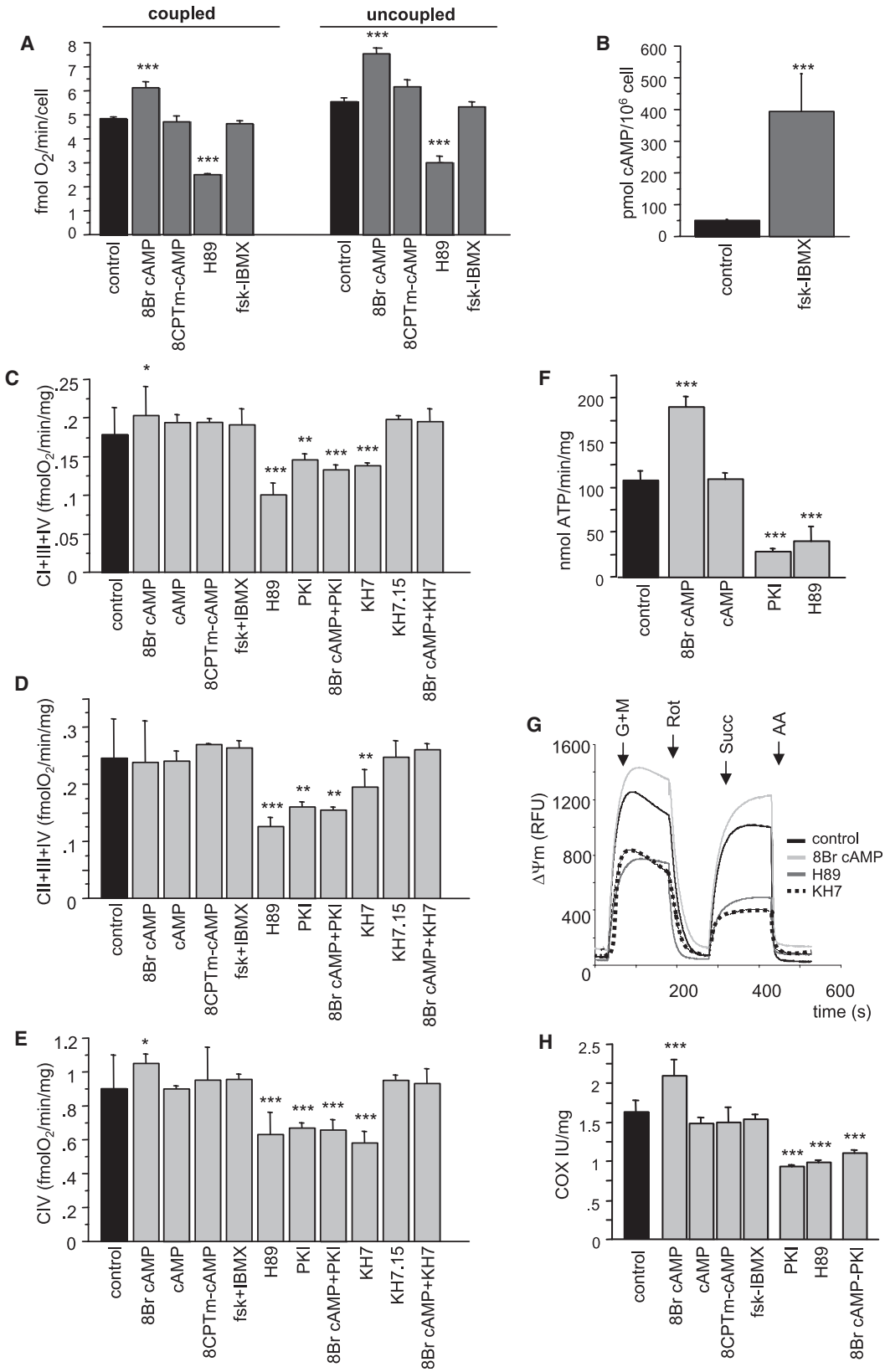
A
coupled
uncoupled
fmol O2/min/cell
control
8Br cAMP
8CPTm-cAMP
H89
fsk-IBMX
B
pmol cAMP/10^6 cell
C
CI+III+IV (fmolO2/min/mg)
cAMP
PKI
8Br cAMP+PKI
KH7
KH7.15
8Br cAMP+KH7
D
CII+III+IV (fmolO2/min/mg)
E
CIV (fmolO2/min/mg)
F
nmol ATP/min/mg
G
ΔΨm (RFU)
G+M
Rot
Succ
AA
time (s)
H
COX IU/mg
8Br cAMP-PKI

8Br-cAMP, which activates all cAMP-dependent kinases. We measured oxygen consumption as an indicator of mitochondrial respiratory chain function. 8Br-cAMP (1 mM for 30 min) resulted in a 25% ($p < 0.0001$) increase in oxygen consumption, as compared to untreated cells (Figure 1A). Then, we uncoupled oxygen consumption from ATP synthesis by inclusion of carbonylcyanide-4-(trifluoromethoxy)-phenylhydrazone (FCCP). Under these conditions, where respiratory chain activity is independent from ATP synthesis by the F_1F_0 ATPase, 8Br-cAMP still increased oxygen consumption. Note that the residual ATP content in mitochondria treated with FCCP for 5 min was approximately 60% of the pre-FCCP content (2.5 ± 0.3 and 4.1 ± 0.2 nmol/mg protein, respectively). Thus, there still was sufficient ATP for phosphorylation of PKA target proteins. The exchange protein activated by cAMP-selective agonist, 8CPT methyl-cAMP, did not change coupled or uncoupled respiration.

Conversely, H89 at 1 μM, a concentration that selectively blocks PKA, resulted in a 50% decrease in coupled and uncoupled respiration. RpcAMP (25 μM), which inhibits PKA by a different mechanism, also caused a significant decrease (20%, $p < 0.001$) in oxygen consumption (data not shown). The effects of PKA agonists and antagonists were replicated in 143B human osteosarcoma and 293T-HEK (data not shown), except that the increase in respiration induced by FCCP was higher (i.e., approximately 100% in 143B and 293T compared to 20% in HeLa cells), reflecting different coupling between oxygen consumption and ATP synthesis.

Stimulation of tmAC with forskolin in combination with the phosphodiesterase (PDE) inhibitor 3-Isobutyl-1-methylxanthine (IBMX) did not affect mitochondrial respiration, despite an 8- to 10-fold increase in cytoplasmic cAMP (Figure 1B). Therefore, mitochondrial respiration is enhanced through PKA activation by membrane-permeant cAMP analogs, but not by cytoplasmic cAMP, suggesting that the PKA that modulates respiration is inside mitochondria. It was suggested that tmAC-generated cAMP enters the mitochondrial matrix. However, our data demonstrate that cytoplasmic cAMP does not have access to the intramitochondrial PKA pool. DiPilato and colleagues used a reporter protein targeted to mitochondria, but the mitochondrial import was partial, with a portion of the protein remaining on the cytosolic surface or in the mitochondrial intermembrane space (DiPilato et al., 2004), where it remained accessible to cytosolic cAMP.

To further explore the role of intramitochondrial PKA in modulating OXPHOS, we examined isolated mitochondria from mouse liver.

First we measured state III (phosphorylating) respiration driven by different substrates: glutamate/malate (G + M) specific for complex I (Figure 1C), succinate for complex II (Figure 1D), and TMPD + ascorbate for complex IV (Figure 1E). Similar to intact cells, 8Br-cAMP produced a small but significant increase in respiration with glutamate/malate (12%, $p < 0.05$) and TMPD/ascorbate (13%, $p < 0.05$). Succinate-dependent respiration was unchanged, indicating that it cannot be upregulated by cAMP. As expected, addition of exogenous, membrane-impermeant cAMP, or 8CPT methyl-cAMP, or forskolin + IBMX had no effect on oxygen consumption (Figures 1C–1E). Similar to whole cells, the PKA inhibitor, H89, decreased oxygen consumption driven by all complexes (44% for glutamate/malate, $p < 0.0001$; 50% for succinate, $p < 0.0001$; 30% for TMPD/ascorbate, $p < 0.0001$). Another PKA-specific inhibitor, myristoylated PKI 14-22, also inhibited respiration (20% for glutamate/malate, $p < 0.001$; 36% for succinate, $p < 0.001$; 25% for TMPD/ascorbate, $p < 0.0001$). 8Br-cAMP was inert in the presence of PKI 14-22, confirming the role of PKA in modulating respiration.

Second, we showed that ATP synthesis (Figure 1F) was also enhanced by 8Br-cAMP (75%, $p < 0.0001$), inhibited by H89 and PKI 14-22 (63% and 74%, respectively, $p < 0.0001$), and unchanged by membrane impermeant cAMP.

Third, the capacity to generate mitochondrial membrane potential ($\Delta\Psi m$) was measured fluorimetrically under nonphosphorylating conditions. Figure 1G shows representative fluorescence traces. 8Br-cAMP increased membrane potential driven by glutamate/malate or succinate (21% ± 8% and 29 ± 6%, respectively; $p < 0.01$), whereas H89 decreased it (37% ± 8% and 51% ± 10%, respectively; $p < 0.0001$).

Because PKA inhibitors decreased oxygen consumption independent of which electron transfer complex was stimulated (Figures 1C–1E), the modulating effect of PKA likely targets COX, the terminal component of the respiratory chain. Consistently, COX activity (rate of oxidation of reduced cytochrome c) was stimulated by 8Br-cAMP (25%, $p < 0.0001$; Figure 1H), but not by cAMP, 8CPT methyl-cAMP, or forskolin + IBMX, and was inhibited by H89 and PKI 14-22 (22%% and 18%, respectively; $p < 0.0001$). The stimulation by 8Br-cAMP was blocked by PKI 14-22.

There were no changes in steady-state protein levels of COX subunits I and IV after modulation of PKA (Figure S1), suggesting that the activity changes depend on posttranslational modification of the enzyme kinetics. Consistently, it was previously proposed that COX is regulated via protein phosphorylation

Figure 1. Regulation of OXPHOS by cAMP-PKA Agonists and Antagonists

(A) Respiration (coupled and uncoupled) in HeLa cells after 8Br-cAMP (n = 6), 8CPT methyl-cAMP (8CPTm-cAMP) (n = 3), H89 (n = 6), for 0.5 hr or with forskolin + IBMX (fsk-IBMX) (n = 3). Control, untreated cells (n = 33). Values are fmoles O_2 per min per cell.

(B) Cellular cAMP levels after stimulation of tmAC with fsk-IBMX. Values are pmol cAMP per 10^6 cells.

(C–E) OXPHOS in mouse liver mitochondria. State III (phosphorylating) mitochondrial respiration driven by glutamate/malate (C); succinate (D), or TMPD/ascorbate (E). Compounded number of replicas were the following: control (n = 21); 8Br-cAMP (n = 9); cAMP (n = 3); 8CPTm-cAMP (n = 3); forskolin + IMBX (fsk + IBMX, n = 3); H89 (n = 9); PKI 14-22 (n = 3); 8Br-cAMP + PKI (n = 3); KH7 (n = 9); KH7.15 (n = 3); and 8Br-cAMP + KH7 (n = 3).

(F) ATP synthesis with 8Br-cAMP (n = 3), cAMP (n = 3), H89 (n = 3), and PKI 14-22 (PKI, n = 3). Values are nmoles ATP per min per mg of mitochondrial protein.

(G) Safranin-O fluorescence curves showing changes in mitochondrial membrane potential ($\Delta\Psi m$) driven by G + M and inhibited by rotenone (Rot), or driven by succinate (Succ) and blocked by the complex III inhibitor antimycin A (AA). Values are relative fluorescent units (RFU). The plots are representative of three independent determinations, which showed similar responses.

(H) COX Vmax (IU per milligram of protein, n = 9). Error bars indicate standard deviations. *$p < 0.05$; **$p < 0.001$; ***$p < 0.0001$.

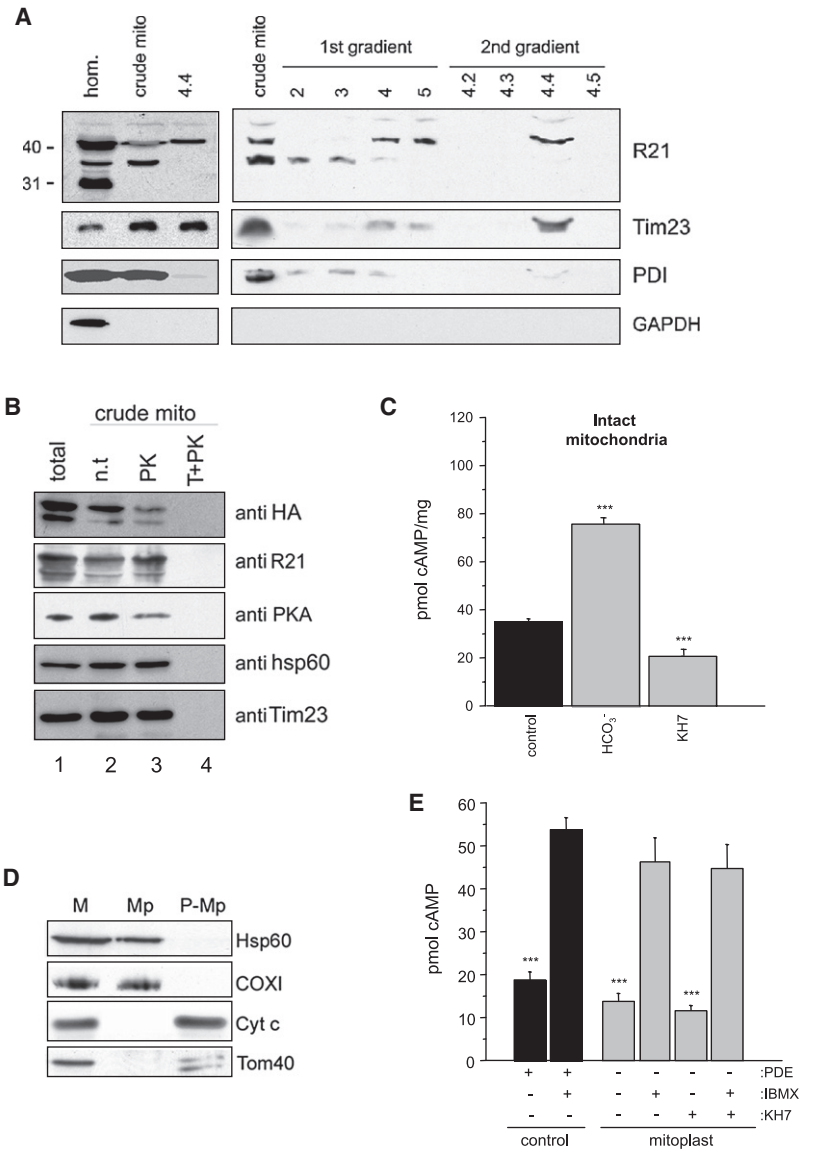

Figure 2. sAC Is Localized and Generates cAMP in Mitochondria

(A) Mitochondria isolated from mouse liver after to two rounds of Nycodenz gradient purification. Lanes 2, 3, 4, and 5 were from the first round. Fractions 4.2, 4.3, 4.4, and 4.5 were from a second round of purification of fraction 4. Tim 23, mitochondrial marker. PDI, protein disulfide isomerase; ER, marker; GAPDH, cytoplasmic marker; Hom, homogenate.

(B) Expression of sAC_t-HA in total cell homogenate of transiently transfected COS cells and in crude nontreated (nt) mitochondrial fractions detected by R21 and HA antibodies. PK, Proteinase K; T + PK, Triton X-100 and PK. Hsp60 and Tim23 are markers of the matrix and the inner membrane, respectively.

(C) cAMP levels in intact mouse liver mitochondria in the presence of bicarbonate (HCO_3^-) or KH7. Values are pmol cAMP per mg mitochondrial protein (n = 3).

(D) Mitoplasts purity tested using protein markers for the different mitochondrial compartments: Hsp60 (matrix), COXI (inner membrane), cytochrome c (Cyt c, intermembrane space), Tom40 (outer membrane). M, (intact mitochondria), Mp (mitoplasts), P-Mp (post-mitoplast fraction).

(E) Residual cAMP levels after 50 pmol cAMP were added to a reaction mixture containing sonicated mitoplasts (mitoplast) or no mitoplasts (control), with and without PDE + calmodulin (PDE), IBMX, or KH7. n = 3 for each reaction. Error bars indicate standard deviations. ***$p < 0.0001$.

(Bender and Kadenbach, 2000; Lee et al., 2005; Miyazaki et al., 2003).

As expected for a short-term adaptation mechanism, the cAMP-induced changes in PKA modulation of COX activity were transient and readily reversible upon washout of the agonist (Figure S2).

sAC Is a Source of cAMP in Mitochondria

Membrane-impermeant cAMP had no effect on OXPHOS response, suggesting that a source of cAMP must reside within mitochondria. We previously showed that sAC immunoreactivity colocalizes and sAC activity copurifies with mitochondria (Zippin et al., 2003). We now show that western blotting using the R21 monoclonal anti-sAC antibody (Zippin et al., 2003) identifies multiple bands in the liver homogenate (Figure 2A), consistent with multiple sAC splice isoforms (Buck et al., 1999; Farrell et al., 2008; Geng et al., 2005; Jaiswal and Conti, 2003). However, purified mitochondria contained only one sAC isoform of approximately 48kDa (Figure 2A, lane 4). This band was confirmed in mitochondria highly purified by a second gradient step (Figure 2A, lanes 4.4). Instead, ER-rich fractions contained a distinct sAC isoform migrating at approximately 35kDa (Figure 2A, lanes 2 and 3). Glyceraldehyde 3-phosphate dehydrogenase (GAPDH) was absent from the mitochondrial and ER fractions excluding detectable contamination with cytoplasmic proteins.

A highly active isoform of rat sAC (sAC_t) (Chaloupka et al., 2006) containing an N-terminal HA tag was expressed in COS cells. In cell homogenates (Figure 2B, lane 1) sAC_t was detected both by the R21 and the HA antibodies. The crude mitochondrial fraction contained the same immunoreactive sAC_t bands (Figure 2B, lane 2). Likewise, endogenous PKA was detected in the mitochondrial fraction (Figure 2B, lane 2). A proteinase K protection assay performed on the mitochondrial fraction showed that portions of sAC_t and endogenous PKA were resistant to digestion, indicating that they resided in a protected mitochondrial compartment (Figure 2B, lane 3). Detergent solubilization of mitochondria allowed for complete digestion of sAC_t, PKA, as well as hsp60 and Tim23, localized in the mitochondrial matrix and inner membrane, respectively (Figure 2B, lane 4).

sAC is stimulated by bicarbonate (Chen et al., 2000), and adenylyl cyclase activity in mouse liver mitochondria demonstrated a significant bicarbonate stimulation (Figure 2C, $p < 0.0001$) and inhibition by the sAC-specific inhibitor, KH7 (Hess et al., 2005),

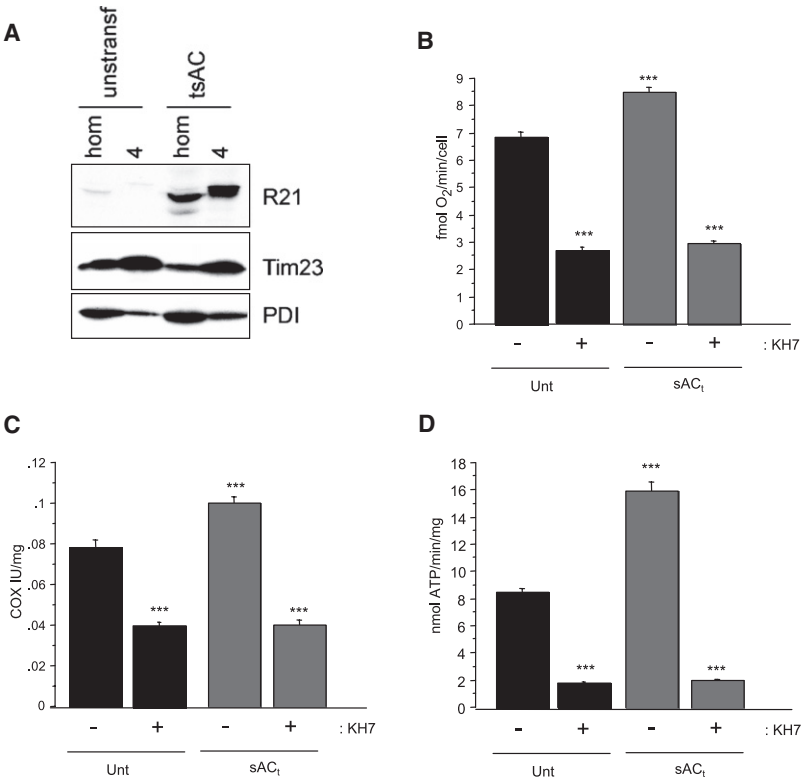

Figure 3. Transgenic sAC_t Localizes to Mitochondria and Increases OXPHOS

(A) Localization of tsAC in untransfected (unstransf) and sAC_t overexpressing (sAC_t) cells in homogenates (hom. lane) and pure mitochondria from fraction 4 of the Nycodenz gradient (lane 4). The major 48 kDa immunoreactive band corresponds to the molecular size of sAC_t. A similar size band, faintly detectable in untransfected 293T cells, presumably corresponds to an isoform of endogenous sAC.

(B) Mitochondrial respiration was increased in cells expressing sAC_t in comparison to untransfected ones (n = 9) in a KH7-sensitive manner (n = 3). sAC_t overexpression stimulated COX-specific activity (C, n = 9) and ATP synthesis (D, n = 9). The increase in both COX and ATP synthesis was KH7 sensitive (n = 3, C and D). Error bars indicate standard deviations. ***p < 0.0001.

indicating that the mitochondrial component of sAC is enzymatically active.

The reversibility of the cAMP signal predicts that phosphodiesterase (PDE) should also be contained inside mitochondria. To test this hypothesis we isolated mitoplasts (i.e., mitochondria stripped of their outer membrane) from mouse liver. Mitoplasts contained inner membrane and matrix proteins (COX I, and Hsp60, respectively), but no intermembrane space or outer membrane proteins (Cyt c and Tom40, respectively), whereas the postmitoplasts supernatants only contained Cyt c and Tom 40 (Figure 2D). After the contents of the matrix were made accessible by sonication, they degraded exogenous cAMP (Figure 2E). This cAMP catabolic activity was fully inhibited by IBMX, confirming the presence of intramitochondrial PDE activity.

Modulation of Intramitochondrial sAC Regulates OXPHOS

We used two distinct methods of increasing intramitochondrial sAC-generated cAMP to demonstrate a functional role for sAC in modulating OXPHOS activity.

First, sAC_t was stably overexpressed in 293T-HEK cells, and was found in both the whole cell homogenate and in isolated mitochondria (Figure 3A, lanes hom and 4, respectively). sAC_t overexpression increased respiration by approximately 25% (Figure 3B, $p < 0.0001$), as compared to untransfected cells. Consistently, COX activity (Figure 3C) and ATP synthesis (Figure 3D) were also increased (by 28% and 87%, respectively; $p < 0.0001$). These effects were antagonized by the sAC-specific inhibitor, KH7.

Second, we stimulated endogenous mouse liver sAC in isolated mitochondria with bicarbonate. We found that maximum stimulation of COX activity occurred at 30 mM bicarbonate (Figure 4A), which is consistent with the physiological intramitochondrial bicarbonate concentration (ranges between 10 and 40 mM) (Simpson and Hager, 1979). As predicted, bicarbonate enhanced ATP synthesis by 32% (Figure 4B, $p < 0.001$), and bicarbonate-dependent stimulation of COX activity at least partially accounted for this effect (18%) (Figure 4C, $p < 0.001$).

To confirm that bicarbonate stimulates OXPHOS, isolated mitochondria were exposed to the CO_2-generating combination of α-ketoglutarate dehydrogenase complex (KGDHC), its substrates ketoglutaric acid + NAD+, and its cofactors coenzyme-A and cocarboxylase. KGDHC stimulated COX-driven respiration by 32%, using TMPD/ascorbate as substrates (Figures 4D and 4E, $p < 0.0001$). Addition of the carbonic anhydrase inhibitor (CAI) acetazolamide diminished COX driven respiration by 10% ($p < 0.01$), indicating that CO_2 diffusing through the mitochondrial membranes is converted into bicarbonate that activates sAC and stimulates COX.

We note that, since OXPHOS activity is increased by both bicarbonate and by exogenously generated CO_2, in a carbonic anhydrase-dependent manner, these effects cannot be due to pH changes (or ionic strength), because bicarbonate addition increases pH while CO_2 addition decreases it.

To further demonstrate the role of sAC in modulating OXPHOS activity, we used three independent methods of blocking intramitochondrial sAC.

First, KH7, but not an inactive congener, KH7.15 (Wu et al., 2006), inhibited state III respiration driven by complexes I, II, and IV by 25%, 22%, and 35%, respectively (Figure 1C–1E, $p < 0.0001$). Inhibition of sAC by KH7 also markedly decreased ATP synthesis (80%) (Figure 4B, $p < 0.0001$). KH7, but not KH7.15, inhibited COX activity by 30% (Figure 4C, $p < 0.0001$). In each case, KH7 inhibition was rescued by membrane permeable 8Br-cAMP. Finally, KH7 decreased $\Delta\Psi m$ in isolated mitochondria by 46% ± 6% with glutamate/malate and by 62% ± 11% with succinate (Figure 1G, $p < 0.0001$). The effects of sAC

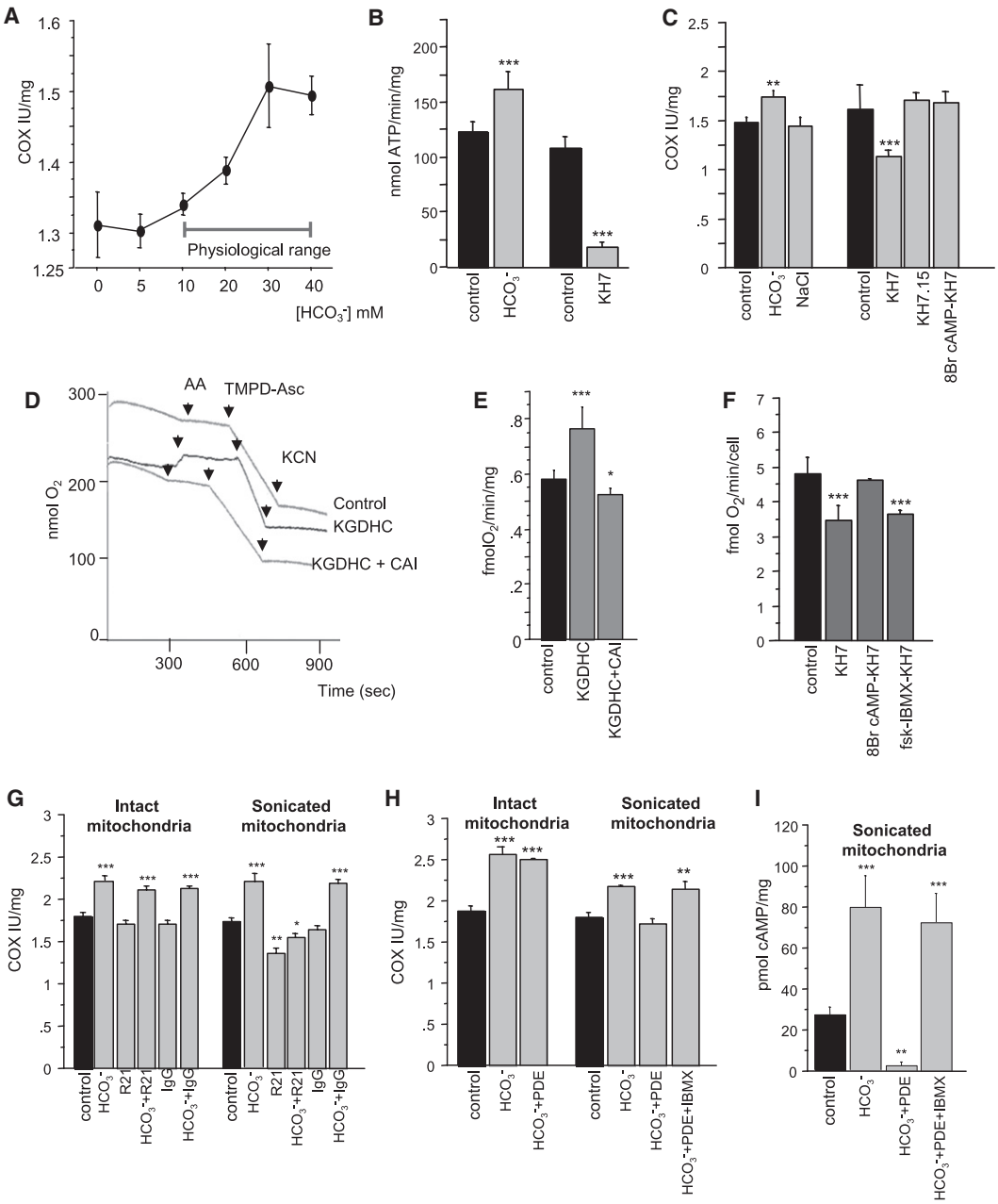

Figure 4. CO_2-TCA and sAC Modulation Regulates OXPHOS

(A) COX Vmax in isolated mitochondria treated with increasing concentration of HCO_3^-, from 5 mM to 40 mM (n = 6).

(B and C) Isolated mitochondria from mouse liver incubated with bicarbonate (HCO_3^-) (n = 4), or NaCl (n = 3) or KH7, (n = 9), KH7.15, (n = 3), KH7 + 8Br-cAMP (n = 3). ATP synthesis (B) was increased by HCO_3^- treatment, whereas KH7 inhibited it. COX Vmax was increased by HCO_3^-, whereas KH7 diminished it (C). COX Vmax decrease was not observed with KH7.15, and was rescued by 8Br-cAMP.

(D) A representative trace of respiration driven by COX using TMPD/ascorbate mouse liver mitochondria. AA is added to mitochondria before TMPD/ascorbate to block electron transfer upstream of COX. KCN is added at the end to inhibit COX. Each addition is marked by downward arrowheads.

(E) Quantification of the experiments shown in D (n = 9).

(F) KH7 (n = 6) reduced respiration in intact HeLa cells, and this inhibition was prevented by 8Br-cAMP (n = 3), but not by forskolin + IBMX (n = 3). Control, untreated cells (n = 33).

(G) COX activity in intact or sonicated mitochondria with or without the inhibitory anti-sAC antibody R21. HCO_3^- stimulation of COX was antibody insensitive in intact mitochondria, whereas it was abolished in sonicated mitochondria by R21 (n = 3).

(H) COX activity in intact or sonicated mitochondria with or without PDE. HCO_3^- stimulation of COX was PDE insensitive in intact mitochondria, whereas it was abolished in sonicated mitochondria by PDE. IBMX prevented the PDE-mediated decrease in COX activity (n = 3).

(I) cAMP levels in sonicated mitochondria were increased by HCO_3^- and reduced by PDE. IBMX prevented the decrease in cAMP. Values expressed as pmol cAMP per mg mitochondrial protein (n = 5). Error bars indicate standard deviations. *p < 0.05; **p < 0.001; ***p < 0.0001.

inhibition on mitochondrial respiration were confirmed in whole cells, where KH7 induced a 30% decrease, which was rescued by 8Br-cAMP but not by cytosolic cAMP induced by forskolin + IBMX (Figure 4F, $p < 0.0001$).

As a second independent method of blocking sAC activity, we used the anti-sAC monoclonal R21antibody, which has inhibitory properties on enzymatic activity (Figure S3). Neither R21 nor nonspecific isotype-matched IgG caused COX inhibition in intact mitochondria. However, R21, but not the IgG control, blocked the bicarbonate-induced increase in COX activity when sAC was made accessible to the antibody by mitochondrial sonication (Figure 4G, $p < 0.01$).

Third, we measured COX activity in mitochondria treated with bicarbonate in the presence or absence of PDE. In intact mitochondria, bicarbonate stimulated COX activity was unaffected by PDE (Figure 4H). Thus, cAMP was produced in a compartment isolated from external PDE. After sonication, PDE degraded intramitochondrial cAMP (Figure 4I, $p < 0.001$), and the bicarbonate-induced COX stimulation was abolished (Figure 4H), in an IBMX sensitive manner.

Taken together, this evidence indicates that the sAC-cAMP-PKA signaling pathway is wholly contained within mitochondria and that it modulates OXPHOS in response to physiologically relevant concentrations of bicarbonate.

cAMP-Dependent Phosphorylation of Mitochondrial Proteins

We investigated the pattern of PKA-dependent mitochondrial protein phosphorylation in isolated mitochondria. Proteins were resolved by isoelectric focusing two-dimensional electrophoresis and detected with a PKA substrate-specific anti-phospho Ser/Thr antibody (Bruce et al., 2002; Schmitt and Stork, 2002). Several of the PKA-phosphorylated proteins detectable in untreated mitochondria (indicated by arrows in Figure S4A, upper panel) disappeared or were markedly reduced in the KH7-treated samples (Figure S4A, lower panel).

Many hydrophobic subunits of the respiratory chain are not amenable to isoelectric focusing (unpublished data). Therefore, to examine respiratory chain complexes, we employed 2D-blue-native gel electrophoresis (Schagger and Pfeiffer, 2000; Schagger and von Jagow, 1991). Phosphoproteins were detected using either anti-phospho Ser/Thr antibody (Figure S5A) or the PKA substrate-specific antibody (Figure S5B). Replicate samples were treated with calf-intestinal phosphatase, which abolished most immunoreactive spots on the membrane probed with anti-phospho Ser/Thr antibody, demonstrating the specificity of the antibody (Figure S6). Both anti-phospho Ser/Thr and the PKA substrate-specific antibodies revealed a marked decrease of several phosphoproteins after KH7 or H89. Membranes were reprobed with antibodies against COX subunits, which revealed two of the phosphorylated proteins (denoted by asterisks in the upper panel of Figure S5A) to be COX I and COX IV type II (COX IV-2). The amounts of phosphorylated COX I and COX IV-2 were respectively reduced to 30% and 20% with H89, and to 25% and 5% with KH7.

These results confirm that phosphorylation of several mitochondrial proteins responds to modulation of the mito-sAC signaling pathway and suggest that certain COX subunits are candidates for the regulation of OXPHOS activity.

Physiological Role of the Intramitochondrial Mito-sAC Pathway in the Regulation of OXPHOS and ROS Production

We hypothesized that the physiological role of mitochondrial sAC is to respond to CO_2 metabolically generated by the TCA cycle. To test this hypothesis, we measured COX activity in isolated mitochondria "fed" with pyruvate and malate, which fuel the TCA cycle to stimulate CO_2 generation. Under these conditions, CAI diminished COX activity by 37% (Figure 5A, $p < 0.001$), suggesting that the CO_2 had to be converted to bicarbonate to sustain COX activity. The inhibitory effect of CAI was reversed by exogenous bicarbonate, which directly stimulates sAC, or by the addition of 8Br-cAMP, which bypasses sAC stimulation. Diminishing CO_2 production by retrograde inhibition of the TCA cycle using the complex III blocker antimycin A (AA) reduced COX activity (25%, $p < 0.001$). As with CAI addition, AA inhibition was rescued by the bicarbonate or 8Br-cAMP (Figure 5A, $p < 0.01$). Changes in mitochondrial cAMP levels paralleled the changes in COX activity; cAMP decreased in the presence of CAI or AA, demonstrating that TCA cycle-generated CO_2 regulates sAC (Figure 5B, $p < 0.0001$). Finally, OXPHOS was inhibited by CAI also in intact cells, where respiration was diminished by 36% and rescued by 8Br-cAMP (Figure 5C, $p < 0.0001$).

To investigate the role of the mito-sAC signaling pathway in the physiological adaptation to changes in substrate availability, we cultured cells in medium containing galactose instead of glucose as the main carbon source. Because galactose is utilized in the glycolytic pathway at a much slower rate than glucose, cells are forced to maximize mitochondrial OXPHOS activity to meet their energy needs. Consistently, respiration was increased by 35% in galactose as compared to glucose medium (Figure 5D, $p < 0.0001$). In contrast to cells grown in glucose, respiration in cells grown in galactose for 48 hr was unaffected by 8Br-cAMP. Presumably, these cells are insensitive to stimulation because OXPHOS is already fully activated by the mito-sAC signaling pathway. Consistently, the decrease in respiration resulting from inhibition of CA, sAC, or PKA was proportionally more effective in galactose than in glucose (46.8% ± 3.97% and 36.5% ± 3.87%, respectively, $p < 0.0001$).

Activation of the TCA cycle dehydrogenases by increasing mitochondrial calcium (McCormack et al., 1990) with the calcium ionophore A23187 (0.5 μM) stimulated respiration in glucose (Figure 5D, $p < 0.0001$), but not in galactose, because in the latter there was no spare respiratory capacity. Alternatively, calcium could stimulate respiration by uncoupling due to calcium cycling. However, it is unlikely that this mechanism would be sensitive to all three inhibitors of the mito-sAC pathway, which suppress respiration both in glucose and galactose medium. Thus, the only nonconflicting explanation is that the mito-sAC pathway modulates the terminal oxidase of the respiratory chain, which is known to be limiting for respiration in cells (D'Aurelio et al., 2001; Villani and Attardi, 1997; Villani et al., 1998).

Mito-sAC signaling cascade links substrates flux through the TCA cycle with the rate of OXPHOS activity; this linkage could be beneficial to minimize electron leakage from the respiratory chain and prevent ROS generation. Cells grown in galactose produced less ROS than cells grown in glucose (Figure 5E, $p < 0.0001$), but ROS production in glucose was diminished by

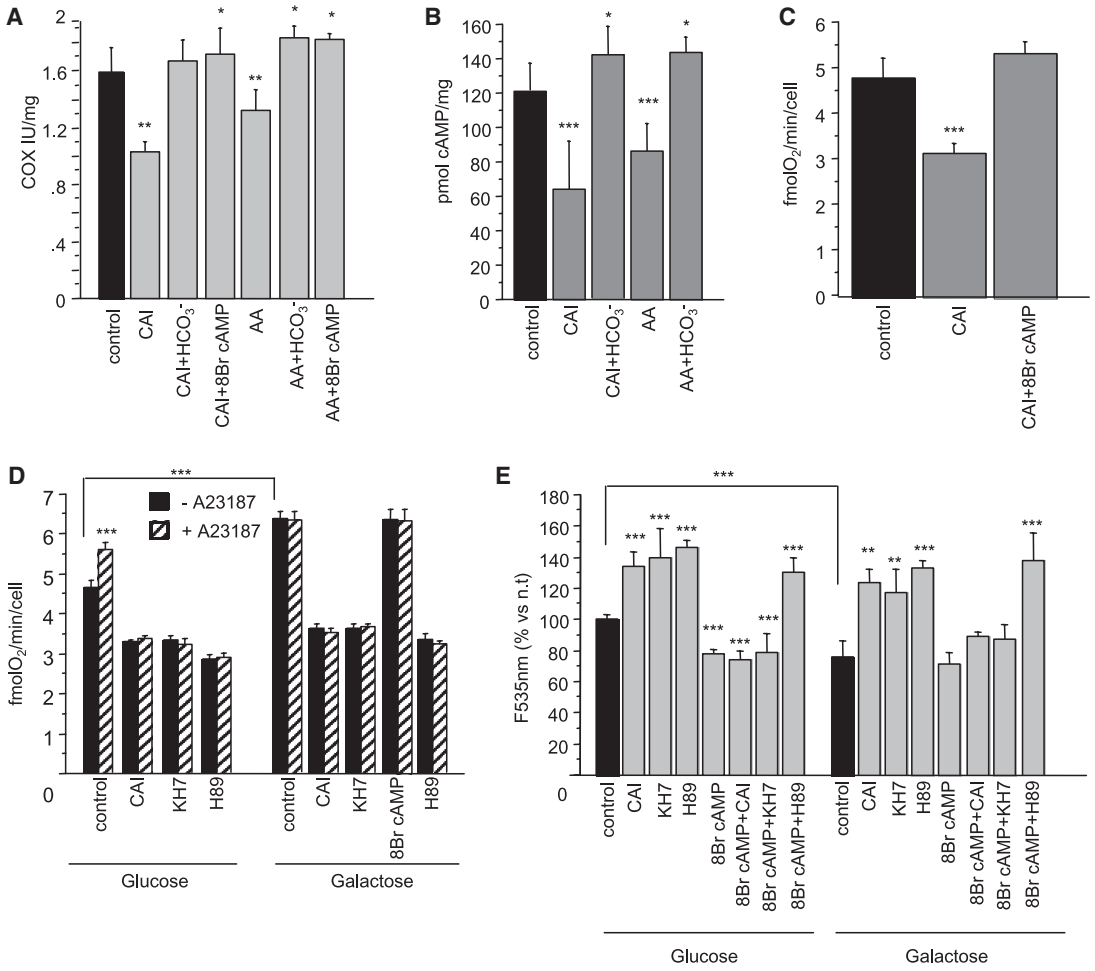

Figure 5. Physiological Role of the Intramitochondrial mito-sAC Pathway in the Regulation of OXPHOS and ROS Production

(A) COX Vmax in mouse liver mitochondria with CAI (n = 9), CAI + HCO_3^- (n = 9) and CAI + 8Br-cAMP (n = 9), and pyruvate and malate as substrates. CAI decreased COX activity, which was rescued by HCO_3^- or 8Br-cAMP. AA (n = 6), blocked CO_2 production by the TCA cycle and decreased COX activity, which was rescued by HCO_3^- or 8Br-cAMP.

(B) cAMP levels in mitochondria decreased when CA or the TCA cycle were blocked with CAI and AA, respectively. HCO_3^- reverted the effects of CAI or AA (n = 8).

(C) CAI (n = 6) decreased respiration in HeLa cells, and this inhibition was prevented by 8Br-cAMP (n = 3). Control, untreated cells (n = 33).

(D) Respiration in cells grown in glucose or galactose medium (black bars) (n = 6) for 48 hr. The calcium ionophore A23187 (dashed bars) increased respiration in control (untreated) cells in glucose.

(E) ROS production in cells grown in glucose or galactose and treated as in (D) (n = 6). Galactose resulted in decreased ROS production in control cells (black bars). All other comparisons are between treated and untreated cells grown under the same conditions (i.e., glucose or galactose medium). Error bars indicate standard deviations. *p < 0.05; **p < 0.001; ***p < 0.0001.

8Br-cAMP. Addition of 8Br-cAMP to galactose grown cells, whose OXPHOS is already maximally stimulated, had no effect. Consistent with the hypothesis that ROS production depends on the mito-sAC pathway, CAI, KH7, or H89 increased ROS production both in glucose and in galactose (Figure 5E, p < 0.001), and 8Br-cAMP reverted the effects of CAI and KH7 on ROS production, but not those of H89, because its inhibition is downstream of cAMP.

Taken together these results indicate that the mito-sAC pathway is engaged in the adaptation of OXPHOS activity in order to optimize the use of substrates for bioenergetic purposes and, at the same time, minimize ROS production.

DISCUSSION

Which are the players involved in the phosphorylation-mediated regulation of OXPHOS function? While many putative mitochondrial phosphoproteins have been identified, most of them have been demonstrated in vitro, making their physiological relevance uncertain. Similarly, the list of kinases and phosphatases identified in mitochondria is constantly expanding (Pagliarini and Dixon, 2006), but their physiological role is still largely unidentified. For example, while both PKA (Livigni et al., 2006; Pagliarini and Dixon, 2006; Prabu et al., 2006; Ryu et al., 2005; Schwoch et al., 1990) and A kinase-anchoring proteins (AKAPs) (Feliciello

et al., 2005; Wang et al., 2001) were found in mitochondria, their substrates and physiological relevance remained controversial. We now show that PKA regulates OXPHOS and that cAMP is generated inside mitochondria in response to metabolically generated CO_2.

We identify sAC as a source of cAMP inside mitochondria. We established the presence and the function of sAC in mitochondria by three independent criteria: (1) sAC is localized inside mitochondria, (2) OXPHOS is decreased by sAC inhibition, and (3) the sAC activator bicarbonate stimulates OXPHOS.

Which are the targets of the mito-sAC pathway? A number of cAMP-dependent phosphorylation events of respiratory chain components have been described. Much work has focused on small subunits of complex I (Papa et al., 1996; Sardanelli et al., 1995; Scacco et al., 2000; Signorile et al., 2002; Chen et al., 2004), although it still remains to be studied whether any of the complex I phosphorylation events are dependent upon the mito-sAC pathway.

Our initial proteomic work has focused on COX, another respiratory chain complex, whose phosphorylation has been studied. COX subunits I, IV-1, and Vb are phosphorylated by PKA in hypoxic cells, resulting in decreased steady-state levels of these proteins and thus COX activity (Prabu et al., 2006). However, changes in COX protein steady-state levels do not occur in our system; therefore, these phosphorylations are unlikely to contribute to the effects described here. Another cAMP-dependent phosphorylation event of COX subunit I occurs on tyrosine residue 304, via PKA regulation of a tyrosine kinase or phosphatase. Tyrosine 304 phosphorylation results in COX inhibition in vitro. However, this tyrosine is on the outer face of the mitochondrial inner membrane (Lee et al., 2005), implying that its phosphorylation should not be dependent upon intramitochondrial cAMP.

cAMP-dependent phosphorylation of subunit I of COX has been postulated to optimize OXPHOS efficiency by keeping the mitochondrial membrane potential low while complex I is fully activated (Bender and Kadenbach, 2000; Kadenbach, 2003). It was also shown that phosphorylation of subunit II of COX by mitochondrial c-Src results in enhanced COX activity in a cAMP-dependent manner (Miyazaki et al., 2003). Either of these mechanisms may be contributing to the increased COX activity described here. COX subunits IV (at amino acid Ser34) and Va (at amino acids Ser4 and Thr35) subunits are phosphorylated in vitro by PKA (Helling et al., 2008). The physiological consequence of these phosphorylation events remains unknown, but because these residues are located on the matrix side of the enzyme (Shinzawa-Itoh et al., 2007), they may be subject to regulation by intramitochondrial PKA.

The mito-sAC pathway is sensitive to metabolic conditions that affect CO_2 production. CO_2 would diffuse throughout a cell, but as it diffuses it encounters discretely localized CA, which speeds up the hydration and dissociation into H^+ and bicarbonate. Thus, diffusing CO_2 would establish a new equilibrium, with elevated bicarbonate wherever it encounters CA. Such bicarbonate elevation would be transient, as bicarbonate would reach a new equilibrium as a function of the changing local P_{CO2}, pH, and buffer capacity. Our data indicate that this occurs within the mitochondrial matrix in response to metabolically generated CO_2. Due to intramitochondrial CA (Dodgson et al., 1980), bicarbonate fluctuates inside mitochondria in direct proportion to the CO_2 generated via the TCA cycle and β-oxidation, and these transient elevations of bicarbonate activate sAC to increase OXPHOS activity and ATP synthesis (Figure 6).

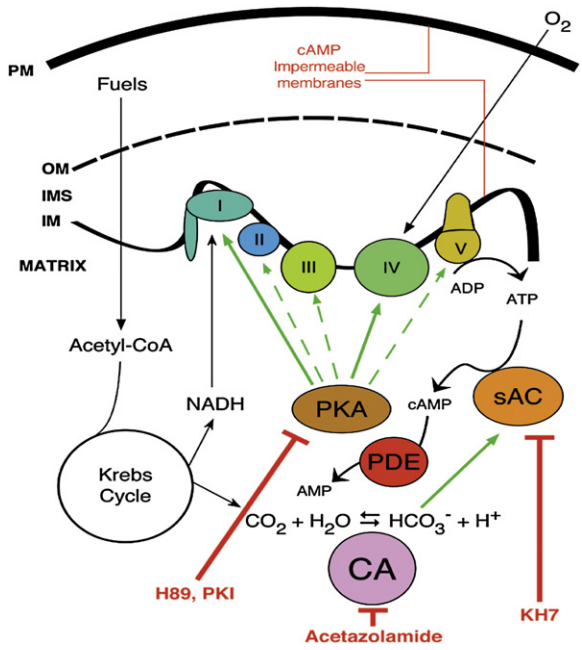

Figure 6. Diagram of the Proposed mito-sAC Regulatory Pathway of OXPHOS

Activators and inhibitors of the various steps of the mito-sAC pathway are indicated. PM, plasma membrane; OM, outer mitochondrial membrane; IMS, inter membrane space; IM, inner mitochondrial membrane; PKA, protein kinase A; sAC, soluble adenylyl cyclase; CA, carbonic anhydrase; KH7, inhibitor of sAC; H89 and PKI (PKI 14-22), inhibitors of PKA; PDE, phosphodiesterase. I through V indicate respiratory chain complexes (I-IV) and complex V (ATPase).

In the well-fed mouse livers used in this study, the mito-sAC pathway appears to be mostly in the "active" state, with high constitutive protein phosphorylation. Thus, we observe a proportionally lower stimulation of OXPHOS by membrane permeable cAMP, bicarbonate, or CO_2 (Figure 1), than downregulation by inhibition of the TCA cycle, carbonic anhydrases, sAC, or PKA (Figures 1 and 4). Physiologically, this pathway mediates OXPHOS activation in response to stimulation of mitochondrial dehydrogenases and utilization of the mitochondrial spare respiratory capacity in cells forced to depend upon OXPHOS for survival in galactose medium. In addition, by providing a mechanism for coupling nutrient utilization with the electron flux, the mito-sAC pathway controls ROS production by the respiratory chain.

With the demonstration that PDE resides inside mitochondria, along with sAC and PKA, we have identified a cAMP microdomain wholly contained within mitochondria. To our knowledge, this represents the first description of a complete signaling cascade inside this organelle. We predict that other itramitochondrial signaling cascades will be identified, which may have evolved in eukaryotes subsequent to endosymbiosis or been retained from primordial bacteria (Margulis and Bermudes, 1985). Interestingly, mammalian sAC is more closely related to

bacterial adenylyl cyclases than it is to other mammalian nucleotidyl cyclases (Buck et al., 1999), and its mechanisms of calcium and bicarbonate regulation are conserved in cyanobacteria (Chen et al., 2000; Steegborn et al., 2005).

By linking nutrient metabolism with ATP synthesis and ROS production, the function of the mito-sAC signaling pathway ensures a proper balance between the supply of reducing equivalent to the electron transport chain and their utilization. This feed forward regulation may have profound implications for energy metabolism in eukaryotic cells.

EXPERIMENTAL PROCEDURES

Cell Culture and Transfection

HeLa, human embryonic kidney (HEK293T), and COS-1 cells were grown in Dulbecco modified Eagle's medium (DMEM) supplemented with 10% fetal bovine serum (FBS), L-glutamine, 1 mM pyruvate, and 4.5 g/L glucose. HEK293T cells expressing sAC_t were generated by stable transfection as previously described (Hess et al., 2005). COS-1 cells were transiently transfected with a pTurbo plasmid containing sAC_t cDNA with an HA tag, using FuGene6 (Roche) following the manufacturer's protocol. Cells were harvested for fractionation and immunoblots after 72 hr.

For galactose growth experiments, HeLa cells were cultured in DMEM without glucose and supplemented with 4.5 g/L galactose, 1 mM pyruvate, L-glutamine, and 10% dyalized FBS.

Measurements of OXPHOS Function in Cells and Isolated Mitochondria

Intact cells (2×10^6) were used for O_2 consumption measurements in an oxygraph equipped with a Clark electrode, as described (Hofhaus et al., 1996). Mouse liver mitochondria were isolated as described (Fernandez-Vizarra et al., 2002) and state III O_2 consumption driven by specific respiratory chain complexes was measured on 75–100 μg of mitochondrial protein as described (Hofhaus et al., 1996). The calcium ionophore, A23187, was used at 0.5 μM. All reagents were purchased from Sigma-Aldrich.

COX enzymatic activity was measured spectrophotometrically on isolated mitochondrial (2–5 μg of protein) or in cell lysates (30–50 μg of protein) as described (Birch-Machin and Turnbull, 2001).

ATP synthesis in isolated mitochondria (15–25 μg of protein) or in cells permeabilized with digitonin (2×10^6 cells) was measured using a kinetic luminescence assay, as described (Vives-Bauza et al., 2007).

ATP content was measured in isolated mouse liver mitochondria incubated with and without the addition of 3 μM FCCP for 5 min using the Enliten ATP Determination Kit (Promega) as described (Vives-Bauza et al., 2007).

Titration of Agonists and Inhibitors

Each agonist and inhibitor used in this study was titrated to determine conditions resulting in a maximal effect on OXPHOS. All experiments, including those where bicarbonate was added, were performed at constant pH and under ambient CO_2.

In intact cells, titrations of compounds were performed by following mitochondrial O_2 consumption. The concentrations of agonists/inhibitors used were as follows: 8Br-cAMP (Sigma-Aldrich), 1 mM; H89 (Calbiochem), 1 μM; RpcAMP (Sigma-Aldrich), 25 μM; KH7, 50 μM; 8-CPT-methyl-cAMP (BioMol International), 1 mM; forskolin (Sigma-Aldrich), 10 μM; 3-Isobutyl-1-methylxanthine (IBMX, Sigma-Aldrich), 50 μM, acetazolamide (carbonic anhydrase inhibitor, CAI, Sigma-Aldrich), 1 μM for 0.5 hr.

Isolated mitochondria were incubated with PKA agonists and inhibitors in MAITE medium (10 mM Tris-HCl, pH 7.4; 25 mM sucrose; 75mM sorbitol; 100 mM KCl; 10 mM K_2HPO_4; 0.05 mM EDTA; 5 mM $MgCl_2$; 1 mg/ml BSA) in the presence of a cocktail of phosphatase inhibitors (Sigma-Aldrich). When bicarbonate was used to stimulate sAC, MAITE containing 300 mM Tris-HCl was used to buffer the pH. Controls for bicarbonate were also run in MAITE 300 mM Tris-HCl. The following conditions were used for all experiments: 1 mM 8Br-cAMP, 1 μM H89, 25 μM KH7, and 30 mM bicarbonate for 10 min. Other agonist/inhibitors used in this study were as follows: cAMP (Sigma-Aldrich), 1 mM; 8-CPT-methyl-cAMP, 1 mM, forskolin, 10 μM + IBMX 50 μM; myristoylated protein kinase inhibitor peptide 14-22 (PKI 14-22, Sigma-Aldrich), 1 μM; KH7.15 25, 1 μM; acetazolamide (CAI), 1 μM.

Membrane Potential Measurements

Mitochondrial membrane potential ($\Delta\Psi m$) was measured in enriched mouse mitochondrial fractions using the dye Safranin-O as previously described (Kwong et al., 2007). $\Delta\Psi m$ was calculated based on the linear response of the dye Safranin-O in the region of our measurements (50–170 mV), corresponding to the difference between the maximal fluorescence induced by the substrates and the minimum fluorescence determined by the inhibitors (Akerman and Wikstrom, 1976; Nedergaard, 1983; Zanotti and Azzone, 1980). Changes in $\Delta\Psi m$ were expressed as a percentage of the untreated mitochondria.

Mitochondrial Purification by Nycodenz Gradient

Crude mitochondria from mouse liver (5 mg) or cultured cells (1 mg) were resuspended in 3.3 ml of 25% Nycodenz solution (50% stock, Gentaur) diluted in 0.25 M sucrose, 1 mM EDTA, 10 mM HEPES-NaOH, pH 7.4. Resuspended mitochondria were applied to a discontinuous Nycodenz gradient composed of the following layers: 1.6 ml of 40%, 1.6 ml of 34%, 2.3 ml of 30%, 3.3 ml of resuspended mitochondria, 2.3 ml of 23%, and 0.7 ml of 20% Nycodenz. Samples were centrifuged at 95,000 *g* for 2 hr in a SW4ITi Sorvall Rotor, and the following fractions were collected: fraction 2 between 20%–23%, fraction 3 between 23%–25%, fraction 4 between 25%–30% and fraction 5 between 30%–34%. Fraction 4 from mouse liver mitochondria was subjected to a second round of Nycodenz gradient fractionation and fractions 2, 3, 4, and 5 (denoted as 4.2, 4.3, 4.4, and 4.5, respectively) were collected.

Mitoplast Preparation

Isolated mitochondria 500 μg (1 mg/ml) were resuspended in MS-EGTA (225 mM mannitol, 75 mM sucrose, 5 mM HEPES, 1 mM EGTA, pH 7.4). Water (1/10 volume) and digitonin (1 mg digitonin/5 mg mitochondrial protein) were added, and the mixture was incubated on ice for 45 min. Then, KCl (150 mM) was added, followed by incubation for 2 min on ice and centrifugation at 18,000 *g* for 20 min at 4°C. The pellet containing the mitoplats fraction was resuspended at 1 mg/ml in 300 mM Tris-HCl, 10 μM $CaCl_2$, pH 7.4. The supernatant containing the postmitoplasts fraction was precipitated with 12% TCA and centrifuged at 18,000 *g* for 15 min at 4°C. The pellet was resuspended in 500 μl acetone and centrifuged at 18,000 *g* for 15 min at 4°C.

Determination of Phosphodiesterase Activity in Isolated Mitoplasts

Mitoplasts were sonicated, and 50 pmol of cAMP was added to each sample. IBMX (50 μM) or KH7 (25 μM) were used to prevent degradation and synthesis of cAMP, respectively. Samples containing 50 pmol cAMP, 0.1 unit of phosphodiesterase (PDE, Sigma-Aldrich), and 10 units of calmodulin (Sigma-Aldrich), with or without IBMX (but no mitoplasts) were used as controls. Reactions were performed at 30°C for 30 min.

Immunoblot Analyses

For western blot analyses of COX subunits in crude mitochondria, 10 μg of protein were separated by 12.5% SDS-polyacrylamide gel electrophoresis (PAGE) and electroblotted onto PVDF filters (BioRad).

For protease protection assays 20 μg of mitochondrial protein from COS cells expressing sAC_t-HA were treated with 20 μg/ml PK for 20 min on ice. Then, PK was inactivated with 2mM phenylmethanesulphonylfluoride for 10 min on ice. Prior to PK treatment, one aliquot of mitochondria was solubilized with 1% Triton X-100 (Sigma-Aldrich) for 15 min on ice.

For isoelectric focusing of mitochondrial samples, 100 μg of protein were processed with a Ready Prep 2D Cleanup kit (BioRad) and resuspended in 125 μl of rehydratation buffer (BioRad). Samples were applied to 3–10 IPG strips (BioRad) and incubated overnight at room temperature. Isoelectric focusing and 2D SDS-PAGE were run under standard conditions, and proteins were transferred onto a PVDF filters.

For blue native (BN) 2D gels (Schagger and von Jagow, 1991), 50–75 μg mitochondrial protein were applied on a 5%–13% gradient BN gel followed by a 12.5% 2D denaturing gel. After electrophoresis, proteins were electroblotted onto PVDF filters and sequentially probed with specific antibodies.

Replicate samples were treated with calf-intestinal phosphatase for 1 hr at 37°C to dephosphorylate mitochondrial proteins.

For protein detection, the following antibodies were used: R21 against human sAC (Zippin et al., 2003), PKA (Millipore), phospho Ser/Thr residues, Tim 23 (BD Transduction Laboratories), phospho Ser/Thr PKA substrate-specific (Cell Signaling Technology), COX I, COX IV-2, GAPDH, and VDAC (Invitrogen), PDI, Hsp60 and cytochrome c (Stressgen), HA (AbCam), and Tom 40 (Santa Cruz Biotechnology).

Phosphodiesterase and Anti-sAC Antibody Treatment of Isolated Mitochondria

Isolated crude mouse liver mitochondria (500 μg), either intact or sonicated with three pulses of 2 s each at half of maximal frequency in a Branson Sonifier 250 sonicator (VWR Scientific), were resuspended in 300 mM Tris-HCl, 10 μM $CaCl_2$, pH 7.4 (1 mg/ml final concentration), and incubated with or without 0.1 unit of phosphodiesterase at 30°C for 30 min. Ten units of calmodulin, a PDE cofactor, were added to all samples. Bicarbonate (30 mM) and IBMX (50 μM) were added to stimulate sAC or inhibit PDE, respectively. For immunoinhibition of sAC, samples were treated with 0.5 μg of the R21 anti-sAC antibody or with mouse IgG subtype K (Sigma). Phosphatase inhibitors were used during the incubations.

Titration of R21 Antibody

Cyclase assays were performed in 100 μl volume with equivalent amounts of total protein in the presence of 50 mM Tris (pH 7.5), 20 mM creatine phosphate, and 100 U/mL CPK where required, substrate 2.5 mM [α^{32}P]ATP and 10 mM $MgCl_2$. Reactions were incubated at 30°C for 30 min, and stopped with 200 μl 2% SDS. [^{32}P]cAMP was recovered using a two-column methods as described in (Salomon, 1979). Kinetic analysis was performed using GraphPad Prism software.

α-Ketoglutarate Dehydogenase Complex Activity Treatment of Isolated Mitochondria

α-ketoglutarate dehydogenase complex (KGDHC) activity was perform in the oxygraph in respiration medium containing cocarboxilase (TPP, Sigma-Aldrich), 0.3 mM: β-nicotidamide adenine dinucleotide (β-NAD^+, Sigma-Aldrich), 0.5 mM; coenzyme A (Sigma-Aldrich), 0.24 mM; α-ketoglutarate (Sigma-Aldrich), 5mM; dithiothreitol (DTT, Sigma-Aldrich), 1 mM; and 0.5 units of KGDHC (Sigma-Aldrich). After 3 min reaction, isolated crude mouse mitochondria (100 μg) were added to the medium and TMPD/ascorbate-dependent respiration was measured after blocking complex III with antimycin A as described above. Control samples were run in the same conditions, but in the absence of the KGDHC enzyme.

cAMP Measurements

cAMP measurements were performed according to manufacturer's instructions using the Direct Correlate-EIA cAMP Kit (Assay Designs, Inc.). One hundred microliters of sample were measured. If necessary, samples were diluted to bring the cAMP level of the sample within the linear range of the assay.

ROS Production Determination

Cells were grown in glucose or galactose medium for 48 hr in a 96-well plate and then incubated with the different compounds for 2 hr at the same concentrations used for the other biochemical assays. Cells were incubated with 2′,7′-dichloroflourescein diacetate (H_2-DCFDA; Invitrogen, 10 μM, 30 min) and then washed with PBS. Fluorescence was measured in a Perkin Elmer HST7000 plate reader (excitation, 485 nm; emission, 535 nm). For each sample, values were normalized by the maximal fluorescence measured after adding 300 μM H_2O_2 for 15 min to correct for potential differences in the loading of the dye.

Statistical Analyses

Comparisons between groups were made using one-way ANOVA. Pair-wise comparisons were made by post hoc Fisher PLSD test. Differences were considered statistically significant at $p < 0.05$. Data analyses were performed using the statistical program StatView. In all experiments, error bars indicate standard deviations (Adept Scientific, UK).

SUPPLEMENTAL DATA

Supplemental Data include six figures and can be found online at http://www.cell.com/cellmetabolism/supplemental/S1550-4131(09)00037-0.

ACKNOWLEDGMENTS

This work was supported by NIH (G.M., D.B., L.R.L., and J.B.), the Muscular Dystrophy Association (G.M.), American Diabetes Association (L.R.L.), Spanish Ministry of Education Fulbright Fellowship (R.A.-P.), United Mitochondrial Disease Foundation (R.-A.P.), Milstein Foundation, and MSTP funding (E.R.S.).

Received: July 23, 2008
Revised: October 31, 2008
Accepted: January 29, 2009
Published: March 3, 2009

REFERENCES

Akerman, K.E., and Wikstrom, M.K. (1976). Safranine as a probe of the mitochondrial membrane potential. FEBS Lett. *68*, 191–197.

Bender, E., and Kadenbach, B. (2000). The allosteric ATP-inhibition of cytochrome c oxidase activity is reversibly switched on by cAMP-dependent phosphorylation. FEBS Lett. *466*, 130–134.

Birch-Machin, M.A., and Turnbull, D.M. (2001). Assaying mitochondrial respiratory complex activity in mitochondria isolated from human cells and tissues. Methods Cell Biol. *65*, 97–117.

Bornfeldt, K.E. (2006). A single second messenger: several possible cellular responses depending on distinct subcellular pools. Circ. Res. *99*, 790–792.

Bruce, J.I., Shuttleworth, T.J., Giovannucci, D.R., and Yule, D.I. (2002). Phosphorylation of inositol 1,4,5-trisphosphate receptors in parotid acinar cells. A mechanism for the synergistic effects of cAMP on Ca2+ signaling. J. Biol. Chem. *277*, 1340–1348.

Buck, J., Sinclair, M.L., Schapal, L., Cann, M.J., and Levin, L.R. (1999). Cytosolic adenylyl cyclase defines a unique signaling molecule in mammals. Proc. Natl. Acad. Sci. USA *96*, 79–84.

Chaloupka, J.A., Bullock, S.A., Iourgenko, V., Levin, L.R., and Buck, J. (2006). Autoinhibitory regulation of soluble adenylyl cyclase. Mol. Reprod. Dev. *73*, 361–368.

Chen, Y., Cann, M.J., Litvin, T.N., Iourgenko, V., Sinclair, M.L., Levin, L.R., and Buck, J. (2000). Soluble adenylyl cyclase as an evolutionarily conserved bicarbonate sensor. Science *289*, 625–628.

Chen, R., Fearnley, I.M., Peak-Chew, S.Y., and Walker, J.E. (2004). The phosphorylation of subunits of complex I from bovine heart mitochondria. J. Biol. Chem. *279*, 26036–26045.

D'Aurelio, M., Pallotti, F., Barrientos, A., Gajewski, C.D., Kwong, J.Q., Bruno, C., Beal, M.F., and Manfredi, G. (2001). In vivo regulation of oxidative phosphorylation in cells harboring a stop-codon mutation in mitochondrial DNA-encoded cytochrome c oxidase subunit I. J. Biol. Chem. *276*, 46925–46932.

DiPilato, L.M., Cheng, X., and Zhang, J. (2004). Fluorescent indicators of cAMP and Epac activation reveal differential dynamics of cAMP signaling within discrete subcellular compartments. Proc. Natl. Acad. Sci. USA *101*, 16513–16518.

Dodgson, S.J., Forster, R.E., 2nd, Storey, B.T., and Mela, L. (1980). Mitochondrial carbonic anhydrase. Proc. Natl. Acad. Sci. USA *77*, 5562–5566.

Farrell, J., Ramos, L., Tresguerres, M., Kamenetsky, M., Levin, L.R., and Buck, J. (2008). Somatic 'soluble' adenylyl cyclase isoforms are unaffected in Sacy tm1Lex/Sacy tm1Lex 'knockout' mice. PLoS ONE *3*, e3251.

Feliciello, A., Gottesman, M.E., and Avvedimento, E.V. (2005). cAMP-PKA signaling to the mitochondria: protein scaffolds, mRNA and phosphatases. Cell. Signal. *17*, 279–287.

Fernandez-Vizarra, E., Lopez-Perez, M.J., and Enriquez, J.A. (2002). Isolation of biogenetically competent mitochondria from mammalian tissues and cultured cells. Methods *26*, 292–297.

Geng, W., Wang, Z., Zhang, J., Reed, B.Y., Pak, C.Y., and Moe, O.W. (2005). Cloning and characterization of the human soluble adenylyl cyclase. Am. J. Physiol. Cell Physiol. *288*, C1305–C1316.

Helling, S., Vogt, S., Rhiel, A., Ramzan, R., Wen, L., Marcus, K., and Kadenbach, B. (2008). Phosphorylation and kinetics of mammalian cytochrome c oxidase. Mol. Cell. Proteomics *7*, 1714–1724.

Hess, K.C., Jones, B.H., Marquez, B., Chen, Y., Ord, T.S., Kamenetsky, M., Miyamoto, C., Zippin, J.H., Kopf, G.S., Suarez, S.S., et al. (2005). The "soluble" adenylyl cyclase in sperm mediates multiple signaling events required for fertilization. Dev. Cell *9*, 249–259.

Hofhaus, G., Shakeley, R.M., and Attardi, G. (1996). Use of polarography to detect respiration defects in cell cultures. Methods Enzymol. *264*, 476–483.

Hopper, R.K., Carroll, S., Aponte, A.M., Johnson, D.T., French, S., Shen, R.F., Witzmann, F.A., Harris, R.A., and Balaban, R.S. (2006). Mitochondrial matrix phosphoproteome: effect of extra mitochondrial calcium. Biochemistry *45*, 2524–2536.

Jaiswal, B.S., and Conti, M. (2003). Calcium regulation of the soluble adenylyl cyclase expressed in mammalian spermatozoa. Proc. Natl. Acad. Sci. USA *100*, 10676–10681.

Kadenbach, B. (2003). Intrinsic and extrinsic uncoupling of oxidative phosphorylation. Biochim. Biophys. Acta *1604*, 77–94.

Kwong, J.Q., Henning, M.S., Starkov, A.A., and Manfredi, G. (2007). The mitochondrial respiratory chain is a modulator of apoptosis. J. Cell Biol. *179*, 1163–1177.

Lee, I., Salomon, A.R., Ficarro, S., Mathes, I., Lottspeich, F., Grossman, L.I., and Huttemann, M. (2005). cAMP-dependent tyrosine phosphorylation of subunit I inhibits cytochrome c oxidase activity. J. Biol. Chem. *280*, 6094–6100.

Lewitt, M.S., Brismar, K., Wang, J., Wivall-Helleryd, I.L., Sindelar, P., Gonzalez, F.J., Bergman, T., and Bobek, G.A. (2001). Responses of insulin-like growth factor (IGF)-I and IGF-binding proteins to nutritional status in peroxisome proliferator-activated receptor-alpha knockout mice. Growth Horm. IGF Res. *11*, 303–313.

Litvin, T.N., Kamenetsky, M., Zarifyan, A., Buck, J., and Levin, L.R. (2003). Kinetic properties of "soluble" adenylyl cyclase. Synergism between calcium and bicarbonate. J. Biol. Chem. *278*, 15922–15926.

Livigni, A., Scorziello, A., Agnese, S., Adornetto, A., Carlucci, A., Garbi, C., Castaldo, I., Annunziato, L., Avvedimento, E.V., and Feliciello, A. (2006). Mitochondrial AKAP121 links cAMP and src signaling to oxidative metabolism. Mol. Biol. Cell *17*, 263–271.

Margulis, L., and Bermudes, D. (1985). Symbiosis as a mechanism of evolution: status of cell symbiosis theory. Symbiosis *1*, 101–124.

McCormack, J.G., Halestrap, A.P., and Denton, R.M. (1990). Role of calcium ions in regulation of mammalian intramitochondrial metabolism. Physiol. Rev. *70*, 391–425.

Miyazaki, T., Neff, L., Tanaka, S., Horne, W.C., and Baron, R. (2003). Regulation of cytochrome c oxidase activity by c-Src in osteoclasts. J. Cell Biol. *160*, 709–718.

Nedergaard, J. (1983). The relationship between extramitochondrial Ca2+ concentration, respiratory rate, and membrane potential in mitochondria from brown adipose tissue of the rat. Eur. J. Biochem. *133*, 185–191.

Pagliarini, D.J., and Dixon, J.E. (2006). Mitochondrial modulation: reversible phosphorylation takes center stage? Trends Biochem. Sci. *31*, 26–34.

Papa, S., Sardanelli, A.M., Cocco, T., Speranza, F., Scacco, S.C., and Technikova-Dobrova, Z. (1996). The nuclear-encoded 18 kDa (IP) AQDQ subunit of bovine heart complex I is phosphorylated by the mitochondrial cAMP-dependent protein kinase. FEBS Lett. *379*, 299–301.

Papa, S., Sardanelli, A.M., Scacco, S., and Technikova-Dobrova, Z. (1999). cAMP-dependent protein kinase and phosphoproteins in mammalian mitochondria. An extension of the cAMP-mediated intracellular signal transduction. FEBS Lett. *444*, 245–249.

Prabu, S.K., Anandatheerthavarada, H.K., Raza, H., Srinivasan, S., Spear, J.F., and Avadhani, N.G. (2006). Protein kinase A-mediated phosphorylation modulates cytochrome c oxidase function and augments hypoxia and myocardial ischemia-related injury. J. Biol. Chem. *281*, 2061–2070.

Ryu, H., Lee, J., Impey, S., Ratan, R.R., and Ferrante, R.J. (2005). Antioxidants modulate mitochondrial PKA and increase CREB binding to D-loop DNA of the mitochondrial genome in neurons. Proc. Natl. Acad. Sci. USA *102*, 13915–13920.

Sardanelli, A.M., Technikova-Dobrova, Z., Scacco, S.C., Speranza, F., and Papa, S. (1995). Characterization of proteins phosphorylated by the cAMP-dependent protein kinase of bovine heart mitochondria. FEBS Lett. *377*, 470–474.

Scacco, S., Vergari, R., Scarpulla, R.C., Technikova-Dobrova, Z., Sardanelli, A., Lambo, R., Lorusso, V., and Papa, S. (2000). cAMP-dependent phosphorylation of the nuclear encoded 18-kDa (IP) subunit of respiratory complex I and activation of the complex in serum-starved mouse fibroblast cultures. J. Biol. Chem. *275*, 17578–17582.

Schagger, H., and von Jagow, G. (1991). Blue native electrophoresis for isolation of membrane protein complexes in enzymatically active form. Anal. Biochem. *199*, 223–231.

Schagger, H., and Pfeiffer, K. (2000). Supercomplexes in the respiratory chains of yeast and mammalian mitochondria. EMBO J. *19*, 1777–1783.

Schmitt, J.M., and Stork, P.J. (2002). PKA phosphorylation of Src mediates cAMP's inhibition of cell growth via Rap1. Mol. Cell *9*, 85–94.

Schwoch, G., Trinczek, B., and Bode, C. (1990). Localization of catalytic and regulatory subunits of cyclic AMP-dependent protein kinases in mitochondria from various rat tissues. Biochem. J. *270*, 181–188.

Shinzawa-Itoh, K., Aoyama, H., Muramoto, K., Terada, H., Kurauchi, T., Tadehara, Y., Yamasaki, A., Sugimura, T., Kurono, S., Tsujimoto, K., et al. (2007). Structures and physiological roles of 13 integral lipids of bovine heart cytochrome c oxidase. EMBO J. *26*, 1713–1725.

Signorile, A., Sardanelli, A.M., Nuzzi, R., and Papa, S. (2002). Serine (threonine) phosphatase(s) acting on cAMP-dependent phosphoproteins in mammalian mitochondria. FEBS Lett. *512*, 91–94.

Simpson, D.P., and Hager, S.R. (1979). pH and bicarbonate effects on mitochondrial anion accumulation. Proposed mechanism for changes in renal metabolite levels in acute acid-base disturbances. J. Clin. Invest. *63*, 704–712.

Salomon, Y. (1979). Adenylate cyclase assay. Adv. Cyclic Nucleotide Res. *10*, 35–55.

Steegborn, C., Litvin, T.N., Levin, L.R., Buck, J., and Wu, H. (2005). Bicarbonate activation of adenylyl cyclase via promotion of catalytic active site closure and metal recruitment. Nat. Struct. Mol. Biol. *12*, 32–37.

Thomson, M. (2002). Evidence of undiscovered cell regulatory mechanisms: phosphoproteins and protein kinases in mitochondria. Cell. Mol. Life Sci. *59*, 213–219.

Villani, G., and Attardi, G. (1997). In vivo control of respiration by cytochrome c oxidase in wild-type and mitochondrial DNA mutation-carrying human cells. Proc. Natl. Acad. Sci. USA *94*, 1166–1171.

Villani, G., Greco, M., Papa, S., and Attardi, G. (1998). Low reserve of cytochrome c oxidase capacity in vivo in the respiratory chain of a variety of human cell types. J. Biol. Chem. *273*, 31829–31836.

Vives-Bauza, C., Yang, L., and Manfredi, G. (2007). Assay of mitochondrial ATP synthesis in animal cells and tissues. Methods Cell Biol. *80*, 155–171.

Wang, L., Sunahara, R.K., Krumins, A., Perkins, G., Crochiere, M.L., Mackey, M., Bell, S., Ellisman, M.H., and Taylor, S.S. (2001). Cloning and mitochondrial localization of full-length D-AKAP2, a protein kinase A anchoring protein. Proc. Natl. Acad. Sci. USA *98*, 3220–3225.

Wu, K.Y., Zippin, J.H., Huron, D.R., Kamenetsky, M., Hengst, U., Buck, J., Levin, L.R., and Jaffrey, S.R. (2006). Soluble adenylyl cyclase is required for netrin-1 signaling in nerve growth cones. Nat. Neurosci. *9*, 1257–1264.

Zaccolo, M., and Pozzan, T. (2002). Discrete microdomains with high concentration of cAMP in stimulated rat neonatal cardiac myocytes. Science *295*, 1711–1715.

Zanotti, A., and Azzone, G.F. (1980). Safranine as membrane potential probe in rat liver mitochondria. Arch. Biochem. Biophys. *201*, 255–265.

Zippin, J.H., Chen, Y., Nahirney, P., Kamenetsky, M., Wuttke, M.S., Fischman, D.A., Levin, L.R., and Buck, J. (2003). Compartmentalization of bicarbonate-sensitive adenylyl cyclase in distinct signaling microdomains. FASEB J. *17*, 82–84.

Cell Metabolism
Article

Adipocyte CREB Promotes Insulin Resistance in Obesity

Ling Qi,[1,5,6] Maziyar Saberi,[2,5] Erik Zmuda,[3] Yiguo Wang,[1] Judith Altarejos,[1] Xinmin Zhang,[4] Renaud Dentin,[1] Susie Hedrick,[1] Gautam Bandyopadhyay,[2] Tsonwin Hai,[3] Jerry Olefsky,[2] and Marc Montminy[1,*]
[1]Laboratories for Peptide Biology, Salk Institute for Biological Studies, La Jolla, CA 92037, USA
[2]Division of Endocrinology and Metabolism, University of California, San Diego, La Jolla, CA 92037, USA
[3]Department of Molecular and Cellular Biochemistry, Ohio State University, Columbus, OH 43210, USA
[4]NimbleGen, Madison, WI 53719, USA
[5]These authors contributed equally to this work
[6]Present address: Division of Nutritional Sciences, Cornell University, Ithaca, NY 14853, USA
*Correspondence: montminy@salk.edu
DOI 10.1016/j.cmet.2009.01.006

SUMMARY

Increases in adiposity trigger metabolic and inflammatory changes that interfere with insulin action in peripheral tissues, culminating in beta cell failure and overt diabetes. We found that the cAMP Response Element Binding protein (CREB) is activated in adipose cells under obese conditions, where it promotes insulin resistance by triggering expression of the transcriptional repressor ATF3 and thereby downregulating expression of the adipokine hormone adiponectin as well as the insulin-sensitive glucose transporter 4 (GLUT4). Transgenic mice expressing a dominant-negative CREB transgene in adipocytes displayed increased whole-body insulin sensitivity in the contexts of diet-induced and genetic obesity, and they were protected from the development of hepatic steatosis and adipose tissue inflammation. These results indicate that adipocyte CREB provides an early signal in the progression to type 2 diabetes.

INTRODUCTION

During fasting, mammals maintain energy balance by shifting from glucose to fat burning. Circulating catecholamines mobilize triglyceride stores from white adipose tissue (WAT) by increasing lipolysis (Joost et al., 1986, 1988; Laakso et al., 1992) and by reducing glucose uptake in fat through activation of the cAMP pathway (Joost et al., 1986, 1988; Laakso et al., 1992). Although they decrease membrane targeting of the GLUT4 transporter, catecholamines also downregulate adipocyte *GLUT4* gene expression in adipose in response to fasting and type 2 diabetes (Berger et al., 1989; Garvey et al., 1989; Kahn et al., 1989; Sivitz et al., 1989).

Superimposed on these metabolic effects, catecholamines also inhibit the expression and secretion of certain adipocytokine hormones, most notably adiponectin, a key modulator of systemic insulin sensitivity (Delporte et al., 2002; Fu et al., 2007; Ricci et al., 2005; Scriba et al., 2000). Depletion of adiponectin in adipose reduces insulin sensitivity (Kubota et al., 2002; Maeda et al., 2002; Nawrocki et al., 2006) while overexpression of adiponectin enhances it, in part through effects on hepatic glucose production (HGP) (Berg et al., 2001; Combs et al., 2001; Kim et al., 2007; Satoh et al., 2005; Yamauchi et al., 2002b).

The CREB family of cAMP-responsive transcription factors (CREB1, CREM, ATF1) has been found to mediate effects of catecholamines and other fasting hormones on cellular gene expression (Herzig et al., 2001; Zhang et al., 2005a). Following its phosphorylation at Ser133, CREB stimulates transcription through recruitment of the histone acetylase CBP and through an association with the CREB Regulated Transcriptional Coactivator (CRTC, also known as TORC2) family of latent cytoplasmic coactivators (Chrivia et al., 1993; Ravnskjaer et al., 2007; Xu et al., 2007). CREB promotes glucose homeostasis during fasting, for example, by triggering expression of the gluconeogenic program in liver (Herzig et al., 2001). Hepatic CREB activity is constitutively upregulated in diabetes, where it contributes to hyperglycemia and insulin resistance (Dentin et al., 2007, 2008). The extent to which adiponectin or other adipose-derived hormones modulate hepatic gluconeogenesis via CREB remains unclear, however.

In addition to its function in liver, CREB also appears to promote expression of the adipogenic program in preadipocytes (Zhang et al., 2004), although its role in mediating effects of cAMP in mature adipocytes has not been addressed. We found that adipocyte CREB is activated in obesity, when it disrupts insulin action and promotes systemic insulin resistance. Blocking CREB activity in adipocytes prevented the development of inflammatory infiltrates in adipose as well as systemic insulin resistance under obese conditions. These results point to a central role for adipose tissue in coordinating systemic insulin action and in modulating energy balance in part through obesity-related increases in CREB activity.

RESULTS

Insulin Sensitivity in Obese Mice with Reduced Adipocyte CREB Activity

CREB family members (CREB1, CREM, ATF1) exhibit considerable functional redundancy (Mayr and Montminy, 2001; Shaywitz

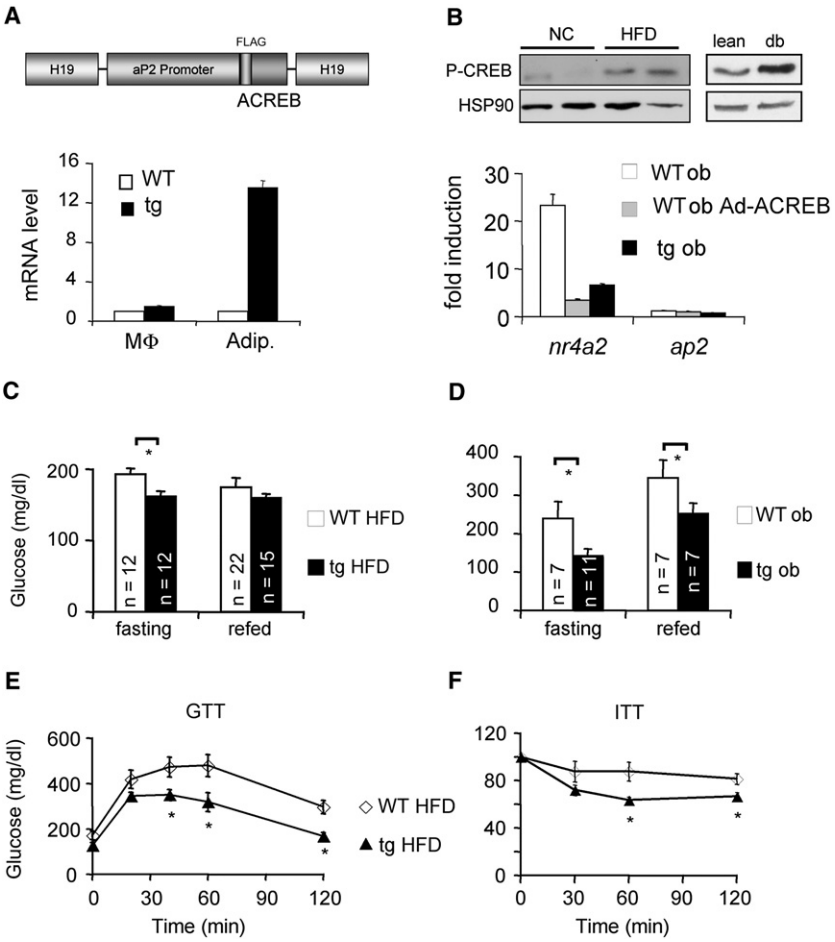

Figure 1. Mice Deficient in Adipocyte CREB Activity Remain Insulin Sensitive under Obese Conditions

(A) Top shows schematic of dominant-negative ACREB transgene expressed from the fat-specific aP2 promoter in FAT-ACREB (F-ACREB) C57/Bl6 mice. Bottom shows Q-PCR analysis of ACREB mRNA amounts in peritoneal macrophages (MΦ) and adipocytes from wild-type (WT) or transgenic (tg) F-ACREB littermates.

(B) Top, immunoblot showing relative amounts of phospho (Ser133) CREB (P-CREB) in adipose from mice maintained on normal chow (NC) or high-fat diet (HFD). Right shows relative P-CREB amounts in adipose from lean or genetically obese (db) mice. Bottom shows effect of forskolin (FSK) exposure (4 hr) on CREB target gene expression (NR4A2) in cultured adipocytes expressing ACREB through adenoviral infection (ob Ad-ACREB) or chronically in cells from F-ACREB transgenic (tg ob) mice.

(C and D) Relative circulating blood glucose concentrations in control (WT) and F-ACREB (tg) mice under HFD (C) and genetically obese conditions (*ob/ob*) (D; WT ob and tg ob). Glucose levels were evaluated in overnight-fasted and 2 hr-refed mice.

(E and F) Glucose (E) and insulin (F) tolerance testing of F-ACREB mice relative to WT littermates maintained under HFD conditions for 9.5 weeks. Unless stated otherwise, mice were maintained on HFD for 8–12 weeks, while *ob/ob* mice were analyzed at 12–16 weeks of age (*; $p < 0.05$). Data are means ± SEM.

and Greenberg, 1999), and mice with individual knockouts show only limited phenotypes (Bleckmann et al., 2002; Blendy et al., 1996; Hummler et al., 1994). To block the activity of all CREB family members in mature adipocytes, we generated transgenic mice that express the dominant-negative CREB inhibitor ACREB, a synthetic polypeptide that heterodimerizes with and disrupts binding of CREB1, CREM, and ATF1 but not unrelated bZIP proteins to DNA (Ahn et al., 1998). Because CREB has been found to promote adipogenesis (Tseng et al., 2005; Zhang et al., 2004), we targeted ACREB expression specifically to mature adipocytes using the adipose-specific *aP2* promoter.

ACREB mRNA was detected in adipocytes but not in peritoneal macrophages or in adipose-derived stromal vascular cells from two independent FAT-ACREB (F-ACREB) founder lines established on different genetic backgrounds (CB6 and C57/Bl6) (Figures 1A and S1). Expression of ACREB, either acutely by adenoviral delivery or chronically in cells from F-ACREB transgenic mice, reduced mRNA amounts for the CREB target gene *NR4A2* in primary adipocyte cultures exposed to the cAMP activator forskolin (FSK) (Figure 1B). F-ACREB mice grow normally and are indistinguishable from control littermates under normal chow (NC) conditions (Figure S2).

In the insulin-resistant state, chronic elevations in circulating insulin paradoxically potentiate catecholamine effects on cAMP signaling in adipocytes (Hupfeld et al., 2003; Zhang et al., 2005a). Indeed, amounts of Ser133-phosphorylated, active CREB were increased following high-fat diet (HFD) feeding and in genetically obese (*db/db*) mice relative to lean controls (Figure 1B). To determine the consequence of CREB activation in this setting, we performed metabolic studies on F-ACREB mice following HFD feeding or after breeding them onto a genetically obese (*ob/ob*) background. Compared to controls, F-ACREB mice had lower circulating blood glucose concentrations despite similar food intake, body temperature, physical activity, weight gain, and fat mass in each group (Figures 1C, 1D, and S3). Whole-body insulin sensitivity was also improved in F-ACREB animals after 9.5 weeks of HFD feeding, as revealed by glucose (GTT) and insulin (ITT) tolerance testing (Figures 1E and 1F).

Systemic Insulin Sensitivity in F-ACREB Mice

To determine the relative effects of adipose-specific ACREB expression on insulin resistance in muscle and liver, we performed euglycemic-hyperinsulinemic clamp studies. After 24 weeks of HFD feeding, basal glucose infusion rates (GIR) during the clamp studies were elevated 5-fold in F-ACREB mice relative to controls, and insulin-stimulated glucose disposal rates (IS-GDR), measures of muscle insulin sensitivity, were increased 10-fold (Figures 2A–2C). Adipose-specific expression of ACREB caused similar changes in liver, where insulin infusion during the clamp study inhibited HGP 3-fold greater in transgenic compared to wild-type (WT) littermates (Figure 2D). Consistent with an increase in insulin signaling, amounts of phosphorylated,

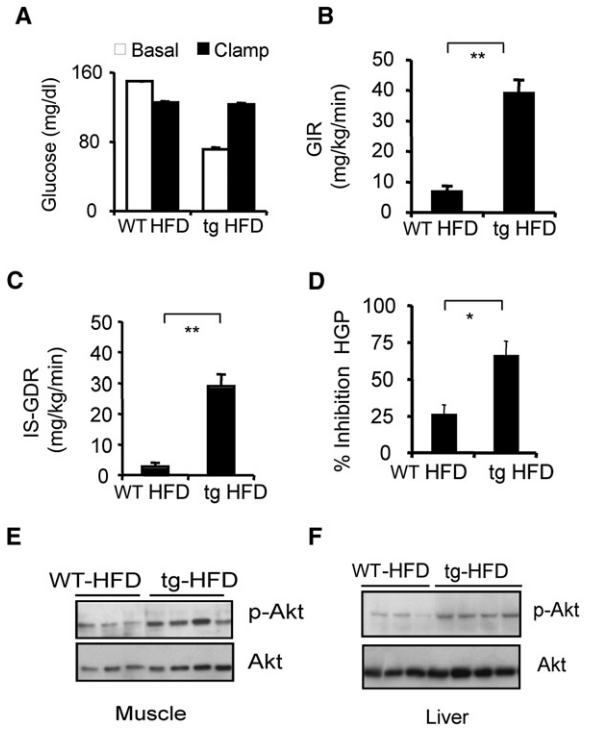

Figure 2. Adipose-Specific Disruption of CREB Activity Enhances Insulin Sensitivity in Muscle and Liver

(A–F) Euglycemic-hyperinsulinemic clamp studies of WT (n = 8) and F-ACREB (n = 9) mice that were maintained on a HFD for 24 weeks. In (A), blood glucose concentrations in HFD-fed F-ACREB (tg) and WT littermates prior to (basal) or after euglycemic clamping (clamp) are shown. Also shown are basal glucose infusion rates (GIRs) (B) and insulin-stimulated glucose disposal rates (IS-GDR) (C) in F-ACREB and control mice under HFD conditions (**; $p < 0.00001$). In (D), relative inhibition of hepatic glucose production (HGP) by insulin in F-ACREB and control mice is shown (*; $p < 0.003$). Also shown are immunoblots of phospho-AKT and total AKT protein amounts in skeletal muscle (E) and liver (F) lysates from F-ACREB and control littermates following insulin injection. Data are means ± SEM.

active AKT were also upregulated in both skeletal muscle and liver from F-ACREB animals following insulin injection (Figures 2E, 2F, and S4).

Despite the elevations in circulating glucose levels in the control group, plasma insulin concentrations were comparable between transgenic and control littermates (Figure S5), suggesting an increased efficiency of glucose-stimulated insulin release in F-ACREB animals. To test this idea, we monitored circulating insulin concentrations under hyperglycemic clamp conditions. In line with their relative insulin sensitivity, GIR were increased 75% in HFD-fed transgenic mice compared to controls (Figure S6). Pointing to an overall improvement in pancreatic islet function, circulating insulin levels rose substantially in glucose-stimulated F-ACREB mice but not in control animals. Taken together, these results indicate that the adipose-specific disruption of CREB activity prevents the development of beta cell failure in the context of obesity.

White adipose stores from obese individuals are often characterized by immune cell infiltrates that further aggravate insulin resistance through the release of inflammatory chemokines (Weisberg et al., 2003; Xu et al., 2003). Although they were abundant in fat pads from HFD-fed controls, immune cells were relatively absent in WAT from F-ACREB mice (Figure 3A). As well, inflammatory pathway gene expression was substantially reduced in WAT from HFD-fed F-ACREB mice compared to WT (Figure S7). Consistent with these improvements, insulin-stimulated glucose uptake was increased in adipocytes from HFD-fed F-ACREB mice (Figure 3B). mRNA and protein amounts for the insulin-sensitive GLUT4 transporter were also elevated.

Enhanced Adiponectin Expression in F-ACREB Mice

We considered that ACREB expression in adipocytes may improve systemic insulin sensitivity in F-ACREB mice by altering the profile of circulating adipocytokine hormones. Although plasma concentrations of resistin, RBP4, tumor necrosis factor (TNF)-α, and IL-1β were similar in both groups (Figure S8), circulating levels of high molecular weight, active adiponectin protein were elevated in F-ACREB transgenic compared to WT controls; adiponectin mRNA amounts in F-ACREB WAT were also increased (Figures 3C and S9). Adiponectin has been found to enhance insulin signaling in liver and other tissues through induction of the Ser/Thr kinase AMPK (Nawrocki et al., 2006; Ruderman et al., 2003; Yamauchi et al., 2002a). Supporting this notion, amounts of phosphorylated, active AMPK were upregulated in livers from F-ACREB mice compared to controls (Figure 3D, top).

AMPK is thought to improve hepatic insulin sensitivity in part by preventing the abnormal accumulation of triglycerides, a condition known as hepatic steatosis. Indeed, large lipid droplets were evident in livers from *ob/ob* controls, but they were relatively scarce in F-ACREB *ob/ob* mice (Figure 3D, bottom). Consistent with these changes, hepatic ketone levels and fatty-acid oxidation gene expression were elevated, while lipogenic gene expression was decreased in F-ACREB *ob/ob* animals compared to controls (Figures 3E, 3F, and S10).

Superimposed on its role in hepatic lipid metabolism, AMPK also reduces glucose production by the liver in part through phosphorylation of the CREB coactivator CRTC2 (Foretz et al., 1998; Lochhead et al., 2000; Koo et al., 2005; Shaw et al., 2005). Indeed, amounts of phosphorylated, inactive CRTC2 were increased in livers from F-ACREB mice, while mRNA amounts for gluconeogenic genes were reduced (Figures 3D, 3F, and S10).

Adiponectin Inhibits CRTC2 Activity

Having seen that hepatic CRTC2 activity is curtailed in F-ACREB animals, we wondered whether adiponectin directly modulates the gluconeogenic program via AMPK-mediated phosphorylation and inactivation of CRTC2. Exposure of cultured primary hepatocytes to FSK triggered CRTC2 dephosphorylation, leading to increases in cAMP response element (CRE)-luciferase reporter activation, gluconeogenic gene expression, and glucose production (Figures 4A–4D). Demonstrating the importance of CRTC2 dephosphorylation, CRE-luciferase activity and glucose output were constitutively elevated in cells expressing phosphorylation-defective, active S171A CRTC2.

Based on the ability for adiponectin (Ad-adiponectin) to lower glucose production following adenoviral delivery into liver (Satoh et al., 2004, 2005), we examined effects of Ad-adiponectin expression in primary hepatocytes on CRTC2 activity. Indeed, Ad-adiponectin blocked the dephosphorylation of CRTC2 and

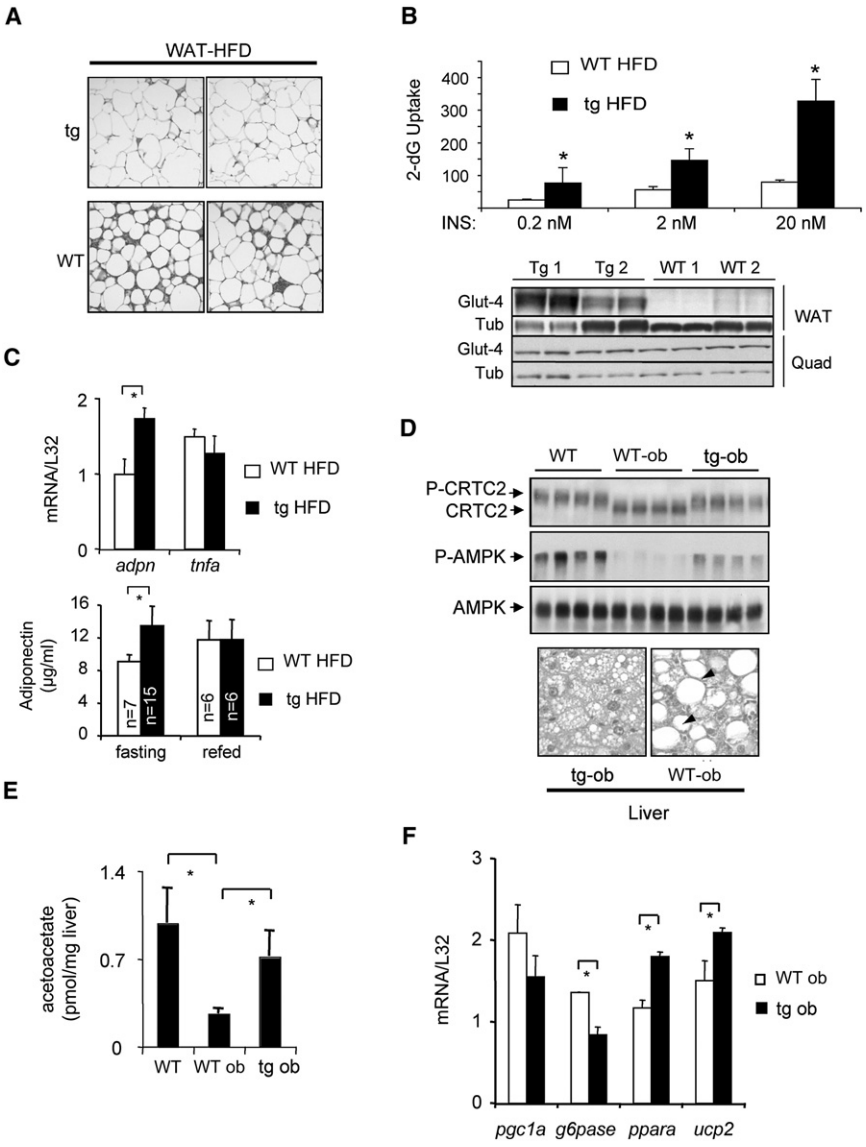

Figure 3. Reduced Adipose Tissue Inflammation and Hepatic Steatosis in F-ACREB Mice

(A) Histological analysis of H&E-stained WAT sections from HFD-fed F-ACREB (tg) and control (WT) littermates showing relative accumulation of inflammatory cell infiltrates.

(B) Top, insulin-stimulated glucose uptake in primary cultured adipocytes from F-ACREB transgenic (tg HFD) and control (WT HFD) littermates under HFD conditions. Relative uptake of [^{3}H]2-deoxyglucose (4 μCi/ml; expressed as counts per minute/10^6 cells) into cultured adipocytes from HFD-fed mice exposed to various concentrations of insulin for 20 min followed by incubation with [^{3}H]2-deoxyglucose for 5 min is shown (*; $p < 0.002$ relative to WT HFD-fed mice; data are means ± SEM). Bottom shows immunoblot of GLUT4 protein amounts in adipose and quadriceps muscle from F-ACREB (Tg1, Tg2) and WT (WT1, WT2) littermates maintained under HFD conditions.

(C) Top, Q-PCR analysis of adiponectin mRNA amounts in adipose tissue from F-ACREB (tg HFD) and WT (WT HFD) littermates maintained under HFD conditions (n = 3 per group; *; $p < 0.05$); bottom, circulating plasma adiponectin concentrations in fasted or 2 hr-refed F-ACREB and control mice.

(D) Top, immunoblot showing phospho-AMPK amounts in liver lysates from WT, *ob/ob* (WT-ob), and F-ACREB transgenic (tg-ob) mice. Amounts of unphospho- and phospho-CRTC2 are also indicated. Bottom shows hepatic sections from F-ACREB transgenic *ob/ob* and control *ob/ob* mice showing relative accumulation of lipid droplets.

(E) Acetoacetate content in livers of F-ACREB *ob/ob* and control *ob/ob* mice relative to lean WT animals (n = 4). (*; $p < 0.05$ transgenic relative to control mice; n = 4; data are means ± SEM.)

(F) Q-PCR analysis of beta oxidation (PGC-1α, PPARα, UCP2) and gluconeogenic (PEPCK, G6Pase) gene expression in livers from *ob/ob* F-ACREB transgenic mice relative to *ob/ob* controls.

correspondingly lowered CRE-luciferase reporter activation in cells exposed to FSK (Figures 4A–4D). As a result, adiponectin also downregulated gluconeogenic gene expression (*G6Pase*, *PEPCK*) and glucose production. But Ad-adiponectin did not reduce CRE-luciferase activity or glucose output in hepatocytes expressing the phosphorylation-defective S171A CRTC2, confirming the importance of Ser171 phosphorylation for these effects. Indeed, exposure of primary mouse hepatocytes to physiologic concentrations of adiponectin (2–15 μg/ml) (Kadowaki et al., 2006) also blocked CRTC2 dephosphorylation and CRE-luciferase reporter activation in cells exposed to FSK (Figures 4E and 4F). Taken together, these results support the notion that adiponectin reduces hepatic gluconeogenesis via the AMPK-mediated phosphorylation of CRTC2 at Ser171.

CREB Stimulates ATF3 Expression in Obesity

Having seen that GLUT4 and adiponectin gene expression in WAT is relatively higher in obese F-ACREB mice over controls, we considered that CREB could inhibit these genes directly or through upregulation of a transcriptional repressor. Arguing against a direct effect, CREB binding over the adiponectin and *GLUT4* promoters was not detectable by chromatin immunoprecipitation assay (Zhang et al., 2005b; data not shown). In gene-profiling assays to characterize putative CREB target genes that are upregulated 2-fold or better in primary adipocytes exposed to FSK and in WAT from HFD-fed compared to NC-fed mice, we identified the transcriptional repressor ATF3 (Chen et al., 1994) as the top-scoring gene (Figure 5A). *ATF3* mRNA and protein amounts were increased nearly 10-fold in WAT from HFD-fed and genetically obese *ob/ob* mice relative to lean controls (Figure 5B, top). Conversely, ATF3 protein and mRNA amounts were decreased in WAT from F-ACREB mice compared to WT littermates (Figure 5B, bottom).

Realizing that the *ATF3* promoter contains a conserved CRE in the proximal promoter (Liang et al., 1996), we tested the role of CREB in modulating this gene directly in adipocytes. Exposure

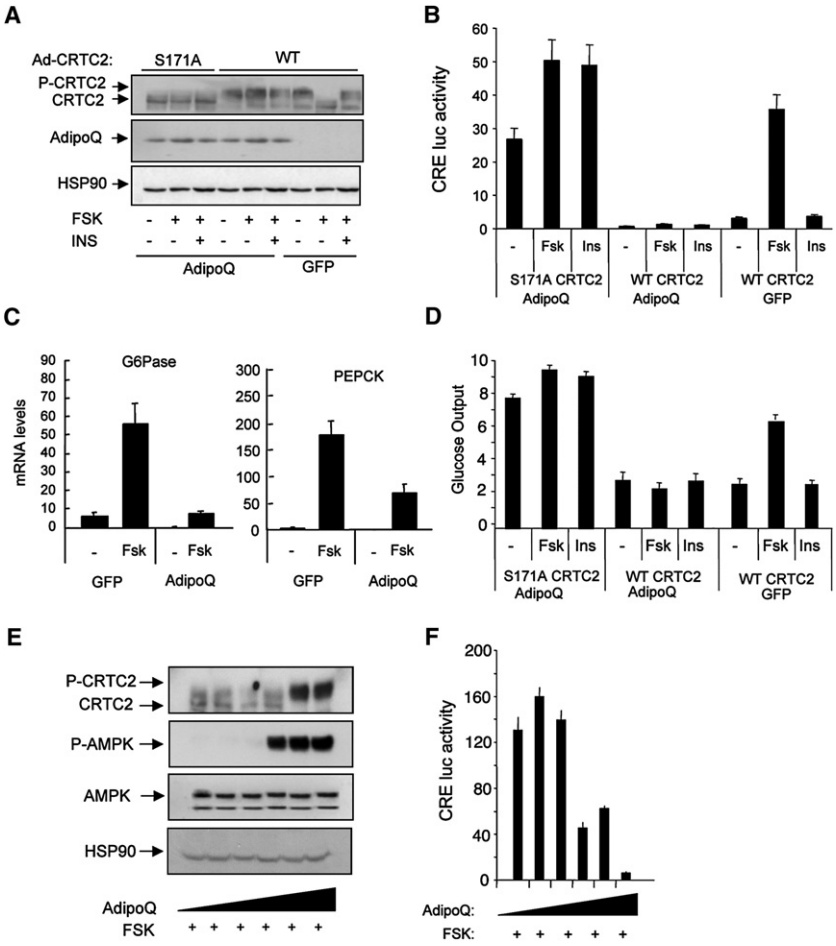

Figure 4. Adiponectin Modulates Hepatic Gluconeogenesis via AMPK-Mediated Phosphorylation of CRTC2

(A–D) Effect of adenoviral adiponectin (AdipoQ) or green fluorescent protein (GFP) expression on amounts of phospho-CRTC2 (A), CRE-luciferase reporter activity (B), gluconeogenic gene expression (C), and glucose secretion (D) from transduced primary hepatocytes exposed to FSK (10 μM) and/or insulin (100 nM). Coinfection with adenoviruses encoding WT or phosphorylation-defective (S171A) CRTC2 are indicated. Data are means ± SEM; n = 3 per group.

(E–F) Phospho-CRTC2 amounts (E) and CRE-luciferase reporter activity (F) in primary hepatocytes exposed to increasing concentrations of adiponectin protein (2–15 μg/ml). Ad-CRE luc activity was measured in cells treated with FSK (10 μM) plus resistin (15 μg/ml) for 5 hr. Representative of three independent experiments shown. Data are means ± SEM; n = 3.

of cultured primary adipocytes or HEK293T cells to FSK increased *ATF3* mRNA amounts; these effects were blocked following expression of adenovirally encoded ACREB (Figure 5C). ATF3 mRNA amounts—elevated in primary adipocytes from *ob/ob* mice—were downregulated in cells from F-ACREB *ob/ob* littermates. Pointing to a direct role for CREB in this process, we recovered the *ATF3* promoter from immunoprecipitates of CREB prepared from gonadal as well as subcutaneous adipose tissue by chromatin immunoprecipitation (ChIP) analysis (Figure 5D).

We examined whether CREB inhibits adiponectin gene expression in adipocytes through the induction of ATF3. Consistent with this idea, ATF3 overexpression disrupted adiponectin promoter activity in transient transfection assays with an adiponectin-luciferase reporter (Figure 6A, top) (Kim et al., 2006). Exposure of primary adipocytes to FSK also reduced adiponectin mRNA amounts; these effects were suppressed when cells were depleted of ATF3 using adenovirally encoded *ATF3* RNAi (Figure 6A, bottom). We also employed *ATF3*$^{-/-}$ mice to determine whether ATF3 mediates the HFD-associated decrease in adiponectin gene expression. In line with the upregulation of *ATF3* mRNA and protein, HFD feeding reduced adiponectin gene expression in WAT from WT littermates (Figure 6B). But adiponectin mRNA amounts remained high in HFD-fed *ATF3*$^{-/-}$ mice, demonstrating the importance of ATF3 in this setting.

In addition to its effects on adiponectin, exposure to FSK also inhibited GLUT4 promoter activity; these effects were reversed in cells expressing dominant-negative ACREB protein (Figure 6C). In keeping with the presence of ATF3 binding sites at −508 and −555 on this promoter, exposure to FSK increased ATF3 occupancy over the GLUT4 gene. Correspondingly, ATF3 overexpression reduced GLUT4-luciferase reporter activity, while disruption of the ATF3 gene increased GLUT4 mRNA and protein amounts in WAT from *ATF3*$^{-/-}$ mice (Figures 6C and S11). Taken together, these results support the notion that the CREB-mediated induction of ATF3 in obesity promotes insulin resistance through the subsequent downregulation of adiponectin and GLUT4 expression in adipose (Figure 6D).

DISCUSSION

Obesity triggers a number of perturbations that alter adipose tissue homeostasis (de Luca and Olefsky, 2008; Lumeng et al., 2007). Increases in adipose tissue mass promote local areas of microhypoxia that activate stress and inflammatory pathways within the adipocytes and surrounding stromal vascular cells. The subsequent release of chemokines by adipocytes is thought to cause a large and sustained influx of circulating monocytes that become adipose tissue macrophages (ATMs). Because they also release a variety of cytokines, ATMs further exacerbate the chronic inflammatory state in adipose by promoting lipolysis as well as insulin resistance in adipocytes (Xu et al., 2003). This insulin-resistant state in adipose can then be communicated to the periphery through increases in circulating FFAs and through changes in the repertoire of secreted adipokines, culminating in systemic insulin resistance in both liver and muscle.

We found that the activation of CREB in adipose represents an important step in the development of insulin resistance in

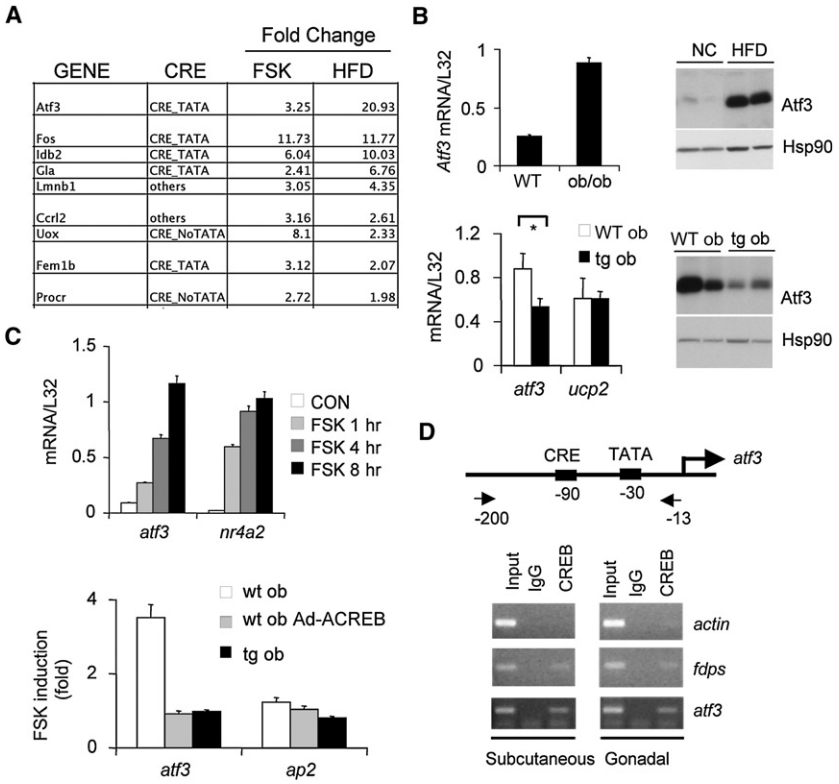

Figure 5. CREB Stimulates Expression of the Transcriptional Repressor ATF3 in Adipose under Obese Conditions

(A) Results from gene profiling studies showing genes induced 2-fold or greater in primary adipocytes following exposure to FSK and in WAT harvested from HFD- relative to NC-fed mice. Presence of conserved CREB binding site (CRE) and TATA box is indicated.

(B) Top left, relative ATF3 mRNA amounts in WAT from lean and *ob/ob* mice. Top right, effect of NC- and HFD-feeding on ATF3 protein amounts in white adipose from WT mice. Bottom shows relative ATF3 mRNA (left) and protein (right) amounts in WAT from F-ACREB *ob/ob* mice compared to control *ob/ob* animals.

(C) Q-PCR analysis of ATF3 mRNA in HEK293T cells (top) and in cultured primary adipocytes of *ob/ob* mice (bottom) following exposure to forskolin. Effect of ACREB expression, either acutely through adenoviral infection (ob Ad-ACREB) or chronically in cells from ACREB transgenic mice (tg ob), is indicated.

(D) ChIP assay of subcutaneous or gonadal WAT showing CREB occupancy over the ATF3 promoter in vivo. CREB binding to positive control (FDPS) and negative control (actin) promoters is shown for comparison. Relative recovery of ATF3 promoter from immunoprecipitates of CREB or nonspecific IgG is also indicated. Position of CREB binding site and TATA box relative to transcription start site on the ATF3 promoter is shown.

obesity. When CREB activity is inhibited, adipose tissue and systemic insulin sensitivity are relatively preserved in obese mice. Because the ACREB transgene is selectively expressed in adipocytes, the systemic insulin-sensitive phenotype must originate within adipose itself. Despite these improvements in insulin sensitivity, F-ACREB animals gain weight comparably to controls in the context of HFD feeding or in *ob/ob* mice, indicating that obesity can be uncoupled from insulin resistance.

In parallel with the increases in adipose tissue insulin sensitivity and glucose transport, pancreatic islet function is also relatively preserved in F-ACREB mice. Although the underlying mechanism is unclear, we imagine that the associated improvements in glucose and lipid homeostasis may protect against deterioration of beta cell function often associated with obesity. Indeed, the systemic changes in F-ACREB mice are reminiscent of those observed in fatty acid binding protein (*FABP4*, *FABP5*) knockout mice, which remain insulin sensitive under obese conditions (Cao et al., 2008). Despite comparable circulating concentrations of free fatty acids, $FABP4^{-/-};FABP5^{-/-}$ knockout mice were protected from hepatic steatosis due to increases in circulating concentrations of the "lipokine" hormone palmitoleate. Further studies should reveal whether the composition of circulating free fatty acids is similarly altered in F-ACREB animals.

ATM content and inflammatory gene expression were also reduced in F-ACREB mice, and these animals were protected from the subsequent development of insulin resistance in the other major insulin target tissues, muscle and liver. The secretion of TNF by ATMs has been shown to increase adipocyte insulin resistance through the activation of the Ser/Thr kinase JNK1, which in turn phosphorylates the insulin receptor substrate 1 (IRS1) on serine (Sabio et al., 2008). These localized changes in adipocyte insulin resistance are transmitted to the liver through the release of interleukin 6 (IL-6) from adipocytes, leading to hepatic upregulation of SOCS3, an inhibitor of insulin receptor signaling. Although we did not observe changes in circulating concentrations of IL-6 in F-ACREB relative to control mice, it is interesting to note that the IL-6 promoter contains a number of CREB binding sites that can potentially mediate induction of this gene in response to cAMP signals (Zhang et al., 2005b).

CREB was found to compromise adipocyte function in part by stimulating the expression of ATF3, a repressor that binds to and inhibits transcription of the adiponectin and *GLUT4* genes. Supporting this idea, ATF3 has been found to inhibit adiponectin gene expression in 3T3-L1 adipocytes in response to ER stress signals (Kim et al., 2006; Koh et al., 2007). Disrupting CREB activity in adipocytes was sufficient to promote relatively normal glucose homeostasis in the contexts of dietary and genetic obesity. Indeed, modest overexpression of adiponectin or GLUT4 in fat also appears to enhance glucose tolerance and insulin sensitivity and, in the case of adiponectin, to reduce inflammatory pathway signaling (Berg et al., 2001; Carvalho et al., 2005; Combs et al., 2001; Kim et al., 2007; Satoh et al., 2005; Yamauchi et al., 2002b).

In addition to its effects on ATF3, CREB may modulate the expression of other cellular genes that influence lipid metabolism in adipocytes. For example, cAMP appears to increase mRNA amounts for the inhibitor of DNA binding 2 (Id2), a helix-loop-helix protein that has been found to promote adipogenesis by

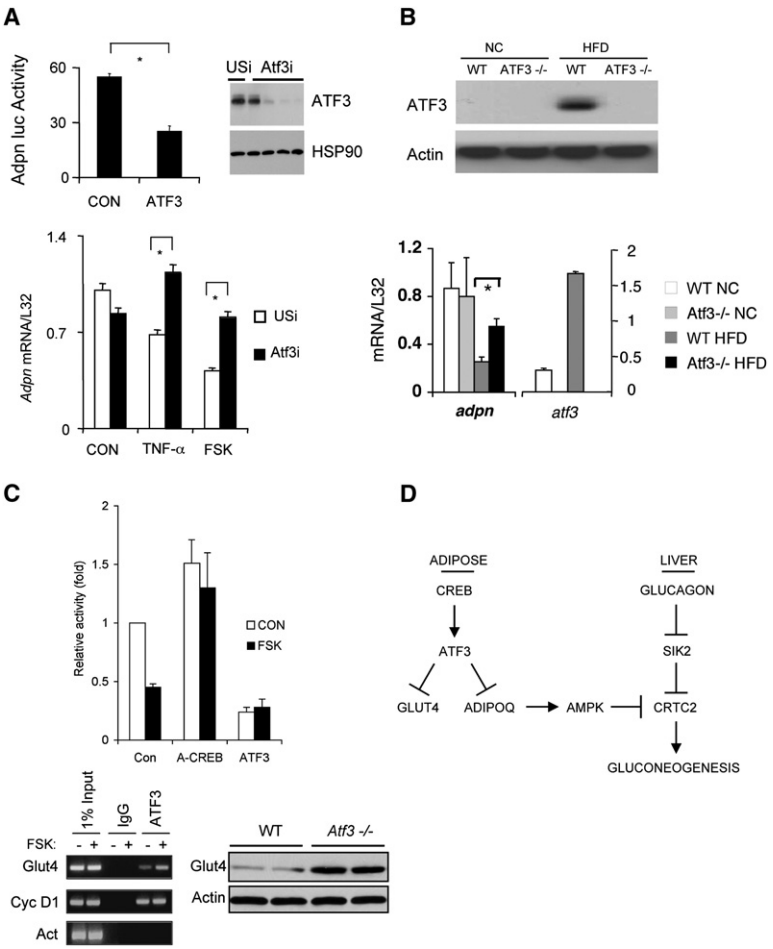

Figure 6. ATF3 Mediates Inhibitory Effects of CREB on GLUT4 and Adiponectin Gene Expression in Adipose under Obese Conditions

(A) Top left, transient assay showing adiponectin-luciferase reporter activity in control and ATF3 overexpressing HEK293T cells. At the top right, an immunoblot shows the effect of adenovirally encoded ATF3 RNAi or control (USi) RNAi on amounts of ATF3 protein in primary adipocytes. Bottom shows Q-PCR analysis of adiponectin mRNA amounts in primary adipocytes infected with adenovirally encoded unspecific (USi) or ATF3 RNAi. Cells exposed to TNF-α or FSK for 24 hr are indicated.

(B) Top, immunoblot of ATF3 protein amounts in WAT from WT and *Atf3*$^{-/-}$ mice under NC and HFD conditions. Bottom shows Q-PCR analysis of adiponectin and ATF3 mRNA amounts in WAT from *Atf3*$^{-/-}$ and control littermates maintained on NC or HFD.

(C) Top, transient assay of HEK293T cells showing effect of A-CREB or ATF3 overexpression on GLUT4-luciferase reporter activity in HEK293T cells under basal conditions and following exposure to FSK for 4 hr. at bottom left, a ChIP assay shows recovery of GLUT4 promoter from immunoprecipitates of ATF3 or nonspecific IgG prepared from HEK293T cells following exposure to FSK as indicated. Recovery of positive control (cyclin D1) or negative control (actin) promoters in immunoprecipitates of ATF3 is included for comparison. At bottom right, GLUT4 protein amounts in white adipose from *Atf3*$^{-/-}$ and WT littermates are shown.

(D) Adipocyte CREB promotes insulin resistance in obesity. Under lean conditions, increases in circulating adiponectin reduce hepatic glucose output during fasting by triggering the AMPK-mediated phosphorylation of the CREB coactivator CRTC2 in hepatocytes. Adipocyte CREB is activated in obesity, where it promotes insulin resistance via the ATF3-mediated inhibition of adiponectin and GLUT4 gene expression.

stimulating the expression of PPARγ in adipose (Park et al., 2008). Indeed, adipocyte *Id2* gene expression is increased in obesity, while mice with a knockout of *Id2* gene have reduced adipose stores at birth. Based on the presence of conserved CREB binding sites in the *Id2* gene and the ability for cAMP to stimulate *Id2* gene expression, CREB may modulate the lipogenic program in adipocytes through upregulation of this transcription factor.

Taken together, these results show that targeting therapies to adipose tissue and, in particular, to the CREB signaling system could have important therapeutic benefits in a variety of insulin-resistant states. Further analysis of other adipocyte genes that are modulated by CREB under obese conditions should provide greater insight into this process.

EXPERIMENTAL PROCEDURES

Mice

A 5.6 kb fragment of the aP2 promoter and a 256 bp fragment encoding FLAG-ACREB were subcloned into the pWhere vector containing two H19 chromatin insulators (InvivoGen). F-ACREB transgenic mice were generated on the B6 and CB6 backgrounds. Mice were genotyped using the following primer sets for ACREB transgene: F tg, GTCCAGTGATCATTGCCAGG; F WT, TGCTGCCGCATCAGGCAAT; and R, AGCACTGCCACTCTGTTCTC (WT = 230 bp, tg = 380 bp). Ob/+ mice were purchased from Jackson Laboratory and bred in the Salk transgenic facility. Transgenic mice were crossed to ob/+ mice to obtain tg-ob/+ mice and WT-ob/+ mice. This intercross generated tg; *ob/ob* (tg-ob) and WT; *ob/ob* (WT-ob) mice. For HFD studies, 8-week-old male mice were fed on 60% HFD for 12–24 weeks. ATF3$^{-/-}$ mice (Hartman et al., 2004) were maintained on 45% HFD or 12% NC diet for 12 weeks.

Cells and Reagents

HEK293T cells were maintained in DMEM supplemented with 10% FBS. Adenoviruses encoding TORC2, GFP, Adiponectin, ATF3, ACREB, and ATF3i were generated using the Ad-Track-pAdEasy system (Herzig et al., 2001). Target sequence for ATF3 RNAi is AAGGAACATTGCAGAGCTAAG (nt 527–546). pGL3-Adiponectin-luc (Iwaki et al., 2003) contains 1 kb of the human adiponectin promoter fused to luciferase cDNA. TNF-α (Calbiochem) and FSK (Sigma) were used at 10 ng/ml (in PBS) and 10 μM (in DMSO), respectively. Antibodies include adiponectin (Sigma; 1:8000), Atf3 (Santa Cruz; 1:500), HSP90 (Santa Cruz; 1:5000), p-AMPK and AMPK, p-ACC and ACC, and p-AKT and AKT (Cell Signaling) at 1:1000.

Adiponectin protein was collected in serum-free medium from primary hepatocytes transduced with Ad-adiponectin virus. Multimeric forms of this hormone were confirmed by SDS-PAGE under reducing and nonreducing conditions (Pajvani et al., 2004). Adiponectin protein concentrations were determined by ELISA assay (Linco Research, Inc.; St. Charles, MO).

Primary Hepatocyte Culture

Mouse hepatocytes were harvested, cultured, and infected with adenoviruses as previously described (Dentin et al., 2004). For reporter studies, Ad-CRE luc-infected primary hepatocytes were exposed to FSK for 5 hr, followed by exposure to control medium or insulin for 3 hr. Luciferase activity was normalized to β-gal activity from coinfected Ad-RSV β-gal vector. For glucose output

studies, cells were exposed for 5 hr to FSK, followed by 1 hr INS or control (G5 medium); glucose output was then collected for 1 hr in control medium supplemented with 10 mM lactate and 1 mM pyruvate. For studies with adiponectin protein, active multimeric forms of adiponectin were confirmed by SDS-PAGE analysis under nonreducing conditions.

Primary Adipocyte Culture and Glucose Uptake

Adipocytes were isolated from mouse visceral adipose tissue as described (Karnieli et al., 1981), with the following modifications. Adipose tissue was incubated for 30–45 min with Type I Collagenase (Invitrogen) in Ringer Bicarbonate-HEPES (KRBH) buffer (10 mM bicarbonate, 30 mM HEPES, 200 nM adenosine, 2.5 mM glucose 1% fatty-acid-free BSA [pH 7.4]) at 37°C. The digestion mixture was filtered through a nylon strainer and centrifuged at 400 × *g*. Adipocytes in the supernatant were resuspended in glucose-free KRBH. Glucose uptake was measured using [^{3}H]2-deoxyglucose. Cells were pretreated with insulin for 20 min and incubated at 37°C with 100 nM-labeled deoxyglucose (4 μCi/ml) for 5 min. Labeled cells were collected after centrifugation at 10,000 × *g* for 10 s. Cells were counted directly by scintillation. Cell aliquots were used to determine protein content and cell number for normalization.

Euglycemic-Hyperinsulinemic Clamps

Mice were anesthetized with 100 mg/kg ketamine and 10 mg/kg xylazine. Clamp studies on catheterized mice were performed as described (Hevener et al., 2003). HPLC-purified [3-^{3}H]glucose (0.05 μCi/min, New England Nuclear) was infused for 2 hr (basal infusion period) into 6 hr-fasted mice using microdialysis pumps, and blood samples were collected from the tail vein. Following the basal infusion period, a 120 min euglycemic-hyperinsulinemic clamp period was initiated with a continuous infusion of human insulin (Humulin R) at 12.5 mU/kg/min. Blood samples were collected at 10 min intervals for the measurement of plasma glucose concentrations. A 50% glucose solution was infused at variable rates to maintain euglycemia during the clamp. Plasma was deproteinized with $ZnSO_4$ and $Ba(OH)_2$, dried to remove ^3H_2O, resuspended in H_2O, and counted in scintillation fluid for detection of ^3H.

RNA Analysis

RNA extractions were carried out using TRIzol followed by purification over a QIAEASY RNA column. Reverse transcribed- and quantitative-PCR were carried out as described. The primer sets for *atf3*: AAGACAGAGTGCCTGCA GAA and GTGCCACCTCTGCTTAGCTC (232 bp); for *nr4a2*: CGCCGAAATC GTTGTCAGTA and CGACCTCTCCGGCCTTTTA (101 bp); for *adpn*: AAG GACAAGGCCGTTCTCTT and GAAAGCCAGTAAATGTAGAG (180 bp); for *pgc1a*: CAAGTCTAACTATGCAGACC and ACTTGCTCTTGGTGGAAGCA (67 bp); for *ucp2*: GATGGCTTGGCAGTCAAGAA and GAACTCCTGGAACTCGAG TTA (110 bp); for *l32*: TCTGGTGAAGCCCAAGATCG and CTCTGGGTTTCCG CCAGTT (100 bp).

Blood Metabolites

Glucose, FFA, TG, and ketones were measured using OneTouch Ultra Glucometer, NEFAC (Wako Chemicals USA, 99475409), and Serum TG Determination Kit (Sigma, TR0100), respectively. Insulin, glucagon, adiponectin, and resistin were measured using kits from ALPCO (10115001 and 48-GLUCA-90) and Linco Research, Inc. (EZMADP-60K and CYT292), respectively.

Chromatin Immunoprecipitation

ChIP in 293T cells and tissues was carried out as described (Koo et al., 2005). Lysates were immunoprecipitated with antibodies to CREB (244) as well as ATF3. Primers are as follows for *atf3*: CCGAACTTGCATCACCAGT and CGTTGCATCACCCCTTTTAT, which produce a 198 bp band following amplification. Controls used in this experiment: positive control (*fdps*), GTAAGA CAGGCAGCCAAAGC and CCACACTAAGGGCGGAAATA (267 bp); negative control (*actin*), TGCTATCCCTGTACGCCTCT and CTCCTTAATGTCACG CACGA (227 bp). Annealing temperature Tm = 56°C.

Microarray

Total RNA samples were amplified, labeled, and hybridized to Affymetrix Mouse Genome 430A 2.0 Arrays (Affymetrix; Santa Clara, CA) using standard protocols. Scanned images were analyzed by using DChIP software. Lower bounds of the 90% confidence intervals of fold changes (LFC) were used to identify cAMP-inducible genes. CRE site assignments have been described (Zhang et al., 2005b) and appear on the website http://natural.salk.edu/CREB. Microarray data have been deposited and can be accessed at NCBI GEO (accession number: GSE14363).

Metabolism

Liver glycogen and ketones were determined as described (Qi et al., 2006). Body temperature, food intake, metabolic cages, and histology were carried out as reported (Qi et al., 2006). Effects of insulin on AKT phosphorylation in muscle and liver were determined following administration of insulin i.p. at 0.75 U/kg body weight. Tissues were harvested 15 min after injection.

Statistical Analysis

Results are expressed as mean ± SEM. Comparisons between groups were made by unpaired two-tailed Student's t test. $p < 0.05$ was considered statistically significant. All experiments were conducted on at least two independent occasions.

SUPPLEMENTAL DATA

Supplemental Data include 11 figures and can be found online at http://www.cell.com/cellmetabolism/supplemental/S1550-4131(09)00007-2.

ACKNOWLEDGMENTS

We thank Ichi Shimomura for adiponectin-luciferase constructs and Anh-Khoi for technical assistance. M.M. is supported by NIH grant DK-049777, by the Foundation for Medical Research, and by the Kieckhefer Foundation. This work was supported by a University of California Discovery Biostar Grant and by NIH grants DK033651 (to J.M.O.) and DK074868 (to C.K.G. and J.M.O.). L.Q. is supported by a JDRF fellowship.

Received: July 7, 2008
Revised: October 20, 2008
Accepted: January 14, 2009
Published: March 3, 2009

REFERENCES

Ahn, S., Olive, M., Aggarwal, S., Krylov, D., Ginty, D., and Vinson, C. (1998). A dominant-negative inhibitor of CREB reveals that it is a general mediator stimulus-dependent transcription of c-fos. Mol. Cell. Biol. *18*, 967–977.

Berg, A.H., Combs, T.P., Du, X., Brownlee, M., and Scherer, P.E. (2001). The adipocyte-secreted protein Acrp30 enhances hepatic insulin action. Nat. Med. *7*, 947–953.

Berger, J., Biswas, C., Vicario, P.P., Strout, H.V., Saperstein, R., and Pilch, P.F. (1989). Decreased expression of the insulin-responsive glucose transporter in diabetes and fasting. Nature *340*, 70–72.

Bleckmann, S.C., Blendy, J.A., Rudolph, D., Monaghan, A.P., Schmid, W., and Schutz, G. (2002). Activating transcription factor 1 and CREB are important for cell survival during early mouse development. Mol. Cell. Biol. *22*, 1919–1925.

Blendy, J., Kaestner, K., Weinbauer, G., Nieschlag, E., and Schutz, G. (1996). Severe impairment of spermatogenesis in mice lacking the CREM gene. Nature *380*, 162–165.

Cao, H., Gerhold, K., Mayers, J.R., Wiest, M.M., Watkins, S.M., and Hotamisligil, G.S. (2008). Identification of a lipokine, a lipid hormone linking adipose tissue to systemic metabolism. Cell *134*, 933–944.

Carvalho, E., Kotani, K., Peroni, O.D., and Kahn, B.B. (2005). Adipose-specific overexpression of GLUT4 reverses insulin resistance and diabetes in mice lacking GLUT4 selectively in muscle. Am. J. Physiol. Endocrinol. Metab. *289*, E551–E561.

Chen, B.P., Liang, G., Whelan, J., and Hai, T. (1994). ATF3 and ATF3 delta Zip. Transcriptional repression versus activation by alternatively spliced isoforms. J. Biol. Chem. *269*, 15819–15826.

Chrivia, J.C., Kwok, R.P., Lamb, N., Hagiwara, M., Montminy, M.R., and Goodman, R.H. (1993). Phosphorylated CREB binds specifically to the nuclear protein CBP. Nature *365*, 855–859.

Combs, T.P., Berg, A.H., Obici, S., Scherer, P.E., and Rossetti, L. (2001). Endogenous glucose production is inhibited by the adipose-derived protein Acrp30. J. Clin. Invest. *108*, 1875–1881.

de Luca, C., and Olefsky, J.M. (2008). Inflammation and insulin resistance. FEBS Lett. *582*, 97–105.

Delporte, M.L., Funahashi, T., Takahashi, M., Matsuzawa, Y., and Brichard, S.M. (2002). Pre- and post-translational negative effect of beta-adrenoceptor agonists on adiponectin secretion: in vitro and in vivo studies. Biochem. J. *367*, 677–685.

Dentin, R., Pegorier, J.P., Benhamed, F., Foufelle, F., Ferre, P., Fauveau, V., Magnuson, M.A., Girard, J., and Postic, C. (2004). Hepatic glucokinase is required for the synergistic action of ChREBP and SREBP-1c on glycolytic and lipogenic gene expression. J. Biol. Chem. *279*, 20314–20326.

Dentin, R., Liu, Y., Koo, S.H., Hedrick, S., Vargas, T., Heredia, J., Yates, J., III, and Montminy, M. (2007). Insulin modulates gluconeogenesis by inhibition of the coactivator TORC2. Nature *449*, 366–369.

Dentin, R., Hedrick, S., Xie, J., Yates, J., III, and Montminy, M. (2008). Hepatic glucose sensing via the CREB coactivator CRTC2. Science *319*, 1402–1405.

Foretz, M., Carling, D., Guichard, C., Ferre, P., and Foufelle, F. (1998). AMP-activated protein kinase inhibits the glucose-activated expression of fatty acid synthase gene in rat hepatocytes. J. Biol. Chem. *273*, 14767–14771.

Fu, L., Isobe, K., Zeng, Q., Suzukawa, K., Takekoshi, K., and Kawakami, Y. (2007). Beta-adrenoceptor agonists downregulate adiponectin, but upregulate adiponectin receptor 2 and tumor necrosis factor-alpha expression in adipocytes. Eur. J. Pharmacol. *569*, 155–162.

Garvey, W.T., Huecksteadt, T.P., and Birnbaum, M.J. (1989). Pretranslational suppression of an insulin-responsive glucose transporter in rats with diabetes mellitus. Science *245*, 60–63.

Hartman, M.G., Lu, D., Kim, M.L., Kociba, G.J., Shukri, T., Buteau, J., Wang, X., Frankel, W.L., Guttridge, D., Prentki, M., et al. (2004). Role for activating transcription factor 3 in stress-induced beta-cell apoptosis. Mol. Cell. Biol. *24*, 5721–5732.

Herzig, S., Long, F., Jhala, U., Hedrick, S., Quinn, R., Bauer, A., Schutz, G., Yoon, C., Puisgever, P., Spiegelman, B., and Montminy, M. (2001). CREB regulates hepatic gluconeogenesis via the co-activator PGC-1. Nature *413*, 179–183.

Hevener, A.L., He, W., Barak, Y., Le, J., Bandyopadhyay, G., Olson, P., Wilkes, J., Evans, R.M., and Olefsky, J. (2003). Muscle-specific Pparγ deletion causes insulin resistance. Nat. Med. *9*, 1491–1497.

Hummler, E., Cole, T.J., Blendy, J.A., Ganss, R., Aguzzi, A., Schmid, W., Beermann, F., and Schutz, G. (1994). Targeted mutation of the CREB gene: compensation within the CREB/ATF family of transcription factors. Proc. Natl. Acad. Sci. USA *91*, 5647–5651.

Hupfeld, C.J., Dalle, S., and Olefsky, J.M. (2003). Beta-Arrestin 1 down-regulation after insulin treatment is associated with supersensitization of beta 2 adrenergic receptor Galpha s signaling in 3T3-L1 adipocytes. Proc. Natl. Acad. Sci. USA *100*, 161–166.

Iwaki, M., Matsuda, M., Maeda, N., Funahashi, T., Matsuzawa, Y., Makishima, M., and Shimomura, I. (2003). Induction of adiponectin, a fat-derived antidiabetic and antiatherogenic factor, by nuclear receptors. Diabetes *52*, 1655–1663.

Joost, H.G., Weber, T.M., Cushman, S.W., and Simpson, I.A. (1986). Insulin-stimulated glucose transport in rat adipose cells. Modulation of transporter intrinsic activity by isoproterenol and adenosine. J. Biol. Chem. *261*, 10033–10036.

Joost, H.G., Habberfield, A.D., Simpson, I.A., Laurenza, A., and Seamon, K.B. (1988). Activation of adenylate cyclase and inhibition of glucose transport in rat adipocytes by forskolin analogues: structural determinants for distinct sites of action. Mol. Pharmacol. *33*, 449–453.

Kadowaki, T., Yamauchi, T., Kubota, N., Hara, K., Ueki, K., and Tobe, K. (2006). Adiponectin and adiponectin receptors in insulin resistance, diabetes, and the metabolic syndrome. J. Clin. Invest. *116*, 1784–1792.

Kahn, B.B., Cushman, S.W., and Flier, J.S. (1989). Regulation of glucose transporter-specific mRNA levels in rat adipose cells with fasting and refeeding. Implications for in vivo control of glucose transporter number. J. Clin. Invest. *83*, 199–204.

Karnieli, E., Zarnowski, M.J., Hissin, P.J., Simpson, I.A., Salans, L.B., and Cushman, S.W. (1981). Insulin-stimulated translocation of glucose transport systems in the isolated rat adipose cell. Time course, reversal, insulin concentration dependency, and relationship to glucose transport activity. J. Biol. Chem. *256*, 4772–4777.

Kim, H.B., Kong, M., Kim, T.M., Suh, Y.H., Kim, W.H., Lim, J.H., Song, J.H., and Jung, M.H. (2006). NFATc4 and ATF3 negatively regulate adiponectin gene expression in 3T3-L1 adipocytes. Diabetes *55*, 1342–1352.

Kim, J.Y., van de Wall, E., Laplante, M., Azzara, A., Trujillo, M.E., Hofmann, S.M., Schraw, T., Durand, J.L., Li, H., Li, G., et al. (2007). Obesity-associated improvements in metabolic profile through expansion of adipose tissue. J. Clin. Invest. *117*, 2621–2637.

Koh, E.H., Park, J.Y., Park, H.S., Jeon, M.J., Ryu, J.W., Kim, M., Kim, S.Y., Kim, M.S., Kim, S.W., Park, I.S., et al. (2007). Essential role of mitochondrial function in adiponectin synthesis in adipocytes. Diabetes *56*, 2973–2981.

Koo, S.H., Flechner, L., Qi, L., Zhang, X., Screaton, R.A., Jeffries, S., Hedrick, S., Xu, W., Boussouar, F., Brindle, P., et al. (2005). The CREB coactivator TORC2 is a key regulator of fasting glucose metabolism. Nature *437*, 1109–1111.

Kubota, N., Terauchi, Y., Yamauchi, T., Kubota, T., Moroi, M., Matsui, J., Eto, K., Yamashita, T., Kamon, J., Satoh, H., et al. (2002). Disruption of adiponectin causes insulin resistance and neointimal formation. J. Biol. Chem. *277*, 25863–25866.

Laakso, M., Edelman, S.V., Brechtel, G., and Baron, A.D. (1992). Effects of epinephrine on insulin-mediated glucose uptake in whole body and leg muscle in humans: role of blood flow. Am. J. Physiol. *263*, E199–E204.

Liang, G., Wolfgang, C.D., Chen, B.P., Chen, T.H., and Hai, T. (1996). ATF3 gene. Genomic organization, promoter, and regulation. J. Biol. Chem. *271*, 1695–1701.

Lochhead, P.A., Salt, I.P., Walker, K.S., Hardie, D.G., and Sutherland, C. (2000). 5-aminoimidazole-4-carboxamide riboside mimics the effects of insulin on the expression of the 2 key gluconeogenic genes PEPCK and glucose-6-phosphatase. Diabetes *49*, 896–903.

Lumeng, C.N., Deyoung, S.M., Bodzin, J.L., and Saltiel, A.R. (2007). Increased inflammatory properties of adipose tissue macrophages recruited during diet-induced obesity. Diabetes *56*, 16–23.

Maeda, N., Shimomura, I., Kishida, K., Nishizawa, H., Matsuda, M., Nagaretani, H., Furuyama, N., Kondo, H., Takahashi, M., Arita, Y., et al. (2002). Diet-induced insulin resistance in mice lacking adiponectin/ACRP30. Nat. Med. *8*, 731–737.

Mayr, B., and Montminy, M. (2001). Tanscriptional regulation by the phosphorylation dependent factor CREB. Nat. Rev. Mol. Cell Biol. *2*, 599–609.

Nawrocki, A.R., Rajala, M.W., Tomas, E., Pajvani, U.B., Saha, A.K., Trumbauer, M.E., Pang, Z., Chen, A.S., Ruderman, N.B., Chen, H., et al. (2006). Mice lacking adiponectin show decreased hepatic insulin sensitivity and reduced responsiveness to peroxisome proliferator-activated receptor gamma agonists. J. Biol. Chem. *281*, 2654–2660.

Pajvani, U.B., Hawkins, M., Combs, T.P., Rajala, M.W., Doebber, T., Berger, J.P., Wagner, J.A., Wu, M., Knopps, A., Xiang, A.H., et al. (2004). Complex distribution, not absolute amount of adiponectin, correlates with thiazolidinedione-mediated improvement in insulin sensitivity. J. Biol. Chem. *279*, 12152–12162.

Park, K.W., Waki, H., Villanueva, C.J., Monticelli, L.A., Hong, C., Kang, S., MacDougald, O.A., Goldrath, A.W., and Tontonoz, P. (2008). Inhibitor of DNA binding 2 is a small molecule-inducible modulator of peroxisome proliferator-activated receptor-gamma expression and adipocyte differentiation. Mol. Endocrinol. *22*, 2038–2048.

Qi, L., Heredia, J.E., Altarejos, J.Y., Screaton, R., Goebel, N., Niessen, S., Macleod, I.X., Liew, C.W., Kulkarni, R.N., Bain, J., et al. (2006). TRB3 links the E3 ubiquitin ligase COP1 to lipid metabolism. Science *312*, 1763–1766.

Ravnskjaer, K., Kester, H., Liu, Y., Zhang, X., Lee, D., Yates, J.R., III, and Montminy, M. (2007). Cooperative interactions between CBP and TORC2 confer selectivity to CREB target gene expression. EMBO J. *26*, 2880–2889.

Ricci, M.R., Lee, M.J., Russell, C.D., Wang, Y., Sullivan, S., Schneider, S.H., Brolin, R.E., and Fried, S.K. (2005). Isoproterenol decreases leptin release from rat and human adipose tissue through posttranscriptional mechanisms. Am. J. Physiol. Endocrinol. Metab. *288*, E798–E804.

Ruderman, N.B., Saha, A.K., and Kraegen, E.W. (2003). Minireview: malonyl CoA, AMP-activated protein kinase, and adiposity. Endocrinology *144*, 5166–5171.

Sabio, G., Das, M., Mora, A., Zhang, Z., Jun, J.Y., Ko, H.J., Barrett, T., Kim, J.K., and Davis, R.J. (2008). A stress signaling pathway in adipose tissue regulates hepatic insulin resistance. Science *322*, 1539–1543.

Satoh, H., Nguyen, M.T., Miles, P.D., Imamura, T., Usui, I., and Olefsky, J.M. (2004). Adenovirus-mediated chronic "hyper-resistinemia" leads to in vivo insulin resistance in normal rats. J. Clin. Invest. *114*, 224–231.

Satoh, H., Nguyen, M.T., Trujillo, M., Imamura, T., Usui, I., Scherer, P.E., and Olefsky, J.M. (2005). Adenovirus-mediated adiponectin expression augments skeletal muscle insulin sensitivity in male Wistar rats. Diabetes *54*, 1304–1313.

Scriba, D., Aprath-Husmann, I., Blum, W.F., and Hauner, H. (2000). Catecholamines suppress leptin release from in vitro differentiated subcutaneous human adipocytes in primary culture via beta1- and beta2-adrenergic receptors. Eur. J. Endocrinol. *143*, 439–445.

Shaw, R.J., Lamia, K.A., Vasquez, D., Koo, S.H., Bardeesy, N., Depinho, R.A., Montminy, M., and Cantley, L.C. (2005). The kinase LKB1 mediates glucose homeostasis in liver and therapeutic effects of metformin. Science *310*, 1642–1646.

Shaywitz, A.J., and Greenberg, M.E. (1999). CREB: a stimulus-induced transcription factor activated by a diverse array of extracellular signals. Annu. Rev. Biochem. *68*, 821–861.

Sivitz, W.I., DeSautel, S.L., Kayano, T., Bell, G.I., and Pessin, J.E. (1989). Regulation of glucose transporter messenger RNA in insulin-deficient states. Nature *340*, 72–74.

Tseng, Y.H., Butte, A.J., Kokkotou, E., Yechoor, V.K., Taniguchi, C.M., Kriauciunas, K.M., Cypess, A.M., Niinobe, M., Yoshikawa, K., Patti, M.E., and Kahn, C.R. (2005). Prediction of preadipocyte differentiation by gene expression reveals role of insulin receptor substrates and necdin. Nat. Cell Biol. *7*, 601–611.

Weisberg, S.P., McCann, D., Desai, M., Rosenbaum, M., Leibel, R.L., and Ferrante, A.W., Jr. (2003). Obesity is associated with macrophage accumulation in adipose tissue. J. Clin. Invest. *112*, 1796–1808.

Xu, H., Barnes, G.T., Yang, Q., Tan, G., Yang, D., Chou, C.J., Sole, J., Nichols, A., Ross, J.S., Tartaglia, L.A., and Chen, H. (2003). Chronic inflammation in fat plays a crucial role in the development of obesity-related insulin resistance. J. Clin. Invest. *112*, 1821–1830.

Xu, W., Kasper, L.H., Lerach, S., Jeevan, T., and Brindle, P.K. (2007). Individual CREB-target genes dictate usage of distinct cAMP-responsive coactivation mechanisms. EMBO J. *26*, 2890–2903.

Yamauchi, T., Kamon, J., Minokoshi, Y., Ito, Y., Waki, H., Uchida, S., Yamashita, S., Noda, M., Kita, S., Ueki, K., et al. (2002a). Adiponectin stimulates glucose utilization and fatty-acid oxidation by activating AMP-activated protein kinase. Nat. Med. *8*, 1288–1295.

Yamauchi, T., Oike, Y., Kamon, J., Waki, H., Komeda, K., Tsuchida, A., Date, Y., Li, M.X., Miki, H., Akanuma, Y., et al. (2002b). Increased insulin sensitivity despite lipodystrophy in Crebbp heterozygous mice. Nat. Genet. *30*, 221–226.

Zhang, J., Hupfeld, C.J., Taylor, S.S., Olefsky, J.M., and Tsien, R.Y. (2005a). Insulin disrupts beta-adrenergic signalling to protein kinase A in adipocytes. Nature *437*, 569–573.

Zhang, J.W., Klemm, D.J., Vinson, C., and Lane, M.D. (2004). Role of CREB in transcriptional regulation of CCAAT/enhancer-binding protein beta gene during adipogenesis. J. Biol. Chem. *279*, 4471–4478.

Zhang, X., Odom, D.T., Koo, S.H., Conkright, M.D., Canettieri, G., Best, J., Chen, H., Jenner, R., Herbolsheimer, E., Jacobsen, E., et al. (2005b). Genome-wide analysis of cAMP-response element binding protein occupancy, phosphorylation, and target gene activation in human tissues. Proc. Natl. Acad. Sci. USA *102*, 4459–4464.

Cell Metabolism
Article

Pref-1 Regulates Mesenchymal Cell Commitment and Differentiation through Sox9

Yuhui Wang[1] and Hei Sook Sul[1,*]
[1]Department of Nutritional Science and Toxicology, University of California, Berkeley, Berkeley, CA 94720, USA
*Correspondence: hsul@nature.berkeley.edu
DOI 10.1016/j.cmet.2009.01.013

SUMMARY

Pref-1 is an EGF repeat-containing transmembrane protein that produces a biologically active soluble form by TACE-mediated cleavage. Although Pref-1 inhibition of adipogenesis has been well established, the specific target(s) of Pref-1 or the Pref-1 function in mesenchymal cell commitment/differentiation are not known. Here, we show that Sox9 downregulation is required for adipocyte differentiation and that Pref-1 inhibits adipocyte differentiation through upregulating Sox9 expression. Sox9 directly binds to the promoter regions of C/EBPβ and C/EBPδ to suppress their promoter activity, preventing adipocyte differentiation. Furthermore, we also show that, by inducing Sox9, Pref-1 promotes chondrogenic induction of mesenchymal cells but prevents chondrocyte maturation as well as osteoblast differentiation, with supporting in vivo evidence in Pref-1 null and Pref-1 transgenic mice. Thus, Sox9 is a Pref-1 target, and Pref-1 directs multipotent mesenchymal cells to the chondrogenic lineage but inhibits differentiation into adipocytes as well as osteoblasts and chondrocytes.

INTRODUCTION

Preadipocyte factor 1 (Pref-1) was originally cloned by us as a preadipocyte transmembrane protein that inhibits adipogenesis (Smas and Sul, 1993). The full-length form of Pref-1 (Pref-1A) is a protein of 385 amino acids. Pref-1 contains an extracellular domain with six EGF-like repeats, a juxtamembrane region, a single transmembrane domain, and a short cytoplasmic tail (Smas et al., 1994). The extracellular domain of Pref-1 is cleaved from Pref-1 by a disintegrin and metalloproteinase 17 (ADAM17, also named TNF-α converting enzyme [TACE]) to generate the biologically active soluble Pref-1 (Mei et al., 2002; Smas et al., 1997; Wang and Sul, 2006). Pref-1 mRNA and protein levels are high in 3T3-L1 preadipocytes, but Pref-1 expression decreases during adipocyte differentiation and is absent in mature adipocytes. Dexamethasone (DEX), a component of adipogenic agents routinely used for adipocyte differentiation, suppresses Pref-1 expression. Thus, Pref-1 is commonly used as a unique preadipocyte marker. Constitutive expression of Pref-1 inhibits adipocyte differentiation, and absence of Pref-1 accelerates/increases the degree of adipocyte differentiation in cultured cells (Smas et al., 1999; Smas and Sul, 1993). Although the direct target of Pref-1 is not known, Pref-1 activates ERK/MAPK to inhibit adipocyte differentiation (Kim et al., 2007). The function of Pref-1 in adipogenesis in vivo has been firmly established. Pref-1 null mice display enhanced adipose tissue formation with higher expression of adipocyte markers, showing increased circulating lipid levels, a characteristic usually associated with obesity (Moon et al., 2002). Conversely, overexpression of Pref-1 in adipose tissue decreases adipose tissue mass and impairs adipocyte differentiation (Lee et al., 2003). In adults, Pref-1 expression is restricted mainly to preadipocytes of adipose tissue, although Pref-1 is detected in some neuroendocrine cell types and was identified as a gene (dlk1) expressed in neuroblastoma cells (Laborda et al., 1993). During embryonic development, however, Pref-1 is widely expressed in multiple embryonic tissues, including liver, lung, and developing vertebra. Thus, the soluble form of Pref-1 has been purified from fetal circulation and named as fetal antigen 1 (FA1) (Bachmann et al., 1996). Pref-1 is coded by a paternally expressed imprinted gene, and a majority of imprinted genes code for proteins that regulate fetal growth and organogenesis (da Rocha and Ferguson-Smith, 2004). Although Pref-1 function in embryonic development has not been studied, we observed defects in bone development in both Pref-1 null and Pref-1 transgenic mice (Lee et al., 2003; Moon et al., 2002).

Multipotent mesenchymal cells can commit and differentiate into various cell types, including adipocytes, chondrocytes, and osteoblasts (Gesta et al., 2007). Adipogenesis occurs late in embryonic development and in postnatal periods. C/EBPα and PPARγ play critical roles in adipogenesis and induction of adipocyte markers, including adipocyte fatty acid-binding protein (aP2/FABP4) (Farmer, 2006; Gregoire et al., 1998; Rosen and MacDougald, 2006). Chondrogenesis and osteogenesis during skeletal development, however, occur in early embryonic stages. Chondrogenesis occurs from mesenchymal condensations, and osteogenesis of some bones occurs directly from mesenchymal condensations by intramembranous ossification. Most bones, however, are formed by endochondral ossification. Mesenchymal condensations first become immature chondrocytes that undergo maturation to become hypertrophic, when some of the surrounding mesenchymal cells invade the zone of hypertrophic chondrocytes to become osteoblasts. Sox9 is required for mesenchymal condensation and for initiation of early chondrogenesis to generate immature chondrocytes that express cartilaginous matrix proteins, such as type II and IX collagens (Col) and aggrecan (Akiyama et al., 2004; Bi et al., 2001). Thus, Sox9 is expressed in all chondro-osteoprogenitor cells and in mesenchymal condensations and promotes chondrogenic commitment. During chondrocyte hypertrophy and early osteogenesis, Runx2 is upregulated, and Col X and osteocalcin are

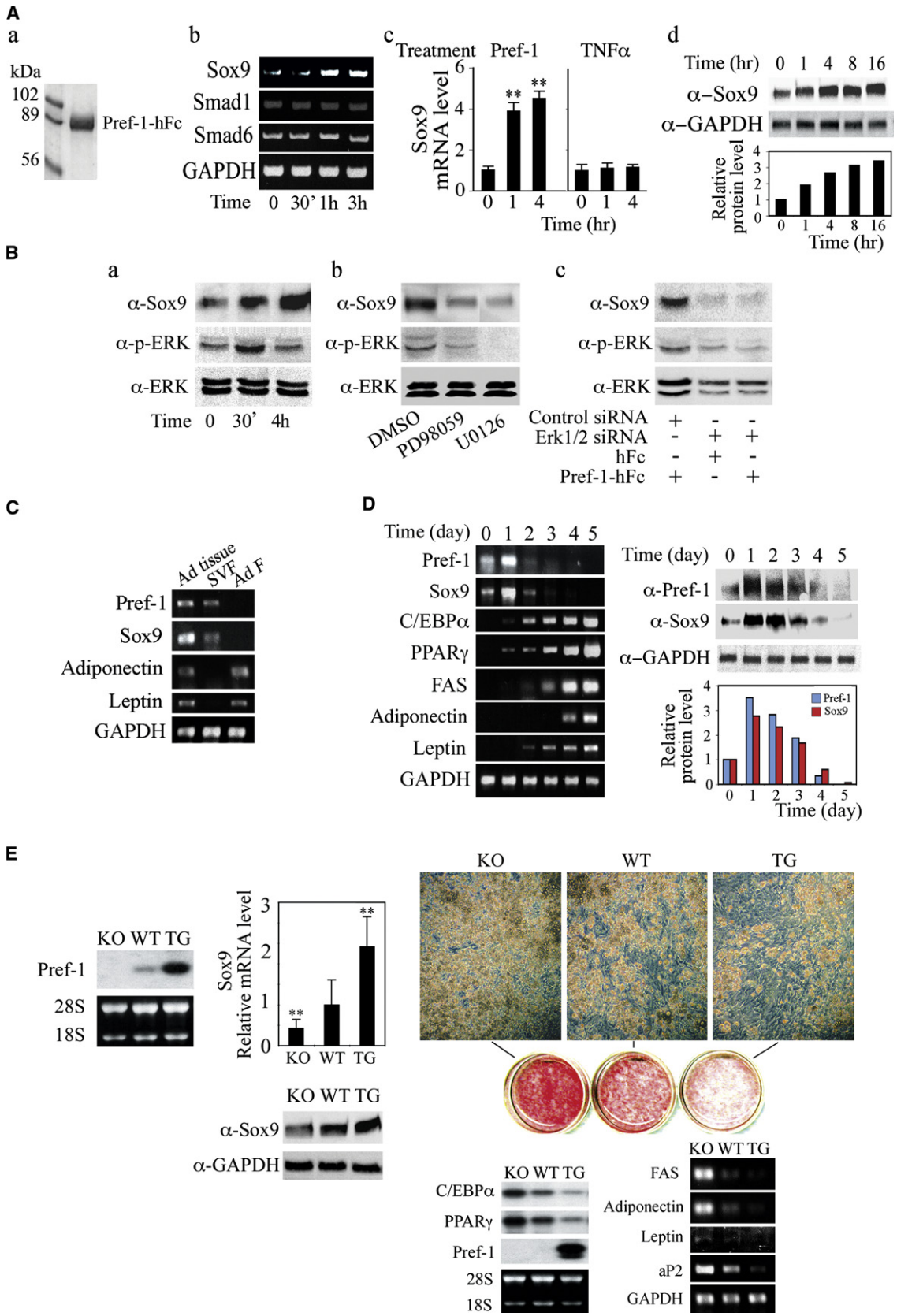
A
a
kDa
102
89
56
Pref-1-hFc
b
Sox9
Smad1
Smad6
GAPDH
Time 0 30' 1h 3h
c
Treatment Pref-1 TNFα
Sox9 mRNA level
Time (hr)
d
Time (hr) 0 1 4 8 16
α–Sox9
α–GAPDH
Relative protein level
B
a
α-Sox9
α-p-ERK
α-ERK
Time 0 30' 4h
b
DMSO PD98059 U0126
c
Control siRNA
Erk1/2 siRNA
hFc
Pref-1-hFc
C
Ad tissue SVF Ad F
Pref-1
Sox9
Adiponectin
Leptin
GAPDH
D
Time (day) 0 1 2 3 4 5
Pref-1
Sox9
C/EBPα
PPARγ
FAS
Adiponectin
Leptin
GAPDH
α-Pref-1
α-Sox9
α-GAPDH
Relative protein level
Time (day)
E
KO WT TG
Pref-1
28S
18S
Sox9 Relative mRNA level
α-Sox9
α-GAPDH
C/EBPα
PPARγ
FAS
Adiponectin
Leptin
aP2

induced (Takeda et al., 2001). However, Sox9 downregulation is a prerequisite for chondrocyte maturation and osteogenesis. Sox9, therefore, plays a critical role in skeletogenesis. Since Sox9 is found in chondro-osteoprogenitor cells and regulates skeletogenesis, it is possible that Sox9 may also affect differentiation of adipocytes that are derived from the common mesenchymal cells, but this possibility has not been examined before.

The present study was to elucidate the molecular target and effect on mesenchymal cell commitment/differentiation by Pref-1. Here, we show that Sox9 directly binds to C/EBPβ and C/EBPδ promoters to suppress their promoter activity, preventing adipocyte differentiation. Thus, constitutive Sox9 expression inhibits and Sox9 knockdown enhances adipocyte differentiation. More importantly, Pref-1 inhibition of adipose conversion is by preventing Sox9 downregulation. Furthermore, by inducing Sox9, Pref-1 promotes chondrogenic induction of mesenchymal cells to generate immature chondrocytes, but Pref-1 inhibits chondrocyte maturation as well as osteoblast differentiation. Overall, by inducing Sox9, Pref-1 promotes the chondrogenic commitment of mesenchymal cells but inhibits adipocyte, chondrocyte, and osteoblast differentiation.

RESULTS

Sox9 Downregulation Is Required for Adipocyte Differentiation, and Pref-1 Inhibition Is through Sox9 Regulation

During the search for Pref-1 targets by microarray analysis and other candidate approaches, we detected regulation of Sox9 expression by Pref-1. We found that treatment of Pref-1 null MEFs with Pref-1-hFc increased Sox9 expression rapidly by 4-fold within 1 hr, and this high level of expression was maintained for up to 4 hr (Figure 1A). A similar increase in Sox9 at the protein level is also detected. Pref-1 treatment increased Sox9 expression in multipotent mesenchymal C3H10T1/2 cells as well as in 3T3-L1 preadipocytes (data not shown). Expression of other factors with documented effects on embryonic development, such as Smad1 and Smad6 for TGFβ/BMP family, remained the same upon Pref-1 treatment. TNFα, a cytokine that can inhibit adipocyte differentiation, also was ineffective in upregulating Sox9, suggesting that upregulation of Sox9 is Pref-1 specific. We previously have shown that Pref-1 inhibition of adipocyte differentiation is through Pref-1-mediated ERK1/2 activation. Therefore, we examined whether ERK1/2 phosphorylation is required for Pref-1 induction of Sox9 (Figure 1B). As previously shown, Pref-1 treatment transiently increased ERK1/2 phosphorylation at 30 min of Pref-1 treatment in Pref-1 null MEFs but decreased to basal levels after 4 hr. In these cells, we detected an increase in Sox9 protein level 30 min after Pref-1 treatment, and the Sox9 level was further increased at 4 hr. Thus, ERK phosphorylation/activation by Pref-1 appears to precede Sox9 induction. When we treated these cells with MEK inhibitors PD98059 or U0126, we did not observe any increase in Sox9 levels upon Pref-1 treatment. Similarly, siRNA-mediated knockdown of ERK1/2 prevented the increase in Sox9 level by Pref-1 treatment. Overall, these results demonstrate that, by activating ERK1/2, Pref-1 induces Sox9 expression.

Expression of Sox9 was easily detected in adipose tissue (Figure 1C). However, unlike adipocyte markers such as adiponectin and leptin, Sox9 mRNA was not detected in adipocyte fraction but was found in stromal vascular fraction that contains preadipocytes as well as other cell types such as macrophages/endothelial cells. Interestingly, Sox9 mRNA levels were lower in adipose tissue from high-fat diet-induced as well as genetically obese *ob/ob* mice (Figure S2 available online). In this regard, mRNA levels of preadipocyte marker, Pref-1, were lower in adipose tissue from these obese mouse models, whereas mRNA levels of various adipocyte markers such as C/EBPα, PPARγ, and leptin were higher. We next examined Sox9 expression during MEF differentiation into adipocytes (Figure 1D). As expected, upon treatment with adipogenic agents DEX/MIX, there was a time-dependent increase in expression levels of adipogenic transcription factors, C/EBPα and PPARγ, as well as other adipocyte markers, including FAS, adiponectin, and leptin, as MEFs underwent adipocyte differentiation. As we have reported previously, unlike the decrease observed during 3T3-L1 adipocyte differentiation, during MEF differentiation, Pref-1 expression displayed a transient increase at day 1 but rapidly decreased and was not detectable at day 5 after conversion into adipocytes. Interestingly, we found that the Sox9 expression also was transiently increased and then decreased during MEF differentiation, closely following the Pref-1 expression. Protein levels of Sox9 and Pref-1 showed a similar pattern, although the decrease was slower than that observed for mRNA levels (Figure 1D, right panels). The difference in the time course of Pref-1 downregulation during adipocyte differentiation between MEFs and 3T3-L1 cells has been noticed previously (Kim et al., 2007; Smas et al., 1999). In this regard, unlike 3T3-L1 cells that are committed to adipocyte lineage, MEFs are multipotent mesenchymal cells, and Pref-1 levels may increase during commitment to adipocyte lineage when these cells are treated with adipogenic agents. Likewise, Sox9 expression may be transiently induced in this culture condition. Regardless, the parallel patterns of Pref-1 and Sox9 expression support a notion that Pref-1 regulates Sox9 expression, thereby inhibiting adipocyte differentiation.

Figure 1. Pref-1 Regulates Sox9 Expression

(A) Regulation of Sox9 expression by Pref-1. Coomassie staining of purified Pref-1-hFc (a). RT-PCR (b), RT-qPCR (c), and western blotting (d) in Pref-1 null MEFs treated with 50 nM Pref-1-hFc or 50 ng/ml TNFα. Results are mean ± SEM. $^{**}p < 0.01$ compared to that before treatment.

(B) Western blotting of cells with Pref-1-hFc treatment (a), ERK1/2 inhibitor (b), and ERK1/2 siRNA transfection (c).

(C) RT-PCR for adipose tissue (Ad tissue), stromal vascular fraction (SVF), and adipocyte fraction (Ad F).

(D) Pref-1 regulates Sox9 expression during adipocyte differentiation.

(E) Comparison of adipocyte differentiation of MEFs from Pref-1 null, wild-type, and aP2-Pref-1 transgenic embryos. Northern blot (left panel), RT-qPCR, and Western blot analysis (middle panels) in MEFs at confluence. The value for wild-type MEFs was defined as 1. Results are mean ± SEM. $^{**}p < 0.01$ compared to wild-type MEFs. Microscopic morphology, oil red O staining (right upper panels), and adipogenic transcription factors by northern blotting and late adipocyte markers by RT-PCR 8 days after induction of adipocyte differentiation (right lower panels).

We next compared Sox9 expression in MEFs from Pref-1 null, wild-type, and aP2-Pref-1 transgenic mice (Figure 1E). Correlating with Pref-1 expression, Sox9 mRNA and protein levels were 50% lower in Pref-1 null MEFs than in wild-type MEFs, whereas those in Pref-1 transgenic MEFs were ~2-fold higher than in wild-type MEFs. After treatment with adipogenic agents, 80% of Pref-1 null MEFs differentiated into adipocytes, whereas 50% of wild-type MEFs and 20% of Pref-1 transgenic MEFs differentiated as judged by the rounded adipocyte morphology. Oil red O staining for lipid accumulation displayed corresponding differences in the degree of adipocyte differentiation. Likewise, following differentiation, mRNA levels of C/EBPα and PPARγ in Pref-1 null MEFs were 2-fold higher than those in wild-type MEFs, and levels in Pref-1 transgenic MEFs were 65%–70% lower than in wild-type MEFs, reflecting the differences in adipocyte differentiation. As expected, Pref-1 expression was not detected in Pref-1 null MEFs and was completely suppressed in wild-type MEFs during adipocyte differentiation. On the other hand, Pref-1 transgenic MEFs showed a high level of Pref-1 expression due to inhibition of differentiation in addition to expression from the transgene. Overall, these results show that Pref-1 and Sox9 expression changes in a parallel fashion during differentiation and is inversely correlated with the degree of differentiation of MEFs into adipocytes.

We next employed soluble Pref-1-hFc in Pref-1 null MEFs to test whether inhibition of adipocyte differentiation by Pref-1 accompanies changes in Sox9 expression (Figure 2A). Pref-1-hFc caused a marked decrease in adipocyte differentiation as judged by Oil red O staining and expression of adipocyte markers, including adiponectin and leptin. In control hFc-treated cells, C/EBPα and PPARγ levels increased by 10- and 5-fold, respectively, whereas, in Pref-1-hFc treated cells, C/EBPα levels increased by only 1.8-fold, and PPARγ expression did not change. We found that Sox9 expression was drastically decreased by 90% during adipocyte differentiation in control hFc-treated cells, whereas, in Pref-1-hFc treated cells, Sox9 expression did not change and remained at levels seen prior to treatment with adipogenic agents. We also examined Pref-1 and Sox9 expression during differentiation of wild-type MEFs into adipocytes (Figure S3). Pref-1 and Sox9 mRNA levels increased ~3-fold at day 1 (after DEX/MIX treatment) and then decreased precipitously to very low levels upon differentiation. In cells treated with Pref-1-hFc, the expression levels also decreased but did so slowly and not below those in preadipocytes. Overall, these results show that, during Pref-1 inhibition of adipocyte differentiation of MEFs, Pref-1 prevents the decrease in Sox9 expression that normally occurs during adipose conversion.

Next, we tested the role of Sox9 in adipocyte differentiation of Pref-1 null MEFs by infecting Sox9 lentivirus. The high levels of Sox9 in nucleus after lentivirus infection were first verified (Figure 2B), and Sox9 expression driven by the CMV promoter would remain the same during differentiation. Upon treatment of Pref-1 null MEFs with adipogenic agents, more than 80% of cells infected with control empty lentivirus differentiated into adipocytes, whereas only 40% of cells infected with Sox9 lentivirus differentiated, as judged by morphology and expression of the adipocyte markers FAS, adiponectin, and leptin and adipogenic transcription factors. Thus, Sox9 lentivirus-infected cells had 70% lower C/EBPα and PPARγ levels compared to empty lentivirus-infected cells after adipose conversion (Figure 2C). We conclude that constitutive overexpression of Sox9 inhibits adipocyte differentiation. Furthermore, Sox9 lentivirus-infected cells treated with Pref-1-hFc showed a similar degree of adipocyte differentiation to that observed in cells infected with Sox9 lentivirus alone. This observation indicates that Pref-1 and Sox9 did not have additive effects on adipocyte differentiation, suggesting a common underlying mechanism for inhibition of adipocyte differentiation.

We next employed 3T3-L1 cells to test the role of Pref-1 and Sox9 in adipocyte differentiation. As expected, during 3T3-L1 differentiation, various adipocyte markers such as FAS, adiponectin, and leptin increased late during differentiation, whereas the increase in C/EBPα and PPARγ expression was detected somewhat earlier and continued to increase up to day 5 (Figure 3Aa). Expression of C/EBPβ and C/EBPδ increased even earlier, by 16- and 10-fold, respectively, 24 hr after the addition of adipogenic agents (Figure 3Ab). On the other hand, both Pref-1 and Sox9 expression decreased in parallel by 50% 12 hr after the addition of adipogenic agents and further decreased by 80%–90% by day 2 (Figure 3Ac). The decrease in Pref-1 at the protein level appears to precede that of Sox9 (Figure 3C, bottom panel). We have previously reported that, of the two adipogenic agents, DEX, but not MIX, suppresses Pref-1 expression. Similarly, we found that DEX, but not MIX, effectively decreased Sox9 mRNA levels by 70% after 12 hr of treatment (Figure 3Ad). We conclude that suppression of Pref-1 and Sox9 is an early event that precedes C/EBPα and PPARγ induction but better coincides and, in fact, precedes C/EBPβ/C/EBPδ induction.

We next tested whether Sox9 can inhibit 3T3-L1 adipocyte differentiation, as was the case for MEF differentiation into adipocytes. Both Pref-1 hFc treatment and constitutive overexpression of Pref-1 by 4-fold by Pref-1 lentivirus infection attenuated adipocyte differentiation as judged by cell morphology, oil red O staining, and expression of adipocyte markers FAS, adiponectin, leptin ADSF/resistin, and aP2, as well as the adipogenic transcription factors C/EBPα and PPARγ (Figure 3B). Conversely, knockdown of Sox9 by 80% at the protein level by Sox9 siRNA transfection resulted in enhanced adipocyte differentiation compared to the control cells as judged by adipocyte morphology, oil red O staining, and expression of adipocyte markers (Figure 3C). Furthermore, in Sox9 siRNA-transfected cells, Pref-1-hFc treatment could not bring about inhibition of differentiation as observed by the same degree of adipocyte differentiation as in Sox9 siRNA-transfected cells treated with control hFc. These data clearly show that Sox9 inhibits adipocyte differentiation and provide evidence that Pref-1 inhibition of adipocyte differentiation is through Sox9.

We previously demonstrated Pref-1 inhibition of adipogenesis in vivo by generating mice lacking Pref-1 as well as mice expressing soluble Pref-1 in adipose tissue. Sox9 ablation in mice causes embryonic lethality and thus could not be used to study adipogenesis that occurs mainly late after birth. In testing the Sox9 effect in vivo, we generated 3T3-F442A-GFP cells that either stably overexpress Sox9 by 6-fold or have knockdown of Sox9 by 65%. These cells were implanted subcutaneously into immunodeficient SCID mice. At 2 weeks after implantation, we determined lipid accumulation and adipocyte marker expression. As

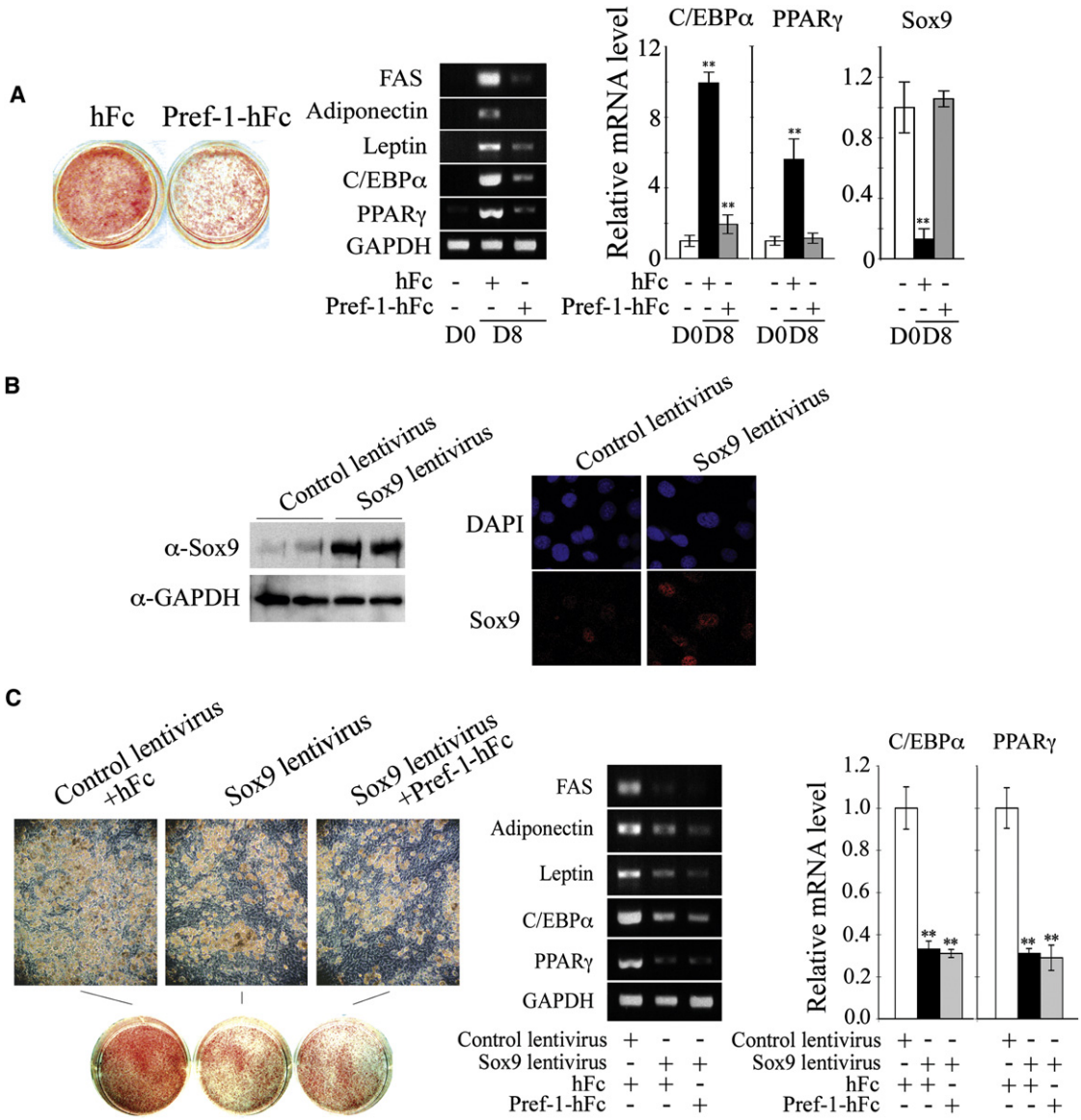

Figure 2. Forced Expression of Sox9 Prevents Pref-1 Inhibition of MEF Differentiation into Adipocytes

(A) Pref-1 null MEFs were subjected to adipocyte differentiation in the presence of Pref-1-hFc or control hFc for 8 days. Oil red O staining (left panel), RT-PCR (middle panel), and RT-qPCR (right panel). Results are mean ± SEM. **$p < 0.01$ compared to the cells in D0.

(B) Expression level of Sox9 was verified by western blotting (left panel) and by immunofluorescence 48 hr after infection (right panel).

(C) Pref-1 null MEFs overexpressing Sox9 by lentivirus infection were subjected to adipocyte differentiation in the presence of Pref-1-hFc or control hFc. Results are mean ± SEM. **$p < 0.01$ compared to differentiated cells infected with control lentivirus or in the presence of hFc.

shown in Figure 3D, control cells formed a substantial number of adipocytes. On the other hand, the adipocytes that arose from the implanted cells overexpressing Sox9 formed fewer adipocytes. They showed lower oil red O staining, higher expression of Pref-1, and lower expression of adipocyte markers such as PPARγ, adiponectin, and leptin. Conversely, implanted cells expressing Sox9 shRNA formed a higher number of adipocytes as detected by higher lipid staining and by lower expression of Pref-1, as well as higher expression of PPARγ, adiponectin, and leptin. These results clearly demonstrate the inhibitory role of Sox9 in adipogenesis in vivo.

Sox9 Binds C/EBPβ and C/EBPδ Promoters to Suppress Promoter Activity in Mediating Pref-1 Inhibition of Adipogenesis

Because the decrease in Pref-1 and Sox9 expression upon treatment with adipogenic agents precedes the early induction of C/EBPβ and C/EBPδ (Figure 3A), we hypothesized that Sox9 may regulate C/EBPβ and C/EBPδ expression to affect adipocyte differentiation. As shown in Figure 4A, overexpression of Sox9 did not affect C/EBPα and PPARγ mRNA levels but significantly suppressed C/EBPβ and C/EBPδ expression by 55% and 70%, respectively. Furthermore, cotransfection of Sox9 with

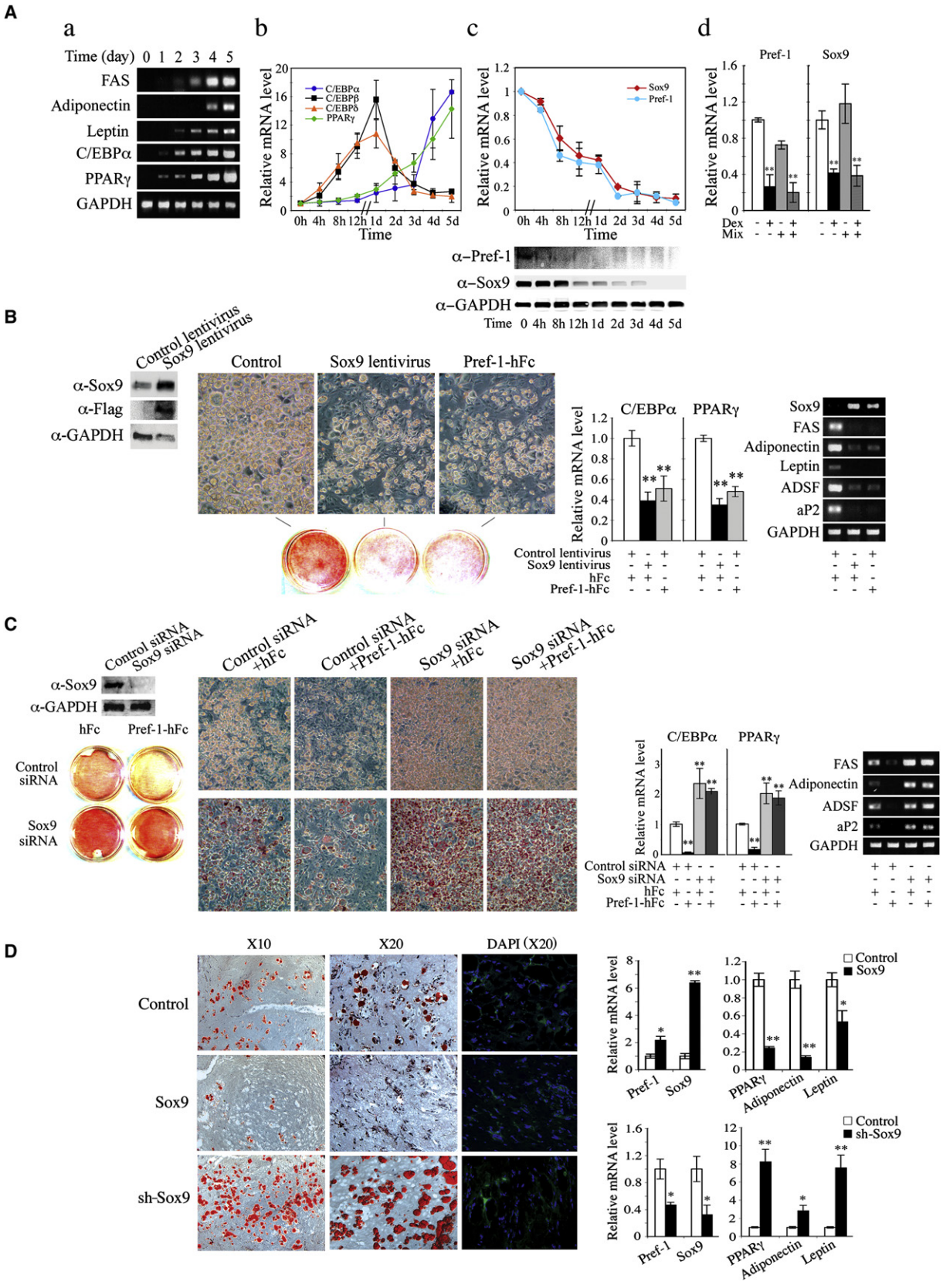
A
a
Time (day) 0 1 2 3 4 5
FAS
Adiponectin
Leptin
C/EBPα
PPARγ
GAPDH
b
Relative mRNA level
C/EBPα
C/EBPβ
C/EBPδ
PPARγ
0h 4h 8h 12h 1d 2d 3d 4d 5d
Time
c
Relative mRNA level
Sox9
Pref-1
0h 4h 8h 12h 1d 2d 3d 4d 5d
Time
d
Pref-1
Sox9
Relative mRNA level
Dex
Mix
α–Pref-1
α–Sox9
α–GAPDH
Time 0 4h 8h 12h 1d 2d 3d 4d 5d
B
Control lentivirus
Sox9 lentivirus
α-Sox9
α-Flag
α-GAPDH
Control
Sox9 lentivirus
Pref-1-hFc
C/EBPα
PPARγ
Relative mRNA level
Control lentivirus
Sox9 lentivirus
hFc
Pref-1-hFc
Sox9
FAS
Adiponectin
Leptin
ADSF
aP2
GAPDH
C
Control siRNA
Sox9 siRNA
α-Sox9
α-GAPDH
hFc
Pref-1-hFc
Control siRNA
Sox9 siRNA
Control siRNA +hFc
Control siRNA +Pref-1-hFc
Sox9 siRNA +hFc
Sox9 siRNA +Pref-1-hFc
C/EBPα
PPARγ
Relative mRNA level
Control siRNA
Sox9 siRNA
hFc
Pref-1-hFc
FAS
Adiponectin
ADSF
aP2
GAPDH
D
X10
X20
DAPI (X20)
Control
Sox9
sh-Sox9
Relative mRNA level
Pref-1
Sox9
PPARγ
Adiponectin
Leptin
Control
Sox9
Relative mRNA level
Pref-1
Sox9
PPARγ
Adiponectin
Leptin
Control
sh-Sox9

1.0 kb C/EBPβ-Luc or 2.0 kb C/EBPδ-Luc suppressed promoter activities by 80% or 85%, respectively (Figure 4B). However, cotransfection of Sox9 with the shorter promoter-reporter constructs, 0.5 kb C/EBPβ-Luc or 1.0 kb C/EBPδ-Luc, did not affect the promoter activities. These data suggest that repression of C/EBPβ and C/EBPδ genes by Sox9 might be through Sox9 binding between −1.0 and −0.5 kb of the C/EBPβ promoter and between −2.0 and −1.0 kb of the C/EBPδ promoter.

Examination of C/EBPβ and C/EBPδ promoter sequences revealed the presence of, respectively, five and eight core consensus binding sites for Sox9 (Figure 4C). ChIP analysis detected evidence for Sox9 binding when specific primer pairs 3 and 4 for C/EBPβ and specific primer pairs 3 and 4 for C/EBPδ, but not other primer sets, were used. Furthermore, EMSA with in vitro translated Sox9 protein and oligonucleotides corresponding to the various Sox9 consensus sites showed that Sox9 can bind the −675–−645 of the C/EBPβ promoter and −1770–−1740 of C/EBPδ promoter (Figure 4D). Excess cold oligonucleotides prevented the signals (Figure 4D, left panels), whereas the oligonucleotides containing mutations of the core Sox9 binding CAAT sequence did not affect the binding (Figure 4D, right panels). Overall, these results demonstrate that Sox9 directly binds its sites in the C/EBPβ and C/EBPδ promoter regions to suppress promoter activity in mediating Pref-1 inhibition of adipocyte differentiation.

Pref-1 Inhibits Osteoblast Differentiation by Maintaining Sox9 Expression

Because we previously observed bone malformation in Pref-1 null and Pref-1 transgenic mice, we tested the effect of Pref-1 on osteoblast differentiation. First, we compared osteoblast differentiation of MEFs from Pref-1 null, wild-type, and Pref-1 transgenic embryos. After 21 days of osteogenic induction, the intensity of von Kossa staining was 3-fold higher in Pref-1 null MEFs than in wild-type MEFs, whereas the staining was barely detected in Pref-1 transgenic cells (Figure 5A, left panel). As predicted, northern blotting showed an absence of Pref-1 in Pref-1 null cells, whereas, in wild-type cells, endogenous Pref-1 was detected at a low level, which was completely suppressed after differentiation. In contrast, Pref-1 expression was high in Pref-1 transgenic cells, and the levels remained high after treatment with osteogenic agents. After 21 days of osteoblast differentiation, expression of ALPase and osteocalcin, respective early and late osteogenic markers, increased drastically in Pref-1 null cells to levels exceeding those in wild-type cells, whereas expression in Pref-1 transgenic cells was very low and did not change. Similarly, ALPase activity in Pref-1 null cells was significantly higher than in wild-type cells after 7 days, and the difference was more marked as differentiation proceeded. Thus, after 21 days of differentiation, ALPase activity in Pref-1 null cells increased by 15-fold, a level 3-fold higher than in wild-type cells. The increase in ALPase activity was only 2-fold in Pref-1 transgenic cells, 60% lower than the 5-fold increase detected in wild-type cells. These data suggest that overexpression of Pref-1 inhibits, whereas lack of Pref-1 enhances, osteoblast differentiation in vitro. The inhibitory effect of Pref-1 on osteoblast differentiation was further tested by using Pref-1-hFc. As expected, the ALPase activity in Pref-1 null cells treated with control hFc increased drastically and reached a 12-fold increase at day 18 (Figure 5B). In contrast, ALPase activity in cells treated with Pref-1-hFc increased in a delayed fashion and was only 4-fold higher at day 18. ALPase and osteocalcin mRNA levels at day 14 were markedly lower in cells treated with Pref-1-hFc, showing Pref-1 inhibition of osteoblast differentiation (Figure 5B).

We next examined the effect of Pref-1 on Sox9 expression early in osteoblast differentiation of MEFs (Figure 5C). Treatment with osteogenic agents drastically decreased Sox9 expression after 24 hr in Pref-1 null MEFs (Figure 5Ca). Importantly, Pref-1-hFc prevented this decrease. Expression of Runx2, a transcription factor required for initiation of osteogenesis as well as chondrocyte maturation, on the other hand, increased markedly, and this increase was also prevented by Pref-1-hFc treatment. Similar to the effects observed in MEFs, Sox9 expression also decreased drastically in C3H10T1/2 cells upon treatment with osteogenic agents, which was prevented by Pref-1-hFc treatment (Figure 5Cb). Unlike in MEFs and MC3T3 cells, however, we could not detect Runx2 expression in C3H10T1/2 cells. After 24 hr of osteogenic treatment, Runx2 was clearly detected, and Pref-1-hFc treatment prevented this Runx2 induction (data not shown).

To further test the Pref-1 effect on Sox9 expression during osteogenesis, we transfected Sox9 siRNA into C3H10T1/2 cells. As expected, Sox9 siRNA transfection decreased Sox9 levels markedly (Figure 5Cc). After 24 hr of treatment with osteogenic agents, Pref-1-hFc prevented the drastic decrease in Sox9 expression observed in control siRNA-transfected cells. Expression of Runx2 was 3-fold higher in Sox9 siRNA-transfected cells compared to control cells. More importantly, Pref-1 suppressed Runx2 expression by 90% in control siRNA-transfected cells treated with osteogenic agents, whereas Pref-1 was unable to suppress Runx2 expression in Sox9 siRNA-transfected cells (Figure 5Cc). These results show that Pref-1 inhibits osteoblast differentiation by preventing Sox9 downregulation. We also detected the Pref-1 effect by comparing osteoblast differentiation of primary osteogenic cells from wild-type, Pref-1 null, and Pref-1 transgenic E18.5 limbs and ribs (Figure S4). Overall, these

Figure 3. Pref-1 Inhibits 3T3-L1 Adipocyte Differentiation through Sox9

(A) RT-PCR (a) and RT-qPCR (b and c) for various adipocyte markers during 3T3-L1 adipocyte differentiation. RT-qPCR after 12 hr treatment (d). Results are mean ± SEM. $^{**}p < 0.01$ compared to untreated cells.

(B) Sox9 protein level after 48 hr of infection (left panel). Morphology, oil red O staining (middle panel), and RT-qPCR and RT-PCR for adipocyte markers (right panels). Results are mean ± SEM. $^{**}p < 0.01$ compared to the cells infected with control lentivirus and treated with hFc.

(C) Sox9 knockdown enhances adipocyte differentiation. Western blotting after 48 hr siRNA transfection (left panel). Morphology, oil red O staining, and adipocyte marker expression after adipocyte differentiation. $^{**}p < 0.01$ compared to the cells transfected with control siRNA and treated with hFc.

(D) 3T3-F442A-GFP preadipocytes stably overexpressing or with knockdown of Sox9, or control cells (3×10^7 cells mixed with Matrigel matrix [BD] per site) were injected subcutaneously into the back of SCID mice. The resulting tissues were dissected for oil red O and DAPI staining and RT-qPCR (n = 4/group). Results are mean ± SEM. $^{*}p < 0.05$. $^{**}p < 0.01$ compared to the control.

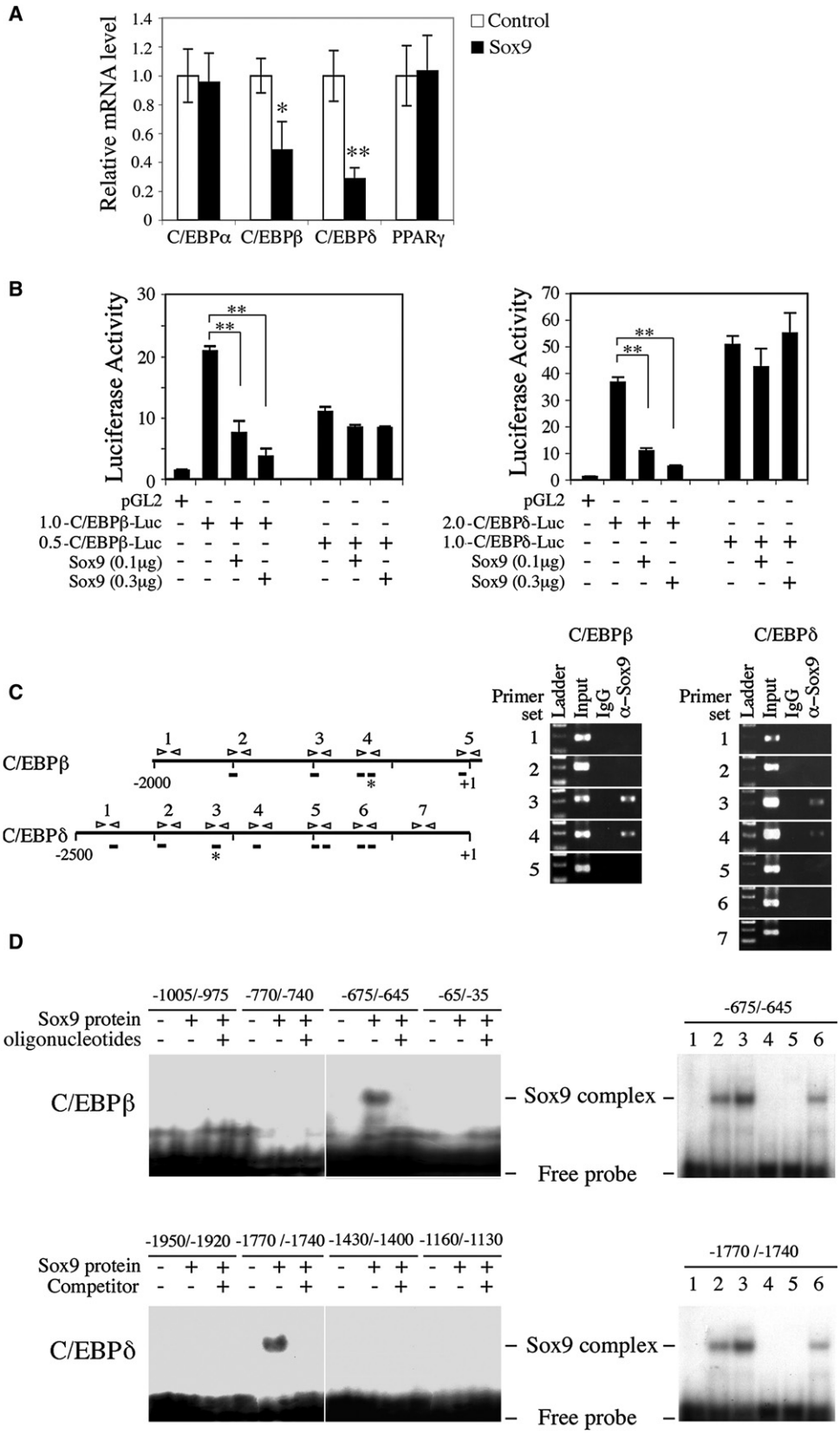
A
Relative mRNA level
Control
Sox9
C/EBPα C/EBPβ C/EBPδ PPARγ
B
Luciferase Activity
pGL2
1.0-C/EBPβ-Luc
0.5-C/EBPβ-Luc
Sox9 (0.1μg)
Sox9 (0.3μg)
2.0-C/EBPδ-Luc
1.0-C/EBPδ-Luc
C
C/EBPβ
C/EBPδ
-2000
-2500
+1
Primer set
Ladder
Input
IgG
α–Sox9
D
-1005/-975 -770/-740 -675/-645 -65/-35
Sox9 protein
Cold oligonucleotides
C/EBPβ
Sox9 complex
Free probe
-1950/-1920 -1770 /-1740 -1430/-1400 -1160/-1130
Competitor
C/EBPδ

results clearly show that Pref-1 inhibits osteoblast differentiation through Sox9 regulation.

The effect of Pref-1 on osteoblast differentiation was also tested in preosteoblastic MC3T3 cells (Figure 5D). Pref-1 expression was not detectable in MC3T3 cells (Figure 5D, top-left panel). Osteocalcin and ALPase expression were very low in confluent cells but increased markedly after 7 days of treatment with osteogenic agents. These increases were blunted in cells infected with Pref-1 lentivirus or upon Pref-1-hFc treatment. Similarly, ALPase activity rapidly increased at day 3 and further increased at days 6 and 9 after osteogenic stimulation (Figure 5D, top-right panel). The increase in ALPase activity was delayed and significantly blunted at all time points in cells infected with Pref-1 lentivirus or upon Pref-1-hFc treatment. We also examined the effect of Pref-1-hFc on expression of Sox9 early during osteogenesis in these cells (Figure 5D, bottom panels). During early osteogenesis, expression of Sox9 was rapidly downregulated by 50% within 1 hr after osteogenic stimulation in control hFc-treated cells, and Sox9 levels further decreased up to 2 days after treatment, whereas expression of Runx2 was rapidly induced, reaching a maximum of 3-fold at 4 hr that gradually decreased. In contrast, the Sox9 expression level was maintained in cells treated with Pref-1-hFc, whereas Runx2 expression did not increase in these cells upon treatment with osteogenic agents. Overall, these results show that Pref-1 prevents Sox9 downregulation and thereby inhibits mesenchymal cell differentiation into osteoblasts.

Pref-1 Directs Multipotent Mesenchymal Cells to Chondrogenic Commitment but Inhibits Maturation of Chondrocytes by Inducing Sox9 Expression

Because Pref-1 inhibits osteoblast differentiation and osteoblasts and chondrocytes are from common mesenchymal progenitor cells, we hypothesized that Pref-1 may regulate chondrocyte formation also (Gaur et al., 2005; Lengner et al., 2004). Therefore, we compared MEFs from Pref-1 null, wild-type, and Pref-1 overexpressing transgenic embryos in micromass culture for chondrogenesis. Alcian blue staining showed the effect of Pref-1 on chondrogenesis (Figure 6A, left panel): Pref-1 null cells showed the weakest staining, and wild-type cells showed a 4-fold higher intensity of staining, which was even higher by 8-fold in transgenic cells. We used Col II and Col IX as immature chondrocyte markers and Col X and ALPase as hypertrophic chondrocyte markers. After 14 days of culture in the presence of chondrogenic agents, wild-type cells showed 4.3-fold higher Col II levels, and Pref-1 transgenic cells displayed 6.7-fold higher Col II expression compared to Pref-1 null cells (Figure 6A, right panel). On the contrary, Col X and ALPase expression were highest in Pref-1 null cells. Upon treatment with chondrogenic agents, ALPase expression decreased by 4.7-fold in wild-type cells but was not detected in Pref-1 transgenic cells. Col X expression was also lower in Pref-1 transgenic cells. These results show that Pref-1 promotes mesenchymal cell commitment to the chondrogenic lineage but inhibits chondrocyte maturation in vitro.

Next, to test the effect of Pref-1 and Sox9 on chondrogenesis, we infected Pref-1 null MEFs with Sox9 lentivirus or treated Pref-1 null MEFs with Pref-1-hFc and subjected them to micromass culture (Figure 6B). We found that Pref-1-hFc treatment or lentivirus-mediated Sox9 overexpression in MEFs caused increased immature chondrocytes as judged by Alcian blue staining and Col II and Col IX expression. Furthermore, overexpression of Sox9 along with Pref-1-hFc treatment did not produce additive effects, suggesting that Pref-1 and Sox9 may affect chondrogenesis by the same mechanism. Similar results were obtained from C3H10T1/2 cells subjected to chondrogenesis (data not shown). To further examine the role of Sox9 in mediating the Pref-1 effect on chondrogenesis, we treated the Pref-1 null MEFs transfected with Sox9 siRNA with soluble Pref-1-hFc (Figure 6C). As judged by Alcian blue staining and chondrogenic marker expression, we found that Pref-1-hFc treatment did not have an effect on chondrogenesis in cells transfected with Sox9 siRNA, compared to control cells treated with Pref-1 that had increased immature chondrocytes. Overall, these data from MEFs and C3H10T1/2 cells are consistent with the notion of Sox9 mediating the Pref-1 effect and clearly demonstrate that, like Sox9, Pref-1 can promote chondrogenic induction of uncommitted mesenchymal cells in micromass culture.

We also tested the involvement of Sox9 and Pref-1 in chondrocyte maturation by employing committed chondrogenic cells from skinned tails from newborn mice in micromass culture (Figures 7A and 7B). After 14 days of culture, compared to wild-type cells, Pref-1 null cells displayed a lower intensity of Alcian blue staining with a lower expression of Col II and Col IX but higher expression of Col X and ALPase. In contrast, Pref-1 transgenic cells displayed stronger Alcian blue staining with higher Col II and Col IX but lower Col X and ALPase expression (Figure 7A). In addition, Sox9 expression was lower, whereas Runx2 was higher in Pref-1 null cells than in wild-type cells, and Pref-1 transgenic cells showed higher Sox9 expression but lower Runx2 expression. We also found that expression of the prehypertrophic marker, Ihh, was higher in Pref-1 null cells but was lower in Pref-1 transgenic cells than in wild-type cells. These observations demonstrate that Pref-1 increases immature chondrocytes but inhibits maturation of chondrocytes. Furthermore, Pref-1 lentivirus infection or Pref-1-hFc treatment increased immature chondrocytes as judged by Alcian blue staining and chondrogenic marker expression with increased Col II and Col IX expression but decreased Col X expression. These observations

Figure 4. Sox9 Directly Binds C/EBPβ and C/EBPδ Promoters and Suppresses Their Transcription

(A) RT-qPCR for various transcription factors 72 hr after Sox9 transfection into 3T3-L1 cells. *$p < 0.05$ and **$p < 0.01$ compared to cells transfected with empty vector.

(B) C/EBPβ and C/EBPδ promoter activity after cotransfection with Sox9 into 293FT cells. pRL-SV40 was used as internal control. Results are mean ± SEM. **$p < 0.01$.

(C) Numbering denotes primer sets in the C/EBPβ and C/EBPδ promoter regions used for ChIP (left panel). ChIP for C/EBPβ and C/EBPδ using 3T3-L1 cells (right panel). Bar, sites with core consensus Sox9 binding sequence. Star, actual Sox9 binding sites.

(D) EMSA for Sox9 binding sites. In vitro translated Sox9 protein and ^{32}P-labeled oligonucleotides were used for EMSA. Probe only (lane 1); 1 μl (lane 2) and 2 μl (lane 3) of Sox9 translation reaction with probe; 1 μl of Sox9 with 100 × wild-type competitor (lane 4); 1 μl of translation reaction of empty pcDNA3.1 vector with probe (lane 5); 1 μl of Sox9 with 100 × mutant competitor (lane 6).

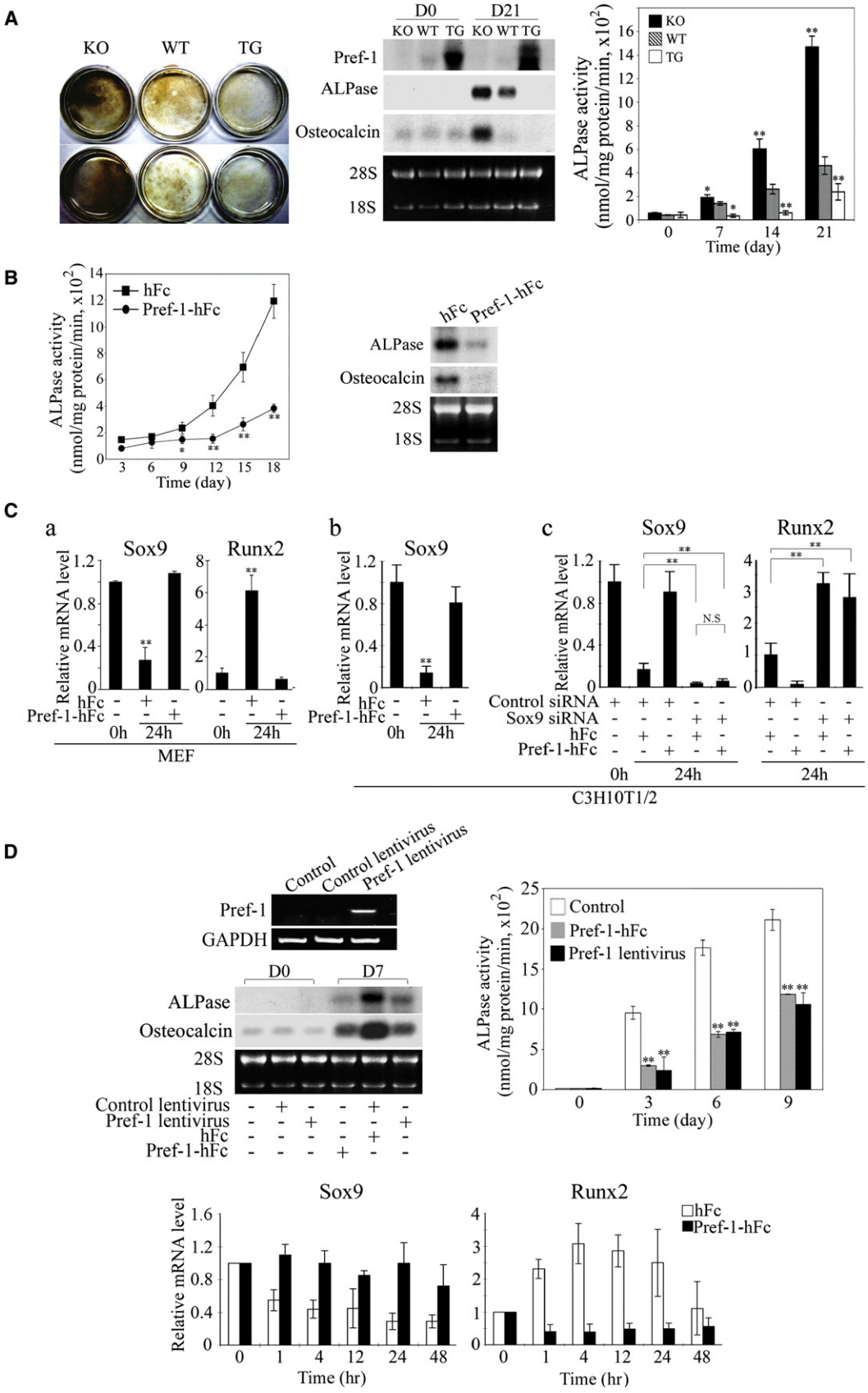
A
KO
WT
TG
D0
D21
KO WT TG KO WT TG
Pref-1
ALPase
Osteocalcin
28S
18S
ALPase activity (nmol/mg protein/min, x10^2)
Time (day)
B
hFc
Pref-1-hFc
C
a
b
c
Sox9
Runx2
Relative mRNA level
Control siRNA
Sox9 siRNA
N.S
0h
24h
MEF
C3H10T1/2
D
Control
Control lentivirus
Pref-1 lentivirus
GAPDH
D0
D7
Pref-1 lentivirus
Time (hr)

provide further evidence that Pref-1 promotes chondrogenic induction/early chondrocyte differentiation but inhibits chondrocyte maturation. Thus, Pref-1 maintains the chondrocytes in an immature state and prevents their differentiation into mature chondrocytes in vitro. When we tested the effect of Pref-1 on Sox9 and Runx2 expression in Pref-1 null primary chondrogenic cells (Figure 7B, left panel), Sox9 expression increased by 4.6-fold after 1 hr of Pref-1-hFc treatment. On the other hand, we did not detect any significant changes in Runx2 expression at this time point, further suggesting that Pref-1 function is through Sox9 induction.

As mentioned, in adults, Pref-1 expression is mainly restricted to preadipocytes as well as some neuroendocrine cell types, but Pref-1 is widely expressed during embryonic development with prominent expression in developing vertebra as shown by in situ hybridization at day E13.5 (Figure 7C). In vertebra, Pref-1 expression was restricted to the periphery of vertebral bodies but was undetectable in hypertrophic zones (Figure 7C, bottom panel), suggesting that Pref-1 functions in immature chondrocytes, but not in hypertrophic chondrocytes. To demonstrate the effects of Pref-1 on chondrogenesis in vivo, we examined embryonic developmental stages by comparing Pref-1 null, wild-type, and Pref-1 transgenic embryos. As shown in Figure 7D, we did not observe drastic malformation at E14.5 when mesenchymal condensations start to commit to the chondrocyte linage and, in part, to become prehypertrophic chondrocytes. But, the prehypertrophic marker, Ihh, was strongly expressed in Pref-1 null vertebral bodies compared to wild-type, whereas it was barely detectable in Pref-1 overexpressing vertebral bodies. In contrast, expression of the immature chondrocyte marker, Col II, was lower in Pref-1 null embryos but was strongly expressed in Pref-1 overexpressing embryos. At E16.5 stage, when the central vertebral bodies normally become hypertrophic chondrocytes, both Pref-1 null and Pref-1 overexpressing embryos showed more visible skeletal malformation (Figure 7E). Compared to wild-type, Pref-1 null embryos were smaller, with higher expression of the prehypertrophic and hypertrophic chondrocyte markers, Ihh and Col X, respectively. Pref-1 transgenic embryos were also smaller, with shorter kinky tails, and showed higher expression of the immature chondrocyte marker Col II and markedly lower expression of the prehypertrophic and hypertrophic markers, Ihh and Col X.

Phenotypes were more severe in the newborn stage (Figure 7F). Histological staining of the vertebral region showed that, compared to wild-type mice, Pref-1 null mice had a 40% increase in the hypertrophic zone, whereas the hypertrophic zone was absent in Pref-1 transgenic mice (Figure 7F). Similarly, we detected a 40% increase in the hypertrophic zone in Pref-1 null long bones (E18.5 femurs) compared to wild-type mice, whereas we found a 25%–30% decrease in the hypertrophic zone in Pref-1 transgenic mice (data not shown). Conversely, the zone of immature chondrocytes was 30% lower in Pref-1 null mice, whereas Pref-1 transgenic mice had only immature chondrocytes without an obvious hypertrophic zone. As expected, by northern blot analysis, Pref-1 was not detected in Pref-1 null mice but was markedly higher in Pref-1 transgenic mice. Similarly, Sox9 expression was significantly lower in Pref-1 null mice compared to wild-type mice but was 6-fold higher in Pref-1 transgenic mice. Examination of chondrocyte/osteoblast marker expression also indicated that the levels of immature chondrocyte markers, including Col II and aggrecan, were lower in Pref-1 null mice but higher in Pref-1 transgenic mice compared to wild-type mice. In contrast, expression of mature chondrocyte marker Col X and hypertrophic/early osteogenic marker ALPase was higher in Pref-1 null mice but barely detectable in Pref-1 transgenic mice. Overall, these data show that Pref-1 brings about chondrogenic induction but inhibits chondrocyte maturation.

Effect of Pref-1 on Bone Marrow Stromal Cell Fate

Because bone marrow mesenchymal stem cells (MSC) can commit and differentiate into adipocytes as well as chondrocytes and Pref-1 is detected in bone marrow, we next examined the presence of adipocytes in bone marrow of 1-week-old vertebral bodies from Pref-1 null, wild-type, and Pref-1 transgenic mice. H&E staining showed that rounded adipose features were higher in Pref-1 null than in wild-type vertebra, and they were barely detectable in Pref-1 overexpressing vertebra (Figure 7G, upper panel). Expression of adipocyte markers in bone marrow from 12-week-old femur bone was inversely correlated with Pref-1 expression. C/EBPα, PPARγ, and adiponectin levels were markedly higher in Pref-1 null bone marrow but were very low in Pref-1 transgenic ones. In contrast, Sox9 expression levels were very low in Pref-1 null bone marrow but were markedly higher in Pref-1 transgenic bone marrow (Figure 7G, lower panel). Overall, these observations indicate a potential in vivo effect of Pref-1 on MSC differentiation into adipocytes.

We next used the human MSC in culture to test whether Pref-1 affects the fate of these cells during adipogenic and chondrogenic commitment/differentiation (Figure 7H). RT-qPCR showed that, 2 days after initiation of adipocyte differentiation, Sox9 as well as endogenous Pref-1 expression levels were significantly higher in Pref-1-hFc-treated cells compared to control hFc-treated cells (Figure 7H, upper panel). On the other hand, expression levels of adipocyte markers, C/EBPβ, C/EBPδ, and PPARγ were lower in Pref-1-hFc-treated cells. Upon treatment with chondrogenic agents of MSC for 2 days, Sox9 and Col II expression levels were significantly higher in Pref-1-hFc-treated cells

Figure 5. Pref-1 Inhibits Osteoblast Differentiation by Preventing the Decrease in Sox9 Expression

(A) Von Kossa staining of MEFs after 21 days of osteoblast differentiation (left panel). Northern blot analysis (middle panel) and ALPase activity (right panel). Results are means ± SEM. *$p < 0.05$ and **$p < 0.01$ compared to wild-type cells at indicated time points.

(B) ALPase activities (left panel) and northern blotting after 18 days of osteoblast differentiation (right panel).

(C) RT-qPCR for Pref-1 null MEFs and C3H10T1/2 cells cultured for in osteogenic media (a and b). siRNA-transfected C3H10T1/2 cells cultured in osteogenic media (c). For Sox9 expression, the value of untreated cells was defined as 1. For Runx2, due to its undetectable level in untreated cells, the value of control siRNA-transfected cells after 24 hr treatment was defined as 1.

(D) RT-PCR after 48 hr lentivirus infection in MC3T3 cells. Northern blot analysis from confluent MC3T3 cells (D0), 7 days osteogenic treatment (D7), and ALPase activity. Results are mean ± SEM. **$p < 0.01$ compared to cells infected with control lentivirus and cultured with hFc at indicated time points. RT-qPCR during osteogenic differentiation (bottom panel).

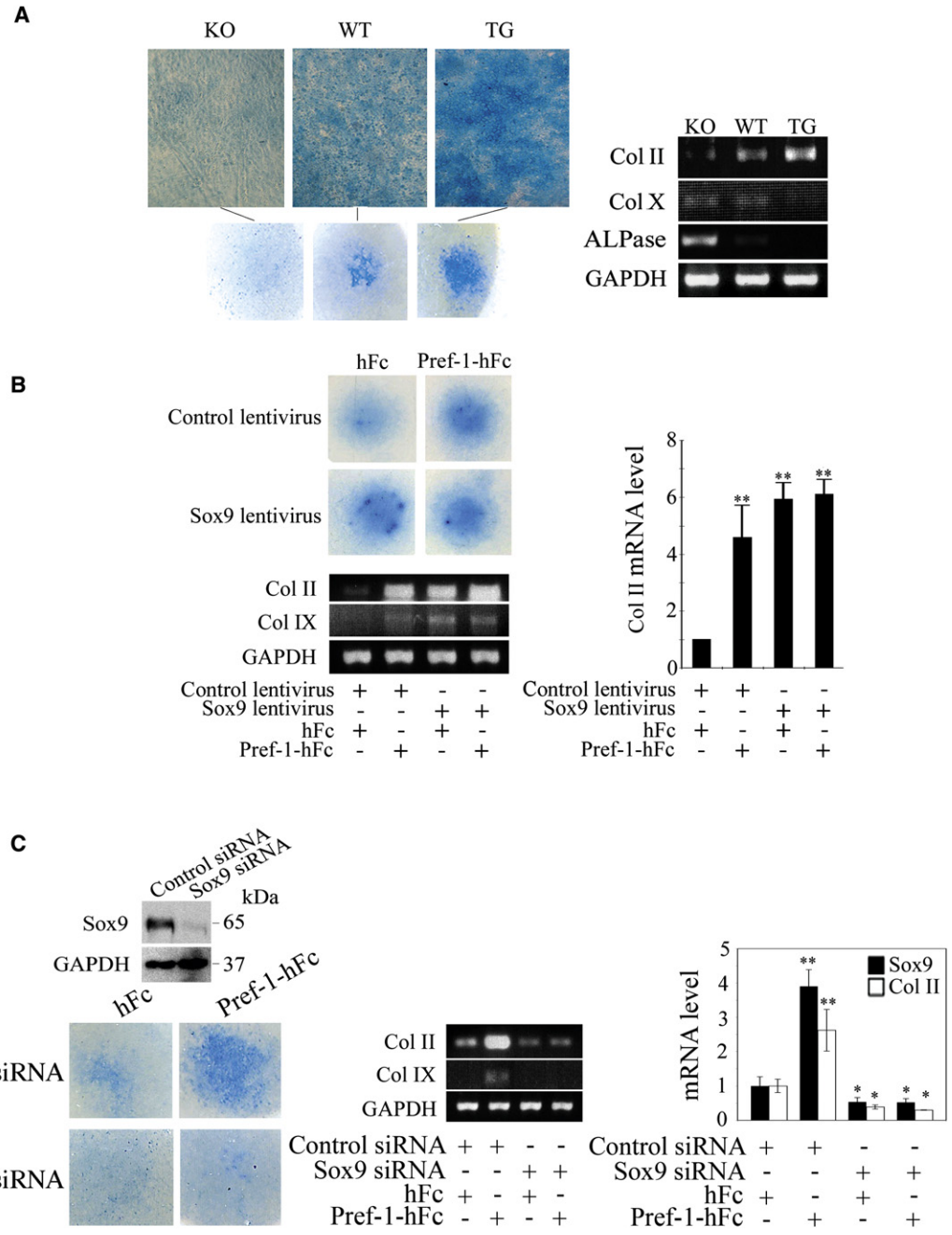

Figure 6. Pref-1 Directs MEF Commitment to Chondrogenic Lineage through Sox9 Regulation

(A) Micromass culture of MEFs. Alcian blue staining (left panel) and RT-PCR for chondrogenic markers (right panel) after 14 days of culture.

(B) Pref-1 null MEFs infected with Sox9 lentivirus after 10 days micromass culture. **$p < 0.01$ compared to differentiated cells infected with control empty lentivirus and in the presence of control hFc.

(C) Knockdown of Sox9 blocks chondrogenic induction by Pref-1. Alcian blue staining for Pref-1 null MEFs transfected with siRNA after micromass culture. Western blotting after 48 hr transfection (left top panel). Results are mean ± SEM. *$p < 0.05$ and **$p < 0.01$ compared to cells transfected with control siRNA and treated with hFc.

compared to control hFc cells, demonstrating promotion to the chondrogenic lineage by Pref-1 (Figure 7H, lower panel). Overall, these results from MSC in culture further confirm that Pref-1 promotes commitment to the chondrocyte lineage but inhibits adipogenesis.

DISCUSSION

We previously reported Pref-1 inhibition of adipocyte differentiation by both in vitro and in vivo approaches. In fact, we originally identified Pref-1 as a protein found in preadipocytes, but not in

adipocytes. During adipocyte differentiation, Pref-1 is extinguished. Constitutive expression of Pref-1 inhibits 3T3-L1 preadipocyte differentiation into adipocytes, and Pref-1 knockdown causes enhanced differentiation. The significance of Pref-1 function in adipogenesis has been documented in vivo in Pref-1 null and Pref-1 overexpressing transgenic mice. Although expression of the two key adipogenic transcription factors C/EBPα and PPARγ clearly is suppressed by Pref-1 treatment, the proximal downstream molecule that mediates Pref-1 inhibition has not been defined. It has been reported previously that HES-1 expression is induced by Pref-1 treatment in thymocytes (Kaneta et al., 2000). However, we could not detect any changes in HES-1 expression by Pref-1 (unpublished data). In the present study, we show that Sox9 is a target of Pref-1, and Pref-1 increases Sox9 expression rapidly in various cell types, including multipotent mesenchymal cells. Although a receptor for Pref-1 has not been identified, we have previously shown that Pref-1 activates the MEK/ERK pathway. The fact that Sox9 is known to be induced by ERK activation (Murakami et al., 2000) and that inhibition of Pref-1-mediated ERK activation prevents Sox9 induction further supports the notion of Sox9 as a downstream target of Pref-1. In this regard, although Sox9 may not be the only target for Pref-1, we found that Pref-1 expression parallels Sox9 expression during adipocyte differentiation of MEFs and 3T3-L1 cells, as well as during in vivo adipogenesis.

Although the role of Sox9 in chondro- and osteogenesis is well understood, its role in adipocyte commitment/differentiation has not been studied. Here, we show that overexpressing Sox9 constitutively or maintaining Sox9 levels by treating the cells with Pref-1-hFc cause inhibition of adipocyte differentiation. We conclude that Sox9 suppression is required before induction of the adipogenic transcription factors PPARγ and C/EBPα for adipocyte differentiation. Furthermore, downregulation of Sox9 coincides with the induction of C/EBPβ/C/EBPδ that occurs earlier than C/EBPα and PPARγ induction. Suppression of Pref-1 decreases Sox9 expression that, in turn, allows C/EBPβ and C/EBPδ induction early at the start of adipocyte differentiation. A synthetic glucocorticoid DEX, routinely used for adipocyte differentiation, suppresses Pref-1 expression. We also found that DEX suppresses Sox9 expression also. We thus predicted that Sox9 might function through regulating C/EBPβ and/or C/EBPδ during adipocyte differentiation. In this regard, glucocorticoids have been reported to induce C/EBPδ expression. In the present study, we detected suppression of C/EBPδ and C/EBPβ upon Sox9 overexpression. Furthermore, cotransfection of Sox9 resulted in decreased C/EBPβ and C/EBPδ promoter activity, and EMSA and ChIP analysis revealed the binding sites of Sox9 at −675–−645 of C/EBPβ and −1770–−1740 of C/EBPδ promoter sequences. Here, we also demonstrate in vivo the role of Sox9 in adipogenesis by subcutaneous implanting (Figure 3D). The present study demonstrates that Sox9 is downregulated during adipocyte differentiation and Sox9 inhibits adipocyte differentiation. Our study also shows that the function of Sox9 is to maintain cells in the preadipocyte stage by directly binding to the C/EBPβ and C/EBPδ promoter regions to suppress transcription.

Pref-1 is expressed in multipotent mesenchymal stem cells that can differentiate into several cell types, including chondrocytes, osteoblasts, and adipocytes. Although the role of Pref-1 in adipogenesis has been extensively studied (Lee et al., 2003; Mei et al., 2002; Moon et al., 2002; Smas et al., 1998), Pref-1 effects on chondrocyte commitment and maturation have not been studied before. Here, we employed MEFs that have the ability to undergo commitment/differentiation into various mesenchymal lineages, including chondrocytes, osteoblasts, and adipocytes. Sox9 and Pref-1 have similar, but not additive, effects on MEF commitment and early differentiation into immature chondrocytes. We also employed bone marrow stromal cells to demonstrate that Pref-1 inhibits adipogenesis while promoting chondrogenic commitment. Examination of the bone marrow clearly shows that Pref-1 expression is inversely correlated with adipose morphology in vivo. Moreover, chondrogenic induction by Pref-1 in micromass culture is abolished in the absence of Sox9, evidence that Sox9 mediates the Pref-1 effect of promoting chondrogenic induction. It is well recognized that Sox9 plays an essential role in recruiting mesenchymal cells to undergo chondrogenic commitment and early chondrogenesis but inhibits maturation to hypertrophic chondrocytes (Akiyama et al., 2004). Sox9 function in chondrogenesis has been documented by loss- and gain-of-function studies in vitro and in vivo (de Crombrugghe et al., 2001). Inactivation of Sox9 before mesenchymal condensation in mice results in the complete prevention of condensation and cartilage formation. Thus, Sox9 deficiency and Sox9 overexpression in mice result in smaller skeletons as seen in Pref-1 null and Pref-1 transgenic mice. Pref-1 null mice appear to have, albeit less severely, phenotypes of skeletal development resembling phenotypes found when Sox9 is knocked down or mutated, whereas the phenotypes of Pref-1 transgenic mice have similarities to the Sox9 transgenic mouse model. In this regard, deficiencies in some of the known growth factors/hormones that affect skeletogenesis, at least in part, through Sox9 regulation also have similar phenotypes (Karaplis et al., 1994; Liu et al., 2002). Regardless, these apparent phenotypic similarities of in vivo gain and loss of function further support the notion that Pref-1 effects are through regulation of Sox9 expression.

With our present study demonstrating the role of Pref-1 on chondrogenesis, the Pref-1 effect on bone formation could be an indirect one. However, the Pref-1 effect on MEFs, as well as preosteoblastic MC3T3 cells that can undergo osteoblast differentiation in vitro, indicates a direct inhibitory effect of Pref-1 on osteoblast differentiation. This idea is also supported by a previous report of Pref-1 leading to inhibition of osteoblast differentiation of human bone marrow stromal cells (Abdallah et al., 2004). More importantly, we demonstrate here that Pref-1 prevents Sox9 downregulation and thereby inhibits osteoblast differentiation and the expression of the osteogenic transcription factor Runx2. Progenitor cells in early mesenchymal condensations have dual differentiation potentials, as they coexpress Sox9 and Runx2. Runx2 has been shown to accelerate chondrocyte maturation to become hypertrophic chondrocytes and to promote osteogenesis (Takeda et al., 2001). Runx2 appears to exert its function only when Sox9 is downregulated in hypertrophic chondrocytes or in osteoblasts. We conclude that Pref-1 inhibits osteoblast differentiation by preventing downregulation of Sox9.

In conclusion, we show here that Sox9 downregulation is required for adipocyte differentiation. Sox9 suppresses C/EBPβ/C/EBPδ expression by directly binding to its sites in the promoter regions of these genes. Importantly, we demonstrate that Pref-1

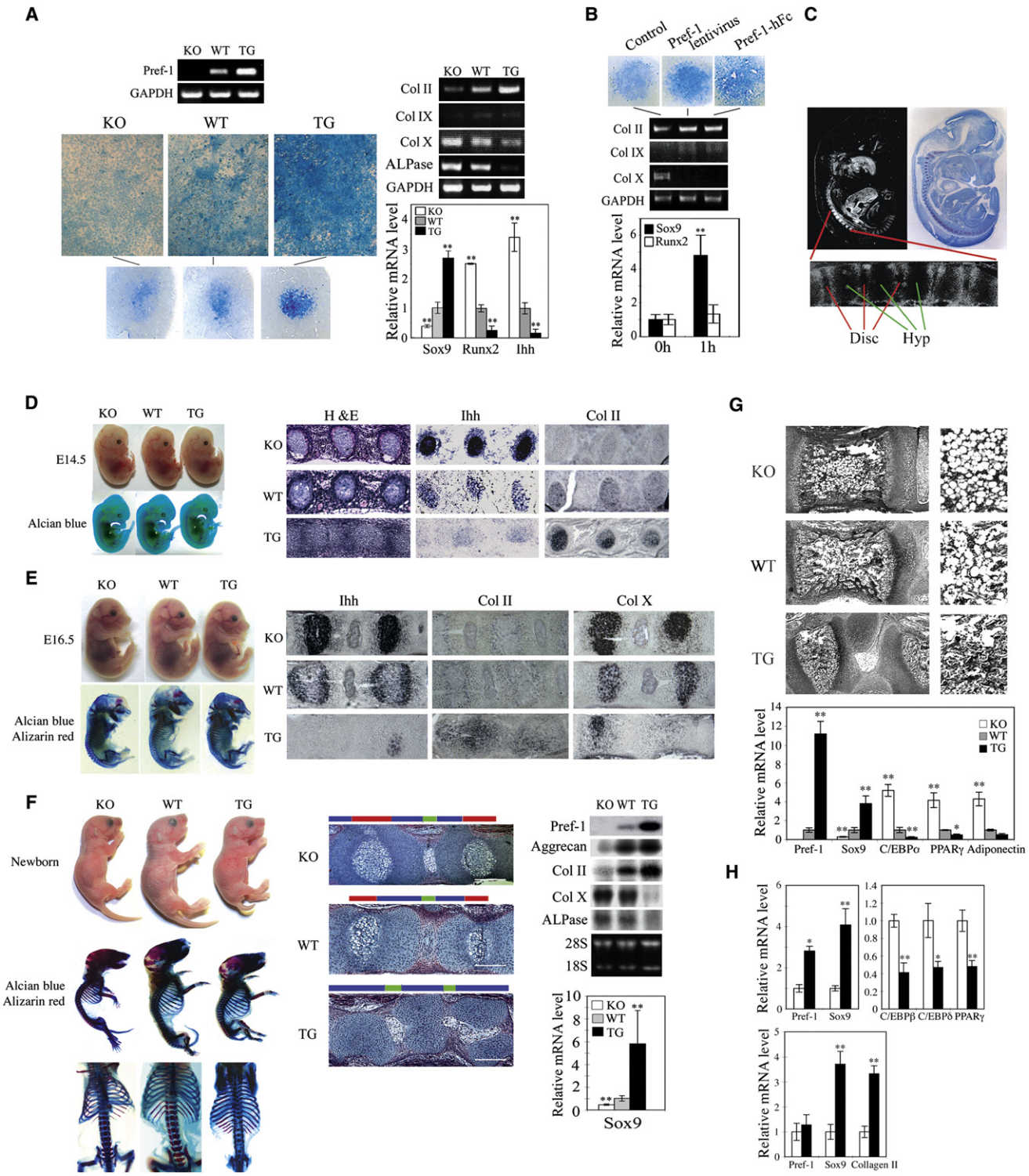

Figure 7. Pref-1 Promotes Chondrogenic Induction but Inhibits Chondrocyte Maturation through Upregulation of Sox9

(A) Micromass culture of cells from newborn tails. Alcian blue staining and RT-PCR and RT-qPCR for chondrogenic markers. **$p < 0.01$ compared to wild-type.

(B) RT-qPCR after 1 hr treatment with 50 nM Pref-1-hFc (left panel). **$p < 0.01$ compared to untreated cells. RT-PCR in cells 48 hr after infection.

(C) In situ hybridization of E13.5 embryos with ^{33}P-labeled Pref-1 antisense probe (left panel) and bright field view with hematoxylin staining (left panel). Thoracic-abdominal vertebra region is enlarged (bottom). Disc, spinal disc. Hyp, hypertrophic zone.

(D–F) Embryos and mice and their skeleton staining (Alcian blue for cartilage and alizarin red for bone) in various developmental stages.

(F) Thoracic-abdominal vertebra was used for in situ hybridization with digoxigenin labeled antisense probe. H&E staining of fourth through fifth coccyges from newborn mice (middle panel). Color bars represent the length of different histological area. Red bar, zones of hypertrophic chondrocytes. Blue bar, the area of

inhibition of adipogenesis is through maintaining Sox9 expression. We also show that, by inducing Sox9, Pref-1 promotes chondrogenic induction of mesenchymal cells but prevents chondrocyte maturation as well as osteoblast differentiation, with supporting in vivo evidence in Pref-1 null and Pref-1 transgenic mice. Overall, Sox9 is a Pref-1 target, and Pref-1 directs multipotent mesenchymal cells to the chondrogenic lineage but inhibits differentiation into adipocytes, as well as osteoblasts and chondrocytes.

EXPERIMENTAL PROCEDURES

Lentiviral and Plasmid Constructs and Animals

The lentiviral construct was made by subcloning Sox9 into pLenti6/V5-D-TOPO vector. Sox9 was also subcloned into pcDNA3.1. The 1.0-C/EBPβ-luc, 0.5-C/EBPβ-luc, 2.0-C/EBPδ-luc, and 1.0-C/EBPδ-luc were generated by inserting 1.0 and 0.5 kb C/EBPβ and 2.0 and 1.0 kb C/EBPδ 5′ flanking regions into the pGL2 basic vector (Promega). Sox9 shRNA plasmid was purchased from SABiosciences. The generation of Pref-1 null and Pref-1 transgenic mice were described previously (Lee et al., 2003; Moon et al., 2002). Scid mice were purchased from the Jackson laboratory.

Cells and siRNA Transfection

MC3T3 cells were cultured in α-MEM (Invitrogen) containing 10% FBS. MEFs were prepared from E13.5 embryos as described previously (Wang and Sul, 2006). Human-derived marrow stromal cells (MSC) and MSC media were purchased from Allcells. Sox9 target-specific siRNA (sc-36534) (Santa Cruz) and the control siRNA (sc-36869) were transfected into cells using transfection reagent (Santa Cruz).

Chromatin Immunoprecipitation and Electrophoretic Mobility Shift Assay

For chromatin immunoprecipitation (ChIP) analysis, 1×10^7 3T3-L1 cells were crosslinked with 1% formaldehyde before nuclei preparation. After sonication, DNA sizes were 0.3–0.9 kb. Ten percent of the total volume was used as input, and the rest was divided into two fractions: one for control IgG and the second for 5 μg of Sox9 antibody immunoprecipitation. Purified DNA was used in PCR reactions.

Sox9 protein was in vitro translated using Promega TNT Translation Systems and used in electrophoretic mobility shift assay (EMSA). Sense and antisense oligonucleotides (30 bp) containing potential Sox9 core-binding sequence CAAT were labeled by γ ^{32}P-dCTP. Mutant competitors were the oligonucleotides mutated CAAT to CCAT. Samples were separated by 5% native polyacrylamide gel electrophoresis before exposure to film.

Statistical Analysis

Data are expressed as the mean ± SEM. The statistical differences in mean values were assessed by Student's t test. All experiments are repeated at least twice, and representative data are shown. All scanned images were quantified by NIH image software.

SUPPLEMENTAL DATA

The Supplemental Data include Supplemental Experimental Procedures and five figures and can be found with this article online at http://www.cell.com/cell-metabolism/supplemental/S1550-4131(09)00038-2.

ACKNOWLEDGMENTS

This work was supported, in part, by the National Institutes of Health grant, DK50828, to H.S.S. We thank Dr. Benoit de Crombrugghe (University of Texas M.D. Anderson Cancer Center, Houston) and Dr. Ormond A. MacDougald (University of Michigan Medical School, Ann Arbor) for Sox9 plasmid and MC3T3 cells. We thank Roger Wong for technical help and Drs. Mary Ann Williams, Robin Duncan, and Maryam Ahmadian for careful reading of the manuscript.

Received: July 7, 2008
Revised: December 1, 2008
Accepted: January 30, 2009
Published: March 3, 2009

REFERENCES

Abdallah, B.M., Jensen, C.H., Gutierrez, G., Leslie, R.G., Jensen, T.G., and Kassem, M. (2004). Regulation of human skeletal stem cells differentiation by Dlk1/Pref-1. J. Bone Miner. Res. *19*, 841–852.

Akiyama, H., Lyons, J.P., Mori-Akiyama, Y., Yang, X., Zhang, R., Zhang, Z., Deng, J.M., Taketo, M.M., Nakamura, T., Behringer, R.R., et al. (2004). Interactions between Sox9 and beta-catenin control chondrocyte differentiation. Genes Dev. *18*, 1072–1087.

Bachmann, E., Krogh, T.N., Hojrup, P., Skjodt, K., and Teisner, B. (1996). Mouse fetal antigen 1 (mFA1), the circulating gene product of mdlk, pref-1 and SCP-1: Isolation, characterization and biology. J. Reprod. Fertil. *107*, 279–285.

Bi, W., Huang, W., Whitworth, D.J., Deng, J.M., Zhang, Z., Behringer, R.R., and de Crombrugghe, B. (2001). Haploinsufficiency of Sox9 results in defective cartilage primordia and premature skeletal mineralization. Proc. Natl. Acad. Sci. USA *98*, 6698–6703.

da Rocha, S.T., and Ferguson-Smith, A.C. (2004). Genomic imprinting. Curr. Biol. *14*, R646–R649.

de Crombrugghe, B., Lefebvre, V., and Nakashima, K. (2001). Regulatory mechanisms in the pathways of cartilage and bone formation. Curr. Opin. Cell Biol. *13*, 721–727.

Farmer, S.R. (2006). Transcriptional control of adipocyte formation. Cell Metab. *4*, 263–273.

Gaur, T., Lengner, C.J., Hovhannisyan, H., Bhat, R.A., Bodine, P.V., Komm, B.S., Javed, A., van Wijnen, A.J., Stein, J.L., Stein, G.S., and Lian, J.B. (2005). Canonical WNT signaling promotes osteogenesis by directly stimulating Runx2 gene expression. J. Biol. Chem. *280*, 33132–33140.

Gesta, S., Tseng, Y.H., and Kahn, C.R. (2007). Developmental origin of fat: Tracking obesity to its source. Cell *131*, 242–256.

Gregoire, F.M., Smas, C.M., and Sul, H.S. (1998). Understanding adipocyte differentiation. Physiol. Rev. *78*, 783–809.

Kaneta, M., Osawa, M., Sudo, K., Nakauchi, H., Farr, A.G., and Takahama, Y. (2000). A role for pref-1 and HES-1 in thymocyte development. J. Immunol. *164*, 256–264.

Karaplis, A.C., Luz, A., Glowacki, J., Bronson, R.T., Tybulewicz, V.L., Kronenberg, H.M., and Mulligan, R.C. (1994). Lethal skeletal dysplasia from targeted disruption of the parathyroid hormone-related peptide gene. Genes Dev. *8*, 277–289.

resting and proliferating chondrocytes and prehypertrophic chondrocytes. Green bar, spinal disc. White bar, 200 μm. Northern blotting and RT-qRCR for skinned tails of newborn mice. Results are mean ± SEM. **p < 0.01 compared to wild-type.

(G and H) Role of Pref-1 in MSC commitment and differentiation.

(G) H&E staining (upper panel) of fifth coccyges of 1-week-old mice and higher magnitude of bone marrow region (right). RT-qPCR for femur bone marrow from 12-week-old mice (n = 5) (lower panel). Results are mean ± SEM. **p < 0.01 compared to wild-type.

(H) RT-qPCR of human primary MSC after 2 days adipogenic (upper panel) or chondrogenic treatment (lower panel). Results are mean ± SEM. *p < 0.05 and **p < 0.01.

Kim, K.A., Kim, J.H., Wang, Y., and Sul, H.S. (2007). Pref-1 (preadipocyte factor 1) activates the MEK/extracellular signal-regulated kinase pathway to inhibit adipocyte differentiation. Mol. Cell. Biol. *27*, 2294–2308.

Laborda, J., Sausville, E.A., Hoffman, T., and Notario, V. (1993). dlk, a putative mammalian homeotic gene differentially expressed in small cell lung carcinoma and neuroendocrine tumor cell line. J. Biol. Chem. *268*, 3817–3820.

Lee, K., Villena, J.A., Moon, Y.S., Kim, K.H., Lee, S., Kang, C., and Sul, H.S. (2003). Inhibition of adipogenesis and development of glucose intolerance by soluble preadipocyte factor-1 (Pref-1). J. Clin. Invest. *111*, 453–461.

Lengner, C.J., Lepper, C., van Wijnen, A.J., Stein, J.L., Stein, G.S., and Lian, J.B. (2004). Primary mouse embryonic fibroblasts: A model of mesenchymal cartilage formation. J. Cell. Physiol. *200*, 327–333.

Liu, Z., Xu, J., Colvin, J.S., and Ornitz, D.M. (2002). Coordination of chondrogenesis and osteogenesis by fibroblast growth factor 18. Genes Dev. *16*, 859–869.

Mei, B., Zhao, L., Chen, L., and Sul, H.S. (2002). Only the large soluble form of preadipocyte factor-1 (Pref-1), but not the small soluble and membrane forms, inhibits adipocyte differentiation: Role of alternative splicing. Biochem. J. *364*, 137–144.

Moon, Y.S., Smas, C.M., Lee, K., Villena, J.A., Kim, K.H., Yun, E.J., and Sul, H.S. (2002). Mice lacking paternally expressed Pref-1/Dlk1 display growth retardation and accelerated adiposity. Mol. Cell. Biol. *22*, 5585–5592.

Murakami, S., Kan, M., McKeehan, W.L., and de Crombrugghe, B. (2000). Up-regulation of the chondrogenic Sox9 gene by fibroblast growth factors is mediated by the mitogen-activated protein kinase pathway. Proc. Natl. Acad. Sci. USA *97*, 1113–1118.

Rosen, E.D., and MacDougald, O.A. (2006). Adipocyte differentiation from the inside out. Nat. Rev. Mol. Cell Biol. *7*, 885–896.

Smas, C.M., and Sul, H.S. (1993). Pref-1, a protein containing EGF-like repeats, inhibits adipocyte differentiation. Cell *73*, 725–734.

Smas, C.M., Green, D., and Sul, H.S. (1994). Structural characterization and alternate splicing of the gene encoding the preadipocyte EGF-like protein pref-1. Biochemistry *33*, 9257–9265.

Smas, C.M., Chen, L., and Sul, H.S. (1997). Cleavage of membrane-associated pref-1 generates a soluble inhibitor of adipocyte differentiation. Mol. Cell. Biol. *17*, 977–988.

Smas, C.M., Kachinskas, D., Liu, C.M., Xie, X., Dircks, L.K., and Sul, H.S. (1998). Transcriptional control of the pref-1 gene in 3T3-L1 adipocyte differentiation. Sequence requirement for differentiation-dependent suppression. J. Biol. Chem. *273*, 31751–31758.

Smas, C.M., Chen, L., Zhao, L., Latasa, M.J., and Sul, H.S. (1999). Transcriptional repression of pref-1 by glucocorticoids promotes 3T3-L1 adipocyte differentiation. J. Biol. Chem. *274*, 12632–12641.

Takeda, S., Bonnamy, J.P., Owen, M.J., Ducy, P., and Karsenty, G. (2001). Continuous expression of Cbfa1 in nonhypertrophic chondrocytes uncovers its ability to induce hypertrophic chondrocyte differentiation and partially rescues Cbfa1-deficient mice. Genes Dev. *15*, 467–481.

Wang, Y., and Sul, H.S. (2006). Ectodomain shedding of preadipocyte factor 1 (Pref-1) by tumor necrosis factor alpha converting enzyme (TACE) and inhibition of adipocyte differentiation. Mol. Cell. Biol. *26*, 5421–5435.